CNEA NT - 13/80

Progress Report

1978 - 1979

Department of Physics

Comisión Nacional
de Energía Atómica

Dirección de
Investigación y Desarrollo

Gerencia de
Investigaciones

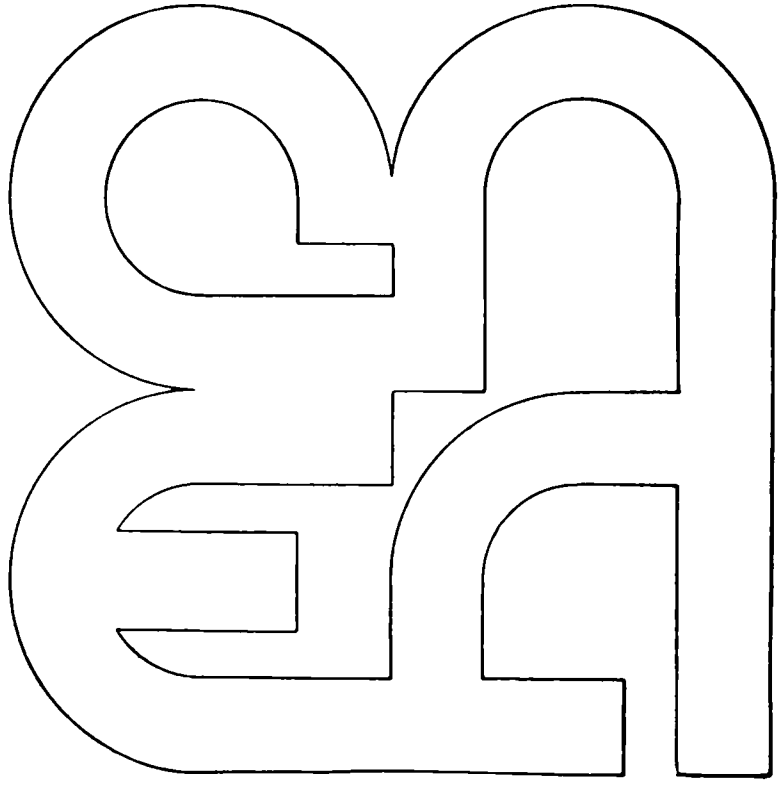

Buenos Aires - Argentina
1980

CNEA NT - 13/80

Progress Report

1978 - 1979

Department of Physics

Comisión Nacional
de Energía Atómica

Dirección de
Investigación y Desarrollo

Gerencia de
Investigaciones

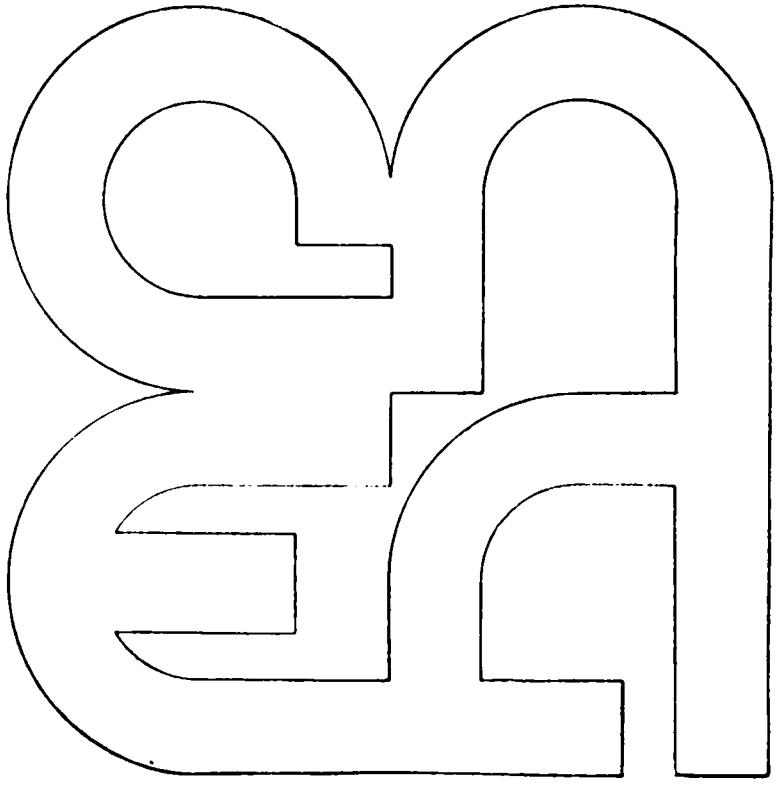

Buenos Aires - Argentina
1980

SCULPTURE BY E. IOMMI AT THE TANDEM SITE

INTRODUCTION

This Progress Report brings together for the first time the contributions of both the Nuclear and Solid State Physics Divisions. While this change implies a larger and perhaps less convenient format, we regard it as a positive additional step in promoting the unity of the local physics community, a policy which we find important to pursue. Given the contribution of our Department to the total effort carried out in physical research in the country, this policy has proven to be relevant well beyond CNEA's boundaries.

It is perhaps opportune to recall that up to 1976 Nuclear Physics constituted one department and the Solid State Group was part of another. After that date these two activities merged together and since then we believe that both have gradually benefited from the interaction with each other.

The period covered by this report has witnessed an increase in the research output and in the effort to acquire better equipment and facilities.

The Solid State group has continued to work on the relationship between physical properties and the structure of crystalline materials and of their modifications by physical parameters such as temperature, pressure and radiation. Phase transitions are of particular interest and the close collaboration of theorists and experimentalists in this field is noteworthy. New facilities have been and are being installed such as a modern automatic microdensitometer designed to perform photographic analyses of X-ray diffraction diagrams and electronic micrography. This equipment will be shared with the radiobiologists. Also a powerful Fourier interferometer and a differential calorimeter have been purchased for infrared spectroscopy and specific heat measurements.

Both the Synchrocyclotron and Cockcroft-Walton accelerators were used intensely. With the Synchrocyclotron the research program on doubly odd Tl isotopes and Br and Rb isotopes was fruitfully continued. Experimentally one important development was the setting up of a facility to measure on line conversion electrons. An adequate description of the parallelism between ^{76}Br and ^{77}Kr was achieved and preliminary evidence for this phenomenon in ^{78}Br and ^{79}Kr was obtained. Part of the work carried out on these nuclei, particularly the most neutron deficient ones, was done in collaboration with the Brookhaven National Laboratory Tandem Group. The new ion source for non-gaseous fragments of the mass-separator which is used in conjunction with the Cockcroft-Walton accelerator to study short lived fission products has yielded a large amount of new and interesting spectroscopic data in the rather unexplored but

important region around ^{132}Sn.

The Nuclear Field Theory has been succesfully applied to the description of deformed systems in two dimensions and it is being extended to three dimensions. Results have been obtained with the Principal Series Approximation which adds the non-vanishing diagrams corresponding to an infinite number of particles with infinite degeneracy, providing a novel way to understand the postulates of the Interacting Boson Model. In collaboration with the Sussex Group the mechanisms of α-transfer enhancement were studied. Also a new method to calculate the corrections to the Time Dependent Hartree-Fock theory has been developed.

By large the most important activity besides research was the work on the TANDAR (TANdem ARgentino) project. In the last two years this project, which became a reality in 1976-1977, was definitely consolidated. After signing the contract with National Electrostatics Company for a 20UD Pelletron in December 1977, most of the effort was devoted towards the design, engineering and construction of the accelerator tower and surrounding buildings. It was a tight schedule and in the previous report we anticipated difficulties. These were not absent. A rather unforeseen one, that of selecting the site, turned out to be quite a hard obstacle. Fortunately it was eventually overcome and after that a lot of work was put into reducing the time allocated for the subsequent planned actions so that the original schedule date for starting the installation of the machine (beggining of 1981) could be met. It is a great satisfaction that this has been achieved so far.

The ambitious training program for young physicists which was reported last time has continued at the same pace. Presently thirteen of these young people have been incorporated to the staff. Most of them are now completing their theses abroad, while a new group has initiated the fellowship stage here.

Two valuable study meetings with a view towards the use of the future Tandem were organized in the summers of 1978 and 1979 and held at the Balseiro Institute in Bariloche. We benefited from the participation of colleagues from other countries like Brazil, Chile, Uruguay and U.S.A.. The lines of research to be pursued were discussed and committees were formed to deal with them. We expect to continue holding these meetings once a year as they have proven very profitable. We are also glad to have played hosts to an International Workshop on Nuclear Matter organized by the nuclear physics group from La Plata University.

Toward the end of the period of this report we celebrated two happy

events: the 25th anniversary of the Sinchrocyclotron and the beginning of the excavation work for the tower which will house the 20UD Tandem accelerator. The coincidence of these two events is in itself significant. The Sinchrocyclotron has played a very important role in the development of Nuclear Physics in Argentina. It has been used with an unusually high degree of continuity and effectiveness and it represents the backbone of our relatively short history. The new Tandem, which will be the central facility for the next generation, can be justly regarded as the last and perhaps most significant product of this old machine. In this ocassion lectures on the subject of the different stages in the Synchrocyclotron history were delivered by its main protagonists and at the Tandem site a modern sculpture (shown in the preceding page), by the renowned argentine artist Enio Iommi, was dedicated as a symbol of the spirit of creativeness which should endow the future laboratory.

We very much hope that the next period will be as full of developments as this has been. If everything goes as planned we should be reporting about the first tests at the Tandem in the next issue.

We wish to acknowledge the effort of the editor of this issue, Andrés J. Kreiner and his assistant Mrs. Susana Lires. Also the extra help provided by Mr. Binda, Mrs. M. T. Carmuega and Mrs. M. Gismondi is greatly appreciated.

M.M.
May 1980

TABLE OF CONTENTS

IV. NUCLEAR STRUCTURE

SOLID STATE PHYSICS

I. VIBRATIONAL SPECTROSCOPY

The Tandar Project

THE T A N D A R PROJECT

E.Achterberg, D.Camín, A.Ceballos, N.Fazzini, A.Filevich, H.González
J.Milberg, J.Nicolai, E. Pérez Ferreira, R.Requejo
R.Ribarich, J.Rossi, S.Tau and E.Ventura

In the last Progress Report (1976-1977) the decision of installing a new facility for research in nuclear physics was announced and a very brief description of the first steps of the Project was included in the Introduction. It was also mentioned that a substantial fraction of the activity carried out by the Department during that period was devoted to meet our original schedule, signing the contract with Electrostatics International, Inc. and starting the construction of the accelerator on December 1st, 1977. We were, however, perfectly aware about the fact that the struggle had just started and about the effort to be done along the years to come before reaching our goal of having the facility operative for the middle of 1982.

After two years, we should recognize that all of us had a very optimistic idea about the work behind a project of this magnitude. Namely, the contract with NEC was just the first of a series of 14 other contracts with local and foreign suppliers and constructors and we have suceeded until now in maintaining the project on schedule within an error of three months.

All this had been impossible without the permanent encouragement and support received from the authorities of the National Atomic Energy Commission or without the very particular spirit existing in the Nuclear Physics and the Engineering and Technical Support Divisions of the Physics Department after a tradition of more than 25 years of continuous and fruitful operation and improvement of the 28 MeV Sinchrocyclotron.

The Accelerator

It is a 20 MV tandem accelerator built by NEC according to CNEA specifications. The high voltage terminal will be located inside a 35 m-high, 7.7 m-diameter presure vessel and supported at the middle of the column structure. Four NEC Pelletron chains will provide charge to the terminal and an enclosed corona point system will accomplish uniform distribution of the column and accelerating tube potential. Unwanted charge states will be prevented from being introduced into the high energy acceleration tube by means of a charge selector located at the terminal, where gas and foil strippers

will also be placed. A second foil stripper is foreseen at the first dead section after the terminal. Electrical power to the equipment in the terminal and dead sections will be provided from generators powered by a rotating shaft running the lenght of the column. Monitoring of terminal parameters at the console will be provided by light links.

Three types of negative ion sources, a duoplasmatron, a charge exchange and a sputtering ion source, are included in the provision by NEC as well as the 300 KV injector, a chopper and buncher device to provide pulsed beams and two 90° magnets, a small one for the low energy beam and an analyzing magnet (mass-energy product = 500) mounted on a rotating platform.

The insulating gas for the tandem is pure SF_6 and typical operation pressure will be 8 Kg/cm^2. During servicing operations the insulting gas will be stored in two spherical tanks at a pressure of 22 Kg/cm^3. An inventory of about 240.000 pounds of SF_6 should be maintained.

The provision of a new data hadling system was also included in the contract with NEC and the VAX-1178 was selected as the main component of the designed system.

Also magnetic and vacuum components and basic instrumentation for six experimental lines are to be provided by NEC.

Current state of the Project

About 80 % of the accelerator has been constructed by NEC according to the original schedule. Shipping is foreseen for the end of 1980 and assembling to be initiated on March 1st, 1981.

The civil work includes not only the accelerator building, but also the installations of the rest of the Physics Department and some other laboraries of the Research Branch of CNEA. The construction of the accelerator building begun last November. The main and service towers (72 m-high) should be completed to the level of 13.69 m on June 15 when assembling of the pressure vessel should begin. Civil work in the towers will be interrupted for two and half months during assembling and testing of the tank and reinitiated after tests. Termination time of the tower walls by using sliding concrete forms is estimated in one additional month and finishing up to the point necessary for starting accelerator mounting requires another 5 months, so that the scheduled date of March 1st, 1981 can be met.

Construction of the pressure vessel and gas storage tanks have been

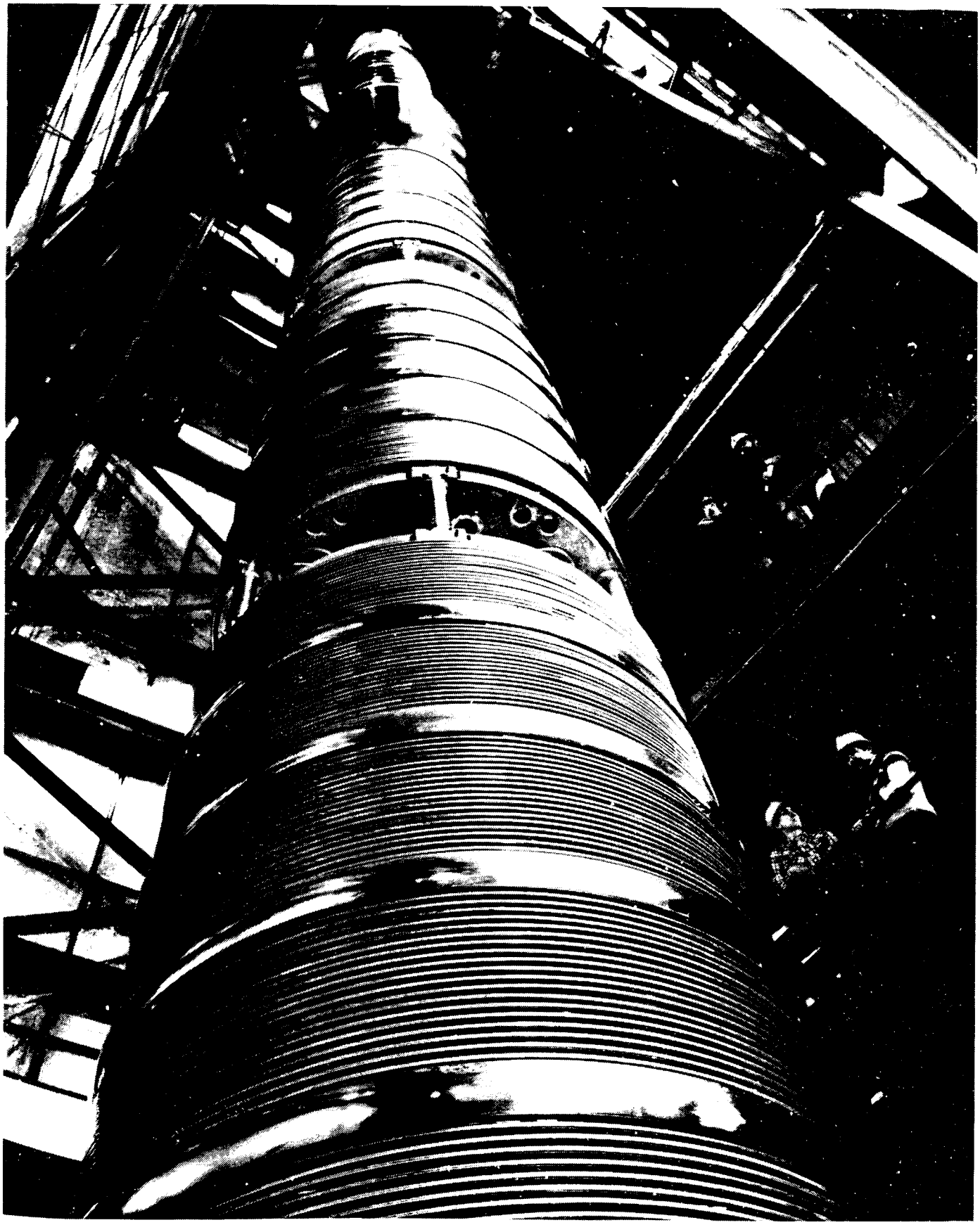

The accelerator column, provisionally assembled at NEC

already contracted with local companies. Provision and assembling of all the electromagnetic equipment in the accelerator building, including the construction of the gas handling system is about to be contracted also with local industry.

The project and development of detailed design for all the local works were elaborated by an argentine engineering company whose personnel worked in close collaboration with CNEA staff.

About a 75 % of the most significant part of the data handling system has been already installed provisionally at the old laboratory and the development of software will begin immediately in order to have it ready for use as soon as the accelerator becomes operative.

In the mean time considerable effort has beem devoted to training both physicists and engineers, to ensure a reasonable utilization of the new facility and its efficient operation and maintenance. Namely, 15 young physicists are being trained both in our laboratories and abroad in relevant subjects of physics where the contribution of the 20 MV Tandem might be significant. We are also indebted to the ORNL for having received 3 of our engineers and one of our senior physicists during the stages of assembling and tests of their 25 UR Pelletron, allowing us to acquire valuable first hand experience on the multiple and unforeseen problems that arise during the installation of these large facilities.

Organization

A great mayority of the staff of the Nuclear Physics and Engineering and Technical Support Divisions collaborates in the different tasks of the Project, some of them full-time, some others on a part-time basis.

Under the Project Manager (E. Pérez Ferreira; alternate M. Mariscotti) there are three groups:

I.- Coordination of local works (E.Ventura, R.Requejo).

II.- Accelerator (N.Fazzini, A.Ceballos).

III.- Planning and coordination of experimental lines (J.Rossi, A.Filevich)

covering the relations with the contractors and coordinating the work of the the following working groups:

1.- Gas handling system (J.Nicolai, H.González)

2.- Safety (S.Tau, A.Ceballos, A.Filevich)

3.- Shieldings (A.Kreiner, M.Mariscotti)

4.- Beam optics (A.Ferrero, A.Ceballos, A.Filevich)

5.- Accelerator control system (S.Tau, D.Camín, J.Mónico)

6.- Vacuum systems (J.Nicolai, H.González)

7.- Ion sources

8.- Data handling system (E.Achterberg, D.Otero)

9.- Targets (A.Ceballos, A.Filevich)

10.- Magnetic spectrometer (J.Rossi)

11.- Short lived isotopes (M.Pérez, J.Rossi)

12.- On line γ-ray spectroscopy (G.García Bermúdez, M.Behar)

13.- Nuclear reactions - Light ions (A.Ceballos, H.Huck)

14.- Nuclear reactions - Heavy ions (D.Otero, A.Proto)

15.- External users (M.Pérez)

16.- Ge(Li) detectors (G.Martí, C.Giménez)

17.- Training of new physicists (E.Maqueda, M.Saraceno, G.García Bermúdez)

18.- Organization of study meetings (R.Perazzo, O.Dragún, J.Rossi)

19.- Inspection of civil work (R.Ribarich, J.Milberg)

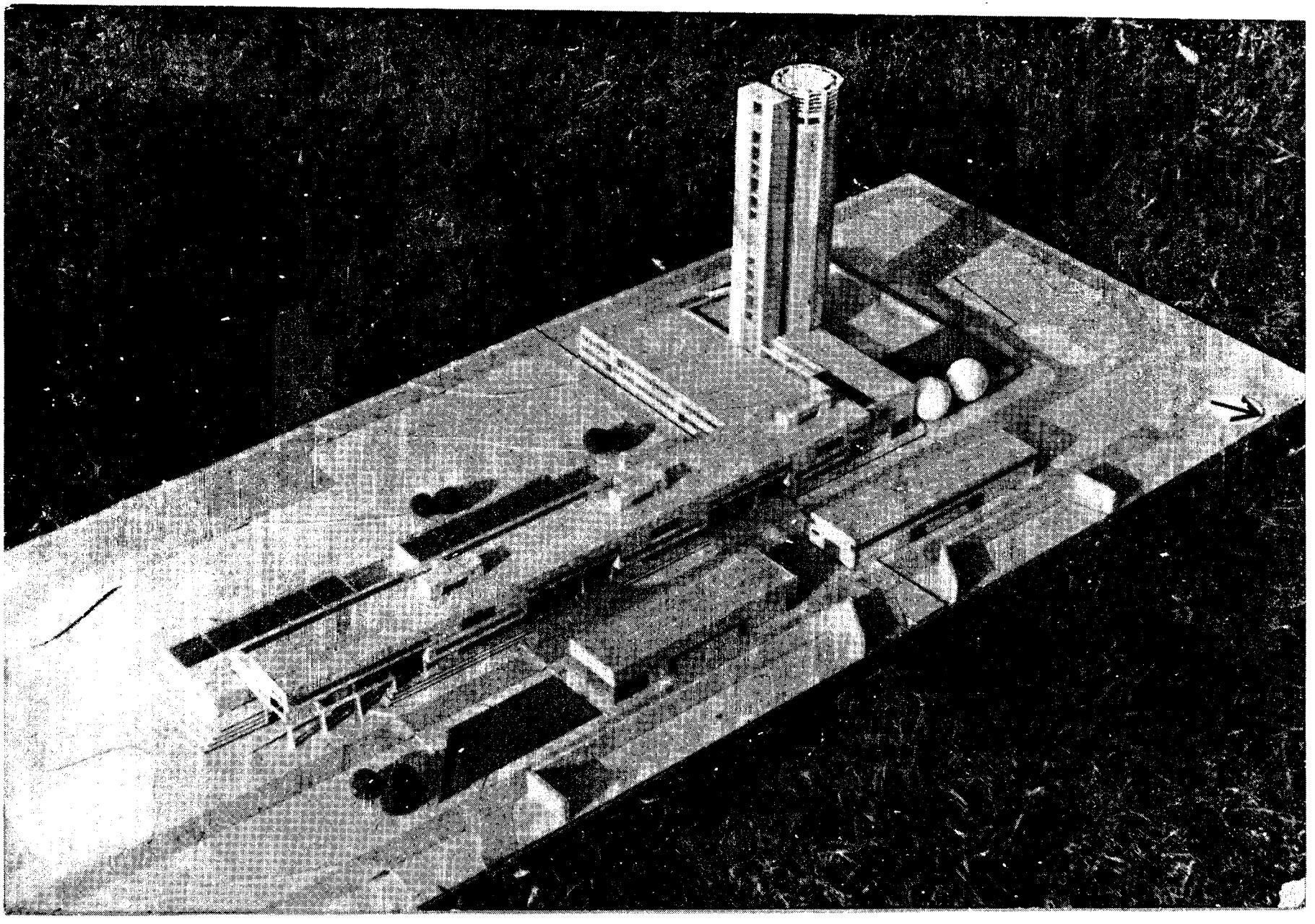

Model of the new Physics Department and the accelerator buildings

Nuclear Physics

In Beam Spectroscopy
Radioactivity
Applied Nuclear Physics
Nuclear Structure
Nuclear Reactions
Instrumentation and Development

I. IN BEAM SPECTROSCOPY

I.1 Band Structure in ^{74}Br

G.García Bermúdez, A.Filevich, A.J.Kreiner, M.A.J.Mariscotti, C.Baktash*, E. der Mateosian* and P.Thieberger*

The observation in ^{76}Br [1] of a Coriolis distorted band built on a low lying 4^+ isomer [2] and satisfactorily described, within the framework of a two non-interacting quasiparticle plus rotor calculation [3], stimulated the present work. The reaction ^{60}Ni(^{16}O,np) has been used to reach levels of the next lighter doubly odd nucleus ^{74}Br. Until now only low spin states$^+$ and the existence of a (4^-) isomeric level at about 200 keV above the $(0, 1^-)$ ground state, had been determined. From excitation function, coincidence and angular distribution measurements, the level scheme shown in Fig. I.1.1 is obtained. The isotopic assignment is mainly based on the determination of relative cross sections and balance between prompt and decay intensities.

Coban et al [4] studied the decay of ^{74}Br to levels of ^{74}Se producing the activity through the ^{63}Cu(^{14}N, 2np) and ^{65}Cu(^{12}C,3n) reactions and established a (4^-) state of 41.5 m half-life. The present decay study shows that both the 25.3 m ground and the isomeric states are populated in the heavy ion reaction. From the analysis of the composite decay (Fig. I.1.2) a 49.5 m half-life is obtained. This result indicates that a new log-ft study is required to reexamine the previous spin parity assignment. The proposed level scheme built on the 49.5 m isomeric state (Fig. I.1.1) displays a $\Delta I = 1$ band structure similar to that found in ^{76}Br. In addition it is worthwhile to note that if the high spin structure in ^{74}Br is analogous to that found in ^{76}Br a prediction [3] indicating the ocurrence of a change in the phase of the staggering above the 9^+ level, would be confirmed.

---

* Department of Physics, Brookhaven National Laboratory, Upton, New York.

[1] M.Behar, A.Filevich, G.García Bermúdez and M.A.J.Mariscotti; Nucl.Phys. A282, 331 (1977).

[2] A.J.Kreiner, G.García Bermúdez, M.A.J.Mariscotti and P.Thieberger; Phys. Lett. 83B, 31 (1979).

[3]) A.J.Kreiner and M.A.J.Mariscotti; Phys.Rev.Lett. 43, 1150 (1979).

[4]) A.Coban, J.C.Lisle, G.Murray and J.C.Willmott; Particles and Nuclei 4, 108 (1972).

+) Piercey et al (ORNL Annual Review, Oct. 1977) studied the ^{60}Ni (^{16}O,xnypzα) reaction and observed a group of unidentified gamma rays which, in the present work, has been proposed to belong to ^{74m}Br.

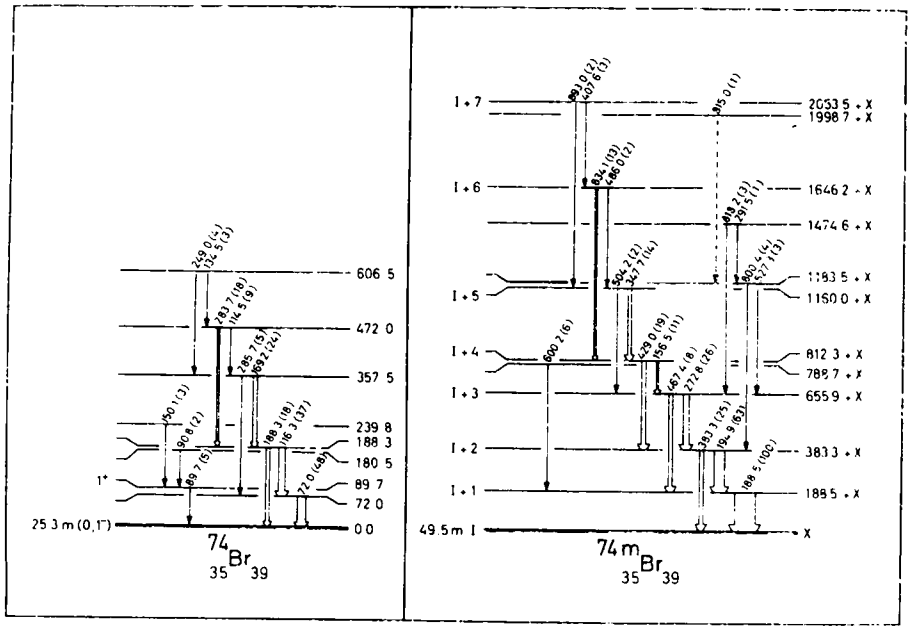

Fig. I.1.1: Proposed level scheme for ^{74}Br.

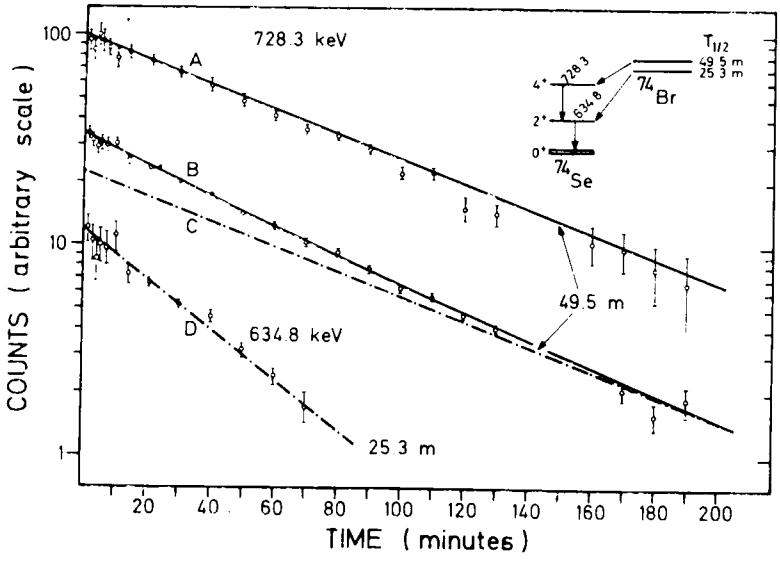

Fig. I.1.2:

Time distribution of (A) 728.3 keV and (B) 634.8 keV transitions in the decay of ^{74}Br to levels of ^{74}Se (see insert). The solid line labeled by B results from a fitting in which a sum of two exponential functions is assumed. The curves labeled by C and D show each term of this sum.

I.2 Long-lived positive parity isomer in ^{76}Br*

A.J.Kreiner, G.García Bermúdez, M.A.J.Mariscotti and P. Thieberger**.

In a recent study[1] of the $^{75}As(\alpha,3n)$ reaction a collective band was found in ^{76}Br which not only shows deviations from a rigid-rotor behaviour similar to those previously observed[2] for the $5/2^+$ ground-state band of the neighboring ^{77}Kr, but the excitation energies of the lowest states in the two bands are very nearly the same.

However, an analysis[3] carried out in terms of the two-quasiparticle-plus-rotor model[4], shows that these features are difficult to understand for a band built on a low-spin state such as the 1^- ground state in ^{76}Br. On the other hand, one has the experimental information that in ^{77}Br a $9/2^+$ decoupled band appears at 106.2 keV[5], which suggests the possible relevance of the positive parity proton states in this connection.

In view of these facts it became tempting to search for a low-lying isomer in ^{76}Br and such was the objective of the present work.

Two lines of 45.5 and 57.1 keV were found to decay with a half-life of 1.32 ± 0.02 s. These lines are identified with ^{76}Br because, (a) there is Br K X-ray characteristic radiation which decays with the same half-life and (b) the mass number A=76 is established by their excitation functions. The new level scheme emerging from this work is shown in Fig.I.2.1. The previously reported $\Delta I=1$ band in ^{76}Br is most likely built on the 4^+ isomer rather than on the 1^- ground state[1]. Indeed, one may expect low-lying high-spin positive parity states of $\tilde{\nu}g_{9/2} \otimes \tilde{\pi}g_{9/2}$ parentage in this region of the periodic table; the neutron Fermi surface is known to lie within the Nilsson multiplet originated in the $g_{9/2}$ orbit as revealed by the spectrum of the neighboring isotone ^{77}Kr (ref.2) and the odd-proton nuclei exhibit low-lying $9/2^+$ isomeric states on top of which decoupled bands develop[5].

---

* Phys. Lett. 83B (1979) 31. Also reported by W.D.Schmidt-ott et. al., Z.Physik A289 (1978) 121.

** Department of Physics, Brookhaven National Laboratory, Upton, N.Y., U.S.A

1) M.Behar, A.Filevich, G.García Bermúdez and M.A.J.Mariscotti; Nucl. Phys. A282 (1977) 331.

2) E.Nolte and P.Vogt; Z. Phys. A275 (1975) 33.

3) A.J.Kreiner and M.A.J.Mariscotti; Phys. Rev. Lett 43 (1979) 1150.

4) A.J.Kreiner; Z. Phys. A288 (1978) 373.

5) M.A.Deleplanque et.al. ; J. de Phys. Lett. 35 (1974) 237.

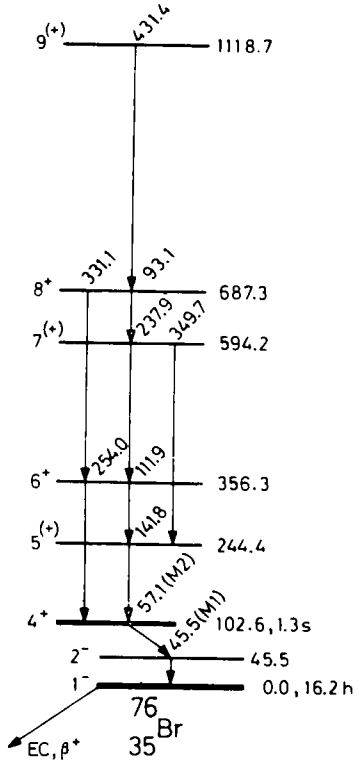

Fig. I.2.1

I.3 High spin states in ^{78}Br

G.García Bermúdez, D.Abriola, M.Behar, M.C.Berisso, J.Fernández Niello, A.Filevich and M.A.J.Mariscotti.

The observation[1] and correct interpretation[2] of a Coriolis distorted band in ^{78}Br built on a low lying 4^+ isomer showing a clear parentage with the ground state band of the next isotone ^{77}Kr, has stimulated the search for similar structures in neighboring doubly odd isotopes. The case of ^{78}Br is of interest because a $4^{(+)}$ isomer has been known in this nucleus for some time. Recently Kluger-Bell et al[4] have studied ^{78}Br using the $^{79}Br(p,d)$, $^{77}Se(\ He,d)$ and $^{75}As(\alpha,n\gamma)$ reactions. From their work a considerable wealth of new spectroscopic data is obtained, including the obser-

vation of new half-lives, but high spin states (I>4) above the $4^{(+)}$ isomer at 180.8 keV are not identified. To reach high spin states in ^{78}Br we used the ^{77}Se(α,2np) reaction between 30 and 55 MeV. From excitation functions, coincidence and angular distribution measurements, the level scheme shown in Fig. I.3.1 is obtained.

Half-lives were determined from two different experiments. In the first one, the natural beam pulsing of the Synchrocyclotron was used to stop a TAC which was triggered by the γ-ray signals from a Ge(Li) detector. In this way evidence was obtained for a 9 ± 1 ns half-life for the 110.2 keV line and 17 ± 2 ns half-life for the 46.3 keV line. In addition the 46 keV line shows a hitherto unreported flat time distribution indicating a longer half-life which could not be determined in this experiment because of the short time span between two beam bursts, but it was established by measuring the time delay between this line and the 110.2 keV γ-ray (see Fig. I.3.2).

Kluger-Bell et al[3] discuss the possibility of finding in ^{78}Br an structure similar to that built on the 4^+ isomer in ^{76}Br and come to the conclusion that such a pattern is not observed in ^{78}Br. In fact the sequence of levels discussed above may provide evidence for such a phenomenon as they show a level staggering resembling to some extent the Coriolis distortions found in ^{76}Br. However to allow elucidation of this point more data are needed, not only for ^{78}Br but also for ^{79}Kr as the underlying description[2] which one would like to test here involves the assumption of a common parentage between the doubly odd nucleus and its odd-A neighbour.

---

[1] M.Behar, A.Filevich, G.García Bermúdez and M.A.J.Mariscotti; Nucl. Phys. A282 , 331 (1977).

[2] A.J.Kreiner and M.A.J.Mariscotti; Phys. Rev. Lett. 43 , 1150 (1979).

[3] B.M.Kluger-Bell, R.E.Anderson, R.J.Peterson, D.E.Prull, R.A.Ristinen and B.L.Smith; J. Phys. G5 , 827 (1979).

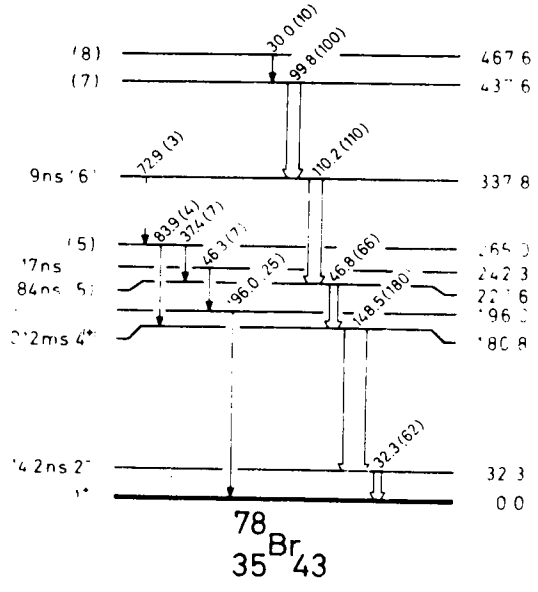

Fig. I.3.1 : Proposed level scheme for ^{78}Br .

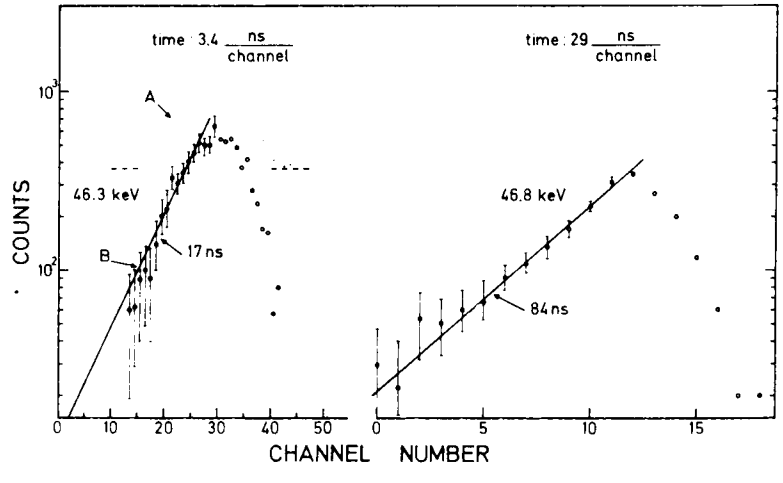

Fig. I.3.2 : Time distribution of the 46.3 and 46.8 keV transitions. A indicates raw data for the 46.3 plus 46.8 keV γ-rays in the R.F.-γ experiment. The dashed lines indicate the level of the long-lived flat time distribution. B shows the time distribution after this flat level is substracted.
The time distribution shown to the right of the figure has been obtained from a γ-γ-time experiment as explained in text.

I.4 Level Structure of ^{82}Rb studied through the ^{81}Br(α,3n) reaction.

M.Behar, A.Filevich, G.García Bermúdez, M.A.J.Mariscotti and L.Szybisz.

The results obtained in previous work[1,2] on excited states of ^{78,80}Rb have stimulated us to search for high spin states in the next odd-odd neighbor ^{82}Rb. Up to now this isotope was scarcely studied and its known level scheme was limited to the $I^{\pi}= 1^{+}$, $T_{1/2}= 1.25$ min g.s. and to an isomeric state at about 100 keV with $I^{\pi}= 5^{-}$ and $T_{1/2}= 6.2$ h . In this work, carried out with the α-particle external beam of the synchrocyclotron we bombarded an 98% enriched 40 mg/cm^2 thick NaBr target to produce the ^{81}Br(α,3n)^{82}Rb reaction. Ge(Li) detectors were used to observe γ-ray spectra. After a careful analysis of the excitation functions, we were able to assign a number of γ-rays as belonging to the ^{82}Rb nucleus. Other open reaction channels show either upgoing or decreasing excitation functions. Recently published data[3,4] allowed the identication of reactions such as (α,2np) , (α,npα) , (α.3p) , (α,2pα) and (α,n2p). Angular distribution results are shown in Fig.I.4.1 and Table I.4.1 shows the data obtained in our measurements. The results of two coincidence experiments (resolving time=40 ns) clearly show the existence of a γ-ray cascade. Only one crossover transition was observed. An upper limit of $T_{1/2} \tilde{=} 5$ ns was found for the 45.9 and 64.5 keV lines. However, the existence of a weak long-lived component cannot be ruled out. The ^{82}Rb level scheme (Fig.I.4.2) contains 6 lines which were placed unambiguously. Other 6 lines have been observed in coincidence with the 45.9 , 64.5 and 123.2 keV γ-rays, but the coincidence experiment does not allow any other conclusion and these lines were not placed in the scheme. The 621.4 keV line shows some evidence of being in coincidence with the 562.7, 980.5 keV γ-rays and the other strong lines of ^{82}Rb, but since its behaviour is not conclusive we kept its placement ambiguous. Two off-beam timing experiments were made to decide whether the level scheme shown in Fig. I.4.2 is based on the $I^{\pi}= 1^{+}$ g.s. ($T_{1/2}= 1.25$ min) or on the $I^{\pi}= 5^{-}$ ($T_{1/2}= 6.2$ h) isomer. In these experiments 20 min and 12 h accumulations were performed after 5 min and 6 h irradiations, respectively. It is difficult to draw any definite conclusion from these measurements because of side feeding effects which mask the intensity balances. However, the behaviour of the first three excited states roughly resembles the one

observed in a similar band in ^{80}Rb [2] and this suggests that the level scheme found in this work can be based in the $I=1^+$ ground state in ^{82}Rb.

---

[1]) M.A.J.Mariscotti et al; Phys. Rev. C19 (1979) 1301.

[2]) M.Behar et al; Nucl. Phys. A287 (1977) 255.

[3]) Table of Isotopes ed. C.M.Lederer and V.S.Shirley (Wiley N.Y.).

[4]) P. von Brentano et al; Proc. topical Conf. on Problems of Vibrational Nuclei, ed. G. Alaga V. Paar and L. Sips (North Holland, Amsterdam, 1975) p. 156 .

TABLE I.4.1

Energies, intensities, angular coefficients of γ-rays and spin sequence for the $^{81}Br(\alpha,3n)^{82}Rb$ reaction at E_α = 45 MeV.

$E_\gamma \pm 0.3$ (keV)	$I_\gamma \pm 10\%$	$(I_T)^{a)}$	A_2/A_0	(A_4/A_0)	Spin Sequence
45.9	100	(200)	-0.61 ± 0.08	0.01 ± 0.09	(I+3) - (I+2)
64.5	190	(260)	-0.42 ± 0.04	-0.02 ± 0.05	(I+2) - (I+1)
84.9	5				
88.7	5				
123.2	340		-0.41 ± 0.04	-0.03 ± 0.05	(I+1) - I
130.4	7				
132.8	3.5				
156.7	12				
386.5	13				
417.8	12				(I+5) - (I+4)
562.7	74		-0.48 ± 0.03	-0.05 ± 0.06	(I+4) - (I+3)
621.4	30				
980.5	45		0.29 ± 0.08	0.07 ± 0.03	(I+5) - (I+3)

a) Total intensity estimate assuming dipolar character for the γ-transitions.

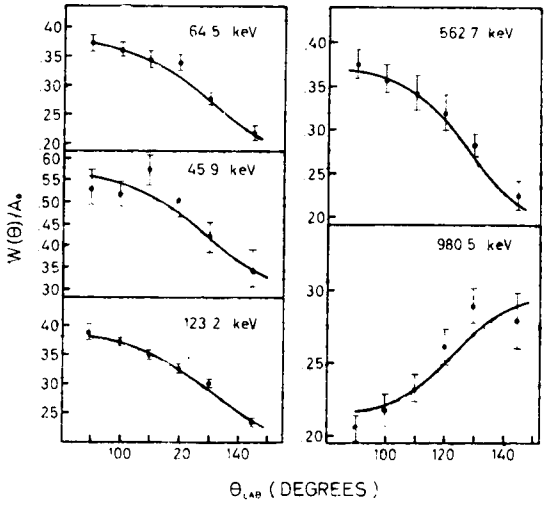

Fig. I.4.1 :

Angular distribution of prominent γ-rays from the $^{81}Br(\alpha,3n)$ ^{82}Rb reaction. The solid lines show the results of least square fits with the parameter A_2 and A_4 listed in Table I.4.1 .

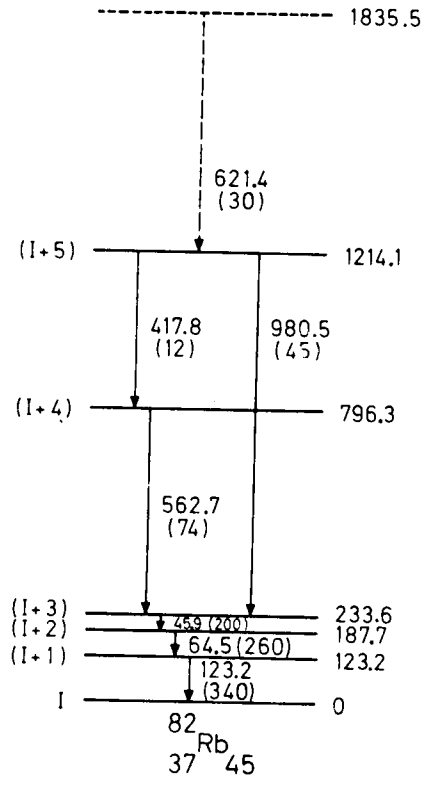

Fig. I.4.2 : Level scheme of ^{82}Rb proposed as result of this work.

I.5 Collective Excitations in ^{88}Y

M.Davidson*, J.Davidson* and M.A.J.Mariscotti

High spin states in ^{88}Y were excited through the ^{87}Rb (α,3n) reaction at energies between 30 and 55 MeV. The population of the previously known[1] 8^+ and 9^+ members of the $\pi g_{9/2} \otimes \nu^{-1} g_{9/2}$ multiplet carry most of the total cross section (see Fig. I.5.1). On top of the 8^+ state a sequence of 5 levels is observed, which can be interpreted as arising from the coupling of this level with the excitations of the ^{88}Sr core[2]. A similar interpretation can be made of the 3206.5 keV state which deexcites into the 9^+ state (see Fig. I.5.2. Only a few of the many low lying-low spin states previously reported are weakly seen with this reaction. The relative cross sections for the different outgoing channels are compared with those observed in the ^{85}Rb(α,xnyp zα) reaction and both sets are in turn combined with earlier data obtained with the Zn isotopes to show that it is possible to attain a systematics for this quantity (see Fig. I.5.3).

*Departamento de Física, Facultad de Ciencias Exactas y Naturales de la Universidad de Buenos Aires.

1) H.W.Baer, R.L.Bunting, J.E.Glenn and J.J.Kraushaar, Nucl. Phys. A218 (1974) 355.

2) S.E.Arnell, A.Nilsson and O.Stankiewicz, Nucl. Phys. A241 (1975) 109.

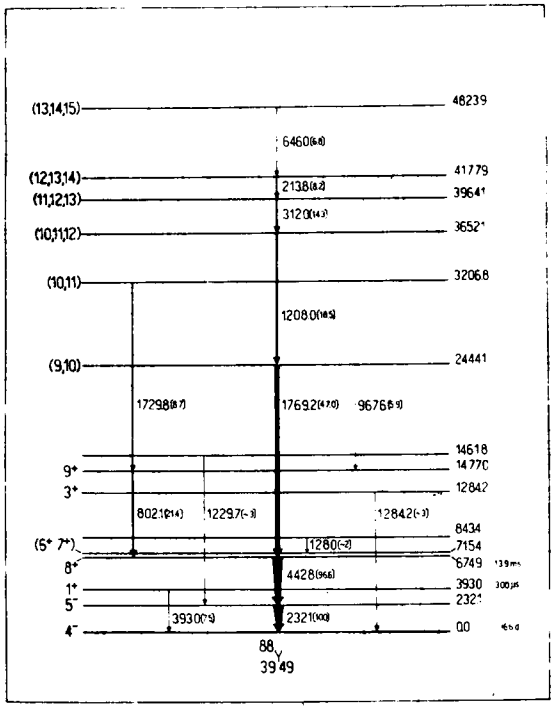

Fig. I.5.1 :

Level scheme of ^{88}Y proposed in the present work.

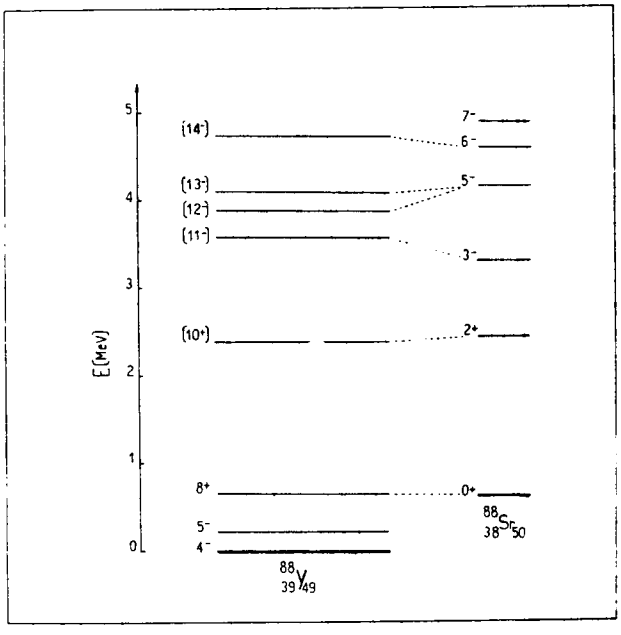

Fig. I.5.2 :

The observed level scheme for ^{88}Y is compared with the high spin states in ^{88}Sr. Since the high spin states in ^{88}Y are interpreted in terms of the $\pi g_{9/2} \otimes \nu^{-1} g_{9/2}$ states, the scale for the ^{88}Sr has been shifted upwards to facilitate the comparison.

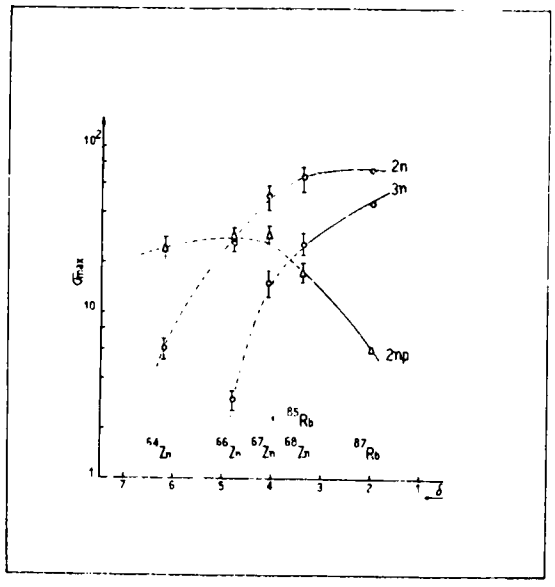

Fig. I.5.3 :

The maximum cross section σ_{mass} versus δ (δ=A-1.7N) which measures the degree of neutron deficiency of the target nuclei was plotted for the Zn and Rb isotopes.

I.6 High Spin Band Structure of ^{192}Tl *

A.J.Kreiner, A.Filevich, G.García Bermúdez, M.A.J.Mariscotti, C.Baktash**, E.der Mateosian** and P.Thieberger**.

High spin states in ^{192}Tl, excited through the ^{181}Ta(^{16}O,7n) and ^{181}Ta(^{18}O,5n) reactions, were studied using standard in-beam γ-ray spectroscopic techniques. The $\tilde{\pi}h_{9/2} \otimes \tilde{\nu}i_{13/2}$ two-quasiparticle band also exists in this case based on an $I^{\pi} = 8^{-}$ isomeric state at 250.6 keV above the known long lived 7^{+} level. The compression trend of the first intraband transition energies already noted in the heavier doubly odd Tl isotopes with A= 198, 196 and 194 towards the neutron deficient side is also confirmed in this nucleus thus providing additional support for the theoretical description (see contribution IV.4.3).

---

* Work performed at Brookhaven National Laboratory under the auspices of CONICET and the National Science Foundation. Phys. Rev. (in press).

** Department of Physics, Brookhaven National Laboratory, Upton, N.Y. 11973, U.S.A.

I.7 In-beam γ-ray spectroscopy in ^{194}Tl *

A.J.Kreiner, M.Fenzl**, U.Heim** and W.Kutschera**

High spin states in ^{194}Tl, excited through the ^{181}Ta(^{18}O,5n) reaction in the energy range E = 80-100 MeV, were studied using in-beam γ-ray spectroscopic techniques. Excitation functions, activity spectra, γ-ray angular distributions and γ-γ coincidences were measured.

The strongly Coriolis distorted $\pi h_{9/2} \otimes \nu i_{13/2}$ two-quasiparticle band already known in ^{196,198}TI (Refs.1,2) has also been found in this case. It is based on an $I^{\pi} = 8^-$ isomeric state located 292.8 keV above ^{194m}Tl($I^{\pi}=7^+$). Fig. I.7.1 shows the level scheme proposed in the present work. The excitation energy of the 7^+ state (≈ 0.30 MeV) can be estimated from systematics. The reason why the cascade is not ending directly on the 8^- isomeric state is primarily connected with the existence of a further low energy (61.5 keV) γ-ray in ^{196}Tl where a very similar band is known[1]. In these heavy nuclei the large internal conversion may easily prevent the observation of such low energy lines. In view of this situation the value of ΔI (Fig. I.7.1) remains open to some extent until its definitive experimental elucidation.

---

* These experiments were performed at the Munich MP tandem facility. Phys. Rev. C (in press).

** Fachbereich Physik der Technischen Universitat Munchen, 8046Garching, Germany.

1) A.J.Kreiner, M.Fenzl and W.Kutschera, Nucl. Phys. A308 (1978) 147.

2) A.J.Kreiner, Z.Physik A288 (1978) 373.

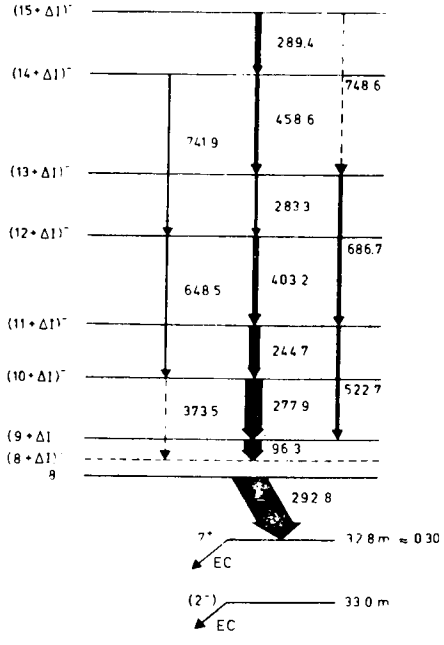

Fig. I.7.1:

Level scheme for ^{194}Tl .

I.8 On-line conversion electron measurements.

M.Debray, A.J.Kreiner, C.Pomar and J.M.Riso

The importance of determining multipolarities of transitions in nuclear spectroscopy work is a well known fact. One of the most powerful tools in this regard is the measurement of internal conversion coefficients. This is a common practice in radioactivity investigations while it is not so generalized in on-line work where it is normally coupled with larger difficulties.

Until now no such measurements were performed in our laboratory, where the main efforts were devoted to γ-ray spectroscopy. In this contribution we report on first successful attempts in obtaining new conversion electron data using the external beam of the Buenos Aires Synchrocyclotron. We investigated the feasibility of acquiring such data with the simplest possible set up without using any magnetic device. Two types of detectors were available. A small (3 mm. thick) Si(Li) detector with a 7.5 μm Be window was used separated from the vacuum of the target chamber by a 0.3 mg/cm^2 Mylar foil. With this set up it is possible to measure satisfactorily electrons of energies down to 150 keV. Limitations are imposed by the window thicknesses and the increasing competition of low energy γ-rays. Fig. I.8.1 showx two spectra obtained with this detector. The lowier one is taken coincidently with the beam bursts and the upper one corresponds to the "silence" periods of the natural μsec time structure of the accelerator. This experiment provides new and complementary information to that obtained on ^{200}Tl measuring only γ-rays within a BNL-Buenos Aires collaboration[1].

The target was approximately lmg/cm^2 thick and the energy of the deuteron beam used for the first time in this kind of studies corresponds to the maximum available at our machine which nevertheless is not large enough to reach the top of the excitation function for the ^{202}Hg(d,4n) reaction. Another case studied was ^{196}Tl through the ^{197}Au(α,5n) reaction at 55 MeV. The other type of detector tried was a 400 μm surface barrier Silicon diode[2] both at room and liquid nitrogen temperature placed directly into the target chamber. In the refrigerated mode results are comparable to the ones obtained with the Si(Li) detector with the advantage of having almost no limitation at low energies. Of course in-beam it is difficult to measure discrete lines below approximately 100 keV because of the very large δ-ray

background.

---

[1]) A.J.Kreiner, M.A.J.Mariscotti, C.Baktash, E.der Mateosian and P.Thieberger; to be published.

[2]) This detector was acquired using financial support from the CONICET (Consejo Nacional de Investigaciones Científicas y Técnicas) which is gratefully acknowledged here.

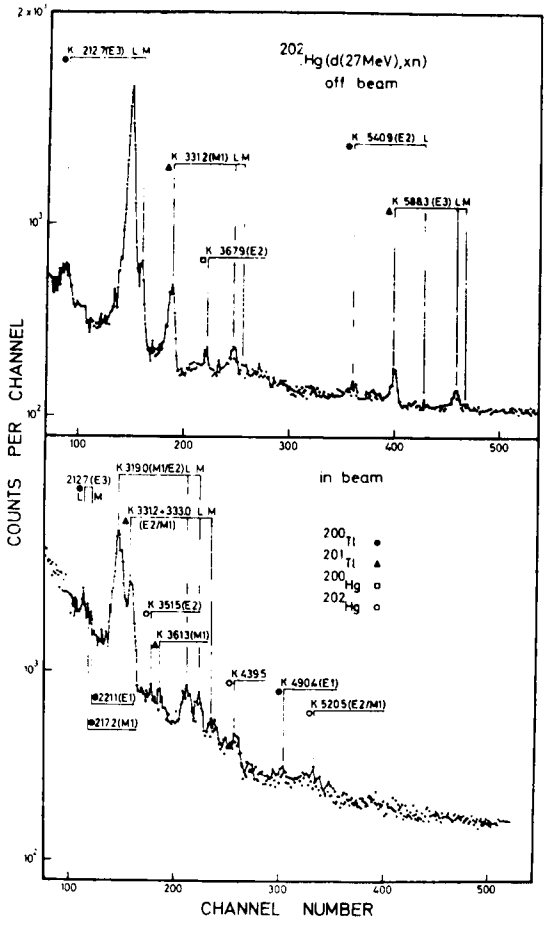

Fig. I.8.1 : In-and off beam spectra from the ^{200}Mg(d,xn) reaction at 27 MeV.

II. RADIOACTIVITY

II.1 Preliminary results on the β decay of ^{129}Sn, ^{130}Sn, ^{131}Sn.

H.Huck, M.L.Pérez, J.J.Rossi.

With the new ion source-uranium carbide target of the I.A.L.E. Project several studies have been initiated in nuclei close to the double magic ^{132}Sn.

Singles γ-ray spectra with different collection times and moving collector speeds were measured in order to assign the γ-lines observed, as well as multispectra runs for half-life determinations.

In all the Sn and Sb decays studied many new γ-lines have been observed as well as some discrepancies in the β feedings or the half-lives involved in the mass 129 decay chain.

Fig.II.1.1 shows a typical mass 131 γ-ray spectrum with the Sn activity enhanced by moving the collector tape.

Carefully made efficiency and energy calibration runs complement these preliminary but encouraging results.

Right now γ-γ coincidence measurements are being performed as well as the preparation for the internal conversion electron measurements.

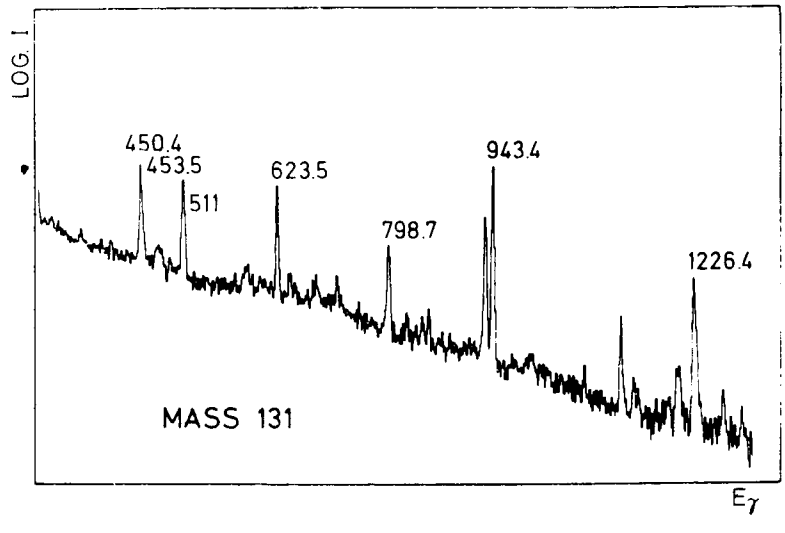

Fig. II.1.1 : Tipical γ-ray spectrum for the mass chain A=131 .

II.2 J^{π} Assignments to the first few levels in ^{138}Cs.

D.Otero, A.N.Proto, E.Duering*, M.L.Pérez.

We improved our previous measurements of conversion electrons in ^{138}Cs[1] using a non-axisymmetric focussing lens and off line measurement[2] (see Fig. II.2.1). In this way the background was substantially reduced and we were able to obtain K/L relations for the 153, 242 and 258 keV transitions (Table II.2.1). The J^{π} values proposed previously for the 258 and 412 keV levels in ^{138}Cs, based on strong arguments, were: $(2^-, 1^-)$, and $(1^-, 0^-)$, respectively[3]. The predominantly M1 character of the 153 and 258 keV transitions allows us now to assign 2^- to the 258 keV level and 1^- to the 412 keV level.

---

* Present address: The Weizmann Institute of Science, Rehovot, Israel.

1) E.Achterberg, F.C.Iglesias, A.E.Jech, J.A.Moragues, D.Otero, M.L.Pérez, A.N.Proto, J.J.Rossi, W.Scheuer and J.F.Suárez, Phys. Rev. C7 (1973) 365.

2) E.Duering, D.Otero, A.N.Proto, Nucl. Instr. Meths., accepted for publication.

3) E.Browne, J.M.Dairiki, R.E.Doebler, Table of Isotopes, VIIth edition, Berkeley 1978, C.M.Lederer and V.S.Shirley, Editors, John Wiley & Sons, N.Y.

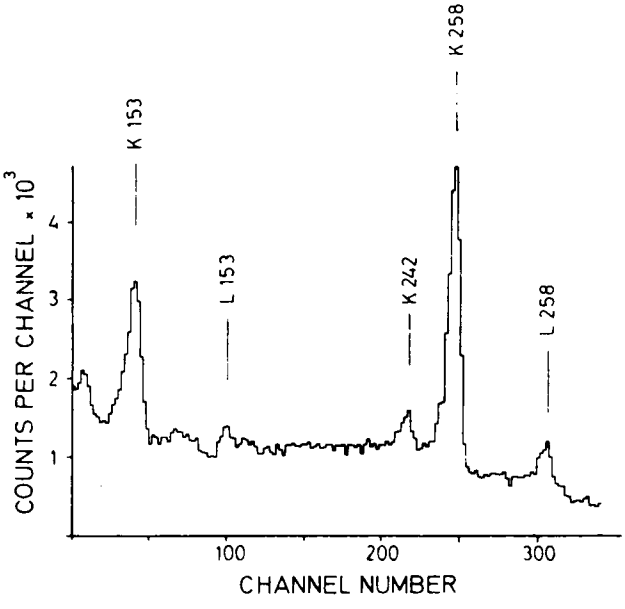

Fig. II.2.1:

Off-line conversion electron spectrum.

Table II.2.1

Transition Energy (keV)	K/L relation	Multipolarity assignment (Present work)	(Ref.1)
153	6.3 ± 0.5	M1(20<E2<46%)	M1(<31%E2)
242	> 5.5	M1(E2<83%)	M1-E2
258	7.0 ± 0.4	M1(12<E2<46%)	M1-E2

II.3 The decay of $^{139}Xe^{*}$

E.Achterberg.

The evaluation of the results of the experimental data obtained in the study of this decay has been completed. These included the analysis of singles and 4096 x 4096 bidimensional coincidence gamma spectra. Special care has been taken with the spectrum analysis and the energy calibrations in order to achieve a significant improvement in the experimental gamma energies over previous data. A list of 271 gamma rays with their corresponding energies and relative intensities has been established. A level scheme with 33 excited levels has been proposed, placing 183 transitions, which account for more than 94% of the total observed gamma intensity. These results should be compared with those provided in Ref.1, based on a private communication by M.A.Lee and W.L.Talbert Jr. . It is to be noted that our level scheme places essentially the same number of gamma rays as in Ref.1, using 17 level less than the 50 shown there, without violating the available coincidence information. Since our energy errors are smaller than those listed in Ref.1 by a factor of 3.5 on the average, we assume that many levels proposed there on the basis of energy sums are probably spurious, specially as in our case we have required that levels without direct coincidence support should be connected by at least 6 gamma rays to other levels, instead of as few as 3 as in the case of Ref.1 . This condition was imposed to reduce the probability of "accidental" levels being proposed on the basis of chance agreements of energy sums within the experimental error limits for the connecting gamma rays to what we believe to be a safe level.

Evidence from systematics for low-lying levels in odd-Z, N=84, and

even-N, Z=55, nuclei, together with our log ft and log f_1t values and information provided by our conversion coefficient determinations, allow us to propose the following spin-parity sequence above the $7/2^+$ ground state of ^{139}Cs: 219 keV, $5/2^+$; 290 keV, $3/2^+$; 394 keV, $(5/2)^+$; 515 keV, $(5/2, 7/2)^+$; 647 keV, $(5/2 - 9/2^-)$.

The energy level scheme proposed on the basis of the present work is shown in Fig.II.3.1.

---

* To be published

1) L.R.Greenwood, Nuclear Data Sheets, 12 (1974) 139. Compilation based on data from a private communication by M.A.Lee and W.J.Talbert Jr., to the Nuclear Data Group.

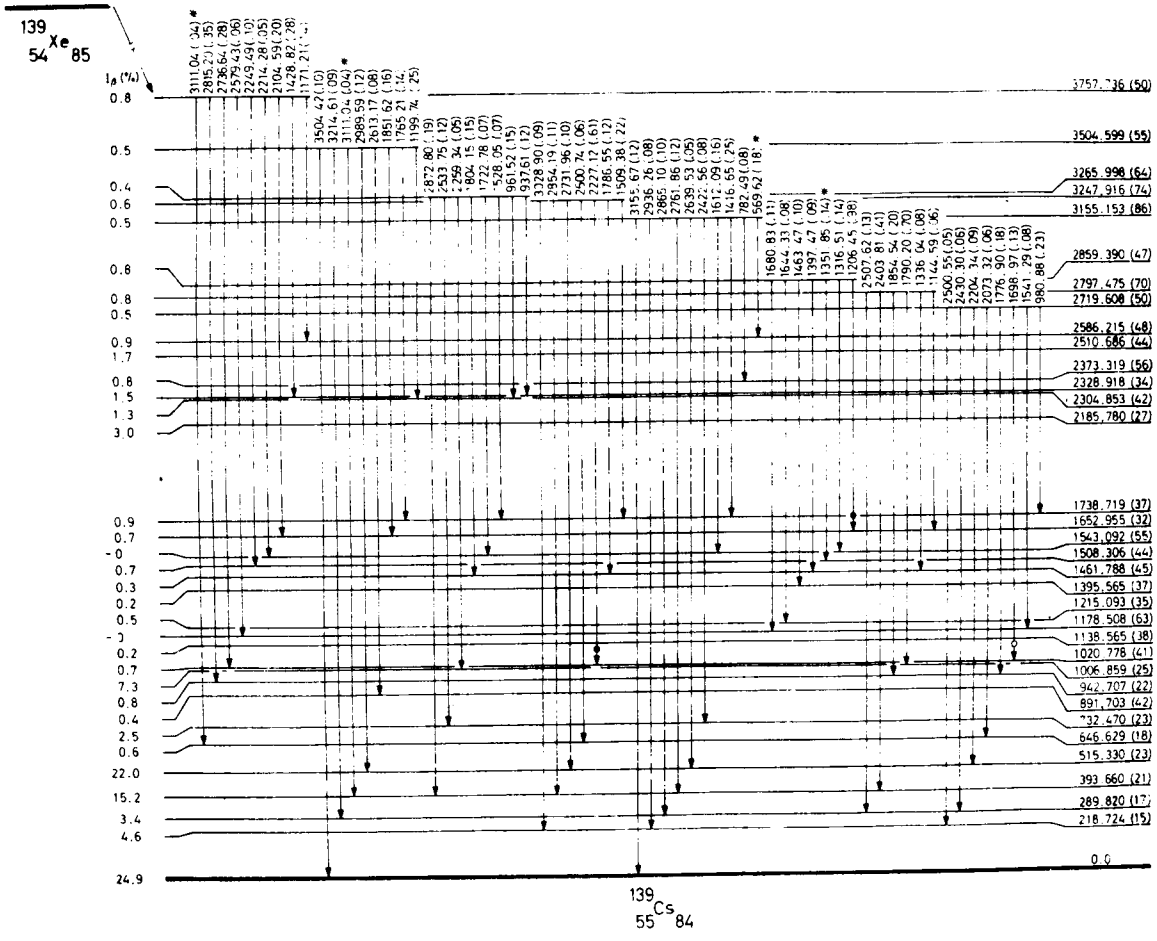

Fig.II.3.1(part a): Proposed level scheme for ^{139}Cs .

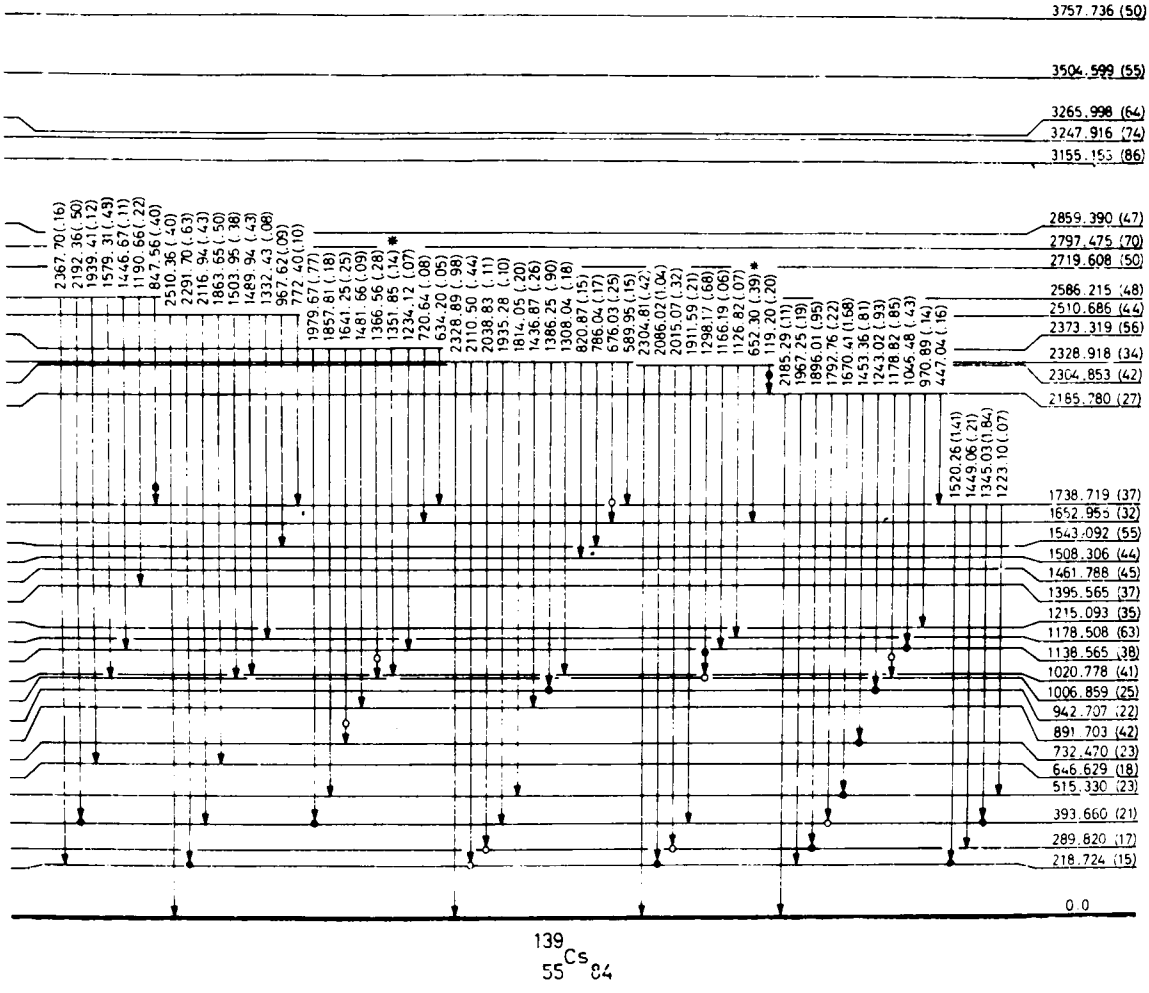

Fig. II.3.1 (part b)

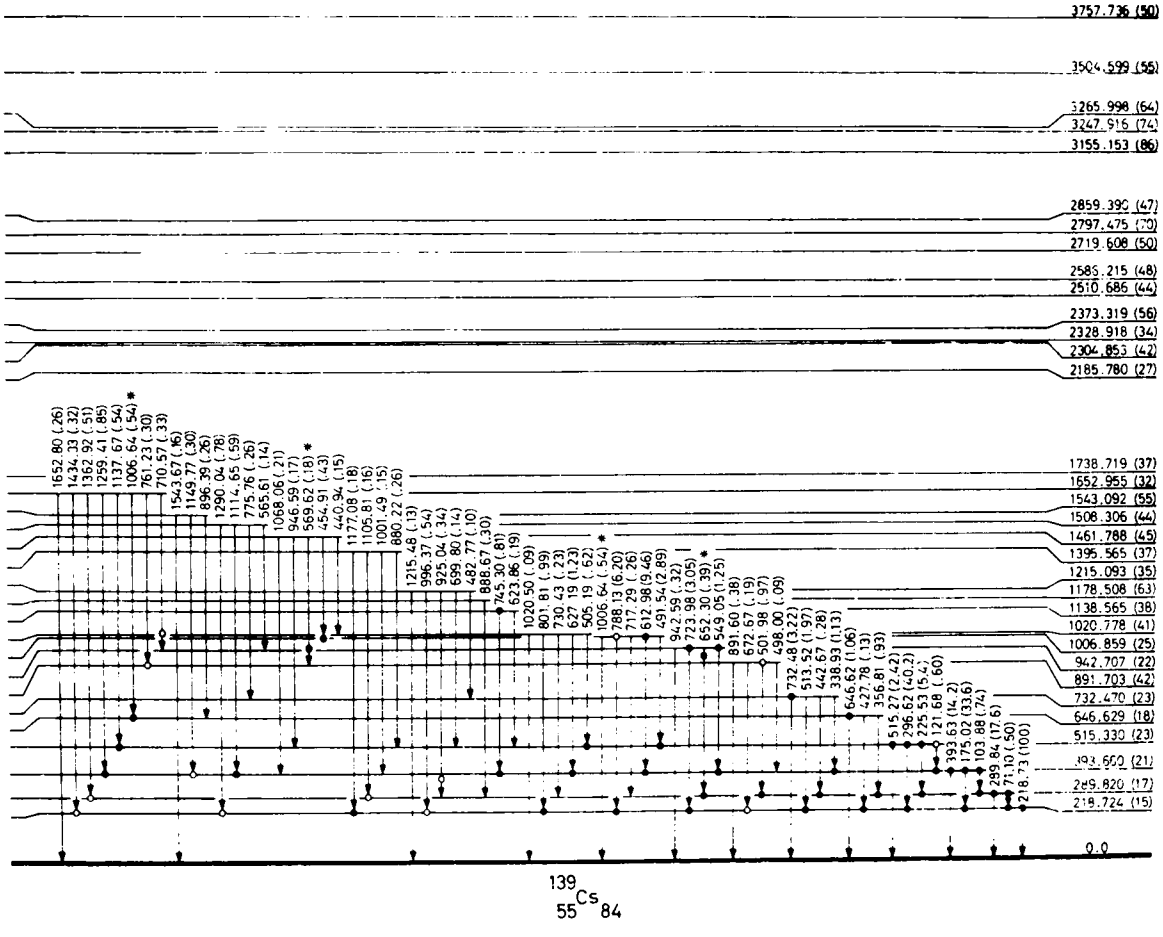

Fig. II.3.1 (part c)

II.4 ^{140}Cs Level Scheme.

D.Otero, A.N.Proto, E.Duering*, M.L.Pérez.

Using biparametric Ge(Li)-Ge(Li) coincidence techniques, several changes in the previously proposed ^{140}Cs level scheme were made. We observed coincidences in the energy ranges of: 10-150 keV vs. 150-1500 keV, and 50-1500 keV vs. 200-1500 keV.

A quantitative coincidence analysis allowed us to find two new transitions: 38.34 and 9.5 keV, although they could not be observed directly. We established their gamma and total transition intensities.

Through equilibrium radioactive measurement of γ-rays belonging to the ^{140}Xe$\rightarrow^{140}$Cs$\rightarrow^{140}$Ba mass chain, we normalized the γ-activity per hundred decays, determining the β feeding to the ground state. The level scheme was completed using sum relations with a χ^2 test[2]. We added three excited levels to the previously proposed level scheme (Fig. II.4.1). We calculated the log ft values and found a new 1^+ level at 2324 keV (Fig.II.4.2); we also established $J^\pi = 1^-$ for the 64 keV level, instead of the $J^\pi = 3^-$ postulated in a previous work[3].

---

* Present address: The Weizmann Institute of Science, Rehovot, Israel.

1) W.C.Schick, Jr., W.L.Talbert, Jr., J.R.Mc Connell; Phys. Rev. C4 (1971) 507.

2) E.Achterberg, PhD Thesis, unpublished, (1979).

3) J.P.Adams, F.K.Wohn, W.L.Talbert, Jr., W.C.Schick, Jr., J.R.Mc Connell; Phys. Rev. C10 (1974) 1467.

Fig. II.4.1 : Low-energy region of the proposed level scheme for ^{140}Cs. Transition intensities per 100 disintegrations and adopted multipolarities are given. Doubly placed γ-rays are marked with asterisks, solid dots and open circles point out definite and doubtful coincidence results.

Fig. II.4.2 : High energy region of the proposed level scheme.

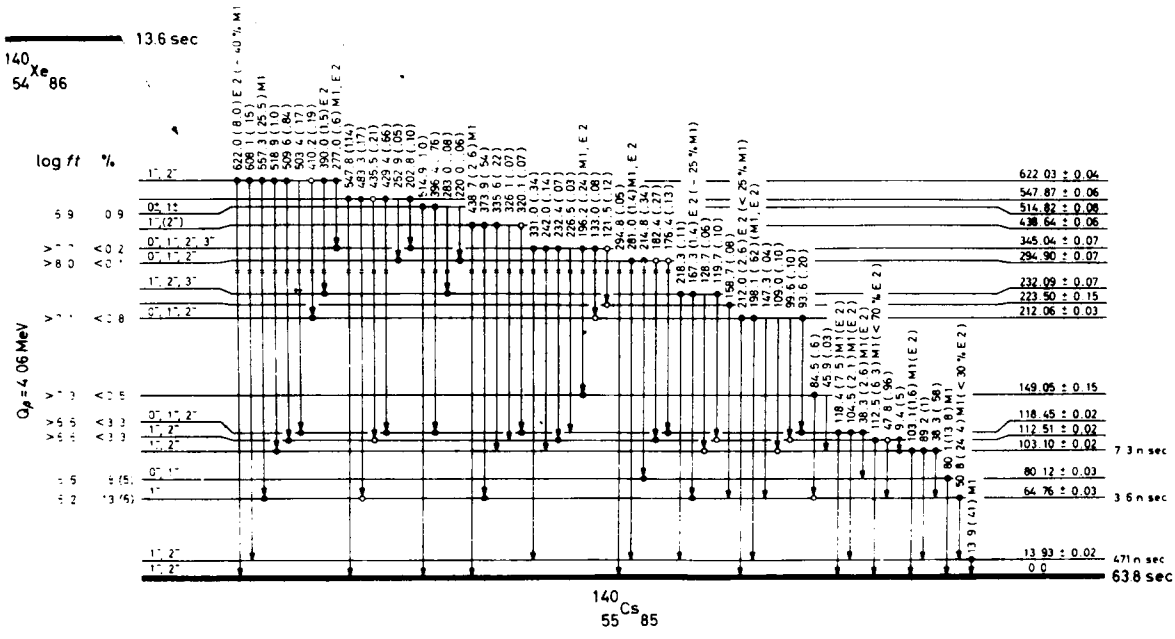

Fig. II.4.1

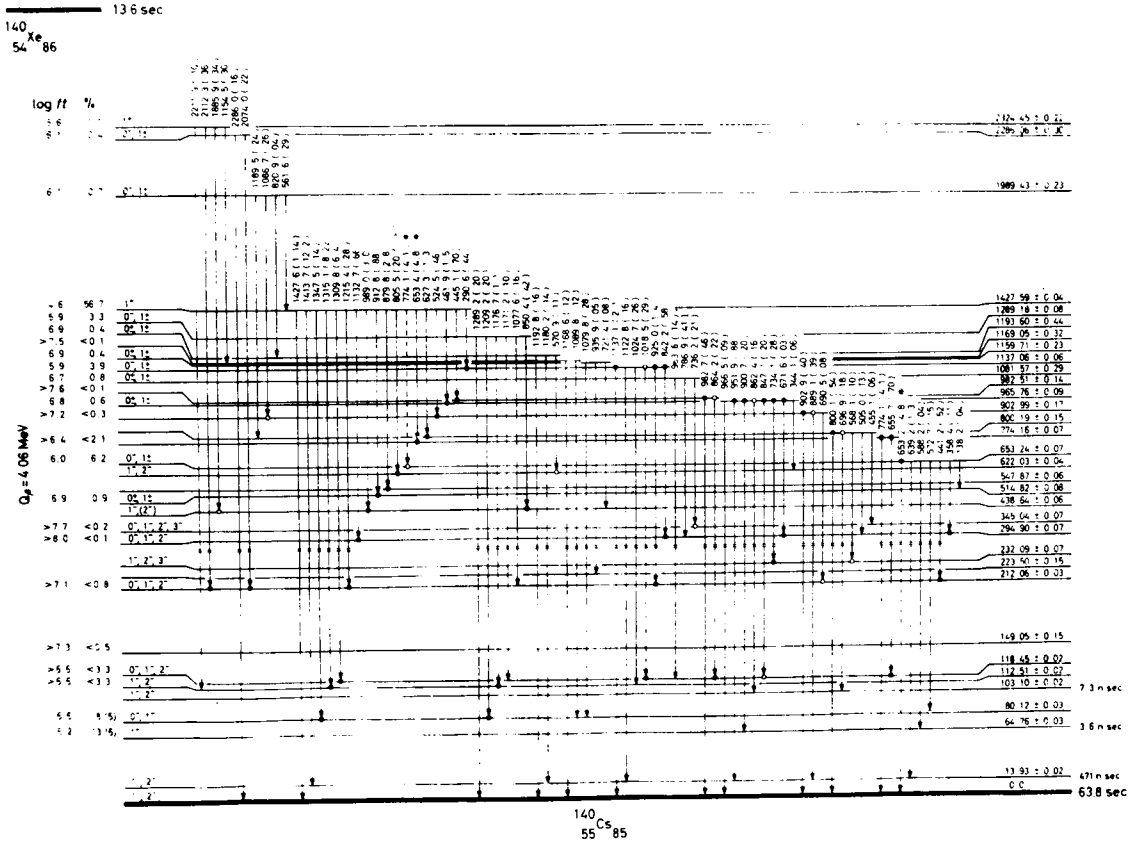

Fig. II.4.2

II.5 Conversion Coefficients in ^{140}Cs: NPG and XPG Methods.

D.Otero, A.N.Proto, E.Duering* and M.L.Pérez

We obtained conversion coefficients for γ-rays from 14 to 212 keV (α_K and α_L values) and K/L relations. The results are shown in Table II.5.1. Previously, J.P.Adams et al.[1] reported conversion coefficients for transitions above 80 keV and in this energy region our results are in general agreement, except for the assigned multipolarities of the 112 and 212 keV transitions.

Below 80 keV we applied the XPG method, selecting the γ-ray of interest and its X-ray by biparametric coincidences. Thus it was possible to obtain the α_K coefficient of the 38, 51 and 80 keV transitions (Fig.II.5.1). Using the conversion coefficient quoted above, we were able to determine an upper limit, for the α_L coefficient of the 14 keV transition through the technique described in Ref.2 . The intensity balance and log ft value calculations in the ^{140}Xe to ^{140}Cs decay are strongly dependent on the low energy conversion coefficients.

---

* Present address: The Weizmann Institute of Science, Rehovot, Israel.

1) J.P.Adams, E.K.Wohn, W.L.Talbert, Jr., W.C.Schick, Jr., J.R.Mc Connell; Phys. Rev. C10 (1974) 1467.

2) E.Achterberg, F.C.Iglesias, A.E.Jech, J.A.Moragues, D.Otero, M.L.Pérez, A.N.Proto, J.J.Rossi, W.Scheuer and J.F.Suárez; Phys. Rev. C7 (1973) 365.

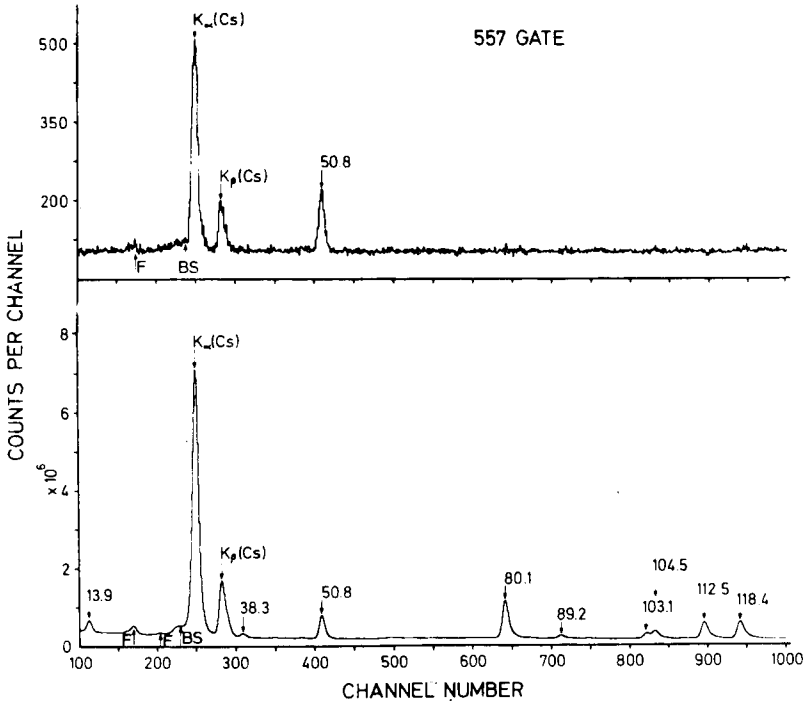

Fig. II.5.1

Table II.5.1

Transition energy	Measured conversion coefficient	Method	Assigned Multipolarity
13.9	$\alpha_L < 36$	XPG	E1 - M1
38.3	$\alpha_K = 12.0 \pm 2.5$	XPGC	M1 - E2
50.8	$\alpha_K = 6.0 \pm 1.1$	XPGC	M1(<30%E2)
80.1	$\alpha_K = 1.8 \pm 0.5$ $\alpha_{L+M} = 0.3 \pm 0.25$	XPGC NPG	M1-E2
103.1 104.5	$\alpha_K = 0.66 \pm 0.10$ $K/L = 3.2 \pm 0.6$	NPG	M1(25%<E2<60%)
112.5	$\alpha_K = 0.7 \pm 0.1$ $K/L = 12 \pm 7$	NPG	M1(<70%E2)
118.4	$\alpha_K = 0.67 \pm 0.10$ $K/L = 13 \pm 7$	NPG	M1(E2)
167.3	$\alpha_K = 0.17 \pm 0.03$ $K/L = 3.2 \pm 0.6$	NPG	E2(~25%M1)
212.0	$\alpha_K = 0.14 \pm 0.03$ $K/L = 3.8 \pm 0.8$	NPG	E2(<25%M1)

III. APPLIED NUCLEAR PHYSICS

III.1 Positron Annihilation in Condensed Matter: Doppler Shift

D.Otero, A.N.Proto, R.Romero*, A.Somoza*, M.Pavioni*, S.Zambrino*.

The observation of the Doppler broadening of annihilation gamma rays from thermalized positrons is the object of the present work. The γ-rays are measured with a Ge(Li) detector. The broad 511 keV peak contains two superimposed contributions: a) the natural response shape of the detector to monochromatic γ-rays and b) the intrinsic Doppler broadening. The latter contains the relevant information and should be obtained from the measured total distribution, which may be written as:

$$F(x) = \int_{-\infty}^{\infty} f(x-x')g(x')dx' \quad , \qquad (i)$$

where g(x) is the detector response and f(x) is the unknown Doppler broadening function. We intend to obtain information about the intrinsic Doppler broadening through the momentum analysis of the functions F(x) and g(x). After the evaluation of the errors introduced by: a) the use of discrete variables instead of an integral, b) considering only a portion of the whole distribution which extends to $\pm\infty$, and c) the statistical errors, we propose the corrections to be made in order to get consistent results for the momenta of the intrinsic distribution.

---

*Universidad Nacional del Centro de la Provincia de Buenos Aires.

III.2 Fluorine Concentration in Zircalloy.

A.N.Proto and D.Otero.

The presence of Fluorine in Zircalloy was detected through the $^{19}F(n,\gamma)^{20}F$ reaction. The neutron flux from the LINAC (CAB)* was of about 10^{10} neutrons/s.cm^2 . The identification of $^{20}F(\tau=11.1$ s) was made through

the 1630 keV γ-ray using a NaI(Tl) detector after an irradiation period of 1 min. The material is extracted from the irradiation point using a rabbit and placed by hand in front of the detector. This new method to determine low quantities of Fluorine in Zircalloy has a sensitivity of about 15 ppm. The following γ-rays were identified from the Zircalloy matrix:

555 keV	$^{92}Zr(\gamma,p)^{91m}Y$	τ = 49 min.
588 keV	$^{90}Zr(\gamma,n)^{89m}Zr$	τ = 4.18 min.
1507 keV	$^{90}Zr(\gamma,n)^{89m}Zr$	τ = 4.18 min.

---

*
Centro Atómico Bariloche.

IV. NUCLEAR STRUCTURE

IV.1 Microscopic aspects of self consistent fields and collective states

IV.1.1 The strength of a multipole residual interaction.

G.G.Dussel, R.P.J.Perazzo and S.L.Reich.

The strength of a residual 2^λ multipole interaction can be determined by a self consistency condition that must fulfill the distortions of the density and of the central potential[1]. This yields, for different assumptions upon the kind of distortions of V(r) and $\rho(r)$:

$$K_\lambda^{(I)} = R_0^2 \int r^2 \frac{\partial V}{\partial r}\Big]_{R_0} \frac{\partial \rho}{\partial r}\Big]_{R_0} dr \quad ; \quad K_\lambda^{(II)} = \int r^4 \frac{\partial V}{\partial r}\Big]_{\alpha=0} \frac{\partial \rho}{\partial r}\Big]_{\alpha=0} dr$$

α being the deformation parameter.

For a harmonic oscillator central potential and a residual interaction $r_1^\lambda r_2^\lambda Y_\lambda(\hat{r}_1) Y_\lambda(\hat{r}_2)$ one obtains[1]

$$K_\lambda^{(BM)} = - \frac{4\pi}{2\lambda+1} \frac{M\omega_0^2}{A\langle r^{2\lambda-2}\rangle}$$

Finally assuming an RPA description of vibrational modes and imposing the condition that the spurious $\lambda=1$ mode lies at zero frequency one obtains:

$$K_\lambda^{(RPA)} = \sum_{mk} \frac{2}{\varepsilon_{km}} \left| \langle m \left\| r^\lambda \frac{\partial V}{\partial r}\right]_{\alpha=0} \right\| k \rangle \right|^2$$

The values of $K_\lambda^{(I),(II),(RPA)}$ are compared in fig.IV.1.1.1 using a Woods Saxon potential well with V_0= 50 MeV; a =.55 fm and r_0= 1.07 fm.

The distribution of the Eλ strength is shown in fig.IV.1.1.2 comparing $K_\lambda^{(BM)}$ (empty bars) with $K_\lambda^{(RPA)}$ (full bars) with the corresponding residual interactions proportional to $r_1^\lambda r_2^\lambda$ and to $r\partial V/\partial r$. For the calculation a schematic model is used simulating the situation prevalent in the ^{208}Pb region.

---

[1]) A.Bohr and B.Mottelson, Nuclear Structure Vol.II (Benjamin, 1975).

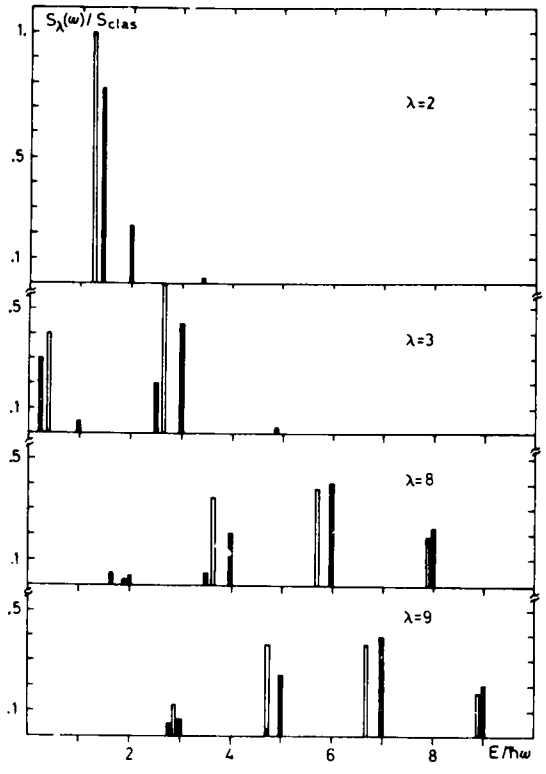

Fig. IV.1.1.1

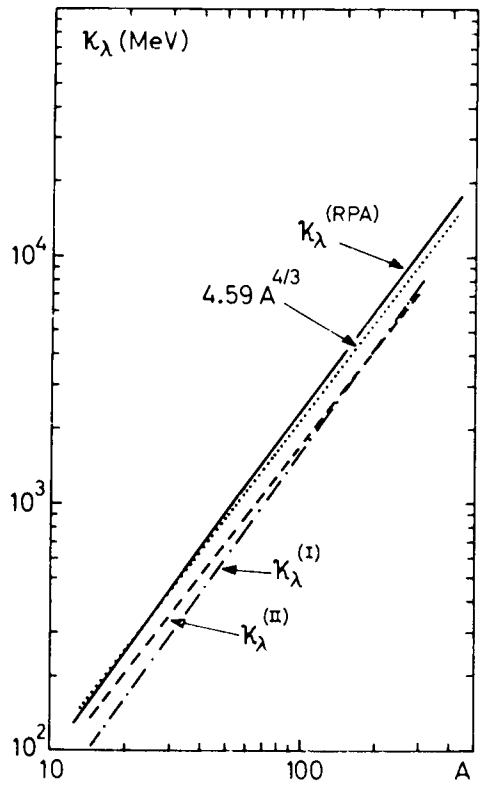

Fig. IV.1.1.2

IV.1.2 One particle transfer fragmentation in the ^{40}Ca region.

G.G.Dussel, R.P.J.Perazzo and S.L.Reich.

The odd neighbours of a doubly magic core have spectra bearing properties that in general depart from a pure single particle pattern. This can be attributed to the admixture of fermionic and collective degrees of freedom.

The spectroscopic factors for one nucleon transfer are the residues of a one body Green's function G. If for G we use the (bare) Hartree-Fock (HF) propagator G_0 , all the strength is concentrated in only one state. The fragmentation into many levels of the same angular momentum and parity occurs when the HF particles couple to other (composite) states. This process gives rise to a renormalized propagator G, defined by the equation:

$$G(jj';t) = G_0(j;t)\,\delta_{jj'} - \sum_{j''} \iint d\tau d\tau' G_0(j;\tau)\,F(j'',j;\tau'-\tau)\,G_0(j;t-\tau) \qquad (1)$$

In this calculation F represents the coupling of HF particles to a one fermion plus one boson (1F1B) state through a diagram in which a fermion line emits and subsequently absorbs a boson line[1].

The input data to eq. (1) are the (bare) single particle energies ε_j, the particle-phonon coupling vertex functions, and the choice of the boson space.

The ε_j's are obtained from the experimental excitation energies E_j^n (E_j^N) of the A=41 (39) nuclei, using the Baranger prescription[2].

$$\varepsilon_j = \sum_n |\langle n|c_j^+|0\rangle|^2 E_j^n + \sum_N |\langle N|c_j|0\rangle|^2 E_j^N \qquad (2)$$

The boson space is defined with the collective states of ^{40}Ca.

The coupling of the i-th nucleon to a λ-multipole collective mode is

$$H_{coup} = -K_\lambda \sum_{\mu,i} r_i^\lambda Y_{\lambda\mu}(\Omega_i)\alpha_{\lambda\mu}^{(n)*} \qquad (4)$$

The present calculation with no adjustable parameters can reproduce the essential characteristics of one body strength distribution (see Fig. IV.1.2.1 and IV.1.2.2 .

---

[1]) D.R.Bes, G.G.Dussel, R.P.J.Perazzo and H.M.Sofía; Nucl.Phys. A293 (1977) 325.

[2]) M.Baranger; Nucl. Phys. A149 (1970) 225.

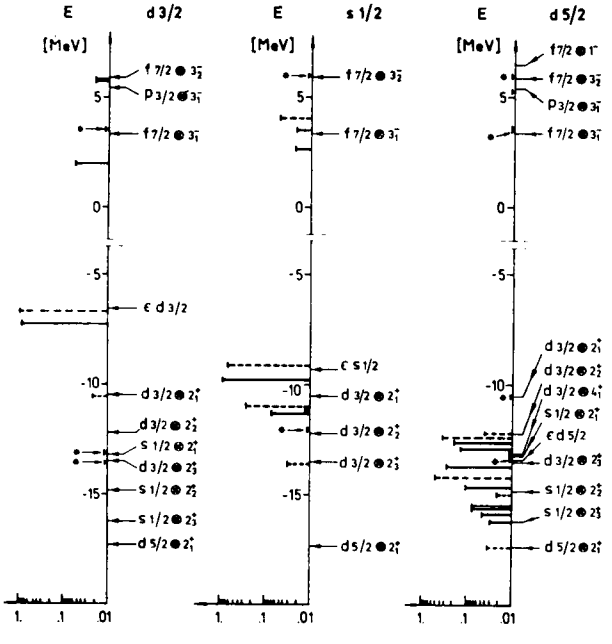

Fig. IV. 1.2.1

Theoretical (dashed bars) and experimental (full bars) spectroscopic factors for one nucleon pick up reactions on a ^{40}Ca target. The strengths (length of the bars) are plotted in a logarithmic scale. Spectroscopic factors $\lesssim$1% are not drawn. Theoretical results $\simeq$ 1% are indicated by stars. The active configurations within the energy range that is plotted are displayed at the right of each axis.

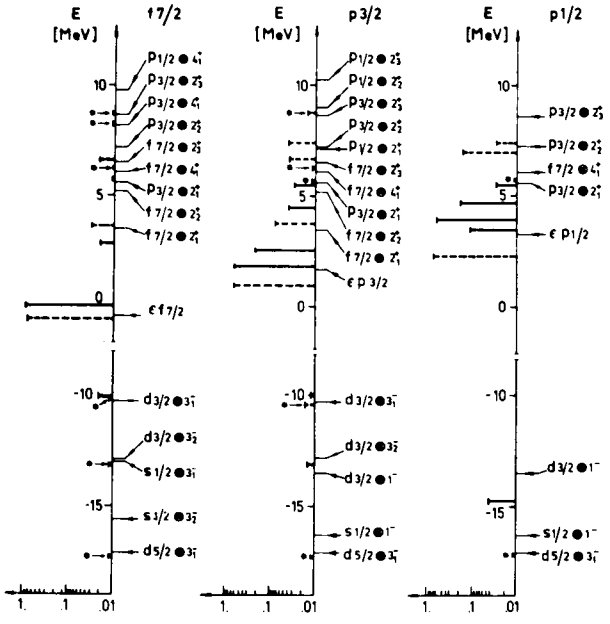

Fig. IV.1.2.2:

The same as Fig. IV.1.2.1 but for one nucleon stripping reactions on a ^{40}Ca target.

IV.1.3 Renormalization of particle and hole states in ^{208}Pb.

R.P.J.Perazzo, S.L.Reich and H.M.Sofía.

The set of diagrams in which a particle line disappears at a given vertex and subsequently reappers and such that the intermediate structure does not interact with the remaining part of the graph, may be replaced by a single diagram with a dressed (renormalized) line. The most familiar example of this procedure is the renormalization of a fermion line in the Hartree-Fock approximation. More complicated processes may also contribute[1], such as the inclusion of a particle-phonon state as intermediate state. We have studied[2] the effects of the last type of processes on the renormalization of particle and hole states in ^{208}Pb. The core polarization is defined as:

$$\delta\omega_0 = \frac{1}{\Omega_p} \sum_{j(part)} (2j+1)\,\delta\varepsilon_j - \frac{1}{\Omega_h} \sum_{j(hole)} (2j+1)\,\delta\varepsilon_j \qquad (1)$$

where $\Omega_{p(h)} = \sum_{j\ part(hole)} (2j+1)$.

This is plotted for different choices of the states that enter in the renormalization procedure in Figs.IV.1.3.1 and IV.1.3.2 . Only the proton results are shown as an example. In Fig. IV. 1.3.1, the core polarization $\delta\omega_0$(eq.1) calculated with this method (full line) is plotted as a function

of the number N of major shells involved in the intermediate fermion space. The curves labelled with F(F+B) correspond to results in which only forward (forward plus backward) diagrams are involved. The dashed lines correspond to first order perturbation theory. The collective space is restricted to $\lambda^{\pi} = 2^{+}$ and 3^{-} particle-hole bosons. The dependence of $\delta\omega_0$ with the angular momentum of the phonon (λ) is shown in Fig.IV.1.3.2 where odd and even multipolarities are separately grouped. The curves labeled with S (S+V) correspond to pure isoscalar (isoscalar plus isovector) boson modes. Dashed lines correspond to first order perturbation theory whereas full lines are obtained with the renormalization procedure.

---

[1]) D.R.Bes, G.G.Dussel, R.P.J.Perazzo and H.M.Sofía; Nucl. Phys. A293 (1977) 350 .

[2]) R.P.J.Perazzo, S.L.Reich and H.M.Sofía; (to be published).

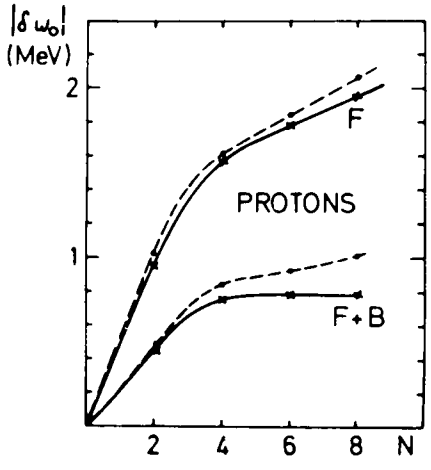

Fig. IV.1.3.1

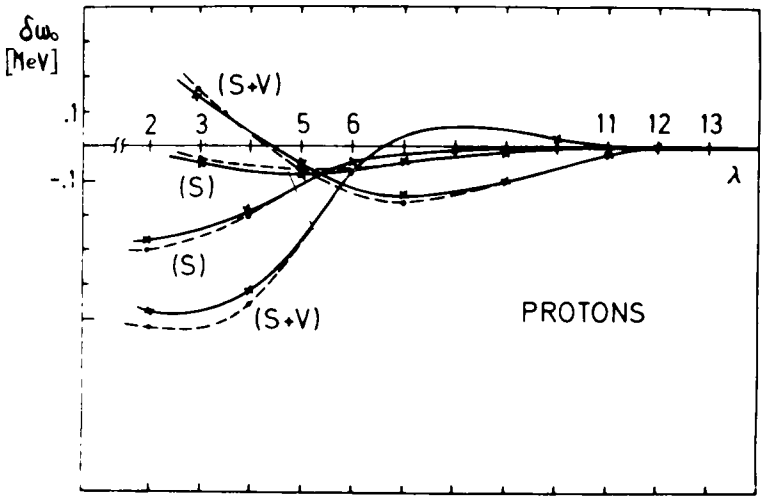

Fig. IV.1.3.2

IV.1.4 The RPA of renormalized fermions.

G.G.Dussel, R.P.J.Perazzo and M.E.Spina.

It is possible to construct RPA modes with dressed fermion lines. The procedure is exemplified within a schematic model and also defining the one body propagator in a semiempirical fashion using energies and residues from experiments.

The main difficulty is to find the proper generalization of the RPA normalization conditions. These were found to be:

$$\sum_p \langle 0|a_2^+a_1|p\rangle\langle p|a_3^+a_4|0\rangle - \langle 0|a_3^+a_4|p\rangle\langle p|a_2^+a_1|0\rangle = \sum_N X_n(13)X_N(42) - X_N(13)X_n(42)$$

$$= \sum_{12,34} \langle p|a_2^+a_1|0\rangle \left(\frac{\partial}{\partial K}\,(S_0^{-1}(12,34;k) - V_{12,34})\right)_{k=\omega_p} \langle 0|a_3^+a_4|p\rangle = 1$$

where $X_n(12) = \langle 0|a_1|n\rangle\langle n|a_2^+|0\rangle$; $X_N(12) = \langle 0|a_2^+|N\rangle\langle N|a_1|0\rangle$ are known amplitudes defined in terms of the residues $\langle 0|a|n\rangle$, $\langle 0|a^+|N\rangle$ of the one body Green's function. The labels $|n\rangle$ ($|N\rangle$) identify the excited states of the systems with one nucleon more (less) than the double closed shell.

The schematic model consists of a Lipkin model in which the dressed fermion line is obtained by adding up to infinite order the process in which a phonon is emitted and subsequently absorbed by a Hartree-Fock line. A dispersion equation is obtained similar to the standard RPA problem in which the matrix elements are conveniently renormalized to act among dressed particles.

A semiempirical one body Green's function is used in the ^{40}Ca region to calculate the distribution of the 3^- strength. The results obtained within a standard and renormalized version of the RPA are covered in Fig. IV.1.4.1 .

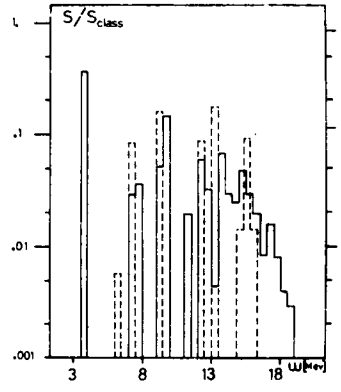

Fig.IV.1.4.1: Distribution of the BE3 strengh given as the fraction of the classical sum rule. The dashed (full) line corresponds to the ordinary (renormalized) RPA results The large concentration at the collective root (3.73 MeV) is the same for both calculations.

IV.1.5 NFT Treatment of the IBM* .

D.R.Bes and R.A.Broglia†.

In one of the versions of the IBM[1] the degrees of freedom of particles outside closed shells are described in terms of four bosons, two for protons and two for neutrons, carrying angular momentum and parity 0^+ (s-bosons) and 2^+ (d-bosons). The only interaction between the boson is

$$H_{\pi\nu} = -\kappa_{\pi\nu}\sqrt{5}(Q_2(\pi)\ Q_2(\nu)\ )_0 \quad , \qquad (1)$$

where $Q_{2\mu}$ is the quadrupole operator.

The phonons of the IBM have been interpreted as pairs of like particles coupled to J=0 and J=2 .

In this work we obtain a theoretical justification of the IBM. We consider a system of multipole proton and neutron pairing vibrations. The properties that completely determine the pairing boson fields are the particle-vibration coupling strength Λ and the energy ω.

Utilizing (1) as the residual Hamiltonian acting between the multipole pairing vibrations, the lowest order NFT contributions to the energy are graphically obtained. The lack of orthogonality of the many-phonon states, as well as the Pauli principle violations are consistently treated in the same footing within the NFT, to lowest order in the NFT expansion parameter Ω^{-1} (where Ω is the effective degeneracy of the shell).

---

* IBM in Nucl.Phys.; F.Iachello ed. Plenum Press, New York (1979) 143.

† The Niels Bohr Institute, University of Copenhagen, DK-2100, Copenhagen Ø Denmark.

[1]) A.Arima, T.Otsuka, F.Iachello and I.Talmi; Phys.Lett. 66B (1977) 205.

IV.1.6 On the convergence of the Nuclear Field Theory perturbation expansion for strongly anharmonic systems† .

P.F.Bortignon*, R.A.Broglia* and D.R.Bes .

In this work we study the convergence properties of the partial summations implied by the NFT by comparing the results of the corresponding perturbative expansion with exact results.

We consider systems with four particles or four holes away from a closed shell moving in a many-level space[1] and interacting via a pairing force of constant matrix elements. In zeroth order, the corresponding states are described in terms of two pairing vibrational bosons . The NFT solutions are worked out in what follows up to third order in the perturbation parameter $1/\Omega$, where Ω is the degeneracy of the shell.

We discuss as examples of many-shell systems the ground state of ^{204}Pb and ^{212}Pb. As mentioned, these states can be described in zeroth order as two phonon pairing vibrational states, i.e.

$$\begin{aligned} |I\rangle &\equiv |gs(^{204}Pb)\rangle = |gs(^{206}Pb) \otimes gs(^{206}Pb)\rangle, \\ |II\rangle &\equiv |gs(^{212}Pb)\rangle = |gs(^{210}Pb) \otimes gs(^{210}Pb)\rangle. \end{aligned} \tag{1}$$

Note that the "rest mass" (correlation energy) of the pair removal mode ($gs(^{206}Pb)$) is 640 keV, to be compared with the experimental value of the phonon-phonon interaction energy

$$B(^{204}Pb)-B(^{208}Pb) - 2\left[B(^{206}Pb)-B(^{208}Pb)\right] = 706 \text{ keV} \quad , \tag{2}$$

where B(A) is the binding energy of the nucleus A. In the case of ^{212}Pb the corresponding numbers are 1237 keV and 169 keV, respectively. We can thus expect convergence problems in the case of ^{204}Pb.

The exact results for the interaction energy of the two systems and for the matrix element of the two-particle transfer operator were obtained diagonalizing the pairing interaction in a basis of four holes (particles), moving around the N=126 closed shell. The levels included in the calculation were taken from experiment. The pairing strengths needed to reproduce the correlation energy of $gs(^{206}Pb)$(-640 keV) and of $gs(^{210}Pb)$ (-1237 keV) are G=0.13 MeV and G=0.10 MeV, respectively.

The resulting values of the interaction energy for the states $|I\rangle$ and $|II\rangle$ are

$$\Delta W_I = 540 \text{ keV} \quad , \quad \Delta W_{II} = 267 \text{ keV}. \tag{3}$$

The NFT results, calculated using RS perturbation theory, are displayed in Table IV.1.6.1 . In the case of ^{204}Pb, already the $1/\Omega$ contribution accounts for 90% of the exact value. The $1/\Omega$ and $1/\Omega$ contributions amount to 8% and 3% of the $1/\Omega$ contribution. Although these values indicate a somewhat slow convergence, they arise from cancellations between

large direct contributions and wave function renormalization type diagrams, as already discussed for the two-level model[1]. For the case of ^{212}Pb the convergence is, as expected, extremely fast.

We conclude that the NFT prescription for summing up the contributions to the different physical quantities, within the framework of the RS perturbation theory, is strongly convergent. Thus, the lowest-order contributions in the parameter $1/\Omega$ give a rather accurate approximation to the exact solution.

Table IV.1.6.1

ORDER	ΔW(keV)	
	I	II
$1/\Omega$	474	262
$1/\Omega^2$	42	4.3
$1/\Omega^3$	14	0.4
	530	266.7
EXACT	540	267

† Ref. 1) .

* The Niels Bohr Institute, University of Copenhagen, DK-2100, Copenhagen Ø Denmark.

1) Phys. Lett. 76B (1978) 153.

IV.1.7 Perturbative treatment of nuclear rotations. Two dimensional case .

D.R.Bes, G.G.Dussel and R.P.J.Perazzo .

In this work we apply a full quantum mechanical perturbative treatment to the coupling between particle and rotational degrees of freedom. The procedure is that of ref.[1] in which the original Hamiltonian is modified by adding a finite restoring force in the angular direction and thus eliminating the infrarred divergences. The symmetry with respect to rotations is restored by overimposing the conservation of the angular momentum.

We consider a problem of particles moving in a single particle potential and coupled by a residual interaction such that the resulting states may be interpreted in terms of two dimensional rotational bands. The framework is completely similar to the one solved by Elliot using SU3 algebra. However, the group of transformations is, in this case, abelian.

The problem may be also cast into the framework of deformed systems. In this case, it is solved through the following steps

i) A transformation to principal axis is performed, thus defining a single-particle (deformed) basis and a residual Hamiltonian acting among the "Nilsson" particles. Neither the independent-particle terms, nor the residual Hamiltonian, separately have the cylindrical symmetry of the total H. This step is common to most treatments of deformed systems.

$$H = H_{sp} + H_Q$$

ii) Next, we introduce the restitutive terms and the symmetry restoring terms in H. This corresponds to a choice of a particular gauge ("freezing" of the system in space) and to a projection to states with good angular momentum L_0 . The final results are to be independent of the particular choice of the gauge (value of α).

$$H' = \lim_{\beta \to 0} \left[H + (L_{op} - L_0)^2/2\beta + \phi_{op}^2/\alpha \right]$$

Here L_{op} and ϕ_{op} are angular momentum and angle operators, respectively.

iii) A perturbative solution of H' is achieved by introducing the collective (RPA) modes and by using the NFT rules as in the case of normal (spherical) systems. One uses as an expansion parameter the inverse of the static quadrupole moment.

The calculation of g.s. energies, moments of inertia, transition probabilities between members of a rotational band and quadrupole matrix elements allow to check that the perturbative and exact results coincide up to the order in which the perturbative expansion has been carried.

Finally, a comparison has been made of the present treatment with a number of other methods, usually impliying semiclassical approximations, that exist in the literature.

---

[1]) V.Alessandrini, D.R.Bes and B.Machet; Nucl. Phys. B142 (1978) 489.

IV.1.8 Collective Coordinates in Fermi Systems.*

V.Alessandrini†, D.R.Bes and B.Machet†.

Collective coordinate methods have been widely used in quantum field theory during the last few years in connection with the semiclassical quantization of extended objects. These classical solutions break in general some symmetry of the theory (like translational invariance in the case of kinks) and consequently the spectrum of small quantum fluctuations around them includes zero frequency modes. These zero modes are an inavoidable consequence of the fact that the symmetry has been spontaneously broken, i.e., one is expanding around a vacuum which is not an eigenstate of the generator of the symmetry transformations but rather a coherent superposition of such eigenstates. Due to the presence of these zero modes, naive perturbation theory fails.

The by now standard way to tackle this problem is to use the collective coordinate method. The constants of the motion associated with the symmetry broken by the ground state are treated as generalized (collective) coordinates and quantized in a straighforward way. One is then left with the problem of quantizing the reduced system, which is the original one plus some constraints arising from the fact that the constants of the motion have been frozen. Perturbation theory, developed for the reduced system, is free of infrared divergencies. The quantization procedure for the reduced system is identical to the one used in the quantization of gauge theories. The major difficulty in the case of fermions is that the zero frequency mode is not just a linear combination of the original canonical variables -as it is the case in boson systems- but it is rather a fermion bound state. The way these zero modes are disposed on in the collective coordinate method is rather more subtle, and this is the problem we have addressed our attention to.

We apply to fermion systems the parth integral formulation of the collective coordinate method developed by Gervais and Sakita[1].

After the collective coordinate method is set up, one is left with path integrals on Fermi variables with delta functionals of composite fields representing bosonic constraints. This delta functionals can obviosly not be integrated over, as it is done for example in the case of kinks. However, one can exploit the fact that -due to the presence of

constraints- one is actually quantizing a gauge theory, and derive Ward identities. One finds that the propagators of the composite operators associated to the collective coordinates, are either zero or contact terms which are pure gauge artifacts. The decoupling of the unwanted zero mode from gauge invariant Green functions is implied by these results[2].

Finally, we introduce a very simple quantum mechanical model consisting of fermions in a single shell with degeneracy 2Ω interacting via a pairing force. This model is exactly soluble and we use it as theoretical laboratory to test how perturbation theory works. The perturbation expansion is in Ω^{-1} and to leading order the system is a superfluid one. We perform some explicit calculations to see how our way of handling the constraint and the gauge condition eliminates the zero-frequency mode. We check to leading order the Ward Identities and show explicitly how the spurious state is automatically projected away when the constraint is enforced. Moreover, we also compute some non-trivial effects in next to leading order and obtain complete agreement with the known exact results [2,3].

---

* Work published in Refs. 2 and 3.

† University of Paris, Orsay, France.

[1]) J.L.Gervais and B.Sakita; Phys.Rev. D, Oct. 2 N° 10 (1975) 2943.

[2]) V.Alessandrini, D.R.Bes and B.Machet; Nucl.Phys. B142 (1978) 489.

[3]) V.Alessandrini, D.R.Bes and B.Machet; Phys.Lett. 80B (1978) 9.

IV.1.9 Quasi Spin pairing and the structure of the Lipkin model†

M.C.Cambiaggio* and A.Plastino*.

The Lipkin model[1] has proved to be extremely useful for studying theoretical approaches to the nuclear many body problem. By introducing the concepts of quasi-spin pairing and quasi-spin seniority , we extend the Lipkin model to a variable number of particles and obtain a simple classification of the excited multiplets.

We deal with N particles, distributed in two (2Ω)-fold degenerate

single particle (s.p) levels separated by the s.p. energy ϵ. The states are characterized by $|p,\mu=\pm 1>$ for $p=1,\ldots,2\Omega$, where $\mu=+1$ (-1) corresponds to the upper (lower) states. In addition to the usual quasi-spin operators I_Z , I_+ and I_- [1] , we introduce the operators

$$\hat{Q}_+ = \hat{Q}_-^\dagger = \sum_p c^+_{p,+}\, c^+_{p,-}$$

$$\hat{Q}_0 = \frac{1}{2} \sum_{p,\mu} c^+_{p,\mu}\, c_{p,\mu-\Omega}$$

which obey angular momentum commutation rules. Moreover, any Q-operator commutes with all I-operators (SU2 x SU2). $\hat{Q}_+$ creates two particles which yield zero contribution to the I_Z value and which could then be said to "couple" to $I_Z=0$. We introduce the quasi-spin seniority v which is the number of particles not "paired" to $I_Z=0$ in a Q-multiplet. v fixes the value of Q and also the value of I.

In the Lipkin model ($N=2\Omega$, $Q_0=0$) the unperturbed ground state multiplet has $v=2\Omega$. The remaining multiplets are those for which v decreases to zero in steps of two. Besides, by allowing Q_0 to vary we can generalize the model to a variable number of particles.

We study then a quasi-spin "pairing" Hamiltonian

$$\hat{H} = \hat{I}_Z - \frac{g}{2} \hat{Q}_+ \hat{Q}_-$$

and find that, as the strength of the interaction grows, the ground state of the system suffers a "phase transition" from the state of maximum quasi-spin seniority to the "superconducting" one in which v=0 and all particles are "paired" to $I_Z=0$.

Following the standard BCS treatment we obtain an approximate solution. The number-projected BCS energy coincides with the exact "superconducting" one. Comparing the properties of quasi-spin pairing with those of ordinary pairing, it can be seen that they are quite similar. The main formal difference lies in the fact that the quasi-spin pairing "pairs" particles of different s.p. energy while the ordinary pairing couples those of the same s.p. energy.

We have also studied the excited states of our system in the quasi-particle approximation and in the quasi-boson one.

Finally, we add to our pairing Hamiltonian the monopole force introduced by Lipkin et al. [1] . So, we have two competing interactions, one favoring states with I=0 and the other trying to get the maximum I for the ground

state. We are thus reminded of the competition between pairing and deformation in atomic nuclei. Studying the exact ground state one sees that the system undergoes the transition from maximum I to I=0 for larger values of g when the monopole coupling constant is greater. A HF solution can also be obtained for this pairing plus monopole Hamiltonian.

For more details see ref.[2].

---

† Z.Physik A288 (1978) 153.

* Departamento de Física, Facultad de Ciencias, UNLP, Bs.As., Argentina

1) H.I.Lipkin, N.Meshkov and A.I.Glick; Nucl. Phys. 62 (1965) 188.

2) M.C.Cambiaggio and A.Plastino; Z.Physik A288 (1978) 153.

IV.2 Beta Decay

IV.2.1 Current State of the Investigation of Superallowed Fermi β Decays†.

Leszek Szybisz*.

At the present time, the crucial point in a systematic study of superallowed 0^+-0^+ transitions is the evaluation of the isospin impurity correction δ_c [1,2]. In the literature, δ_c is decomposed into two parts, δ_{c1} and δ_{c2}. Several estimates of δ_{c1} have been published, while only one is available for δ_{c2}. We analyze the compatibility of the different estimates of δ_{c1} with the most recent surveys of experimental data. The simplest evaluation of δ_{c1} reported some years ago by Damgaard[3] is found to yield the most satisfactory F t values; these provide reliable values of the effective vector coupling constant G'_v (e.g., $G'_v = (1.41242 \pm 0.00023) \times 10^{-49}$ erg cm^3). These values are in excellent agreement with a recent value $G'_v = (1.41248 \pm 0.00044) \times 10^{-49}$ erg cm^3 obtained by Wilkinson et. al[4] on the basis of a phenomenological approach to δ_c. Conversely, the most recent and detailed parentage expansion approaches to δ_{c1} lead to

F t values which increase with Z, showing pronounced slopes. This fact might be due to a relative overestimation of δ_{c1} for the lighter nuclei.

Using the F t values calculated with δ_{c1} as reported by Damgaard, we evaluate the coupling constant for the induced scalar interaction following a procedure described in a previous paper. The mean of such values is $f_s/f_v = (-0.17\pm0.80) \times 10^{-3}$. In addition, we develop an alternative way of determining a limit for f_s/f_v using the phenomenological approach to δ_c suggested by Wilkinson. This new procedure yields $f_s/f_v = (-0.16\pm0.87) \times 10^{-3}$, a result which is in excellent agreement with that obtained using the former method; both values are consistent with a value of zero, supporting the conserved vector current theory. The better accuracy of the experimental data makes it possible to reduce by a factor of two the limit established in a previous work[5].

---

† L.Szybisz; Z.Physik A292 (1979) 49.

* Departamento de Física, Facultad de Ciencias Exactas, UNPL.

1) D.H.Wilkinson; Phys. Lett. 65B (1976) 9.

2) I.S.Towner , J.C.Hardy and M.Harvey; Nucl. Phys. A284 (1977) 269.

3) J.Damgaard; Nucl. Phys. A130 (1969) 233.

4) D.H.Wilkinson, A.Gallmann and D.E.Alburger ; Phys. Rev. C18 (1978) 401.

5) L.Szybisz; Z.Phys. A285 (1978) 223.

IV.3 Multistep Shell Model

IV.3.1 Four Particles-One Hole States in the Multi-Step shell Model Approach .

R.J.Liotta* and C.Pomar.

The method given in ref.[1] to study nuclei with three nucleons outside a closed-shell core has been extended to describe states containing in addition, one particle-hole excitation.

As a preliminary step the three particles-one hole (3p-1h) states $|\alpha>$ of the neighbor A+2 nucleus (A number of nucleons in the core) are studied in the basis:

$$|3p\text{-}1h> \equiv Q^+(q)\ P^+(p)\,|0> \qquad (1)$$

where $P^+(p)$ is the creation operator of the "correlated" two particle states (A+2 nucleus), while $Q^+(q)$ creates 1p-1h "correlated" states in the core (A). Also the four particle (4p) states $|\beta>$ at the A+4 nucleus are studied in the basis :

$$|4p> \equiv P^+(p_1)\ P^+(p_2)\ |\ 0\ > \qquad (2)$$

Basis (1) and (2) are overcomplete. Then before proceeding to diagonalize the respective interaction matrices their corresponding overlap matrices must be evaluated[2].

Once the $|\alpha> = \Gamma^+(\alpha)|0>$ and $|\beta> = \Gamma^+(\beta)|0>$, neighbor nuclei states, have been obtained a new overcomplete basis in the 4p-1h space (A+3 nucleus) is generated. Their basis elements are

$$|4p\text{-}1h>_1 \equiv C_K^+\ \Gamma^+(\alpha)|0> \qquad \text{and} \qquad |4p\text{-}1h>_2 \equiv b_i^+\ \Gamma^+(\beta)|0> \qquad (3)$$

where C_K^+ and b_i^+ are the single-particle and single-hole creation operators respectively. In this basis a coupled dynamical equation in the projections:

$$<\tau|C_K^+\ \Gamma^+(d)|0> \qquad \text{and} \qquad <\tau|b_i^+\ \Gamma^+(\beta)|0> \qquad (4)$$

is written. $|\tau>$ represent the 4p-1h physical states. The energies and wavefunctions of the physical states in the A+2 and A+4 neighbor nuclei(as well as the single-particle and single hole energies) is all we need to determine that system of equations for the A+3 nucleus (no interaction matrix-elements are explicitely involved).

The overcompletness of the basis (3) requires here again the calculation of its overlap matrix to reject the non physical solutions.

The structure of the basis elements (3) allows to evaluate the relative contribution (in the A+3 nucleus) of the neighbor nuclei states. When collective states are involved, drastic truncation can be performed.

The approach described above originated mainly in the fact that the $^{205}Pb(d,d')$ and the $^{204}Pb(d,p)$ reactions[3,4] indicate a strong mixing in the multiplet at ~ 2.6 MeV in ^{205}Pb of some collective states of ^{204}Pb and ^{206}Pb nuclei coupled to a hole- and a particle-state respectively. The numerical calculation for that nucleus is in progress.

---

* Research Institute for Physics, S 10405, Sweden.

1) R.J.Liotta and C.Pomar; Lett. al Nuovo Cimento, in press.

2) C.M.Ko, T.T.S.Kuo and J.B.Mc Grory; Phys. Rev. C8 (1973) 2379.

3) J.H.Bjerrgaard et al.; Nucl. Phys. A302 (1978) 173.

4) C.F.Maguirre et al.; Phys. Rev. C15 (1977) 161.

IV.3.2 Multi-step shell-model approach to ^{202}Pb.

R.J.Liotta* and C.Pomar .

The method given in ref.[1], to solve the problem of three nucleons outside a closed-shell core, has been extended to four- and six-particles outside closed-shell and applied to calculate the spectrum of ^{202}Pb.

The basic idea is to use the calculated states of the two-particle spectrum as the building blocks to construct the four-particle system. Once this has been achieved, the iteration of the method allows, in a second step, to describe the six-particles nucleus, but now with the two- and four- particles states as building blocks. In both steps, the problem is solved in a basis generated by the tensorial product of the two-particle spectrum and the tensorial product of the two- times the four-particle spectrum respectively. Since both basis contain non-orthogonal elements a direct diagonalization does not provide the physical eigenvectors. Then the corresponding overlap matrices must be first evaluated.

The main purpose is to analize the ^{204}Pb and ^{202}Pb spectra and (t,p) reaction[2]. Drastic truncations of the original shell-model basis have been done. Basis up to 50 and 20 elements for the ^{204}Pb and ^{202}Pb respectively have been used, choosing those with the lowest zero order energy.

The results are summarized in Table IV.3.2.1 . It shows the experimental[2] and the present theoretical energies (in MeV) and (t,p) cross section (relative to the lowest state of the corresponding spin and parity in ^{206}Pb) for (a) ^{206}Pb(t,p)^{204}Pb(J^π) (only if $\sigma_{rel} > 0.003$) , (b)^{204}Pb(t,p) ^{202}Pb(J^π) (only if $\sigma_{rel(calc)} > 0.03$). The ground state energies, relative to the ^{208}Pb core, were calculated to be 28.883 MeV in ^{204}Pb (experiment 28.925 MeV)and 43.983 MeV in ^{202}Pb (experiment: 44.112 MeV). The cross-sections were calculated using the code DWUCK[3] with optical parameters as in ref.[2].

---

* Research Institut for Physics, 5 10405, Sweden.

1) R.J.Liotta and C.Pomar; Lett. al Nuovo Cimento, in press.

2) W.A.Landford; Phys. Rev. 16C (1977) 988.

3) P.D.Kunz; unpublished.

Table IV.3.2.1(part a)

^{206}Pb (p,t) ^{204}Pb (J^π)					
	EXP.		THEORY		
J^π	E	σ rel	J^π	E	σ rel
0_1^+	0	1.74	0_1^+	0	1.54
(0_2^+)	1.584	(0.10)	0_2^+	1.561	0.003
0_3^+	1.728	0.17	0_3^+	1.655	0.28
2_1^+	0.899	0.63	2_1^+	0.893	0.54
2_2^+	1.351	0.015	2_3^+	1.446	0.088
2_3^+	1.663	0.12	2_5^+	1.739	0.005
2_4^+	1.958	0.05	2_6^+	1.844	0.089
2_5^+	2.103	0.015	2_9^+	2.156	0.0074
4_1^+	1.274	0.65	4_1^+	1.156	0.68
4_2^+	1.563	0.22	4_2^+	1.431	0.21
4_3^+	1.816	0.05	4_3^+	1.781	0.18
4_4^+	2.897	0.20	4_{12}^+	2.562	0.14
6_1^+	2.808	0.77	6_2^+	2.557	0.79
(5_1^-)	2.257	(1)	5_1^-	2.233	1.26
5_2^-	2.505	0.48	5_2^-	2.432	0.83
(7_1^-)	2.257	(0.70)	7_1^-	2.127	0.57
(7_2^-)	2.399	0.11	7_2^-	2.381	0.054
9_1^-	2.186	0.88		2.148	0.88

Table IV.3.2.1(part b)

^{204}Pb (p,t) ^{202}Pb (J^π)					
	EXP.		THEORY		
J^π	E	σ rel	J^π	E	σrel
0_1^+	0	2.31	0_1^+	0	2.02
2_1^+	0.961	0.56	2_1^+	0.884	0.44
(2_2^+)	1.383	0.026	—	——	——
2_3^+	1.657	0.020	—	——	——
4_1^+	1.383	0.48	4_7^+	1.322	0.65
4_2^+	1.623	0.09	—	——	——
4_3^+	1.915	0.067	—	——	——
4_4^+	2.516	0.086	—	——	——
4_5^+	2.666	0.115	—	——	——
6_1^+	2.747	0.55	6_{18}^+	2.512	0.15
5_1^-	2.040	1.28	5_5^-	2.093	0.64
—	——	——	5_{12}^-	2.577	0.49
9_1^-	2.172	0.93	9_2^-	1.975	0.66
—	——	——	9_4^-	2.273	0.18

IV.4 Rotational States, Doubly Odd Nuclei

IV.4.1 Particle-Rotor Model for Doubly Odd Transitional Nuclei of the Tl-Region *.

A.J.Kreiner.

A model has been investigated describing a situation in which two non-interacting high-j Nilsson-BCS quasiparticles move in the deformed field of an axially and reflection symmetric rotor. According to the positions of the j-shells with respect to the proton and neutron Fermi surfaces structures of different character emerge referred to as semi- and doubly-decoupled. In particular, strongly Coriolis-distorted bands recently re-

ported[1,2] in doubly odd Tl nuclei are discussed. Also $\tilde{\pi}h_{9/2}$ bands in neighbouring odd mass Tl isotopes are analyzed on the same footing. It is shown that the pronounced odd even staggering of the transition energies can be understood as a specific quantal feature associated with the Coriolis interaction.

---

* Z.Physik A288 (1978) 373.

1) A.J.Kreiner, M.Fenzl, S.Lunardi and M.A.J.Mariscotti; Nucl. Phys. A282 (1977) 243.

2) A.J.Kreiner, M.Fenzl and W.Kutschera; Nucl. Phys. A308 (1978) 147.

IV.4.2 On the Coriolis Interaction*.

A.J.Kreiner.

A possible explanation of the intriguing problem of the so-called Coriolis attenuation factors, in the framework of the particle-plus-rotor model is suggested. The explicit inclusion of the recoil term renders unnecessary the assumption of an attenuation factor for the Coriolis interaction, at least for the very distorted positive parity $i_{13/2}$ bands of the rare earth region. The relationship between the particle-plus-rotor and the cranking model has been explored, showing that the largest differences, although not excessively large, appear at low values of the angular momentum where the quantal nature of the core rotation is especially important. Both models become equivalent as fluctuations become more unimportant.

---

* Phys. Rev. Lett. 42 (1979) 829.

IV.4.3 Fermi-level dependence of semidecoupled bands in doubly odd Tl isotopes*.

A.J.Kreiner.

Recent measurements have revealed the existence of strongly Coriolis-distorted bands based on $I^{\pi} = 8^{-}$ isomeric states in doubly odd transitional

Tl nuclei[1,2]. Calculations performed within the framework of the two-quasiparticle plus rotor model have allowed an interpretation of the measured cascades in terms of a two-quasiparticle band where the appropiate frame to describe the intrinsic motion turns out to be the $\tilde{\pi}h_{9/2} \otimes \tilde{\nu}i_{13/2}$ product space[1-3].

The purpose of the present contribution is to discuss the predicted behavior of the $\tilde{\pi}h_{9/2} \otimes \tilde{\nu}i_{13/2}$ structure as a function of neutron number, especially for isotopes lighter than those studied up to now.

In the lower part of fig.IV.4.3.1 we display the excitation energies relative to the 8^- state of some members of the band as a function of the neutron Fermi level λ_n while proton parameters are held fixed in the calculations, as indicated by the remarkable constancy of the $\tilde{\pi}h_{9/2}$ bands in odd-A Tl isotopes over the mass range A=191-197[4]. It is clearly seen how the 8^--11^- multiplet becomes progressively compressed as λ_n merges into the $i_{13/2}$ shell . On the contrary, the portion of the band above the 11^- state remains approximately constant in a relatively wide range of λ_n (for $\lambda_n \gtrsim \varepsilon(\Omega_n=7/2)$. Below this value, level crossings start to occur within the multiplet. For the actual structures in the Tl nuclei which depopulate into long lived 7^+ states, this means that the character of the isomeric transition out of the band will change succesively from E1 (as in ^{198,196}Tl) to M2, etc. in the lighter isotopes giving rise to increasingly longer lifetimes.

---

* Submitted to Phys. Rev. C (Feb.1979).

1) A.J.Kreiner, M.Fenzl, S.Lunardi and M.A.J.Mariscotti; Nucl. Phys. A282 (1977) 243.

2) A.J.Kreiner, M.Fenzl and W.Kutschera; Nucl. Phys. A308 (1978) 147.

3) A.J.Kreiner; Z.Physik A288 (1978) 373.

4) J.O.Newton, F.S.Stephens and R.M.Diamond; Nucl. Phys. A236 (1974) 225.

Fig. IV.4.3.1 Energies of some yrast states for the $\tilde{\pi}h_{9/2} \otimes \tilde{\nu}i_{13/2}$ (odd-odd Tl) and $\tilde{\nu}i_{13/2}$ (odd Hg) systems as a function of the neutron Fermi level ($\hbar\omega = 41/A^{1/3}$). Positions of single-particle energies of the $i_{13/2}$ shell members are also given on the λ_n axis.The position of λ_n for each neutron number (Nexp) is extracted from a fit to the $15/2^+$-$17/2^+$ spacing in the odd Hg $i_{13/2}$ bands.

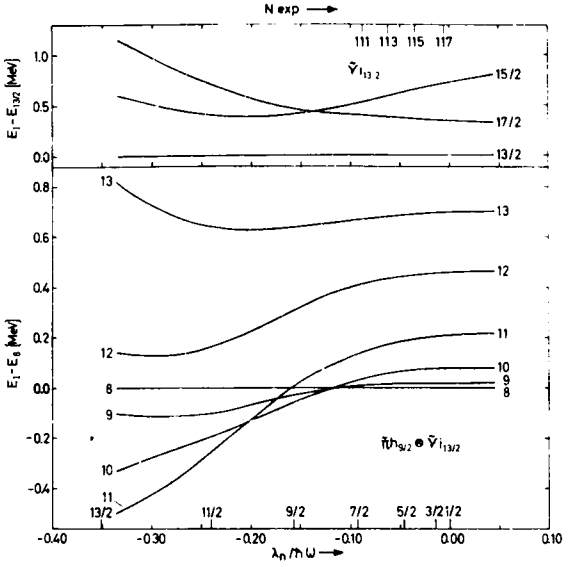

IV.4.4 Coriolis distorted bands of common $g_{9/2}$ parentage in doubly odd and odd N=41 nuclei*.

A.J.Kreiner and M.A.J.Mariscotti.

All features of a ΔI=1 band[1] displaying Coriolis like distortions based on a 4^+ isomeric state, recently discovered in ^{76}Br(ref.2), are successfully described within the framework of a two non-interacting quasiparticle plus rotor calculation. Assuming the intrinsic state to be of $\tilde{\pi}g_{9/2} \otimes \tilde{\nu}g_{9/2}$ parentage it is possible to account in a natural way for the apparent relationship noted between the 4^+ and $5/2^+$ ground state band[3] of the neighboring isotone ^{77}Kr.

---

* Phys. Rev. Lett. 43 (1979) 1150.

1) M.Behar, A.Filevich, G.García Bermúdez and M.A.J.Mariscotti, Nucl. Phys. A282 (1977) 331.

2) A.J.Kreiner, G.García Bermúdez, M.A.J.Mariscotti and P.Thieberger, Phys. Lett. 83B (1979) 31.

3) E.Nolte and P.Vogt, Z.Physik A275 (1975) 33.

IV.4.5 Evidence for a predicted change of phase in the level staggering of bands in doubly-odd nuclei*.

A.J.Kreiner and M.A.J.Mariscotti.

Evidence is discussed for a predicted change of phase in the odd-even level staggering, at a certain spin value, of Coriolis-distorted bands in doubly-odd transitional nuclei. Examples are given, covering different regions of the nuclidic chart, for the likely ocurrence of similar phenomena.

---

* Journal of Physics G Letters, 6 (1980) 13.

IV.5 Nuclear Matter

IV.5.1 Zero order crystallization in the Bethe-Fermi homework problem.

M.C.Cambiaggio*, M.de Llano**, A.Plastino* and L.Szybisz*.

Many recent works have studied the Bethe-Fermi homework problem, i.e., neutron matter with the v_0 potential (the repulsive part of the $^1S_0$ Reid soft-core potential) (see for example Ref.1). We have discussed the possibility of solidification in this problem, restricting ourselves to the zero order solution, and shown that non-trivial results are already found at this stage.

To this end, we evaluated the total energy per particle $\varepsilon=E/N$ as a function of the density ρ, both in a "fluid" and in a "solid" phase. For the "fluid" state we used a Slater determinant of normalized plane waves. For the "solid" phase we followed Ref.2) in which normalized, non-overlapping Wannier-like functions are employed. We studied three different structures: sc, fcc and bcc. The "solid" energy values obtained are lower than the "fluid" ones for the three lattice arrangements, in the physically interesting range of densities ($0.2\ fm^{-3} \leq \rho \leq 3\ fm^{-3}$). The "fluid" to "solid" transition appears at $\rho = 0.16\ fm^{-3}$ for sc structure, $\rho = 0.07\ fm^{-3}$

for fcc and $\rho = 0.09$ fm^{-3} for bcc. Similar calculations were carried out with the v_1 homework potential (which adds attraction to the v_0) but in this case the "fluid" to "solid" transition appears at $\rho \simeq 10^4$ fm^{-3}.

It is remarkable that our zero order "solid" results are fairly close to the energy values obtained in ref.1) through a much more sophisticated calculation. (For example, for $\rho = 1$ fm^{-3} our result is 1010 MeV/particle for the bcc structure and their result is 793 MeV/particle).

We have demonstrated the existence of a Slater determinant (that represents a "solid" phase) whose energy per particle is lower than the corresponding one for plane waves, in the Bethe homework problem. Accordingly, a Hartree-Fock state exists which is periodic and whose energy is less than or equal to our trial one. This finding invalidates a HF-based perturbative approach to this problem which starts with plane waves as the zero order solution.

---

* Departamento de Física, Facultad de Ciencias, UNLP.

** Instituto de Física, Universidad de México.

1) L.J.Lantto and P.J.Siemens; Nucl. Phys. A317 (1979) 55.

2) M. de Llano and S.Ramírez; Ann. Phys. (N.Y.) 79 (1973) 186.

IV.5.2 The self-consistent pseudopotentials in the thermodynamic Limit.The correlation field.

E.S.Hernández*, A.Plastino** and L.Szybisz** .

It is usually believed that correlations induced by two-body interactions characterized by the presence of a hard-core cannot be handled within the framework of the Hartree-Fock (HF) formalism. This assumed failure of the HF theory has lead to the development of powerful methods that are able to deal with the strong short-range repulsion of the nuclear force[1-3]. However, de Llano and Ramírez[4] have shown that in the limit of infinitely repulsive potentials between pairs of particles, there exists for both fermions and bosons, a periodic density HF solution. More recently, Giraud and Orland[5] have demonstrated that non-overlapping orbitals make HF calculations possible in the presence of hard-core interactions.

Let us consider a system of N fermions enclosed in a (one-dimensional) container of volume L in the thermodynamic limit (i.e., $N \to \infty$ and $L \to \infty$) but

$$\rho_0 = \lim_{\substack{N \to \infty \\ L \to \infty}} \frac{N}{L} = \text{finite}. \tag{1}$$

This system is acted upon by a hard-core pair-wise potential; with range b and hard-core radius c. It is the aim of the present note to report that the effect of the strong repulsion in the actual two-body force can be simulated by a constraint. For such a purpose we introduce the correlation function of the system

$$G(x_1, x_2) = \frac{1}{\rho_0^2} \sum_{\lambda,\mu=1}^{N \to \infty} |\psi_{\lambda\mu}(x_1, x_2)|^2 \tag{2}$$

where $\psi_{\lambda\mu}(x_1,x_2)$ is the antisymmetrized two-particle wave function, which is considered purely spatial for simplycity. Assuming that we can perform a Fourier analysis of the single particle wave function $\psi_\lambda(x)$

$$\psi_\lambda(x) = \frac{1}{\sqrt{2\pi}} \int dk\, C_\lambda(k)\, e^{ikx} \tag{3}$$

and that the ground state $|\phi_g>$ is the normalized Slater determinant of these orbitals. Integrating (2) over the center-of-mass coordinate $X_{12} = \frac{1}{2}(x_1 + x_2)$ we obtain a one-body correlation function $g(X_{12} = x_1 - x_2)$. The presence of the hard-core in the potential causes $g(X_{12})$ to vanish at $X_{12} = C$. Our proposal is to include the boundary condition $g(c) = 0$ as a constraint in the variational principle through a Lagrange multiplier α.

It is possible to demonstrate that the Euler-Lagrange equations of the problem are the well known Hartree-Fock integral equations

$$\int dk_1 \left| t(k_1,k_2)\, g(k_1-k_2) + \Gamma(k_1,k_2) \right| C_n(k_1) = E_n\, C_n(k) \tag{4}$$

with

$$\Gamma(k_1,k_2) = \Gamma_1(k_1,k_2) + \alpha\, \Gamma_2(k_1,k_2) \tag{5}$$

Here $t(k_1,k_2)$ stands for the kinetic energy and $\Gamma(k_1,k_2)$ is the self-consistent one-body "pseudopotential". $\Gamma_1(k_1,k_2)$ is due to the regular part

of the two-body interaction and $\Gamma_2(k_1,k_2)$ is a correlation field generated by the imposed constraint.

It is possible to show that the most familiar set of Hartree-Fock solutions, namely the plane waves, do not satisfy eq.(4). In fact, they are not even zero-order approximations since $\Gamma_2(k_1,k_2)$ will diverge if attempted to be evaluated with a plane wave density. So an important feature of the correlation field is to destroy the localization in momentum space and to give rise to subsequent confinement in configuration space. We could thus argue that this may be interpreted as a justification for the widespread use of Overhauser-like orbitals[6] in nuclear matter calculations[7-10]. Furthermore, we may suggest an explanation of the origin of the so-called "density waves" in Fermi systems in the thermodynamic limit. The present investigation shows that waving in the local density is associated with the way in which the correlation function has to bend in order to reach a node at a relative distance equal to the hard-core radius.

---

* Departamento de Física, FCEN, Universidad Nacional de Buenos Aires.

** Departamento de Física, FCE, Universidad Nacional de La Plata.

1) H.A.Bethe; Ann.Rev.Nucl.Sci. 21 (1971) 93.

2) J.W.Clark; Prog. in Part. and Nucl.Phys. (in press).

3) B.D.Day; Rev.Mod.Phys. 50 (1978) 495.

4) M. de Llano and S.Ramírez; Ann. of Phys. (N.Y) 79 (1973) 186.

5) B.G.Giraud and H.Orland; Phys.Rev.Lett. 41 (1978) 1016.

6) A.W.Overhauser; Phys.Rev.Lett 4 (1960) 415.

7) M. de Llano and A.Plastino; Phys.Rev. A13 (1976) 1633.

8) V.Aguilera, M. de Llano, S.Peltier and A.Plastino; Phys.Rev. A15 (1977) 1256; Phys.Rev. C16 (1977) 1642.

9) L.Dohnert, M. de Llano and A.Plastino; Nucl.Phys. A291 (1977) 45; Phys. Rev. A17 (1978) 767.

10) V.Aguilera, S.Andrade, A.Zinerman, L.Dohnert, M. de Llano and A.Plastino; Phys.Rev. C16 (1977) 2081.

IV.6 Time Dependent Hartree Fock (TDHF)

IV.6.1 Geometry of the time dependent variational principle.

P.Kramer* and M.Saraceno

The time dependent variational principle (TDVP) results from the variation of the action

$$S = \int \langle \Psi(x) \mid i \frac{\partial}{\partial t} - H \mid \Psi(x) \rangle dt \qquad (1)$$

and leads to approximate evolution equations

$$\eta_{ij} \dot{X}_j = \frac{\partial \mathcal{H}}{\partial X_j} \qquad (2)$$

with $\mathcal{H} = \langle \Psi(x) | H | \Psi(x) \rangle$ $\qquad \eta_{ij} = \langle \partial_j \Psi(x) | \partial_i \Psi \rangle - \langle \partial_i \Psi | \partial_j \Psi \rangle$

η is a symplectic form completely defined by the chosen parametrization of the wave function. This form defines a generalized phase space or symplectic manifold in which (2) are Hamilton's equations[1].

If the parameters are chosen to be the coordinates of a Lie group a rich geometric structure arises which allows a detailed study of the equations of the TDVP. In particular the degeneracy of η_{ij} can be analyzed and a well known theorem[2] can be applied to show that η_{ij} is non degenerate on the orbits under the coadjoint representation of the group. For semisimple compact groups we give a general procedure to construct the symplectic form based on the Cartan decomposition of the algebra[3]. We give several examples illustrating these concepts. The Weyl group and SU(2) are studied in detail and the latter case is applied to the analysis of the TDHF equations for the Lipkin model[4]. As a more complicated example we take the SU(3) group, which has already most of the complications of the general case. We classify the different types of orbits and find the symplectic structures associated with them.

The SU(M) group, which corresponds to unitary transformation of fermion operators distributed in M single particles levels, underlies the geometry of the time dependent Hartree-Fock equations. We also analyze the TDHF equations from this point of view and we construct explicitly the symplectic form in this case. Finally, to explore the difficulties connected with non compact groups the SU(1,1) group is analyzed.

---

* Institut für Theoretische Physik, Universität Tübigen.

1) P.Kramer and M.Saraceno; to be published.

[2]) V.Arnold, "Mathematical Methods of Classical Mechanics", Springer-Verlag N.Y. (1978).

[3]) R.Gilmore, "Lie Groups, Lie Algebras, and some of its applications", J.Wiley N.Y. 1974.

[4]) H.I.Lipkin, N.Meshkov, A.I.Glick, Nucl. Phys. 62 (1965) 188.

IV.6.2 Intermediate representation and corrections to the TDHF evolution.

M.Saraceno and G.G.Dussel

An intermediate representation provided by a one body evolution operator $U_0(t)$ allows a decomposition of the exact evolution as follows:

$$U(t_2,t_1) = e^{iS_{12}}\, U_0(t_2)\, \tilde{K}(t_2,t_1) U_0^+(t_1) \qquad (1)$$

where $S_{12} = \int_{t_1}^{t_2} \langle \Psi_0 | U_0^+(t) (i \frac{\partial}{\partial t} - H)\, U_0(t) | \Psi_0 \rangle \, dt$ (2)

and where $\tilde{K}$ satisfies the equation

$$i \frac{\partial \tilde{K}}{\partial t}(t,0) = \Delta V_I(t)\, \tilde{K}(t,0) \qquad \tilde{K}(0,0) = 1 \qquad (3)$$

The perturbing operator ΔV_I is given by

$$\Delta V_I(t) = U_0^+(t)(H - i\frac{\partial}{\partial t}) U_0(t) - \langle V_I(t) \rangle$$

We show that the TDHF equations result either from an extremum of the action S_{12} or from the elimination of one body terms in ΔV_I. This is completely analogous to the static case[1]. Recently[2], a decomposition similar to (1) has been proposed based on functional integral techniques. These have the difficulty that they lead to a phase S_{12} that does not include exchange terms and to the Hartree equations. The Fock terms can be recovered through corrections to the Hartree trayectory. We do not have these problems because our zero solution is based on the variational principle and therefore includes the exchange terms.

A perturbation solution to eq.(3) allows the calculation of corrections to the TDHF evolution of an operator A. To first order the corrections are:

$$\delta A(t) = - i \int_0^t \langle \left[A_I(t) , \Delta V_I(\tau) \right] \rangle \, d\tau$$

where $\delta A(t)$ is the difference between the e act and the TDHF evolution.

Only the $\langle \Psi_0 \mid A_I(t) \mid 2 \text{ ph} \rangle$ elements contribute to the corrections in this order. In particular $\delta A(t) = 0$ for one body operators. We apply this formula to the important case of corrections to the dispersion of one-body operators.

---

1) Nozieres , "Theory of Interacting Fermi Systems", W.A.Benjamin, N.Y.1964.

2) S.Levit, J.W.Negele, Z.Paltiel, M.I.T. preprint, CTP #781, May 1979.

IV.6.3 Periodic Trajectories in TDHF.

M.Saraceno .

The periodic trajectories of a classical hamiltonian system with many degrees of freedom allow the determination of semiclassical properties of its bound quantum states[1,2]. The TDHF equations are classical hamiltonian equations and its periodic solutions are the natural generalization of the static Hartree-Fock solutions which are its rest points.

We apply Floquet's theorem[3] on systems of equations with periodic coefficients and the phase expansion[4] for the single particle evolution operator to obtain a necessary condition for the existence of a periodic solution to the TDHF equations. This condition takes the form of a self-consistent requirement analogous to the static equation (HF) and is

$$\left[M\left[\rho(t)\right] , \rho_0 \right] = 0 \qquad (1)$$

Where ρ_0 is the initial condition for the density matrix and M is given by

$$M = \frac{1}{T} \left\{ \int_0^T h(\tau) d\tau + \frac{i}{2} \int_0^t d\tau \int_0^\tau \left[h(\tau) , h(\sigma) \right] d\sigma + \ldots \right\}$$

Here $h(t) = h(\rho(t))$ is the Hartree-Fock Hamiltonian. Higher terms in the expansion can be found in ref.[4]. M is a static single particle field which is a complicated functional of the periodic density $\rho(t)$ with period

T. It is a property of the periodic solution and its eigenvalues provide a generalization of the single particle energies of the static case. When the periodic trajectory contracts to a rest point, M becomes the usual HF Hamiltonian. Although eq.(2) is difficult to use in practical calculations, it suggests naturally an iterative procedure to find a self-consistent periodic trajectory of period T (if it exists) starting from an approximate trajectory of the same period. The procedure is entirely analogous to the usual iteration procedure used to solve the static HF equations.

---

[1]) M.C.Gutzwiller; Jour. of Math. Phys. 12 (1971) 343.

[2]) R.F.Dashen, B.Hasslacher, A.Neveu; Phys. Rev. D10(1974) 4114.

[3]) V.A.Yacubovich, V.M.Starzhinskii; "Linear Differential Equations with Periodic Coefficients", John Wiley & Sons, New York, 1975.

[4]) I.Bialynicki-Birula, B.Mielnik, J.Plebansky; Ann. Phys. 51 (1969) 187.

IV.6.4 Semiclassical quantization of Lipkin's model TDHF.

M.Saraceno and J.M.Carcione.

The TDHF equations for the Lipkin model[1]) are[2]):

$$\dot{\phi} = \varepsilon \chi \sin\phi \sin 2\Psi \qquad \chi = \frac{V(N-1)}{\varepsilon}$$
$$\dot{\Psi} = -\varepsilon (1 - \chi \cos\phi \cos 2\Psi)$$

They can be derived by variation of the action functional with the wave function parametrized as

$$|\Psi,\phi\rangle = \exp(i\Psi(t)K_0) \exp(i\phi(t)K_y) |\, 0\rangle$$

where $|\, 0\rangle$ is the unperturbed ground state with quasi-spin quantum numbers $J = N/2$ and $M = -J$, and N is the (even) number of particles.

With this parametrization the action is

$$S = \frac{N}{2} \int_0^t \dot{\Psi}\cos\phi - H)\, dt$$

Where

$$H(\phi,\Psi) = \langle\Psi,\phi|H|\Psi,\phi\rangle = -(\cos\phi + \frac{\chi}{2}\sin^2\phi\cos 2\Psi)$$

The reduced action

$$S_0 = \frac{N}{2} \int_0^T \cos\phi(t) \quad \dot{\Psi}(t)\, dt$$

computed along a closed T-periodic solution of the equations of motion can be evaluated as a function of energy and used to apply a generalized Bohr-Sommerfeld quantization rule as follows:

$$S_0 (E_n) = 2\pi n \quad (\hbar = 1,\ n = \text{integer})$$

This condition determines the semiclassical eigenvalues E_n which can be compared to the exact numerical diagonalization. The detailed study of the function $S_0(E)$ can be done explicitly in this model and is greatly simplified by the application of the geometrical methods developed in ref.3 .

The exact and semiclassical spectrum are compared in Fig.IV.6.4.1 as a function of the interaction parameter $\chi = \frac{(N-1)V}{\varepsilon}$ for a system with N=14.

Only the positive eigenvalues are plotted because the spectrum is symmetric for negative energies. Salient features emerging from this comparison are the following:

a) The semiclassical results are able to reproduce the overall features of the exact spectrum over a wide range of interaction parameters on both sides of the "phase transition" point $\chi = 1$.

b) The semiclassical ground state energy is always higher than the exact ground state energy. This is a feature of the variational nature of the TDHF equations. If exchange terms are neglected as in TDH equations (in our simple model this means replacing χ by $\chi' = \frac{NV}{\varepsilon}$) this feature is destroyed. The inclusion of exchange is the main difference with a very similar calculation[4] done with functional integral techniques.

c) The analysis of this model is made very simple by the fact that all trayectories are periodic. For more complicated models the analysis of multidimensional hamiltonian systems becomes necessary and quite involved unless constants of motion other than the energy can be found.

---

[1] H.J.Lipkin, N.Meshkov, A.J.Glick; Nucl. Phys. 62 (1965) 188.

[2] S.Y.Krieger; Nucl. Phys. A276 (1977) 12.

[3] P.Kramer, M.Saraceno; (to be published).

[4] S.Levit, J.W.Negele, Z.Paltiel; M.I.T. preprint CTP#781 (May 1979).

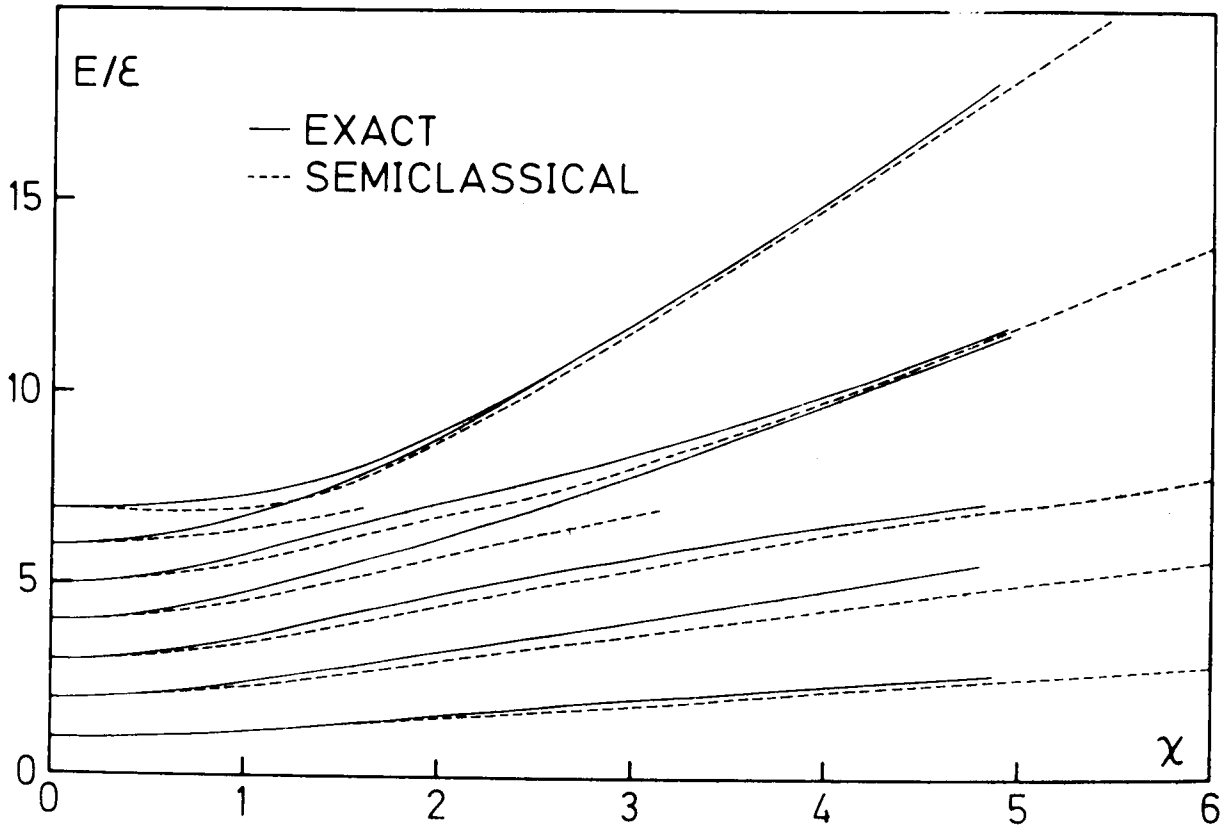

Fig. IV.6.4.1

V. NUCLEAR REACTIONS

V.1 Nuclear Rayleigh and Whispering Gallery Waves Excited in Heavy Ion Collisions.

O.Dragûn and H.Überall*.

The gross structure oscillations recently observed in differential and total heavy-ion elastic or inelastic scattering and fusion cross sections, which are indicative of molecular resonances, are here analyzed in terms of nuclear surface (creep) wave resonances. Their dispersion curves characterize these waves as being of Rayleigh type in some cases, and of Whispering-Gallery type in others.

The gross structure peaks have most clearly been noticed in the quasi-molecular $^{12}C+^{12}C$ (i.e. the ^{24}Mg) system[1], the $^{12}C+^{16}O$ (i.e. the ^{28}Si) system[2], and the $^{12}C+^{28}Si$ (^{40}Ca) and $^{16}O+^{28}Si$ (^{44}Ti) system[3], and have been tentatively fitted to rotational bands by some investigators.

It may be said that our analysis of the resonances observed in heavy-ion scattering in terms of nuclear surface waves on the intermediate (nuclear-molecular) systems seems to provide the first indication for the existence, as well as their classification, of nuclear Rayleigh and Whispering Gallery waves on the curved surface of nuclear matter. These waves agree with their classical counterparts insofar as they constitute a solution of the wave equation (in the nuclear case, the Schrödinger equation), propagate over a boundary of matter and show an equivalent dispersion behavior. They differ from the classical waves as these are actual density waves, while the nuclear creep waves are only the probability amplitudes described by an optical model wave function of two colliding heavy ions. Therefore, rather higher angular momenta, or short wavelenghts, are completely acceptable here even for a relatively light intermediate nuclear system.

---

* Department of Physics, Catholic University, Washington, DC 20064, U.S.A.

1) T.M.Cormier, C.M.Jachcinski, G.M.Berkowitz, P.Braun-Munzinger, P.M.Cormier, M.Gai, J.W.Harris, J.Barrette and H.E.Wegner; Phys. Rev. Lett. 40 (1978) 924.

[2]) D.Shapira, R.M. De Vries, M.R.Clover, R.N.Boyd and R.N.Cherry, Jr., Phys.Rev.Lett. 40 (1978) 371.

[3]) J.Barrette, M.J.Le Vine, P.Braun-Munzinger, G.M.Berkowitz, M.Gai, J.W. Harris and C.M.Jachcinski; Phys.Rev.Lett. 40 (1978) 445.

V.2 Analysis of (p,α) reactions in the pre-equilibrium regime.

O.Dragún, A.Ferrero and A.Pacheco.

In the last years, abundant experimental data have been obtained for inelastic and transfer reactions induced by light ions , leaving the residual nuclei in highly excited states[1,2].

The corresponding continuous energy spectra of outgoing particles have been interpreted in terms of compound and pre-compound processes. We present here one extension of the Multi-step-direct-reaction theory[3] applied to the (p,α) process in the pre-equilibrium regime.

A detailed analysis of the first order contribution of a triton pick-up is made, as a function of the target mass and incident proton energy. Within the scope of the present approximation, the double differential cross-section is given by:

$$\frac{d\,\sigma^{\text{one step}}}{d\Omega\, dE}(\bar{E}_\alpha,\theta) = \binom{A}{3} N \frac{d^2(\bar{E}_\alpha)}{\hbar\omega} \sum_{\Lambda,L,N} \frac{d\,\sigma^{DWBA}_{LN}}{d\,\Omega}(\bar{E}_\alpha,\theta)\,\delta_{\Lambda,2N+L}$$

where A is the target mass, N is the normalization factor that contains D_0^2 and the averaged fractional parentage coefficient, $\frac{d^2(E\alpha)}{\hbar w}$ plays the role the spectroscopic density and $\bar{E}_\alpha$ is an intermediate outgoing α-energy belonging to an actual energy interval ΔE_α . The sum over the quantum numbers L and N (representative of the triton's center of mass motion) takes into account the final states belonging to ΔE_α, in the frame of an oscillator shell model calculation. The differential cross-sections $d\,\sigma^{DWBA}_{LN}/d\,\Omega$ are calculated using a triton-cluster form factor. The sets of optical parameters for the incoming and outgoing channels are the same for all target nuclei.

The impressive agreement between experimental data and theory is shown in Figures V.2.1 and V.2.2 . It is interesting to note how the theory adjusts angular distributions , outgoing energy spectra and rela-

tive intensities. A single "ad hoc" parameter has been used; the strength W_0 of the absorptive potential in the outgoing α-channel. Contributions of higher order could change the small value of W_0 (approximate 6 MeV) of the present calculation.

---

[1]) F.E.Bertrand and R.W.Peelle; Phys. Rev. C8 (1973) 1045.
Oak Ridge National Laboratory Report, ORNL-4455 (1969) and ORNL-4638 (1971).
R.W. West, Phys. Rev. 141 (1966) 1033.

[2]) E.Gadioli, I.Iori, N.Molho and L.Zetta; Report INFN/BE-73/5 (1973).
A.M.Ferrero, I.Iori, N.Molho and L.Zetta; Report INFN/BE-78/6 (1978).

[3]) T.Udagawa, T.Tamura and K.S.Low; Phys. Rev. Lett. 34 (1975) 30.
T.Tamura, T.Udagawa, D.H.Feng and K.K.Kan; Phys. Lett. 66B (1977) 109.
T.Tamura and T.Udagawa; Phys. Lett. 71B (1977) 273.

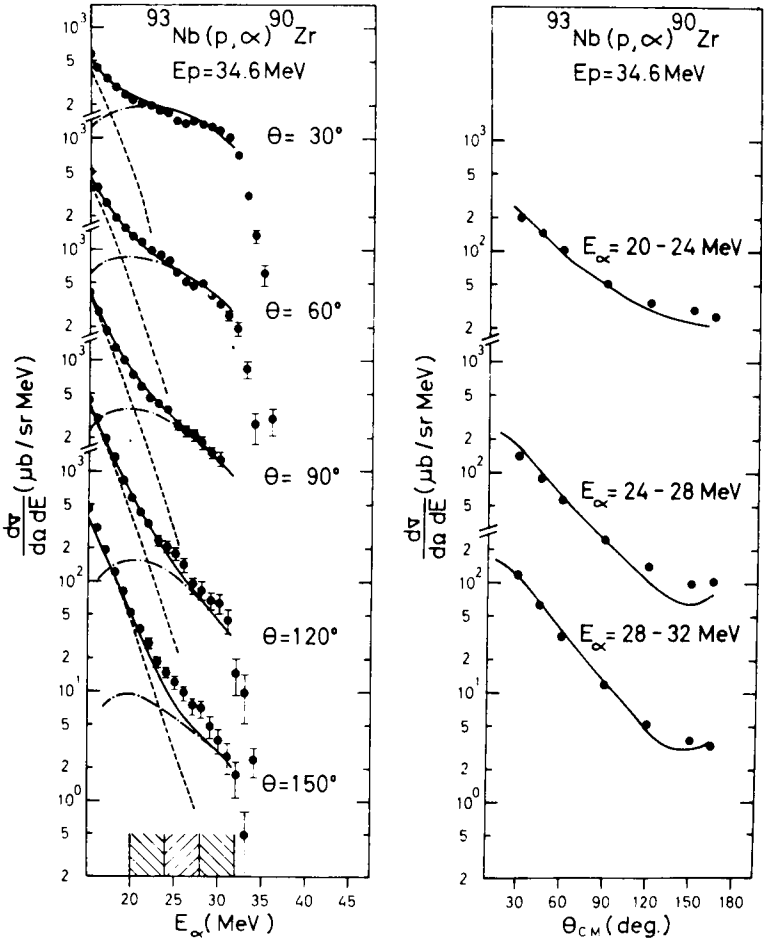

Fig. V.2.1 :

Experimental and theoretical energy spectrum for the ^{93}Nb (p,α)^{90}Zr reaction.

a) Dashed curves are compound components. Dotted dashed curves are one step contributions with a relative normalization equal 1 for all of them. Full lines contributions are the sum of compound and one step.

b) Experimental and theoretical angular distributions. Experimental points are averaged on 4 MeV bins showed at the bottom of a).

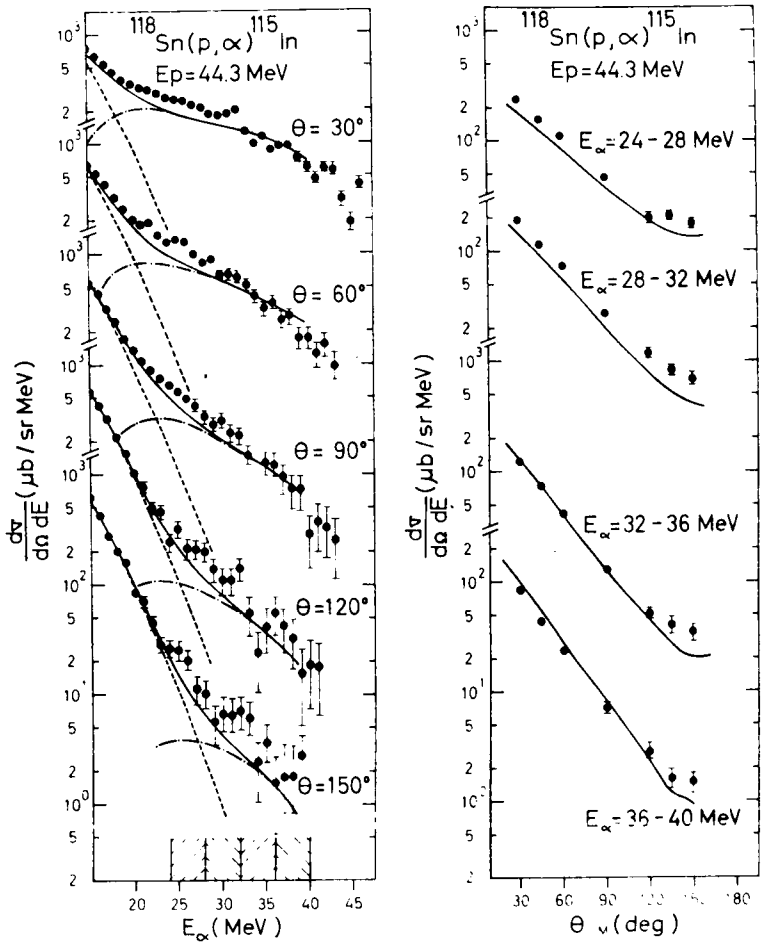

a) b)

Fig. V.2.2: Same as fig.V.2.1 for the ^{118}Sn $(p,\alpha)^{115}In$ reaction.

V.3 Isospin-dependent Optical Potentials and Two-nucleon Transfer Reactions.

O.Dragún and E.Maqueda.

In ref.[1] a formalism was developed in order to work with distorted waves of definite isospin. In that way the nuclear isovector component of the optical potentials is fully taken into account. The method neglects a term arising from the Coulomb potential which though cancelling largely in the nuclear interior[3], may contribute significantly between the nuclear and matching radii[4]. The asymptotic boundary conditions that both projectile

(exit particle) and target (residual nucleus) have known charges, is to be imposed in this approximation through modifications of the usual DWBA codes.

Other authors (see for instance ref.[2]) have used a different approach. The distorted waves in the entrance and exit channels are chosen to have well defined isospin projections for both projectile and target. This individual-charge defined treatment has the practical advantage of working in a basis where the imposition of the asympotic boundary conditions with respect to isospin projections is straight-forward. The Coulomb potential is diagonal in this basis but the nuclear isospin dependent terms of the optical-model potentials produce couplings between channels with different isospin projections. The effects of these couplings are neglected in the DWBA treatments[5,6].

If the different parts neglected by each of the above approximations were insignificant, both treatments should lead to the same results when applied to the calculation of ratios of cross sections of isobaric analogue reactions. Of course the relative importance of any difference is to be pondered, taking into consideration the errors of the respective experimental data. In fact, even if an upper estimate of 30% is allowed for the experimental errors, the comparison of both approximations indicates[1] a sizable discrepancy. It is therefore desirable to perform a calculation where no approximation in the treatment of the isospin-dependent terms is made. With this purpose in this note we present a charge-coupled-channel calculation and compare the results with those of the approximate treatments.

The method is applied to two-nucleon transfer reactions populating $J^{\pi} = 0^{+}$ states in nuclei of the first part of the fp shell. This is a region where these reactions have been investigated in relation to studies of the isoscalar pairing degree of freedom[6]. A reliable analysis of the experimental evidence has to behave properly under isospin symmetry tests as indicated above. In this sense, we compare the cross sections of (τ,p) and (τ,n) reactions populating members of isospin multiplets, namely,

$$r_0 = d\sigma(\tau,n)/d\sigma(\tau,p) \qquad (1)$$

and the ratios

$$R_0 = r_0^{exp}/r_0{}^{th} \qquad (2)$$

obtained with the exact ISOCCBA calculation with the T_z and T approximations. This comparison can be done analyzing the values of

$$\rho(T \text{ or } T_z) = \frac{R_0(T \text{ or } T_z) - R_0(\text{ISOCCBA})}{R_0(\text{ISOCCBA})} \qquad (3)$$

for nineteen pairs of reactions in the fp-region, which are displayed in fig. V.3.1 . From the values of ρ shown there, it is possible to conclude that the isospin-defined (T) approximation is in better agreement with the exact result than the charge-defined (T_z) approximation. In fact, except for a few cases in which both approximations give essentially the same result, for all the other pairs of reactions the differences between the T-approximation and the exact results are smaller than those corresponding to the T_z approximation

1) O.Dragún, D.R.Bes and E.E.Maqueda; Nucl.Phys. A258 (1976) 10.

2) J.D.Garrett and O.Hansen; Nucl.Phys. A212 (1973) 600.

3) D.Robson; Phys.Rev. 137 (1965) B535.

4) B.Bayman; Proc.Int.School of Physics Enrico Fermi, Course 40, 1967 (Academic Press, New York, 1969) p.380.

5) D.Evers, W.Assmann, K.Rudolph, S.J.Skorka and P.Sperr; Nucl.Phys. A193 (1972) 268; A230 (1974) 109.

6) D.R.Bes, R.A.Broglia, O.Hansen and O.Nathan; Phys.Reports 34C (1977) 1.

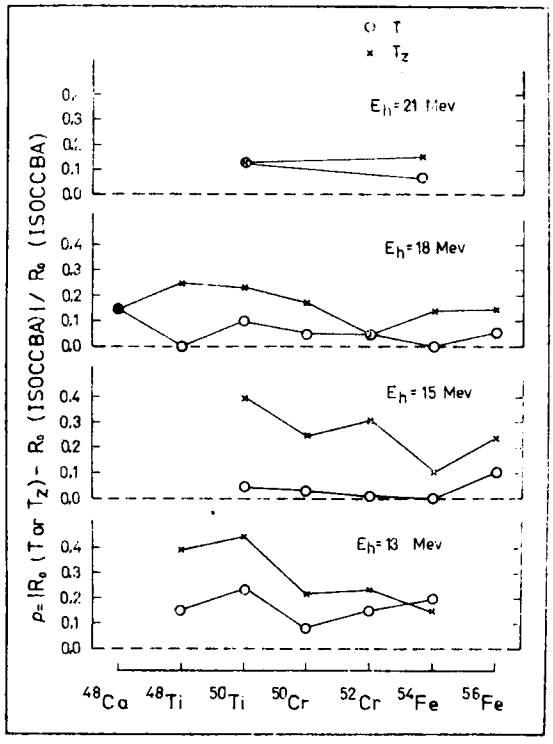

Fig V.3.1 :

The values of ρ from formula (3) as function of the target masses and incident projectile energy in the (τ,n) reaction.

VI. INSTRUMENTATION AND DEVELOPMENT

VI.1 Isotope Separator

VI.1.1 Non-axisymmetric focusing lenses for the beam of a mass-separator.

E.Duering*, D.Otero and A.N.Proto.

An electrostatic lens device was developed to improve the quality of the radioactive sources obtained at the Buenos Aires ISOL (Isotope Separator On-Line) system[1].

The focusing lenses were designed with the aim of correcting the asymmetric spot broadenings and to get well defined spots of less than 1 mm diameter at distances between .5 and 3 m from the focal plane of the mass separator. These sources are required to improve angular correlation and electron conversion measurements.

A view of the lenses is shown in fig.VI.1.1.1 . They are formed by three quadrupolar elements of cylindrical geometry enclosed in a lucite tube and placed on the focal plane of the mass separator.

The potential of a quadrupolar system can be written as:

$$\phi/\phi_0 = k_1(x^2 - y^2) - \frac{1}{12}\left(\frac{d^2 k_1}{dz^2}\right)(x^4 - y^4) + k_2(x^6 - y^6) - \left(15\, k_2 - \frac{1}{24}\,\frac{d^4 k_1}{dz^4}\right)$$

$$(x^2y^2)\,(x^2 - y^2) - \ldots$$

where k_1 and k_2 are determined by electrode shape and length. We preferred cylindrical geometry because it provides easier assembling properties and optical centering. For this case, $k_1 = 1.267$ and $k_2 = 0.41$. This means that the electric field is 27% more effective than in the case of equilateral hyperbolas, although a k_2 value different from zero implies the existence of additional aberrations. The largest distortion points to the gap between adjacent electrodes (see Fig. VI.1.1.2). In our case the gap amplitude is of 5°, a variation between 0° and 20° produces a change in R of about 4%. As under working conditions we used only 30% of the entrance area, the additional aberration term appearing is only 1% of the focusing term in the gap direction.

---

* Present Adress: Weizmann Institute, Rehovot, Israel.

[1]) E.Achterberg, F.C.Iglesias, A.E.Jech, A.Kasulin, E.Kerner, J.Mónico, J.A.Moragues, D.Otero, M.L.Pérez, M.Pinamonti, A.N.Proto, R.Requejo,J.J. Rossi, W.Scheuer and J.F.Suárez; Nucl. Instr. Methods 101, 555 (1972).

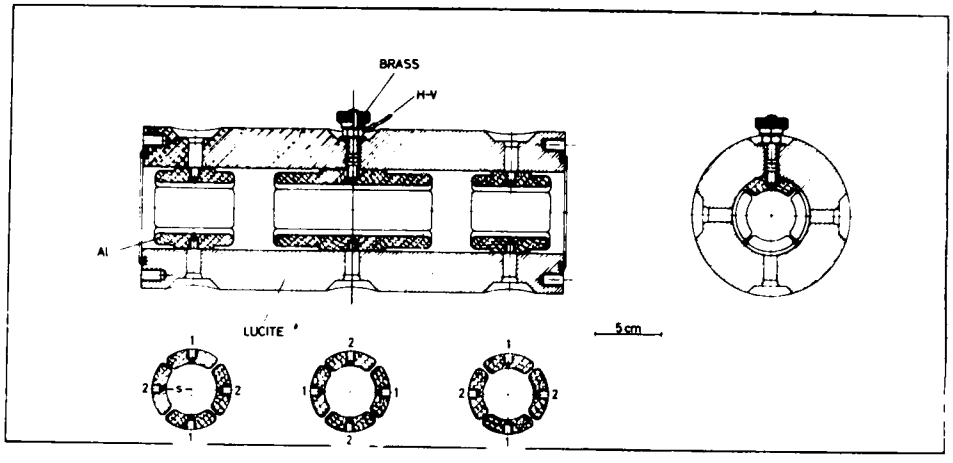

Fig. VI.1.1.1 : Schematic view of the lenses. The operating voltages were: $+V_1 \sim 700$ V and $-V_2 \sim 800$ V. Each electrode can be fed independently.

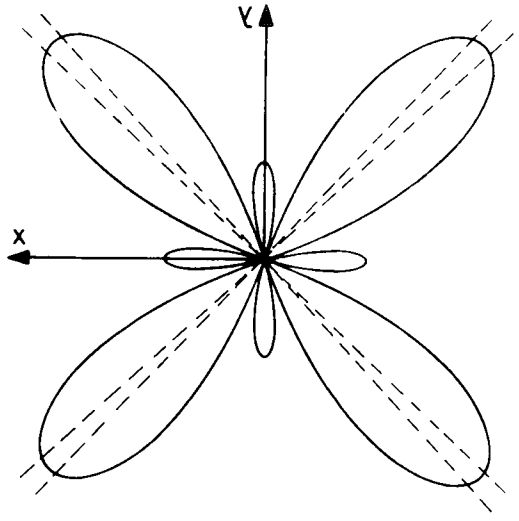

Fig. VI.1.1.2: Plot of R (relation between focusing and aberration terms) under $x^2 + y^2 = 1$ constraint.

VI.1.2 A new ion source with Uranium target for the IALE Project.

R.D'Agostino, H.Huck, C.Miguez, J.Orecchia, M.L.Pérez, M. Ramírez , J.J.Rossi, A.Tersigni and J.Vidallé.

After several years of successful utilization of the Uranil stearate sample[1]) a large effort has been devoted to develop an ion source with an

incorporated Uranium target (see fig. VI.1.2.1).

The finally succesful system consists of a Studsvik type one with extra heater and thermal shields. The Uranium sample, a mixture of Uranium oxide and graphite powder, incorporated as UO_2 in the beginning is transformed to CU after one day running (10-15 hours). It is supported by the classical graphite cloth inside the discharge chamber.

A strong dependence of the shortest half-lives yields with the temperature and with the amount of UO_2 transformed into CU has been observed. Because of our low neutron flux (10^8 n/cm^2 sec), a rather massive uranium target (~5 g) has been used which means longer time of "cooking" and lower yield for short ion gaseous elements.

Anyhow, with our moderated temperatures (2000 °C) it has been possible to obtain activities high enough to make detailed nuclear spectroscopy studies for Cs, Xe, I, Te, Sb, Sn down to halflives as short as 1 sec in the heavy peak of ^{235}U thermal fission.

All the electrostatic lens system has been rebuilt in order to optimize the neutron moderator geometry.

Right now we have started the detailed studies of mass chains 129, 130, 131 etc. and also a survey of activities in the light fission peak is in progress.

---

[1]) E.Achterberg et al.; Nucl. Instr. and Meth. 101 (1972) 555.

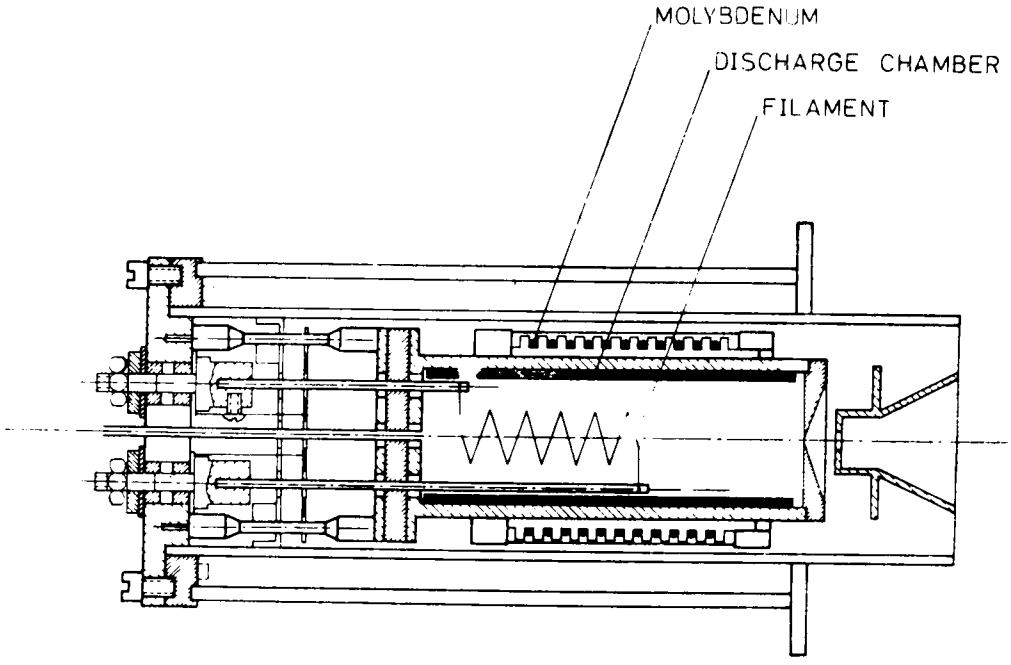

Fig.VI.1.2.1:
Ion source
Scheme

VI.1.3 On the posibilities of an electromagnetic isotope separator on-line with the new 20 UD tandem.

H.Huck, M.L.Pérez and J.J.Rossi.

Taking into account the characteristics of the different ion beams and neutron flux, thermal and fast, that will be available in the new 20 UD tandem several calculations have been performed. Cross sections, thermal and fast fission yields, etc available in the literature as well as typical diffusion rates and ion source efficiences have been used.

These estimations show a very interesting situation with several hundred nuclei available for detailed nuclear spectroscopy studies as is partially shown in fig. VI.1.3.1 .

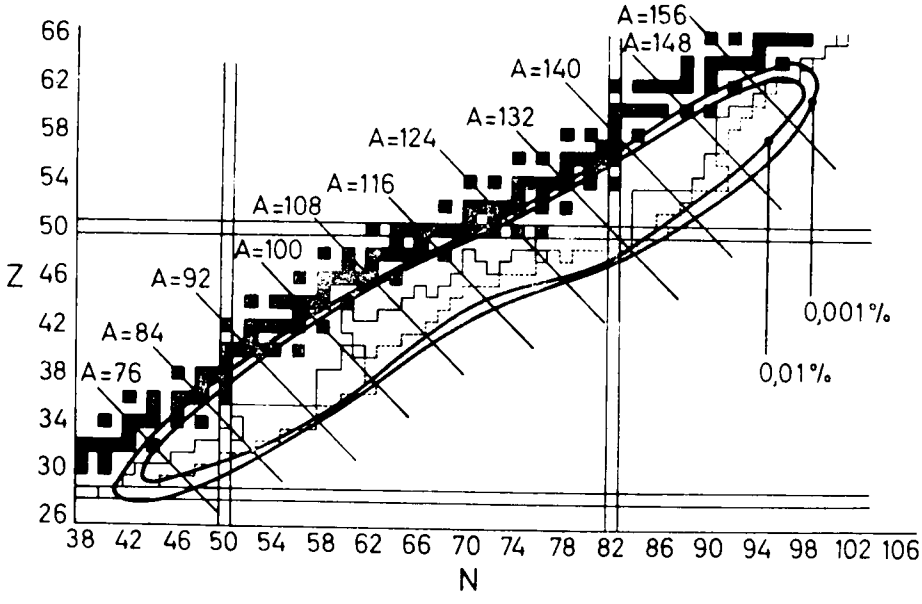

Fig. VI.1.3.1 : Contours of independent fission cross-sections in barn for ^{235}U (n,fission) .

VI.2 Electronic and Computer Hardware Developments

VI.2.1 CAMAC based multichannel analyzer.

J.Milberg, J.Mónico and S.Tau

Originally conceived as a training set-up in CAMAC systems, a multichannel analyzer using a crate and several CAMAC modules is being-developed.

Fig. IV.2.1.1 presents a block diagram where several sections are shown.

a) ACD and ADC CAMAC interface:
The ADC is located in a NIM bin and furnishes digitized analog pulses to the memory control module . At present this is done through its front end input[1] but, using the CAMAC interface, data transfer would be through the dataway. This technique permits direct control of the ADC by the dataway but increases dead times.

b) Memory control module and mass memory:
The control module contains a hardware "add-one" facility suitable for MCHA applications. Three internal registers allow the following functions[1]: overflow detection at any address, overflow detection at a selected Region of Interest (ROI), detection of a matching between any address or ROI address with a present content, and detection of an address overflow.
The signals are a CAMAC LAM (look at me) or an inhibit condition which can be used to stop the accumulation automatically. A control register defines the suitable mode for the above registers and allows to mask selectively LAM and inhibit signals.
Mass memory is connected to memory control module using three private buses (address, data and control) in a typical master-slave arrangement, where the routing, timing and logical control is provided to either write or read data that are stored in the memory.

c) Display modules:
Basically through the point ploter and display driver, display of spectrum is achieved using a storage monitor unit. Vector and character generators could be added to obtain splitted representations or channel contents indication.

d) Autonomous Crate controller:
Is the central processing unit (CPU) which governs the system through the CAMAC bus. Several peripherals help the user to talk with the CPU as shown in Fig. VI.2.1.1 .

A real-time Basic programming language is being used to write the main program, dealing with the display of memory contents. However use of an assembler sub-routine is necessary to have the required speed. Two CAMAC modules[2] (not shown in Fig. VI.2.1.1) and additional software, can be used to write this or any other assembler portions of the program. Also the use of external development systems like Intellec Series II is possible.

A switeh register contained in the Test module will add typical display features in MCHA like: positioning of channel markers at fast or slow speed and blow-up of a selected area of spectrum; or acquisition features (e.g.= change on the mode of overflow registers described above). These last ones could be even conditioned by external signals coming from the experimental set-up, and picked-up by input modules in the same CAMAC crate. On the other hand the CPU can actuate on the experiment by suitable output modules. Then a CAMAC based MCHA offers a closed loop characteristic both by acquisition and control of the data source.

---

1) ORTEC MC024, Memory Control Module, Operating and Service Manual. ORTEC INC.

2) MACAMAC; a modular and interactive instrumentation system with local and high-level software development. Borer Electronics AG.

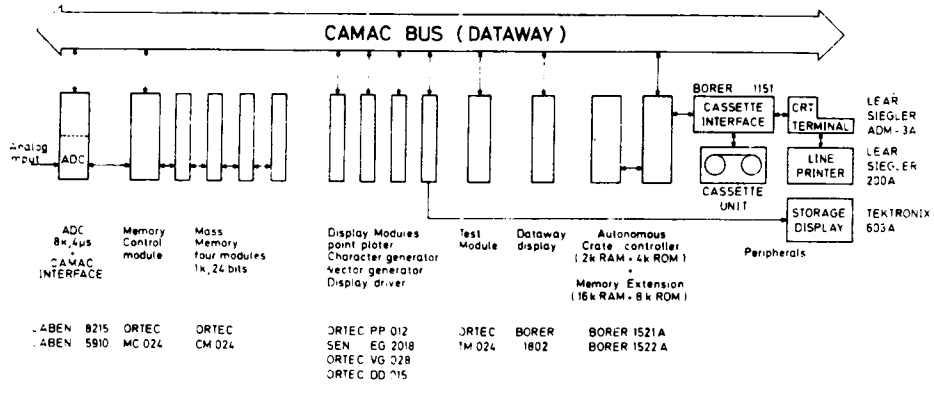

Fig. VI.2.1.1 : Block diagram of a CAMAC based multichannel analyzer.

VI.2.2 Single event recorder[†].

D.V.Camín and S.Keimeesuke[*].

It is normally difficult to observe a single event in an oscilloscope without storage capability. With this equipment in the acquisition mode the single analog waveform is sampled, digitized and stored in a memory.

In the display mode the memory is recirculated and its content is converted into an analog signal through a DAC. A stable, repetitive waveform is obtained capable to be displayed in a single oscilloscope.

Another application is to record a slow moving waveform and, if the memory is later fastly recirculated, the slow waveform can be easily observed in the oscilloscope.

A block diagram is indicated in Fig. VI.2.2.1 .

In order to have a fast analog to digital conversion a special type of ADC was also developed.

Using a low cost DAC a simple ADC is implemented as indicated in Fig. VI.2.2.2 . Here the limitation is speed, as the settling time is 1 µs and the total conversion time for a large pulse should be 256 µs.

The modified version of this ADC uses two clock frequencies and two counting sequences, while the output voltage of the DAC is far from the input voltage, the clock frequency is high and the counting sequence is 0,8, 16,... When V_0 is within a small window, the clock frequency is reduced and the steps are produced sucessively. In this way, the settling time is respected and the conversion time is reduced to aprox. 10 µs. (Fig. VI.2.2.3).

[†] This project was developed at IAEA Nuclear Electronics Course, Dublin (Rep. of Ireland), 1979.

* Office of Atomic Energy for Peace Bangkok 9, Thailand.

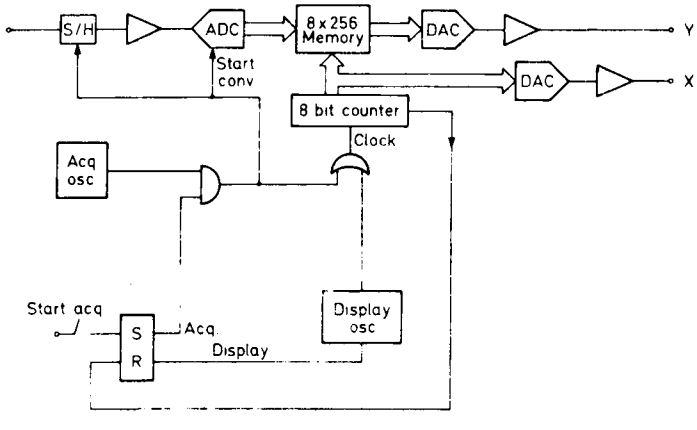

Fig. VI.2.2.1 :

Single event recorder block diagram.

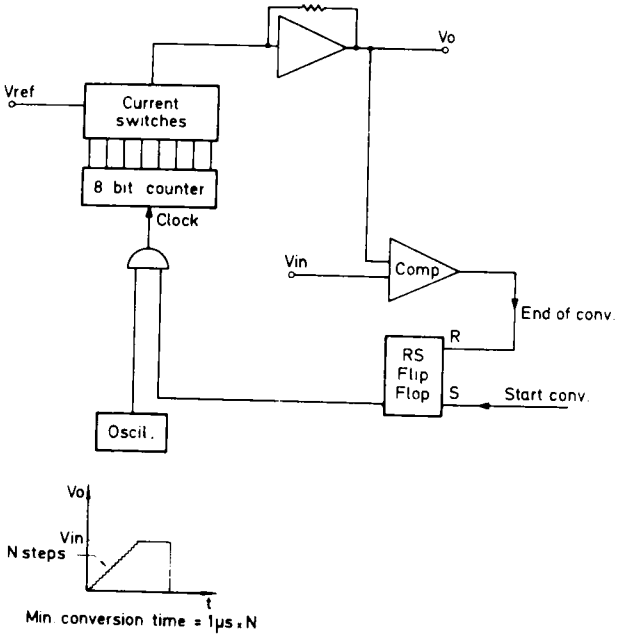

Fig. VI.2.2.2 :

Conventional ADC block diagram.

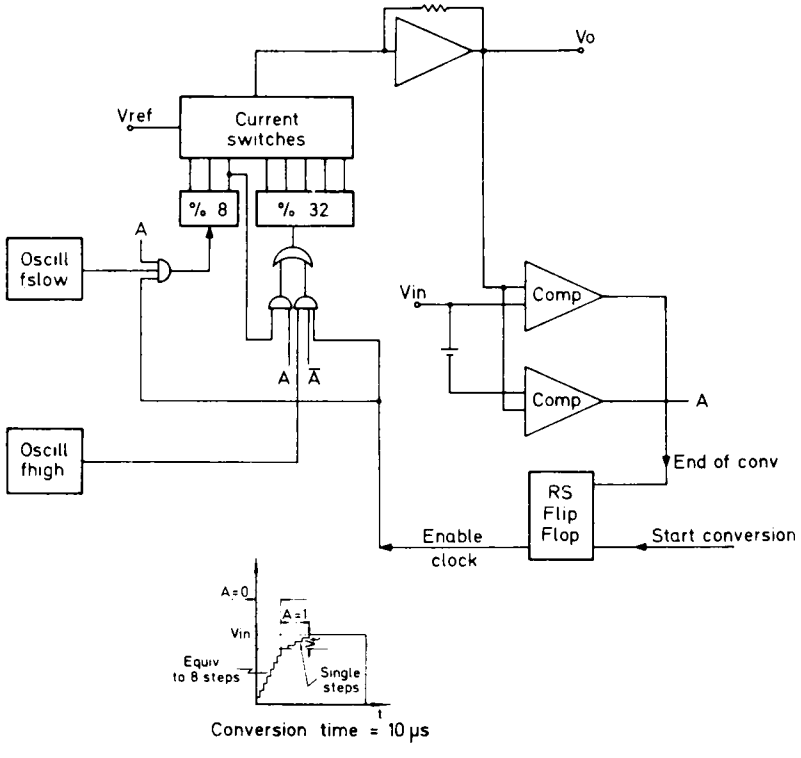

Fig. VI.2.2.3 :

Modified ADC .

VI.2.3 Analog Data Transmission Link.

D.V.Camín, M.Satinosky and S.Swiszcz.

Several power supplies of the isotope separator are mounted on a tray polarized at 150 KV with respect to ground.

For that reason it is not possible to have the meters located on the operator console.

In order to bring the different voltages to the console, a multiplexed system with voltage to frequency converters and optical

isolation was developed.

The block diagram shown is self-explanatory but some points must by remarked (Fig. VI.2.3.1).

1. V/F converters have been implemented with 555 and they are satisfactory linear.
2. Time slot is 10 ms and it is obtained from the line.
3. Frequencies of V/F converters have been selected in order to get a consistent indication in the 3 decade counter.
4. Display is disabled while the counter is being updated and no flickering is noticed.
5. A sync pulse is generated connecting to Vcc one input of the multiplexer. A logic 1 is present during one time slot and no other situation can generate it.

At present development is being finished and the system will be installed soon.

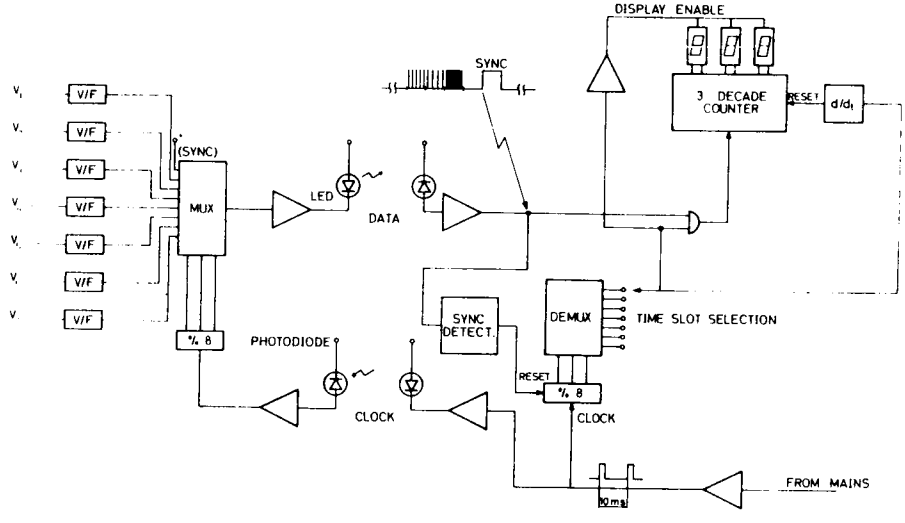

Fig. VI.2.3.1 : Analog data transmission link block diagram.

VI.2.4 Interface between a multichannel analyzer and a programmable calculator†.

D.V.Camín and R.Tzolov*.

The use of a programmable calculator as an output device of a MCA is

feasible using this interface. Basically, this idea is to convert the channel content presented by the MCA as a 20 bit pure binary number into a 6 decade BCD number. The BCD counter sequentially drives reed relays connected to the corresponding calculator digits (Fig. VI.2.4.1).

In order to save integrated circuits, conversion is done in the following way: a 20 bit pure binary counter is loaded in paralell with the channel content. Then it counts down a clock pulse which, at the same time, makes the BCD counter to count up. When a zero is reached in the binary counter, the count stops. The content of the BCD counter is the channel content expressed in BCD.

Afterwards the BCD counter is read sequentially, decoding each decade and driving a corresponding reed relay. A hardware logic controls the process giving a pulse to advance the channel, and storing the number in the calculator, then preparing it for the next channel (see Fig. IV.2.4.2).

A special control logic to perform many other functions is being developed by Mr. Tzolov.

---

† This project was developed at IAEA, Nuclear Electronics Course, Dublin (Rep. of Ireland) 1979.

* Institute of Nuclear Research and Energy, 1113 Sofía, Bulgaria.

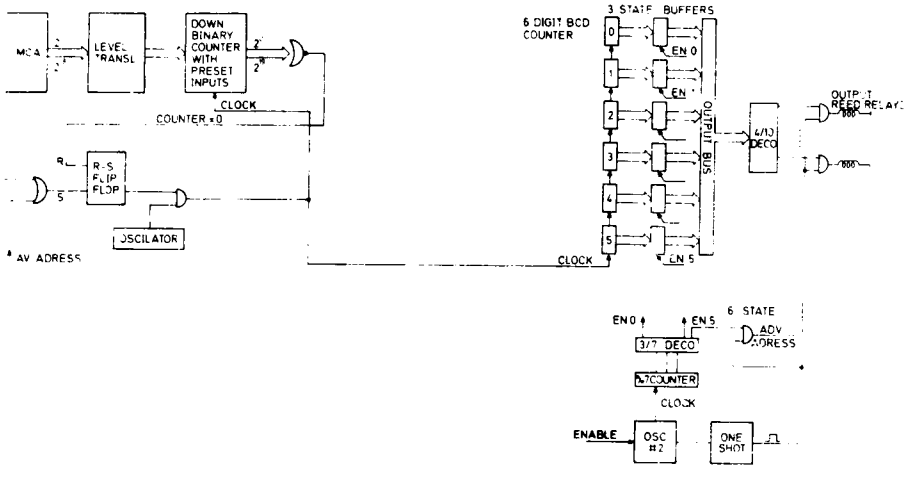

Fig. VI.2.4.1 : Interface block diagram.

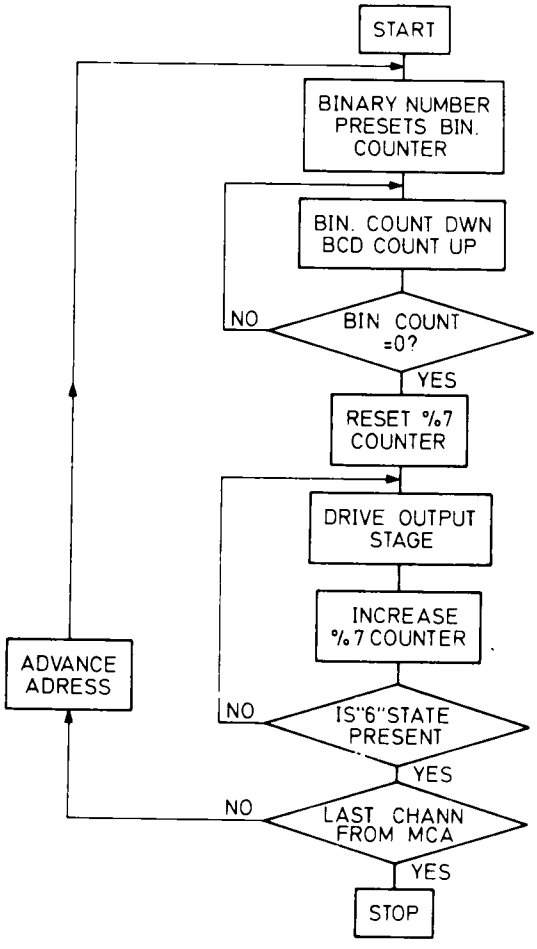

Fig. VI.2.4.2 :

Interface flow chart .

VI.2.5 Interface between a Multichannel analyzer and a computer.

D.V.Camín, J.Mónico and S.Swiszcz.

Besides permitting the transfer of memory data between the equipments mentioned above, this interface allows several multichannel's functions to be controlled by the computer.

Then, change from store to display mode, memory clear and data routing are achieved at the multichannel by remote control of the computer, which is separated some 30 meters.

Also, it is possible to transfer a certain region of interest (ROI) of data by using adequate software (see next contribution).

In Fig. VI.2.5.1 a block diagram is shown. A multiplexer switch is used in order to adequate MCHA word length (24 bits) to computer input register (16 bits).

Encode and Device Flag lines from the computer, are used as handshake signals to govern data transfer.

A front panel rotary switch permits the choice of a zone configuration. Then, routing is achieved using three assigned lines from the output section or

the 16 bit duplex register.

Opto-coupling techniques were used throughout, in order to assure complete electrical isolation between the two equipments.

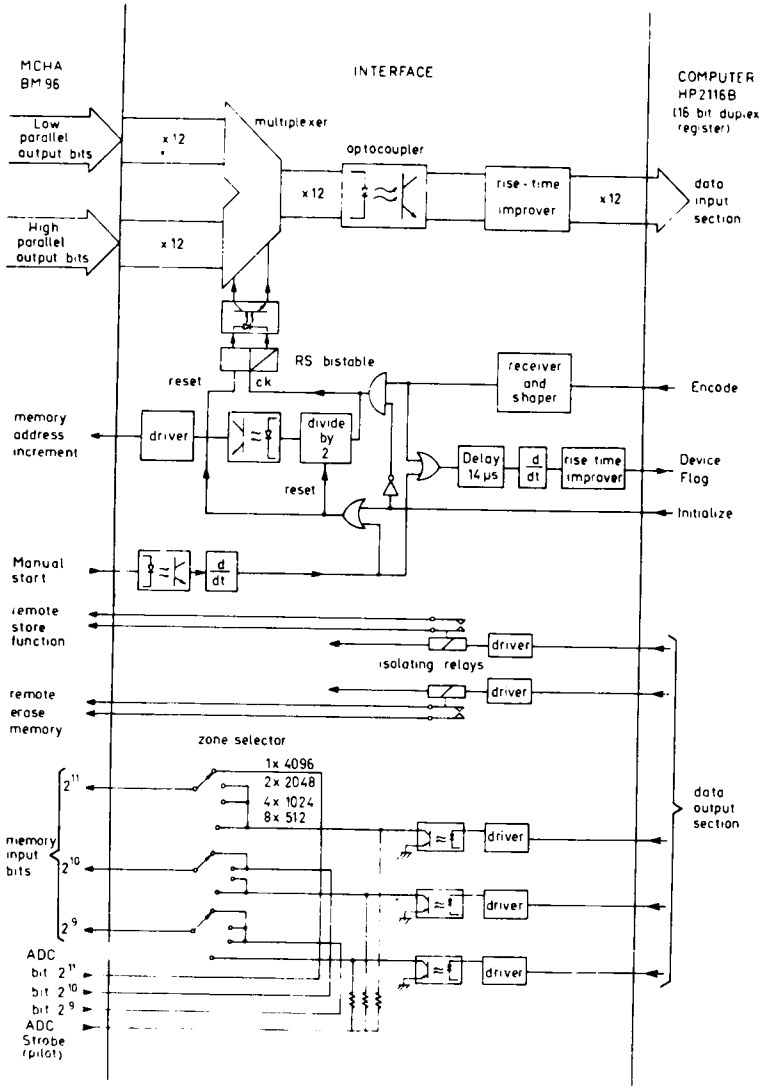

Fig. VI.2.5.1 : Interface block diagram

VI.2.6 Remote operation of an Intertechnique BM96 Multichannel Analyzer.

E.Achterberg.

A facility for the remote operation of an BM96 multichannel analyzer from the console of our HP 5406B nuclear data acquisition system has been developed. The design and constructuion of the corresponding electronics for the hardware interface was performed by the Electronics Group of the Physics Department (see preceding contribution).

The interface connects to a 16-bit parallel bidirectional input/output card in the I/O channel of the HP2116B minicomputer included in the HP 5406B. Data transfer from the multichannel analyzer to the computer memory and control information to the analyzer is by programmed I/O. Operations which have been included are: a) data transfer from arbitrary channel groups in the analyzer to selected portions of the data acquisition system's display memory; b) erasure of analyzer spectrum; c) data accumulation in the multichannel analyzer. Selection of analyzer memory block size is by hardware switching from 8 x 512 channels to 1 x 4096 channels, while routing is under software control. Provision is made in the software for "multi-spectra" mode, with accumulation stepping automatically from one storage zone to the next after a specified accumulation time, with negligible switching time. Spectral data may be either simply transferred to the computer memory, replacing whatever may be contained in the storage region involved, or it may be added to or subtracted from the existing spectrum.

VI.2.7 The data acquisition system for the TANDAR Project.

E.Achterberg, A.Filevich and D.Otero.

Planning has been completed for the preliminary version of the data acquisition system to be provided for the experimental physicists who are going to use the 20 MV Tandem Accelerator of the TANDAR Project, to become operational in early 1982.

The present configuration tries to include as much as possible existing equipment and to simplify the installation of future improvements. It was desired that the system should be able not only to provide data acquisition services properly, in the most versatile way possible, but also to satisfy, in a concurrent manner, the needs for most of the interactive data handling and processing required by the analysis of the collected experimental information.

Figure VI.2.7.1 shows a sketch of the tentative layout of the planned system. Part of the hardware has already been ordered and is to be installed at a temporary site in early 1980.

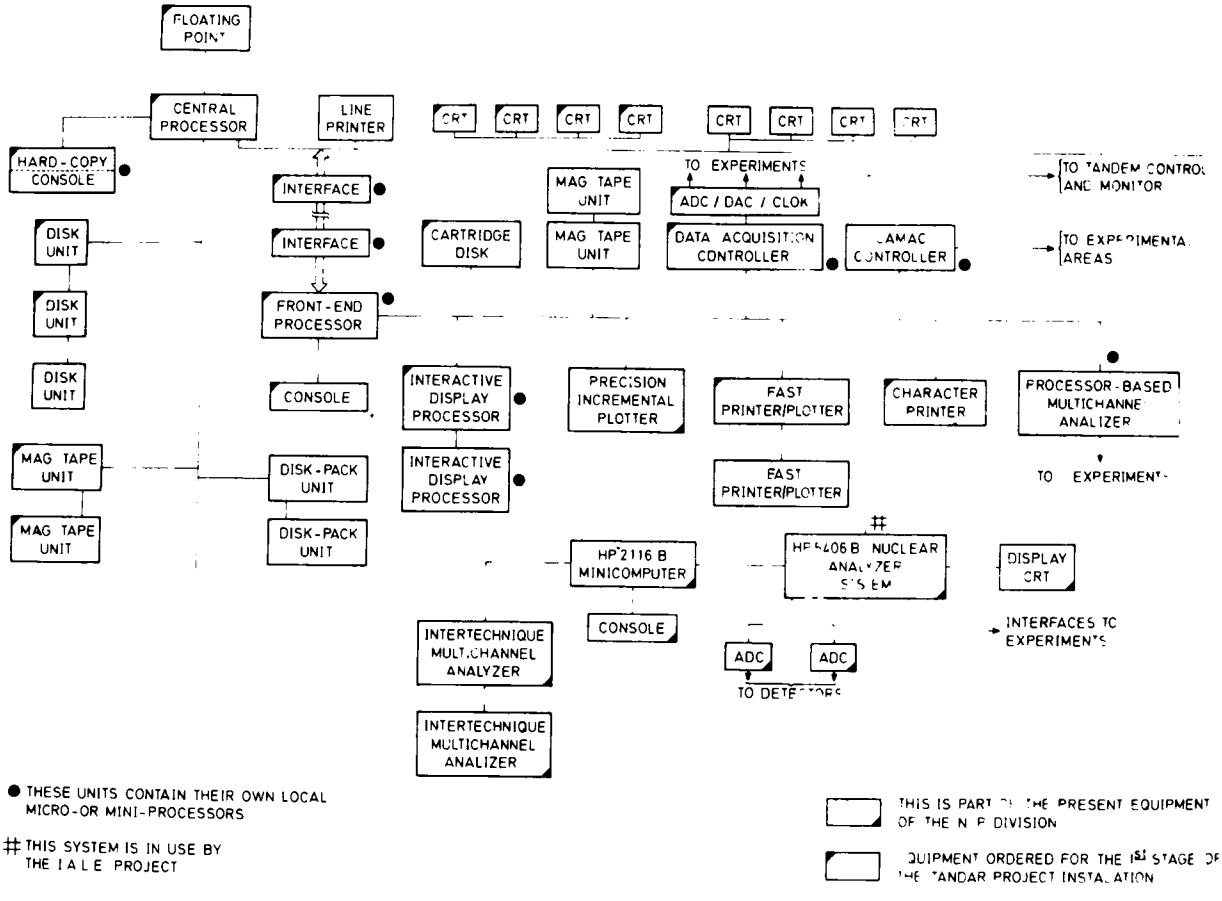

Fig. VI.2.7.1

VI.3 Experimental facilities at the Sinchrocyclotron

VI.3.1 Development of an on-line conversion electron detection system†.

M.Debray, J.M.Riso and A.J.Kreiner.

In order to be able to measure low energy conversion electrons it is necessary to place the detecting device into the vacuum thus eliminating all windows between the detector and the target. In addition and since the surface barrier Silicon detector used has to be cooled down in order to achieve a good resolution one has to build a system capable of providing isolation from atmospheric pressure when operations are performed at the target chamber. For these purposes a telescopic system was constructed which allows the detector, installed at the end of a cold finger, to be moved forward to be used and backwards behind a valve when, for instance, a target

has to be changed. In order to minimize condensation problems at the detector's surface a trap is placed in front of the device having only a small aperture of the size of the sensitive zone. Fig. VI.3.1.1 shows a picture of the assembled system.

---

† This work is part of the Licenciatura Thesis of M.Debray.

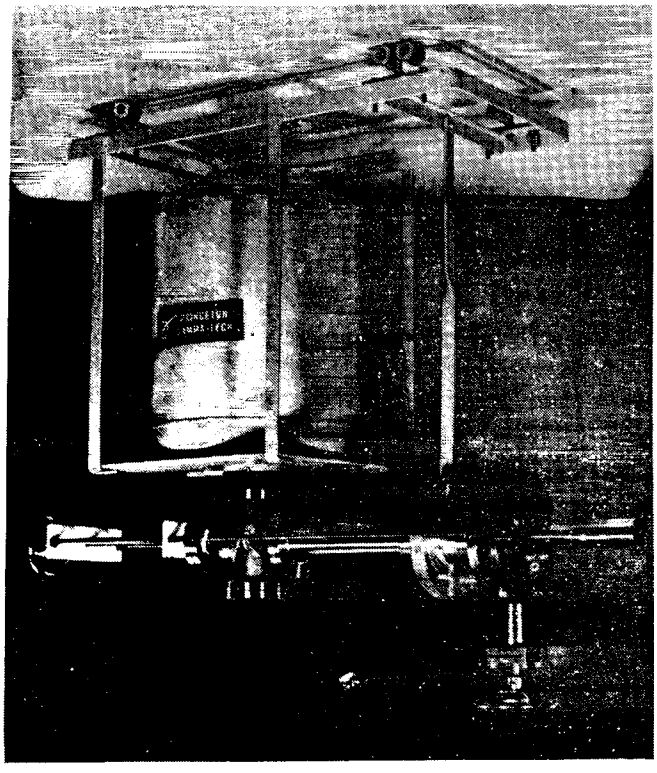

Fig. VI.3.1.1 :

View of the detection system

VI.3.2 Identification of Heavy-Ions.

A.N.Proto, J.M.Riso and D.Otero.

With the aim of identifying heavy-ions, experiments on ^{235,238}U(d,pf) and ^{235,238}U(α,α'f) were made. To perform them it was necessary to develop: a) a technique to prepare thin Uranium targets, b) a TOF technique, c) a detector to measure dE/dx.

The first point was covered by the Electrochemical Division of the CNEA. Briefly, the Uranium is electrodeposited[1] on a metallic backing suitably chosen to minimize background production. In Fig. VI.3.2.1 the results for different electrodeposition times are shown. The target with 10 min. exposure is 0.4 μm thick (~1 mg/cm^2). The fragments were detected with a Si detector 80 μm thick.

In the TOF method for M determination, thin scintillator foils (Pilot B) were used as zero time detectors. Electronic resolution time for a ^{241}Am α source was about 450 ps.

For dE/dx measurements a small aluminium gaseous chamber (60x40x10 cm) was constructed. Fig. VI.3.2.2 shows the resolution for α particles, when used as total energy detector.

---

1) J.J.Magallanes, A.Caridi; VIIth Meeting of the Argentine Soc. for Nuclear Technology, (San Rafael, Mendoza, 1978).

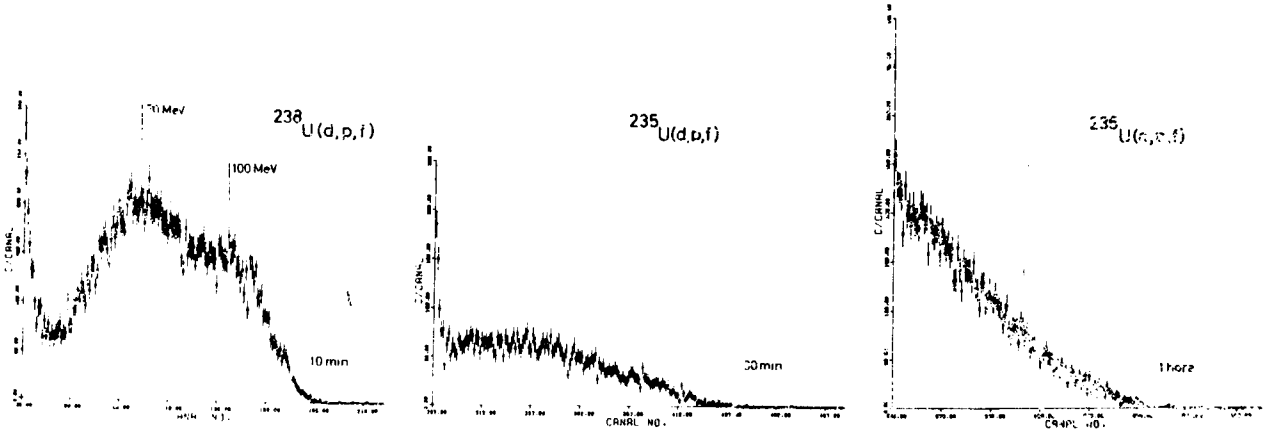

Fig. VI.3.2.1:

Yield of the reactions used in this work. The first graph shows the two fission fragment peaks.

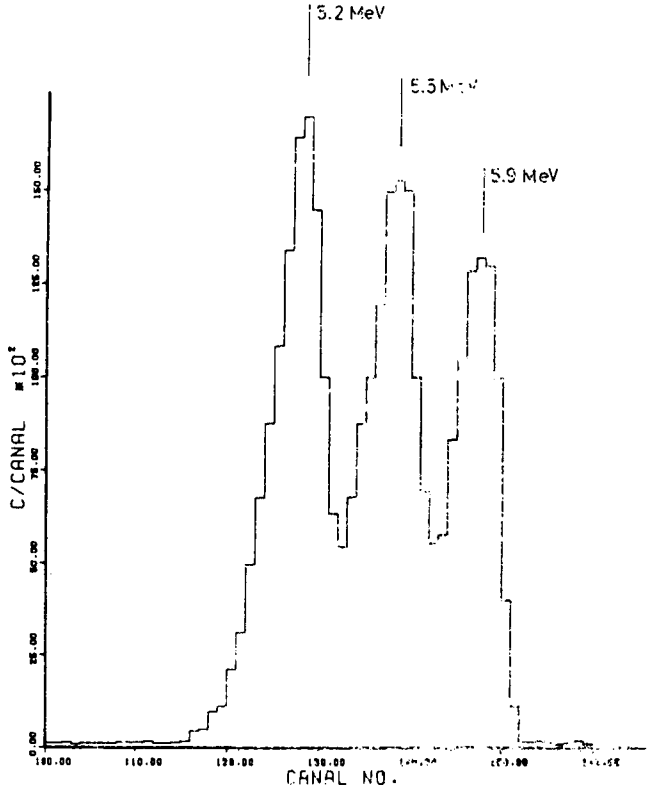

Fig. VI.3.2.2:

The resolution of the gaseous detector when filled with P-10 and used as a total energy detector (about 4.5%) for 5.8 MeV α particles.

VI.4 Ge (Li) Detectors

VI.4.1 Ge(Li) Detectors Fabrication Techniques.

G.Martí and C.Giménez.

Several Lithium drifted true coaxial Germanium detectors were constructed and tested following the usual Lithium drifting techniques.

The material employed was supplied by HOBOKEN and manufacturer specifications were: resistivity between 15 Ωcm and 25 Ωcm, minority carrier lifetime from 600 μseg up to 1150 μseg and etch-pit density ranging from 1900-3500/cm^2 depending on the particular crystal used.

Lithium diffusion[1] was carried out at 400 °C in Argon atmosphere; previously, Lithium was evaporated on the periphery of the crystal surface when vacuum in the diffusion chamber was less than 1 x 10^{-5} mm Hg. Diffusion depths were measured by Copper staining[2] and diodes characteristics were checked after etching crystal surfaces. Another diffusion quality control procedure was the sheet resistance test by the four points probe method[3,4].

The Lithium drift main process[5] was carried out at 24°C in boiling MF-Freon[6] and constant power dissipation during 12 or 17 weeks, depending on crystal sizes and drift-depth desired several diffusions were made in between when it was found necessary to achieve typically 14 mm drift-depth (intrinsic zone) and a fresh diffusion was always done before the clean-up drift at lower temperatures[7]. Those were carried out -25 °C during 2 weeks until theoretical detector capacity was reached at some reasonable voltage (300 or 500 volts).

Previous to mounting, the devices were carefully lapped and etched during 3' in 3:1 (NO_3:FH) or 3:1:6% by volume (NO_3H:FH : NO_3H red fuming), thoroughly rinsed in deionized water (>15MΩ) and short dips in methanol-hidrogen peroxide-methanol were given to obtain the best surface treatment. Finally, they were blown quickly with a jet of dry nitrogen and loaded in their cryostat.

After ≈2 hours of turbo molecular pumping they were put in the liquid-nitrogen container until testing.

The results are summarized in Table VI.4.1.1 where 7 detectors, its remarkable characterisitcs, important features during drift and performances are shown.

Fig. VI.4.1.1 shows γ-spectra of the decay of excited states from 131

mass (^{131}Sn) isotopes populated by β^- decay measured on line with 5B detector.

---

1) A.J.Tavendale; IEEE, Transactions on Nuclear Science NS-13 N°6 (1966).

2) E.J.Rivet; UCRL 18403 (1968).

3) L.Valdés; Proc. I.R.E. 42 (1954) 420.

4) W.L.Hansen y B.V.Jarrett; Nucl. Instr. and Meth. 31 (1964) 301.

5) E.M.Pell; Jour. of App. Phys., Vol 31, N°2 , 291.

6) F.Cappellani et al., Nucl. Instr. and Meth. 37 (1965) 352.

7) F.Cappellani et al., Nucl. Instr. and Meth. 47 (1967) 121.

Table VI.4.1.1

CRYSTAL	RESISTIVITY	MINORITY CARRIER LIFE TIME	ETCH PITS DISLOCATIONS	DIFFUSIONS NUMBER	TOTAL DRIFTING TIME	DRIFT-DEPTH	TOTAL SYSTEM RESOLUTION (1.33 MeV)	CRYSTAL VOLUME	EFFICIENCY (1.33 MeV) REL. INA (3"x3")
	Ω cm	μs	N/cm^2	n	days	mm	keV	cm^3	%
5B	20	1150	2500	9	140	13	2.8	60	7.5
7	25	750	2900-3500	6	91	15.5	3.4	60	6
8A	19	600	1800-3200	9	166	15	5.5	55	2
11A	15	600	1900-2000	4	73	12	3.5	40	4.6
11B	15	600	2000-2100	4	110	14	5.5	35	2.5
11C	15	600	2100-2200	5	72	13.5	4.8	35	4
11D	15	600	2200-2300	3	50	11	4.2	38	3.5

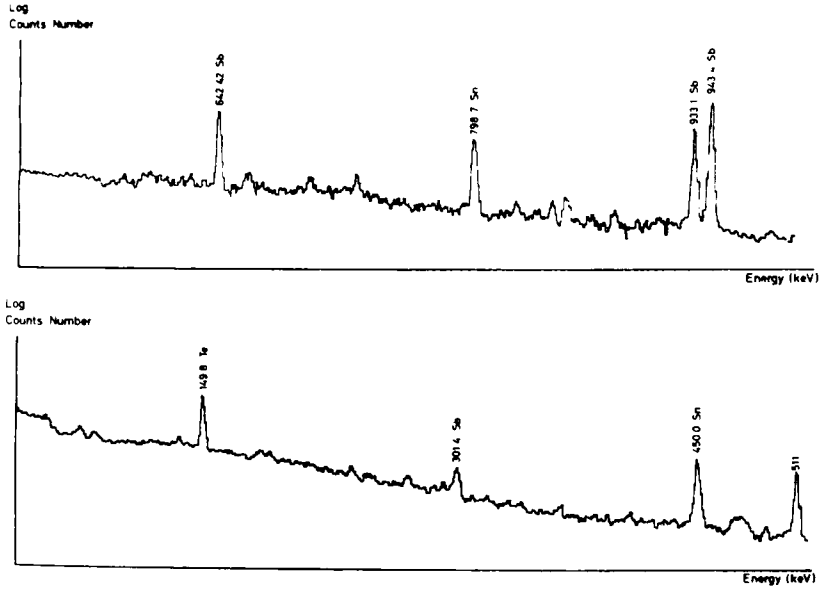

Fig. VI.4.1.1: γ-spectra of the decay of excited states from 131 mass (^{131}Sn) isotopes populated by β^- decay obtained with 5B detector and analyzed on line.

VI.4.2 Surface conductivity effect on the efficiency and resolution of Ge(Li) coaxial detectors.

G.Martí and E.Caselli*.

Surface conductivity is one of the factors that limits the resolution and efficiency of Ge(Li) detectors. When the surface conductivity σ_s [1,2] is different from the volume conductivity σ_v it is not possible to apply the necessary voltage to have an electric field greater than 1000 V/cm in the compensated zone to minimize noise contribution from carrier collection. The breakdown voltage (detector operation voltage) is practically determined by the surface leakage current noise. Another consecuence from σ_s and σ_v discrepancy is the efficiency degradation specially for $E_\gamma < 600$ keV [3]. As surface conductivity is set by etching or another method it is necessary to investigate which kind of surface conductivity is obtained after crystal etching and surface treatment.

The experimental method employed for determining the surface conductivity type consists in obtaining the different ^{241}Am spectra (E_γ=59.6 keV) resulting from collimated irradiation paralell to the crystal simmetry axis in several positions between the p and n regions. For an n-type sur-

face conductiviy (n-channel) as shown in Fig. VI.4.2.1.a we get three different spectra as in Fig. VI.4.2.1.b . Near the n-contact there is only one peak, in the intermediate position there are two, one in the same position as before (principal peak) but with smaller area, and the other one at lower channels (secondary peak). Finally near the p-region the principal peak has a diminished area and the secondary peak becomes very wide and appears as a background. Plotting the full energy peak (FEP) given by the area of the principal peak against the irradiation position one gets a curve which shows a maximum on the n-side. For a p-type surface channel the maximum is near the p-region.

For determining σ_s on HP-Germanium detectors it is only necessary to plot the FEP irradiation position as many authors have done, because only one maximum appears on the curve. For Ge(Li) detectors, on the contrary, one can sometimes observe two maxima near each contact. For getting σ_s it becomes necessary to obtain some spectra with collimated radiation to observe in which region approximately the secondary peak appears. If it occurs near the n-contact or p-contact there is an n-type or p-type surface channel respectively.

Seven detectors were scanned 5B,6B,11A,11B and 11D (constructed in our Lab.) and two ORTEC models 0-0523 and 0-1021.

In Fig. VI.4.2.1.c and VI.4.2.1.d FEP is plotted vs irradiation position for several detectors. 5B and 11D clearly show a p-type surface conductivity, 0-1021 has an intrinsic one showing no maximum, finally 0-0523 shows a curve with two maxima being is necessary to observe the secondary peak position appearance in order to determine the σ_s type. Fig. VI.4.2.1.c shows different spectra from 0-0523 and 11D detector for comparison. Being $\lambda=x/d$ (x: distance from p-contact to irradiation position, d: distance from p-contact to n-contact) we can see that for the 0-0523 detector the secondary peak appears in the neighbourhood of the n-contact ($\lambda=0.25$ $\lambda=0.33$) which confirms that it has a p-type surface conductivity.

In Table VI.4.2.1 two types of etching and different surface treatments employed are listed. The results would indicate that for longer etching times σ_s would be of n-type. As the result of an etching and subsequent rinse is a statistic one we are going to test more detectors in order to verify if the alternative plays an important role in Ge(Li) detector fabrication.

* Present address: Facultad de Ciencias Exactas y Naturales, U.N.B.A.

1) E.Baldinger and E.Haller; Helv.Phys. Acta 43 (1970) 833.

2) R.Dinger; Helv. Phys. Acta 47 (1974) 220.

3) H.L.Malm and R.J.Dinger; IEEE Trans. on Nucl. Sci. Vol. NS 23 (1976) 76.

Table VI.4.2.1

Detector	Etching	Etching time	Rinse	Surface treatm. Meth H_2O_2 Meth	Surface conductivity
5B	3:1	7'	deionized water	1' 20" 1'	p type
11A	3:1	3'	"	1' 25" 1'	n type
11E	3:1	8'	"	1' 10" 1'	p type
11D	3:1:6%	3'	"	1' 30" 1'	p type
6B	3:1:6%	3'	Methanol	- 5" 1'	"strongly" p type
0-0523	———	——	——	————	n type
0-1021	———	——	——	————	intrinsic

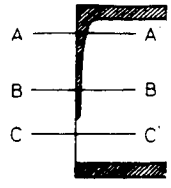

Fig.VI.4.2.1a: n-type surface channel detector. $\bar{A}A'$, $\bar{B}B'$ and $\bar{C}C'$ indicates three differents 60 keV collimated beam irradiation positions and the differents spectra obtained in each position.

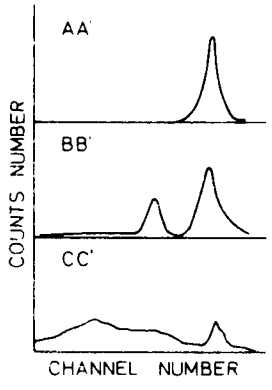

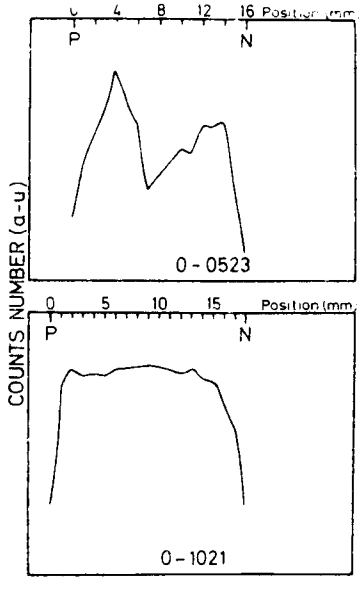

Full energy peak (FED) vs. irradiation position for 0-0523 and 0-1021 detectors. The first one shows a curve with two maxima we can't assure which surface conductivity type it his, the second shows a curve with no maximun the n it has an intrinsic surface conductivity.

:Fig.VI.4.2.1b

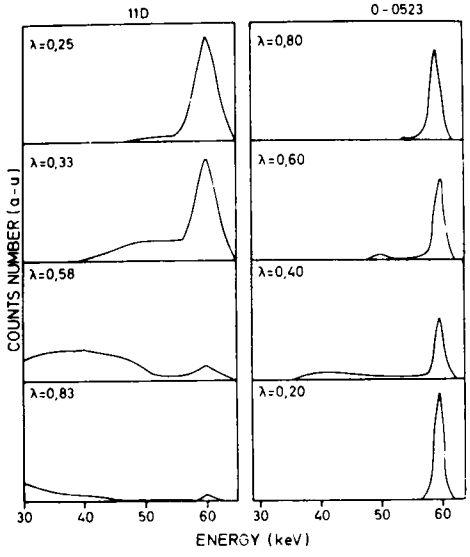

Fig. VI.4.2.1c: several spectra obtained with 60 keV (Am) collimated radiation in differents positions between n and p regions. λ is defined $\lambda = \frac{x}{d}$ being x irradiation position measured from p-contact and d the distance from n contact to p contact.
In 0-0523 detector secondary peak appears near the n-contact then it has n-type surface channel. In 11D detector it appears near the p-contact then it has a p-type surface channels.

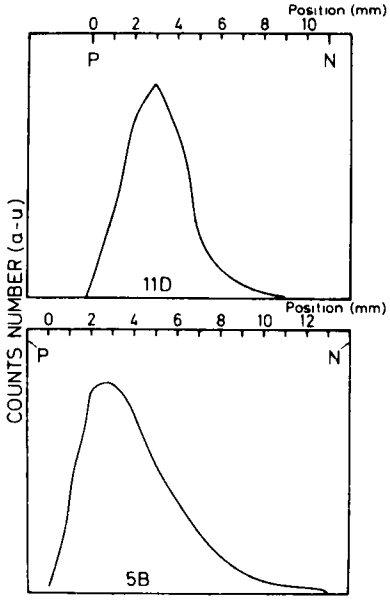

Fig.VI.4.2.1d: Full energy peack (FEP) vs irradiation position for 11D and 5B detector. As the maximun in near p-contact we conclude they have a p-type surface channel.

VI.5 Liquid Nitrogen Production

VI.5.1. Maintenance of the Liquid Nitrogen production facility

J.Bustos, R.Schiavino, J.Laffranchi and J.Nicolai

Different kinds of repairs on the liquid nitrogen machines were made, in order to achieve uninterrupted provision of liquid nitrogen for the whole Nuclear Physics Department and even other sections at CNEA, reaching a volume of 60.000 lts during the 78-79 period.

VI.5.2 Assembling of a new liquid Nitrogen machine with associated pump equipments and storage tank.

J.Nicolai and J.Laffranchi.

The installation of a new liquid Nitrogen machine with a rate of production of 28 lts per hour has been completed. As a consequence the existing plant has increased its production from 30.000 to 100.000 lts per year.

In addition we hope, in the near future, to double the liquid Nitrogen storage capacity which at present is roughly 3.000 lts. Besides that, a termotank mounted on a track with a capacity of 1.500 lts will be added soon, in order to increase liquid Nitrogen availability for CNEA's users.

VI.6 Gas handling system for the 20UD TANDAR Project.

N.Fazzini, J.Nicolai, H.González and R.Requejo.

The functions of this system are: to fill the accelerator tank with the dielectric gas after air removal; to continuously circulate the gas through absorption beds to remove moisture and breakdown products; to extract heat generated within the accelerator tank and to remove and store the SF_6.

The design of the plant has been based on the following requirements:

a) The storage capacity of the plant has to be sufficient to provide an accelerator tank gas pressure of 10 Kg/cm^2 abs.

b) The SF_6 charge and discharge rates have to be compatible with both filling and emptying times of no more than 15 hs.

c) Contamination of the dielectric gas during handling operations has to be eliminated as much as possible by the use of oil-free pumps.

d) All plant operations have to be remotely controlled from a central console with sequential control facilities.

e) A policy has been adopted of using multiple units where possible, so that plant operation can be continued at reduced speed in the event of a breakdown.

A gaseous phase storage system has been adopted based on the following

considerations:

1) It is more simple and safe to operate.

2) The plant has the capability of storaging and handling gas mixtures.

3) The higher cost of the storage tanks is almost compensated by saving costs in compressors, piping, accesories and operation.

The system can be divided into three main parts:

a) Pressure vessel.

b) Gas handling plant.

c) Storage tanks.

The pressure vessel will be located in the accelerator tower.

The gas handling plant will have a special building near the tower and the storage tanks will be mounted outside this building.

Solid State Physics

Vibrational Spectroscopy
Crystal Structure and Phase Transformations
Mössbauer Spectroscopy
Theoretical Solid State Physics
Development and Services

I. VIBRATIONAL SPECTROSCOPY

I.1 Vibrational properties and crystal structure of ortho-diiodobenzene[+] .

C.Faerman and H.Bonadeo.

The unit cell parameters of the crystal of orthodiiodobenzene were determined by X-ray difraction. The study was incomplete, and proposed two space groups, C_{2h}^1 or C_{2h}^2 for the crystal structure.

We have measured the infrared and Raman spectra of the crystal from 275 to 80 °C.

No phase transition was detected in this temperature range. The spectroscopic evidence may be summarized as follows:

i) The threefold symmetry of the molecule, which belongs to the C_{3v} point group, is lowered, as indicated by the appearance of the forbidden a_2 bands.

ii) Some bands are split both in the i.r. and Raman spectra, and the frequencies are non-coincident, indicating the presence of a center of symmetry, and four molecules in the unit cell, at least.

iii) Nine bands were observed in the Raman spectrum of the lattice mode region, pointing again to a centrosymmetric unit cell with 4 molecules.

This information indicates that the unit cell is indeed monoclinic, with 4 molecules in general sites, and factor group C_{2h}; of course, optical spectroscopy does not distinguish space groups with the same factor group.

In order to obtain more information, we performed packing calculations, using the existing unit cell parameters, and atom-atom potential parameters for the intermolecular force field. In spite of many trials and starting points, it was impossible to pack the molecules in the unit cell with symmetries corresponding to the C_{2h}^1 or C_{2h}^2 space groups. Of the remaining primitive unit cells with C_{2h} factor group, C_{2h}^5 is the most probable, mainly because about half of all known organic materials crystallize in that space group. When this symmetry was used, we obtained a rapid convergence of the structure to reasonable values, yielding normal atom-atom distances and a packing energy of the order of that of similar compounds.

In order to check the consistency of the obtained structure with spectroscopic data, we have performed a lattice vibration frequency calculation, using the same atom-atom potential as for the packing calculations. Although no detailed comparison of calculated and measured results is possible due to the lack of a complete asignment of the bands, the overall agreement is good, confirming the results of the packing calculation.

In conclusion, we have shown that the crystal structure of orthodiiodobenzene is most probably C_{2h}^5 ($P2_1/c$) and obtained approximate atomic positions; the structure is compatible with existing unit cell parameters and spectroscopic evidence, and with packing and lattice vibration frequency measurements.

---

† Chem. Phys. Letters (in press)

I.2 Intermolecular forces in brominated benzene crystals.†

E.Burgos and H. Bonadeo

A set of potential parameters of the atom-atom type has been refined taking into account heats of sublimation, structural equilibrium conditions and lattice vibration frequencies of a series of brominated benzene crystals. The atom-atom potential functions chosen for the calculation are of the Buckingham form:

$$V_{ij} = -A\, r_{ij}^{-6} + B \exp(-C\, r_{ij})$$

where r_{ij} is the distance between atoms i and j belonging to different molecules, and A, B and C depend on the nature of atoms i and j. The refinement procedure is discussed in ref.1, and the calculation method for the lattice frequencies in ref.2. One new feature, regarding the intermolecular energy calculation, has been introduced in the present calculation: at a cut-off distance of 5-6 Å, the lattice frequencies and equilibrium conditions are fully calculated, whereas only from roughly 65-80% of the intermolecular energy, depending on the crystal, has been taken into account, and it is necessary to consider interactions of atoms up to 12-25 Å apart to achieve convergence. Since this adds considerable computation time to a lengthy

calculation we have used a simple extrapolation method which allows an analytical expression of the defect energy. The exact calculation is carried out up to a certain cut-off distance r_o , beyond which it is supposed that each atomic species is distributed uniformly in space. We have verified in a large number of crystals that for $r_o \geq 5$ A , this extrapolation method is accurate within 1%.

In the present refinement we have used a set of 44 data, including 28 experimentally assigned frequencies correspoding to optically active lattice vibrations of the crystals of $1,3,5\text{-}C_6H_3Br_3$, $p\text{-}C_6H_4Br_2$ and $p\text{-}C_6D_4Br_2$, 15 equilibrium conditions corresponding to these crystals and to $1,2,4,5\text{-}C_6H_2Br_4$ in its β and γ phases, and the heat of sublimation of $p\text{-}C_6H_4Br_2$. The rigid body approximation has been used throughout, since it was verified that lattice modes mix only weakly with internal frequencies. We have taken Williams'[3] parameters for the CC, CH and HH interactions, and are left with 9 parameters to refine. We have performed refinements using two sets of initial trial parameters obtaining two basically equivalent sets of potential parameters. The agreement between calculated and observed data, for both parameter sets, is satisfactory for this type of calculations.

---

† Chem. Phys. Letters 49 (1977) 475.

1) H.Bonadeo and E.D'Alessio, Chem. Phys. Letters 19 (1966) 117.

2) G.Taddei, H.Bonadeo, M.P.Marzocchi and S.Califano, J.Chem. Phys. 58 (1973) 966.

3) D.E.Williams, J. Chem. Phys. 45 (1966) 3770.

I.3 Lattice dynamics, thermodynamic functions, and phase transitions of p-dichloro- and 1,2,4,5-tetrachlorobenzene

H.Bonadeo, E. D'Alessio, E. Halac and E.Burgos

In the present work we have calculated thermodynamic properties of two phases of p-dichlorobenzene and 1,2,4,5-tetrachlorobenzene, using an intermolecular potential of the atom-atom type; in particular we have observed the free energy in the vicinity of the phase transitions.

For a crystal with M molecules per unit cell and N atoms per molecules the free energy A per unit cell at temperature T is given by:

$$A(T) = \phi_{st} + \frac{1}{2} h \sum_{\alpha} \int_0^{\infty} \nu g_{\alpha}(\nu)\, d\nu + kT \sum_{\alpha} \int_0^{\infty} g_{\alpha}(\nu) \ln \left[1-\exp(-h\,\nu/kT)\right] d\nu$$

where ϕ_{st} is the static crystal energy, α ranges over the 3MN internal and external phonon branches, and $g_{\alpha}(\nu)$ is the corresponding vibrational density of states normalized by $\int_0^{\infty} g_{\alpha}(\nu)=1$.

Once the inter- and intramolecular force fields are established it is possible to calculate the crystal frequencies troughout the Brillouin zone, and then the density of states. For the crystal of p-dichlorobenzene in phases α and β, the complete densities of states were used to calculate (in the rigid body approximation) the contribution of the lattice vibrations to the internal energy, free energy, entropy and specific heat. These calculations are too lengthy, and therefore extremely costly in terms of computer time. For this reason, the Debye-Einstein aproximation to the density of states was used to recalculate the thermodynamic properties. This aproximation was shown to be sufficiently accurate and then it was applied to the crystal of 1,2,4,5-tetrachlorobenzene.

The thermodynamic properties were calculated for the α and β phases of both crystals in a range of temperatures near the phase transitions. The calculations are consistent with the experimental data. The free energies of both phases of p-dichlorobenzene are almost coincident, which is consistent with the fact that the phases are metastable, and the free energy curves for 1,2,4,5-tetrachlorobenzene cross at a temperature which is very near the transition temperature, in coincidence with the well defined transition behaviour.

---

† J. Chem. Phys. 68 (1978) 4714.

I.4 The lattice vibrations of 1,2,4,5-tetrabromobenzene.†.

E.Burgos and H.Bonadeo

In the last years, we have been interested in the problem of intermolecular forces in halogenated benzene crystals; we have studied the

lattice vibrations, intermolecular forces and recently we have refined an intermolecular force field for brominated benzene crystals. The refinement included dynamical and structural data of a series of these crystals; because of the lack of data, the lattice vibrations of 1,2,4,5-tetraromobenzene were not taken into account.

In the present work we study the lattice vibrations of 1,2,4,5-tetrabromobenzene in its β and γ phases using Raman and far infrared spectroscopy, in order to complete the experimental data on the series, and the results are compared with calculations based on the atom-atom interaction model, in order to check the accuracy and transferability of the potential parameters obtained.

In spite of the similar crystal structures, both the spectra and the calculated frequencies of the two phases are widely different. Although we have observed partial polarizations, our results refer to unpolarized spectra of essentially polycrystalline samples. Therefore, we have placed calculated and observed values in correspondence using these indications of partial Raman polarizations and a proximity criterion; this by no means can be regarded as a definitive assignment, but only as a tentative indication. Within these limitations, the agreement between observed and calculated values is reasonable, as compared with the values found for other halogenated benzene crystals.

---

† Chem. Phys. Lett. 57 (1978) 125

I .5 Intermolecular potentials for some crystals of heterocyclic compounds containing nitrogen.

Z.Gamba and H.Bonadeo

In the last years several papers considering potential functions for these crystals have been published. The information, however, is quite heterogeneous: some of the crystals considered are largely hidrogen bonded, some posses dipole moment; most refinements are based on one particular crystal and the tranferability of the parameters is not certain.

Atom-atom potential parameters for a series of chlorinated [1] and brominated [2] benzene crystals have been refined in our laboratory. In both cases, static and dynamic properties of the crystals were very well

reproduced, and later the parameters were found to be transferable to other crystals not included in the fit. In view of the success of these calculations it seemed logical to perform a refinement on heterocyclic ring compounds. We have chosen a group of five crystals: pyrazine, s-tetrazine, pyridazino-(4,5d) pyridazine and the two known phases of s-triazine, which contain nonpolar molecules and are thought not to have hydrogen bonds, in order to clear the calculation of possible side complications.

In our previous refinements the convergence proceeded smoothly and rapidly, and the final error was quite small; in this case, however, the differences between experiments and calculations are quite high.

Therefore the model should be improved to take into account the physical reasons behind the discrepancies. Recently Righini et al.[3] showed that multipole-multipole interactions may give sizable contributions to calculated frequencies. Since the molecules under consideration are all non polar, quadrupolar interactions must be the leading electrostatic term. Unfortunately, the quadrupoles of these molecules are not known; a gross estimation of them was made, and it was found that the effect of the electrostatic term is large.

At this stage, it is not possible to refine atom-atom parameters together with the quadrupole moments, since too many unknowns are introduced. But in any case it seems to be very probable that the inclusion of the appropriate electrostatic interactions may correct the uncommonly large discrepancies between atom-atom calculations and experiments. A more detailed study of the effect of different types of electrostatic interactions is in progress.

---

† Chem. Phys. Lett. (in press)

[1]) H.Bonadeo and E.D'Alessio, Proc. Int. School Phys. "E.Fermi", Course LV, (1972) 136. New York: Academic Press.

[2]) E.Burgos and H.Bonadeo, Chem. Phys. Lett. 49 (1977) 475

[3]) RRighini, N.Neto, S.Califano and S.H.Walmsley, Chem. Phys. 33 (1978) 345

I.6 Vibrational spectra and phase transitions of crystalline bromoform.

E.Burgos, E.Halac and H.Bonadeo.

We have obtained the Raman and infrared spectra of bromoform crystals at different temperatures in the range -175 to 5°C. We have shown the existence of 3 phases of crystalline bromoform: α, stable between the melting point and -5°C; β the stable phase from -5°C to -175°C, obtained when the sample is cooled slowly; and γ, which can be trapped by sudden cooling of the liquid or the α phase to liquid nitrogen temperature, and transforms irreversibly into the β phase at temperatures above about -80°C. We have also shown that under different experimental conditions it is possible to have mixtures of phases β and γ in varying proportions.

Our i.r. and Raman spectra of the β phase point to a centrosymmetric unit cell, either monoclinic or orthorhombic, with two molecules located at C_1 or C_s sites. The spectroscopic evidence for the γ phase, is compatible with a centrosymmetric hexagonal unit cell with 2 molecules located at C_3 sites. For the α phase, the broadening of all the bands, and the general appearance of the lattice mode region Raman spectrum strongly point to the existence of some kind of orientational disorder.

II. CRYSTAL STRUCTURE AND PHASE TRANSFORMATIONS

II.1. A study of the initial stage of the accretion process

O.Nasello*, L.Levi, E.M.de Achaval**, E.Ceppi*

Accretions about 5 mm thick, grown without ventilation at air and deposit temperatures $T_a \simeq -10°C$ and $T_d \simeq -5°C$, are shown to follow the substrate orientation, wether basal or prismatic, with theexception of a few embedded tiny crystals. Thus, in these conditions the preferred orientation, typical of wind tunnel accretions, does not develop. Taking into account these results, experiments where 50-200 μm diameter droplets collide at 10 m $s^{-1}$with a prismatic o basal substrate are carried out. When droplets impinge on a prism surface, forming a nearly continous layer, many new crystals ≃ 40 μm in size are observed, even at T_d just below 0°C. When droplets impinge on a basal surface, they follow the substrate orientation down to $T_a - T_d = -13°C$, i.e. to the temperature where they turn polycrystalline after free fall collision. These results indicate that the accretion structure depends on the speed of the droplets colliding on the substrate. The mechanisms that determine these different behaviours are discussed. The results are applied to the interpretation of the structure of wind tunnel accretions and of natural hailstones throughout their different growth stages.

---

* Instituto de Matemática, Astronomía y Física, Universidad Nacional de Córdoba.

** Servicio Meteorológico Nacional.

II.2 Structure of sodium chloride cleavage surfaces etched in vacuum at moderate temperature.

L.Levi

The structure of NaCl cleavage surfaces subjected to evaporation in vacuum at temperatures between 100° to 300°C has been studied by examination of gold decorated replicas in the electron microscope [1].

The effect of biatomic step splitting [2, 3] and random formation of surface depressions (Fig.II.2.1) is interpreted, assuming a vacancy cluster

nucleation process. The phenomenon is correlated with the similar formation of impurity clusters observed by previous authors[4] on the surface of thermally treated doped crystals.

It is noted that, though split steps largely prevail on thermally etched surfaces, showing that monoatomic steps rarely exist, this fact does not signify that a/2<011> dislocations loops do not form in front of the crack. Such loops left behind by cleavage may change into half loops. In these circumstances the electric forces associated with the surface emergences of the half loops and the charged kinks existing along correlated steps combine to restore electric equilibrium and annihilate the steps generated on the surface.

---

[1]) G.A.Bassett, Phil. Mag. 8 (1958) 1042

[2]) L.Levi, Phil. Mag. 28 (1973) 472.

[2]) M.J.Yacaman and T.Z.Ocaña, J. Appl. Phys. 48 (1977) 418.

[4]) G.A.Bassett and M.J.Yacaman, Thin Solid Films 31 (1976) 375.

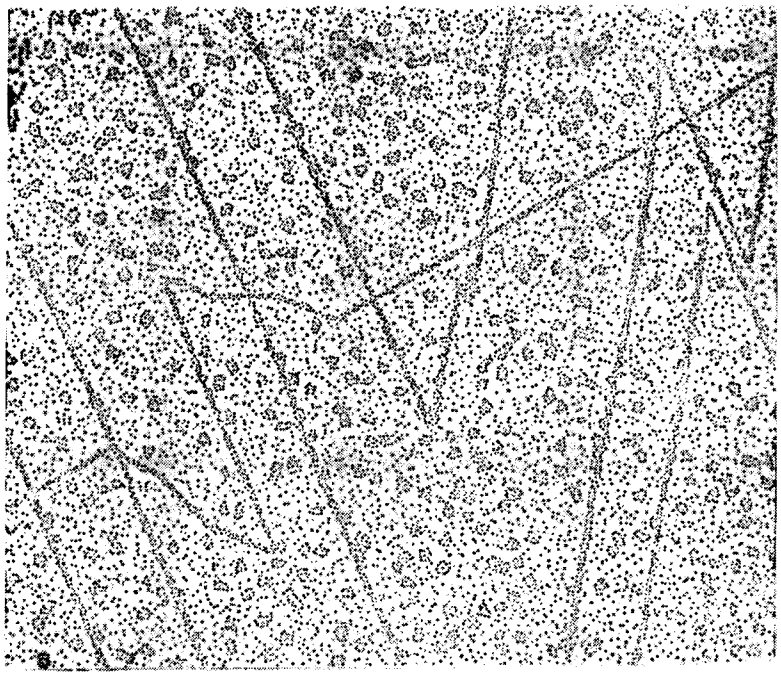

Fig. II.2.1 : Split steps and depresssions on the surfaces of a crystal of the second batch, heated in vacuum at 270°C for 1 hour.

II.3 Crystal structure of droplets frozen on an ice substrate after low speed collision.

L.Levi, O.B.Nasello and E.M. de Achaval*

The freezing behaviour, for droplets colliding at terminal free fall speed with an ice substrate, is studied. The experiments are carried out using droplets of 135 and 75 mm mean volume diameter. The results show that the droplets follow the substrate orientation down to a narrow temperature interval, where the probability of formation of crystals with new orientations increases rapidly from P<10% to P>90%. This behaviour is shown in Fig.II.3.1 for a prismatic substrate and in Fig. II.3.2 for a basal one. These figures show that the transition temperature T^*, corresponding to P=0.5 [1] decreases with the droplet diameter, varying from -18°C to -29°C for a prismatic substrate and from -11°C to -13°C for a basal one. This behaviour is discussed on the basis of the classical nucleation theory [2]. It is found that the energy for nucleation of new orientations on a prismatic and basal substrate may be respectively represented by the following equations:

$$\Delta G^* = (5.6 \times 10^{-11}) / \Delta T^2 \text{ erg/°C}^2$$

$$\Delta G^* = (1.4 \times 10^{-11}) / \Delta T^2 \text{ erg/2C}^2$$

Accretions are also grown, formed by several droplet layers and the differences between their structure and that of wind tunnel accretions [3,4] are discussed.

---

* Servicio Meteorológico Nacional, Bs. As. Argentina.

1) P.J.Rye and W.C.Macklin, Quart. J.R. Meteorol. Soc. 101 (1975) 207

2) I.E.Kuhns and B.J.Mason, Proc. Roy. Soc. (London) A302 (1968) 437

3) L.Levi and A.N.Aufdermaur, J. Atmospheric Sci. 27 (1970) 443

4) L.Levi, E.M.Achaval and L.Lubart, J. Crystal Growth 22 (1974) 303

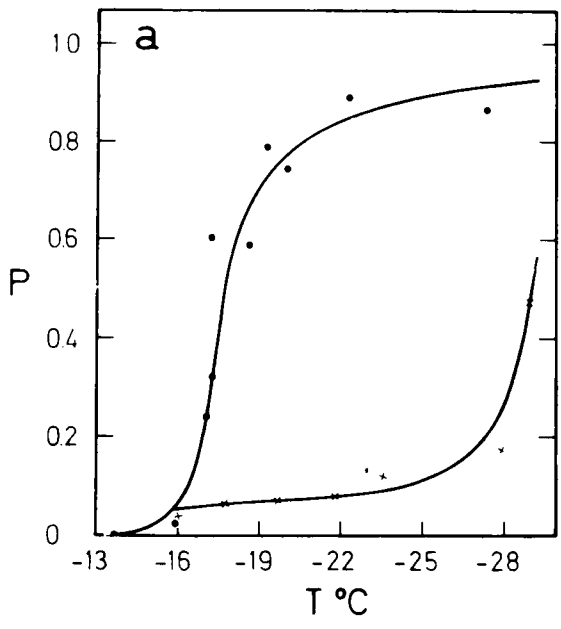

Fig: II.3.1

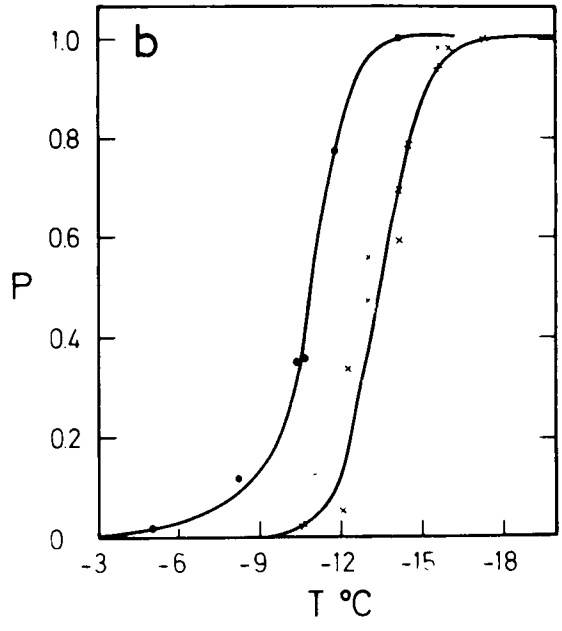

Fig: II.3.2

II.4 Phase transitions in synthetic troegerite: electron microscopy study of surface relief.

C.Sá, M.A.R.Benyacar, L.S.Wainer.

Two phase transitions have been reported [1,2,3] in $H_2(UO_2)_2(AsO_4)_2 \cdot 8H_2O$ (synthetic troegerite): 1) A transition ($T_1 \simeq 20°C$) from a tetragonal phase (phase 1) to a low symmetry antiferroelectric pseudo-tetragonal phase (phase 2). 2) A transition ($T_2 \simeq -20°C$) from the pseudo-tetragonal structure to a ferroelectric noncentrosymmetrical structure (phase 3). Optical microscopy studies showed that phase 2 appears as two sets of 90° domains in the tetragonal matrix. Each domain is usually a composite of two or more subdomains.

The aim of this research was to study the possible differences in surface relief associated with the domains and subdomains present in phase 2 and its modifications with temperature. This information is relevant when considering the different models proposed in ref.3 .

Shadowed and decorated replicas, obtained at different temperatures, of cleavage surfaces of synthetic troegerite crystals, were observed in the electron microscope. Special care was taken to distinguish cleavage structures from those associated with the presence of domains.

The results obtained can be summarized as follows:

1) Replicas of phase 2 crystals show 90°domain structures with domain width

$\leq$0.04μ (Fig.II.4.1), similar to those observed by optical microscopy.

2) It has not been possible to detect any particular structure which could be related to the presence of subdomains.

3) No deviation has been observed in domain walls when they cut through low cleavage steps (height $\leq$100Å).

4) We have observed a difference in the domain structure at both levels of high cleavage steps (height >500Å). We believe this is due to the different stresses present at both levels of a high cleavage step and could be related to a possible ferroelastic character of phase 2.

5) Replicas of crystals kept at temperatures above 30°C (phase 1) show relatively smooth surfaces presenting mostly the characteristic cleavage structures with some evidence of thermal etching. But structures similar to those associated with phase 2 domains are not completely absent in these samples; they tend to disappear as the temperature increases above the transition temperature T_1.

6) Preliminary experiments with crystals kept near T_2 do not show the 90° domain structure. Circular structures (Fig.II.4.2) visible through a difference in nucleation densities, similar to those characteristic of ferroelectric materials appear instead.

From 1) and 2) we conclude that domain walls associated with phase 2 domains do produce resoluble surface relief while that is not the case for subdomains walls. Any model proposed to explain the transformation mechanisms should be able to explain the different behaviour of domain and subdomains walls.

---

[1]) M.A.R. de Benyacar, M.E.J de Abeledo, Am.Mineral 59 (1974) 763.

[2]) M.A.R. de Benyacar, H.L. de Dussel, Ferroelectrics 9 (1975) 241

[3]) M.A.R. de Benyacar, H.L. de Dussel, Ferroelectrics 17 (1978) 469

Fig II.4 1: Electron micrograph of a replica of phase 2 crystals of synthetic troegerite showing a 10° domain structure.

Fig II.4.2: Electron micrograph of a replica of a crystal of synthetic troegerite kept at a temperature near T_2 showing a circular structure.

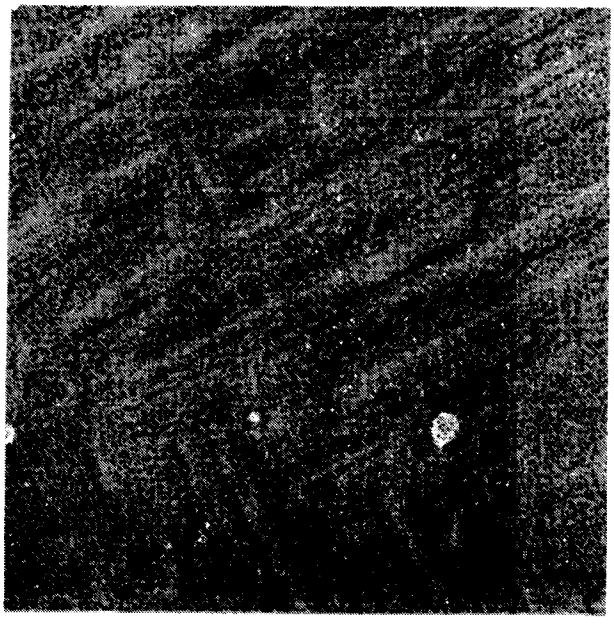

Fig. II.4.1

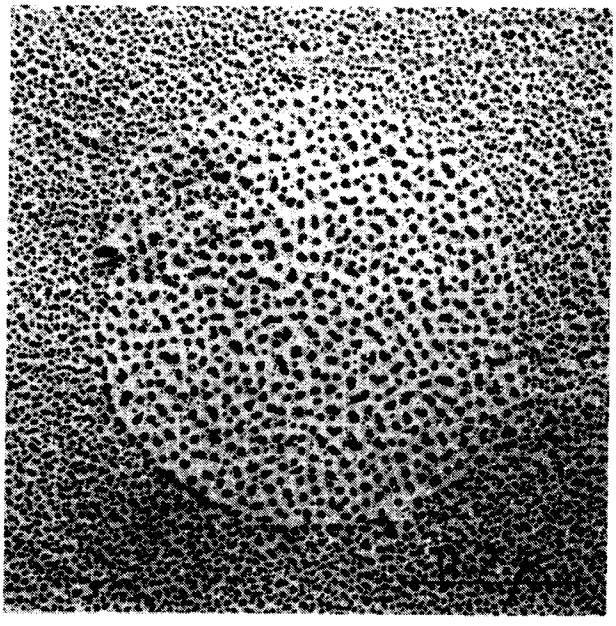

Fig. II.4.2

II.5 Decoration effects on cleavage surfaces of ferroelectric crystals.†

L.S.Wainer, H.L.Dussel, M.A.R.Benyacar.

Charged zones appearing in the cleavage surfaces of ferroelectric materials can be due to the presence of ferroelectric domains and/or to cleavage and fracture structures. All these zones are decorated by the differential nucleation of evaporated materials.

We have compared the patterns obtained in ferroelectric and non ferroelectric materials in order to determine the relationship between ferroelectric domains and decoration patterns.

We have observed similar decoration patterns while studying in the electron microscope replicas obtained evaporating either Au or Te on GASH, GUSH, and TGS crystals. On the other hand, Weidmann et al[1] report an absence of decoration on TGS and $NaNO_2$ crystals when using Au as evaporating material and explain their result as due to the electronegativity of the Te atoms and the electropositivity of the Au atoms. Our observations are not in agreement with theirs and throw doubt upon their tentative explanation.

Mainly two types of decoration patterns can be distinguished in the replicas of the ferroelectric compounds:

1) Closed curved structures, sometimes with lenticular shapes. Their contrast arises from differences in the nucleation density of decorating nuclei.

Similar structures have not been observed in any of the non-ferroelectric substrates studied. From this we conclude that they correspond to ferroelectric domains in agreement with the results obtained by Weidmann et al.[1] working with TGS crystals.

2) Elongated decoration patterns with almost parallel and frequently straight edges, several hundreds of microns long. Their contrast arises also from a difference in the densities of decorating nuclei. Very often they correspond to cleavage and fracture structures. They were present in replicas of the following ferroelectric materials: GASH decorated with Te and Au, GUSH decorated with AgCl, Te and Au, TGS decorated with Te and Au and the non-ferroelectric GZnS decorated with Te and Au. Moreover they appear in ionic cubic centrosymmetrical crystals such as LiF and NaCl, typically non-ferroelectric materials. Cleavage patterns appearing in ferroelectric crystals are probably not always independent of the domain structure[2], but they do not necessarily reproduce the domain shape. There is a strong similarity between these structures and those observed by Weidmann et al. in $NaNO_2$ and intepreted by them as revealing the presence of domains through differential nucleation densities as in the case of TGS, even though in their case the direction of Ps should be almost parallel to the observed surface.

Though decoration is a useful tool for the detection of ferroelectric domains, the decoration patterns should be carefully analyzed and the relationship between the cleavage plane, cleavage direction and the electric polarization vector orientation should be taken into account in order to distinguish between cleavage, fracture and domain structures.

+ Accepted for publication in "Thin solid films"

1) E.J.Weidmann, J.C.Anderson, Thin solid films 7 (1971) 27

2) N.Nakatani, Japan J. Appl. Phys. 15 (1976) 2113

II.6 X-ray studies of Argentine minerals

P.K. de Perazzo

Within the plan of collaboration between Córdoba University and the Solid State Physics Division, some X-ray studies of minerals from Córdoba province were carried out.

Phosphates and oxides of the locality of Tanti, Córdoba province, were obtained and some single crystals were separated. The minerals Rockbrigeite and Columbite-Tantalite were particularly suitable for X-ray analysis. X-ray powder patterns and single crystal precession films were obtained. Rockbrigeite $(Fe, Mn)_5 (P_2O_4)_3 (OH)_5$ was found to be orthorhombic with

a = 13.867 Å
b = 16.917 Å SP = Bbmm
c = 5.190 Å

quite similar to typical Rockbrigeite[1] in spite of having a 2% content of Mn. This is the first time the presence of Rockbrigeite in Argentine has been confirmed.

A mineral supposed to be Axiolite was studied by powder and single crystal method. As the mineral was not previously known in Argentina, it was particularly important to confirm its identification.

X-ray difraction precession films showed the mineral to be really orthorhombic with

a = 5.724 Å
b = 14.027 Å SP = Pcan
c = 5.110 Å

In these films b = 14.027 Å is clearly shown to be a super-cell of a cell with b = 4.676 Å belonging to Axiolite. So data belong not to Axiolite but to Columbite - Tantalite $(Fe, Mn) (Nb, Te)_2O_6$ and single crystal X-ray difraction was the only method capable of differentiating both minerals.

---

1) M.Moore, Am.Miner. vol. 55, (1970) 135-69.

2) E.H.Nickel, J.F.Rowland, R.C.McAdam, Am. Miner. vol. 48 (1963) 961-79.

II.7 The crystal and molecular structure of O-methyl Armepavine Iodomethylate

R.F.Baggio and B.O.Perazzo

The crystal structure of O-methyl Armepavine Iodomethylate ($C_{20}H_{25}NO_3.ICH_3$) has been solved by the heavy atom technique, using photographic methods. Single crystals of the compound were obtained from a saturated methanol solution, and preliminary h0l and 0kl precession photographs gave

the following results:

System: orthorhombic, Space group: $P_{2_12_12_1}$,a=15.61(3) Å, b=16.25(3) Å, c= 9.14(2) Å.

Intensity data were difficult to collect due to pronounced crystal decay, but some 1550 reflexions could be measured from levels hk0 to hk7 taken in a Weissenberg camera, using the equi-inclination technique, and Cu Kα radiation. They were measured by visual estimation with a calibrated strip by two different observers. No absorption corrections were applied.

The usual Patterson and Fourier methods gave the whole structure without serious difficulties, but conventional least squares refinement failed to converge to any sensible model, thus revealing the poor quality of the data.

In order to retrieve any structural information our data could have, a constrained least squares refinement was attempted, with bond lengths stuck to their commonly accepted values. This time the procedure converged smoothly to final values which made chemical sense.

Fig.II.7.1 shows the constrained bond distances used, as well as the interatomic angles after refinement.

Fig.II.7.2 shows a projection of the molecule into its least squares plane. It is apparent from there that the benzyl group is sterically repelled by the substituents in N14 into a region where its effect onto H8 (the H atom attached to C8)is far from negligible. This is in agreement with previous NMR results[1,2].

The special way in which the heterocyclic group is puckered (five carbon atoms laying on a plane with a maximun deviation of 0.02 Å and the N atom moving 0.65 Å away from it) shown in Fig II.7.3, seems quite efficient in reducing overlap of H atoms as well as in preventing the benzyl group from coming too near H8, the actual distance from the plane being 2.6 Å.

---

† Anales Asoc. Quimica Argentina 66 (1978) 345

1) D.R.Dalton, M.P.Cava and T.Buck. Tetrahedron Lett. 31 (1965) 2687

2) M.Tomita, T.Shingu, K.Fugitani and H.Furukawa. Chem. Pharm. Bull. (Tokio) 13 (1965) 921.

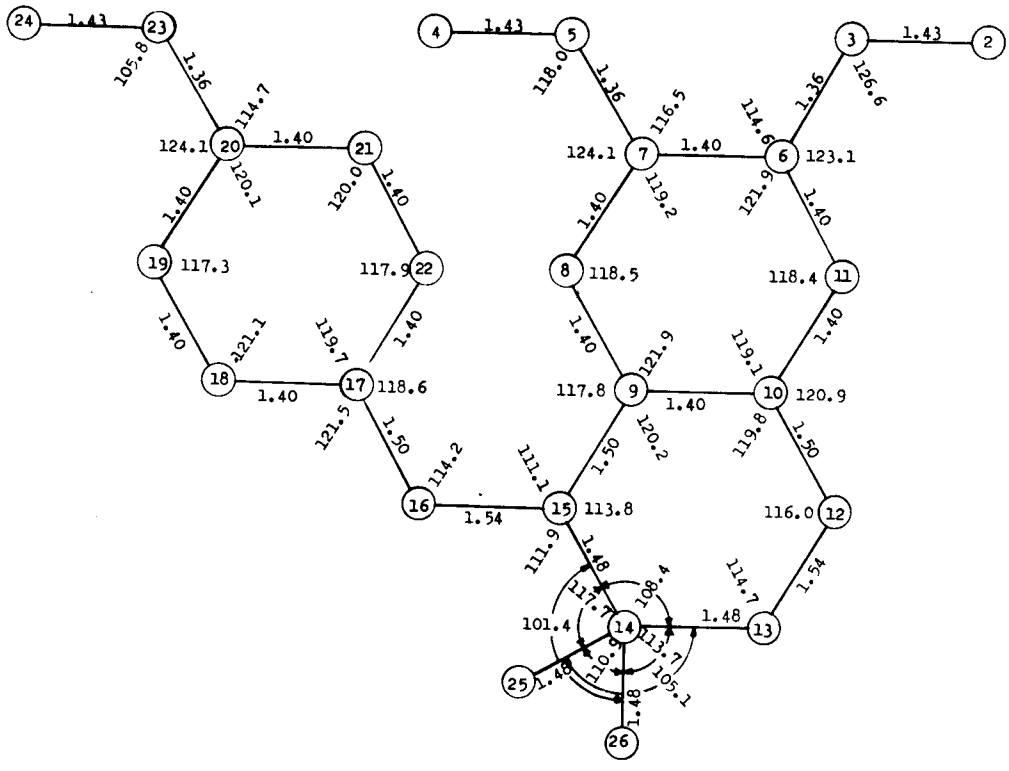

Fig.II.7.1: Bond distances in Å, and angles, in degrees.

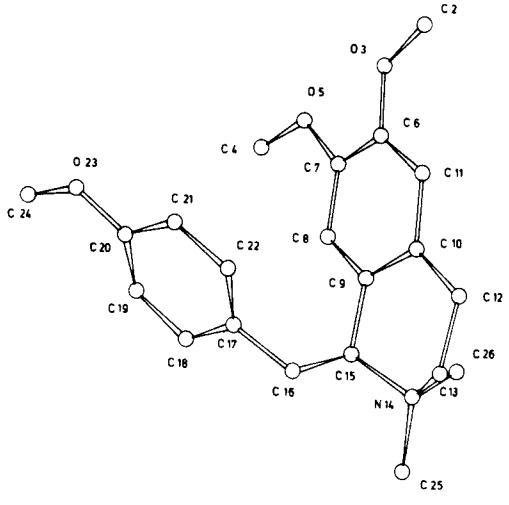

Fig.II.7.2: Projection of the structure onto its least squares plane.

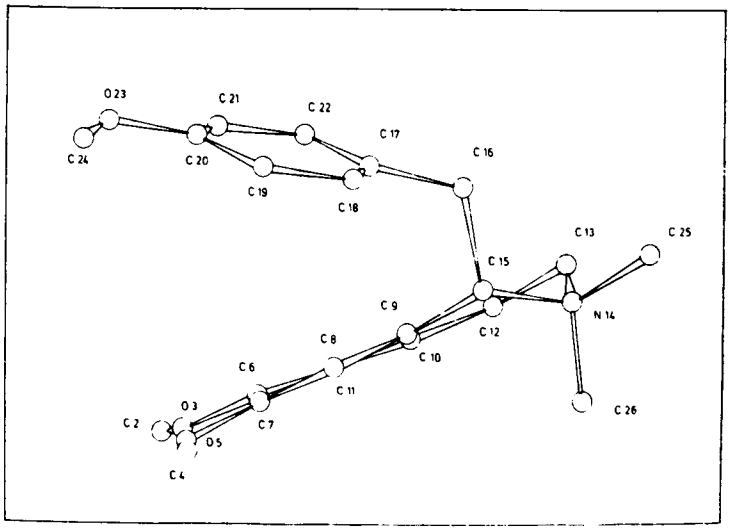

Fig.II.7.3: Projection of the structure along the C8-H8 Bond

II.8 On the application of phase relationships to complex structures: A random approach to structure determination.†

R.F.Baggio and M.M.Woolfson*, and J.P.Declercq and G.Germain.**

In this work the linear equations method for the refinement of phases proposed by one of the authors in a previous paper [1] was analysed in terms of the radius of convergence.

The main (and striking) conclusion of this set of trials was that even for a reasonably large (70 to 80) set of phases linked by some 1000 triple phase relationships there was a significant chance of refining a given, arbitrary set of phases into the same final values where the true ones would converge if allowed to refine into self consistency.

This result was checked and confirmed, starting from random phases, whith some "easy" known structures as well as some "difficult" ones, the qualifications relating to the reluctancy the structures showed to be solved by conventional direct methods.

Although the fraction of successful trials diminished with increasing complexity of the problem as well as with the number of phases involved, there were enough of them (5 to 10% in the first type of structures, 2 to 5% in the second) as to make the method worth considering as a starting step in a multisolution procedure.

New figures of merit had then to be envisaged to isolate the more promising solutions as the conventional ones did not discriminate properly among the different outcomes of the random trials. However, none of those proposed and tested by us seemed to work any better. Some work is still being done on the subject.

Several improvements in the least squares procedure described in the paper by Woolfson[1] were tried, such as an indirect weighting scheme for the linear equations which did not affect the matrix, thus avoiding the need of many time-consuming matrix inversions, and an acceleration procedure to speed the convergence of the method up. A moderate success could be claimed on these subjects.

As a byproduct of our studies, a potentially useful enantiomorph discrimination method was envisaged, which worked extremely well in upgrading a set of phases which had previously been over-refined so that its Fourier map showed two ghost enantiomorph images. After the correction (just a few cycles of a modified least squares refinement) the corresponding Fourier map appeared much less symmetrical, and one of the images could be definitively be isolated from its "ghost".

---

† Acta cryst. A34 (1978) 883

* Department of Physics, University of York, York, England.

** Laboratoire de Chimie Physique et de cristallographe, Universite de Louvain, Belgium.

1) M.M.Woolfson, Acta Cryst. A33 (1977) 219.

II.9 Optical and X-ray characterization of some gel grown crystals†.

F.Lefaucheux*, M.C.Robert*, E.Manghi and H.Arend**

Brushite and lead monetite have been grown in silica gel and in tetramethoxysilane gel (TMS). Two main features characterize these crystals:

-a high growth rate (up to 2 mm/day)

-a good quality.

They are optical clear and show some inclusions at the beginning of growth and a faint line [102] for $CaHPO_2 . 2H_2O$, [401] for $PbHPO_4$.

X-ray topographs reveal dislocations starting from these inclusions, growth sector boundaries and some growth bands. The dislocation density is

higher in silica gel than in TMS either for $PbHPO_4$ or for $CaHPO_4 . 2H_2O$.

Reducing to 1.0006 the gel density for TMS 2%, large parts become dislocation free. The correlation between the gel density and the dislocation density can be explained by the reduction of entrapped particles.

The gel properties can be modified by varying the temperature. For example, experiments with $PbHPO_4$ performed at 32°C (i.e., below 37°C which is the critical temperature for the ferro- to para- electric phase transition) give nearly perfect crystals.

In the case of TMS the pH can be easily reduced while keeping the other grown conditions constants. For brushite crystals, growth experiments have been performed in the pH range 3-5. For low pH the nucleation is reduced, the thickness of (010) platelets is increased, but for long duration experiments dissolution occurs.

X-ray topographs show a similar crystalline quality. Only growth sector boundaries remain visible for (200) reflection. The dislocation and the loops have [001] as Burger's vector. As they lie in (010) planes, they seem to be related to the lamellar structure of this compound.

---

† Contributed paper, Second European Conference on Crystal Growth, Lancaster University, September (1979) 10-15.

* Laboratoire de Cristallographie, Paris VI.

** E.T.H., Zurich, Switzerland.

II.10 Domain structure in ferroelastic $BiVO_4$: I. Electron microscopy of cleavage surfaces

L.S.Wainer, R.F.Baggio, M.A.R.Benyacar

Bismuth vanadate ($BiVO_4$) shows a reversible phase transformation at 255°C[1] from a tetragonal, high temperature phase, space group $I4_1/a$ to a monoclinic, low temperature one, space group I2/a. The low symmetry phase has been described as ferroelastic. Two sets of 90° domain boundaries have been reported.

As a part of a comprehensive research on domain structure in ferroelastic materials a study of the surface relief of cleaved single crystals of $BiVO_4$ was undertaken by scanning electron microscopy (SEM) and the observation of Pt-C replicas in the transmission electron microscope.

Fig.II.10.1 is an electron micrograph of a replica showing the relief associated with the presence of one set of the 90° domains. Structures associated with at

least 3 and possibly 4 different orientation variants were observed for a given orientation of the domain boundary. Work is currently being done to correlate these structures with the orientations predicted for a $I4_1/a \rightarrow I2/a$ transition.

From the work done so far with the SEM (Fig.II.10.2) and replicas (Fig.II.10.1) has not been possible to assign the domains a saw-tooth or a square-step profile. This information would be valuable in determining the transformation mechanism. Glancing angle shadowing will be used to decide between the two possibilities.

---

1) J.D.Bierlein, A.W.Sleight, Solid State Com. 16 (1975) 69.

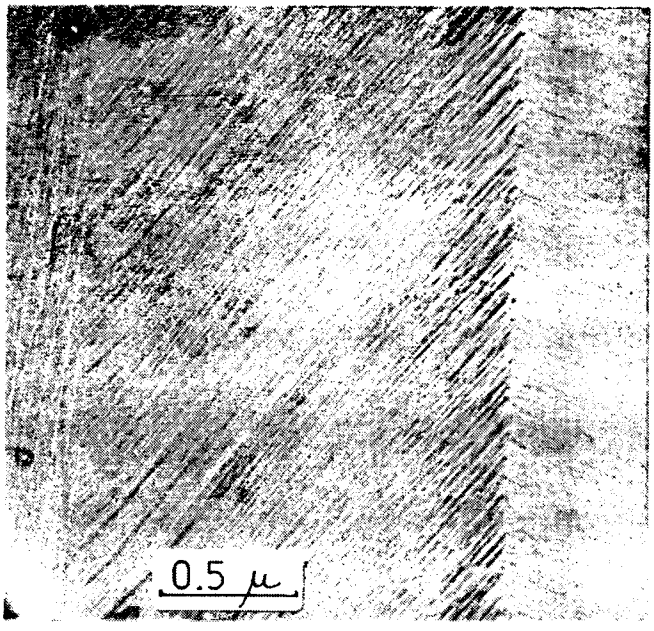

Fig.II.10.1: Electron micrograph of C-Pt replica of $BiVO_4$

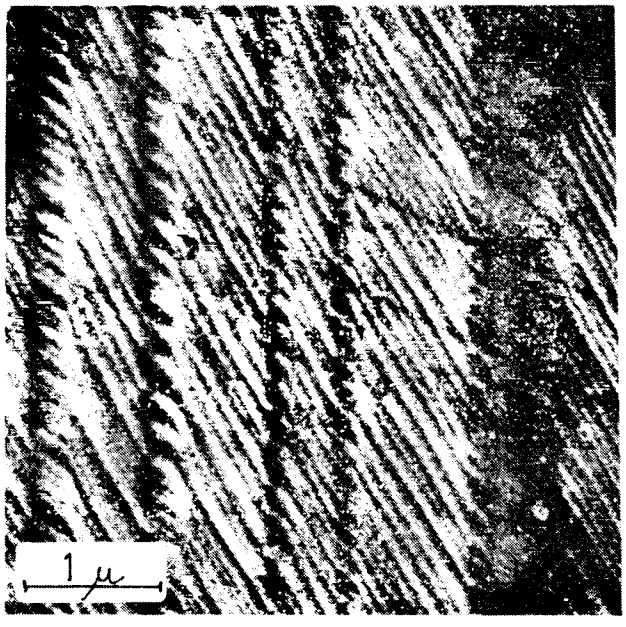

Fig.II.10.2: Scanning electron micrograph of a cleavage surface of a $BiVO_4$ crystal

II.11 Domain structure in ferroelastic $BiVO_4$: II Transmission electron microscopy.

L.S.Wainer, R.F.Baggio, M.A.R.Benyacar.

Single crystals of $BiVO_4$ (bismuth vanadate) were grown from the melt at 940°C. Thin flakes obtained by cleaving the thick crystals proved to be suitable specimens for transmission electron microscopy (TEM). We have been able to observe on a much finer scale (~0.1μ) the two sets of 90°domains already described by optical microscopy[1].

Electron diffraction patterns show a splitting of the diffraction spots due to the presence of different orientation variants.

Figs.II.11.1 and II.11.2 are dark field images obtained each with one of the resolved diffracted beams contributing to the (200) diffraction spot (tetragonal indices). Different orientation variants can be clearly appreciated; we are at present trying to correlate the number of variants observed in the TEM micrographs with those observed with replica techniques.

Fig.II.11.3 is a dark field electron micrograph obtained with all the beams contributing to the (200) diffraction spot (tetragonal indices). We conclude that domain walls are imaged as alternating black and white lines (A-B, C-D); the former are due to the superposition of reflected electron beams from two adjacent domains and the latter are due to an absence of reflected intensity. A similar effect has been observed by X-ray topography[2] in $Gd_2(MoO_4)_3$.

By heating with the electron beam we have been able to change the domain structure (Fig.II.11.4 and II.11.5) usually through the appearance of many smaller domains. We are now trying to observe the behaviour of the domain structure while the crystals are being stressed in situ in the electron microscope.

---

[1]) J.D.Bierlein, A.W.Sleight, Solid State Comm. 16 (1975) 69.

[2]) C.Malgrange, M.Glogarova, Journal de Physique. C2, supp.n°4, Tome 33, C2-159 (1972).

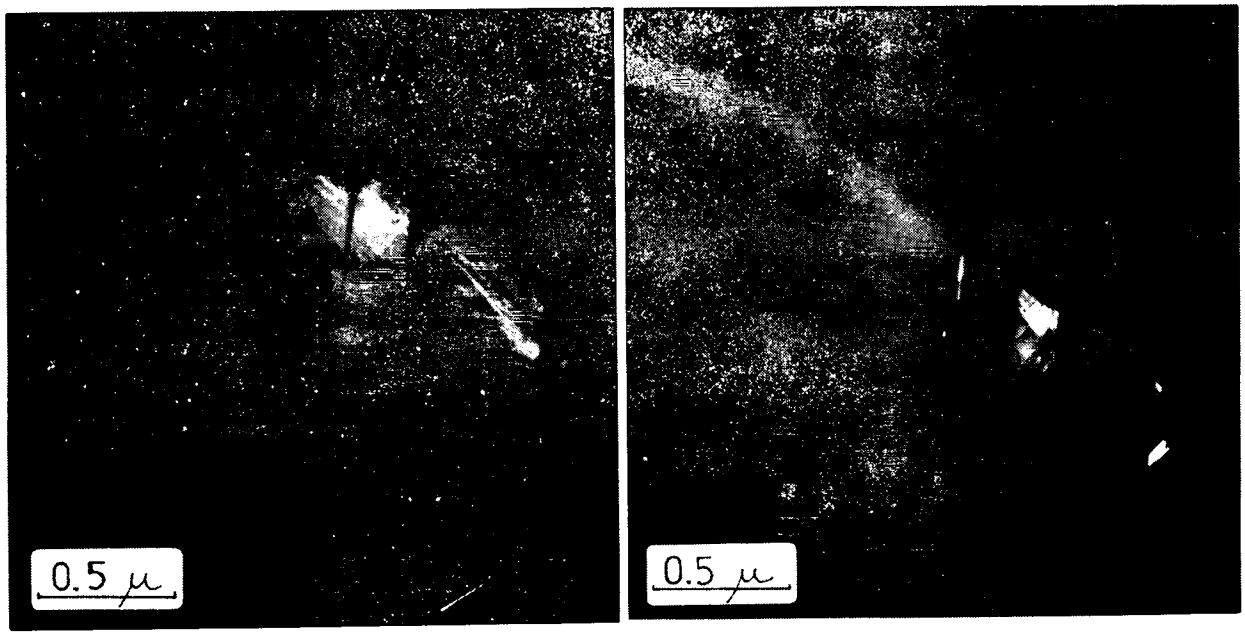

Fig. II.11.1 and II.11.2: Dark field electron micrograph of a $BiVO_4$ crystal taken with different resolved contributors to the (200) tetragonal reflexion.

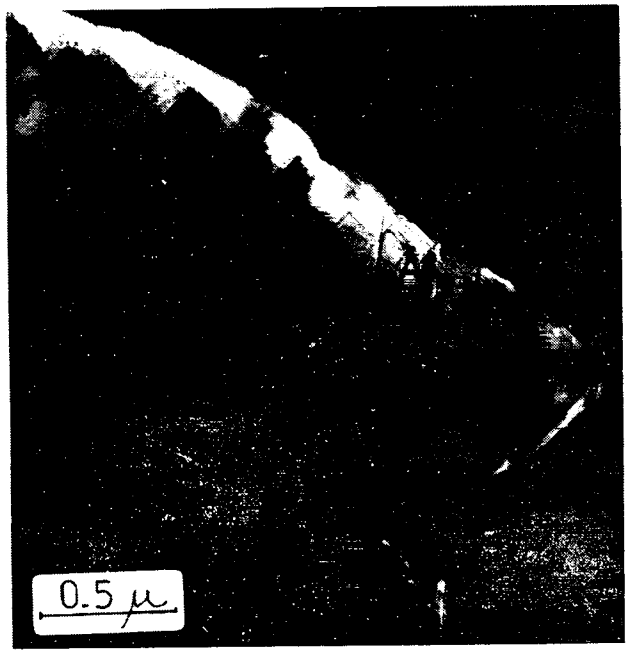

Fig. II.11.3: Dark field electron micrograph taken with all the beams contributing to (200) tetragonal. A-B, C-D: Domain walls.

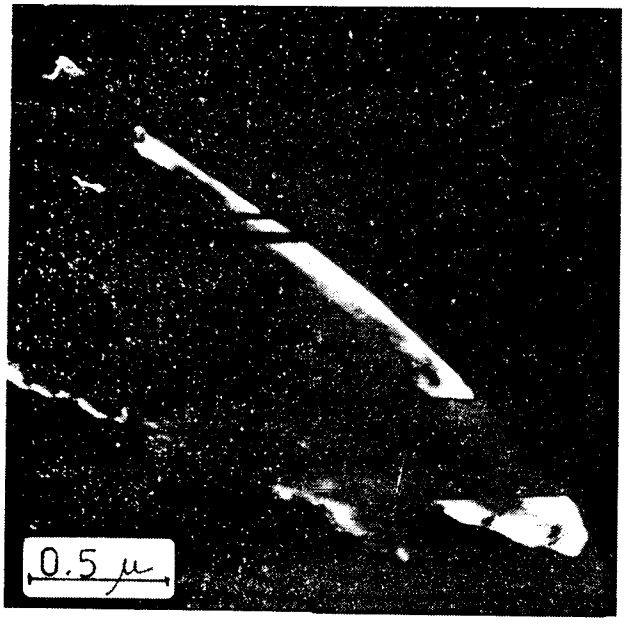

Fig.II.11.4: Dark field electron micrograph (one of the resolved (220) tetragonal) showing a typical domain structure in $BiVO_4$.

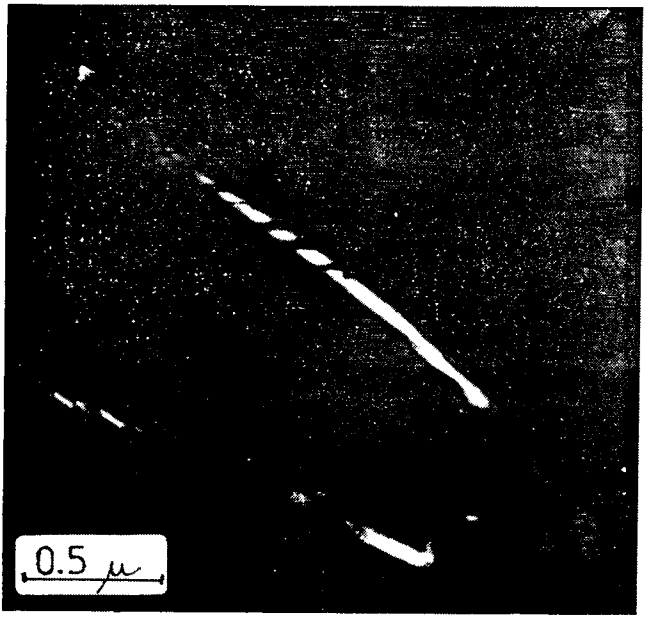

Fig.II.11.5: Idem fig.4, after heating with the electron beam.

III. MÖSSBAUER SPECTROSCOPY

III.1 Study of a low alloy steel rust using Mössbauer Spectroscopy†

I.A.Maier*, C.Saragovi, F.Labenski

Several authors have studied the nature of the oxide products formed on carbon steels using techniques such as reflected polarized light, X-ray and electron diffraction infrared and far infrared spectrophotometries. Osaka[1] observed that the rust consisted of two layers, both of them were composed by α-FeOOH and γ-FeOOH. Miranda[2] found that the whole rust was formed by α-FeOOH and γ-FeOOH and only γ-FeOOH was present in the external layer and α-FeOOH in the inner one. Misawa[3] reported α-FeOOH, γ-FeOOH and a fine particle sized δ-FeOOH or an amorphous FeOOH and that the relative amount of γ-FeOOH was larger in the inner rust than in the outer and that α-FeOOH and amorphous ferric oxihydroxide were abundant in the outers.

In the present work we employed Mössbauer spectroscopy to analyze the composition of the external and internal rust layers of a low alloy steel belonging to the so called "weathering steels", exposed for 10 months in an urban industrial atmosphere, facing north at an 30° angle. The steel composition is shown below. Spectra were taken in transmission geometry and at room and liquid nitrogen temparatures.

Steel Composition

Element	C	Mn	Si	S	P	Cr	Ni	Mo	Sn	Cu	Fe
% weight	0.11	0.37	0.22	0.023	0.085	0.69	0.11	0.10	0.06	0.38	diff.

Internal sample Mössbauer parameters indicate the presence of γ-FeOOH[4] with a relative contribution of 43% and ultrafine α-FeOOH[5] (< 80Å) with an excess of water. External sample Mössbauer parameters indicate also the presence of γ-FeOOH but now its contribution is about 28% of the total, of ultrafine α-FeOOH and of small sized δ-FeOOH(< 100Å) or an amorphous oxihydroxide. Mössbauer spectroscopy shows that the internal layer α-FeOOH particles are smaller than those contained in the external one; that the relative amount of γ-FeOOH is larger in the internal one and that only in the external layer there is evidence of the presence of amorphous oxihydroxide and/or ultrafine δ-FeOOH.

Misawa[3] et al. support the hypothesis that the low corrosion rate of

these steels is due to the formation of a protective layer of amorphous ferric oxihydroxide on the steel surface. Okada[1] also considers that an inner layer of an amorphous spinel-type iron oxide is protective and on the other hand Miranda[2] favours the hypothesis of a protective layer rich in α-FeOOH.

Our results are not in agreement with those obtained by Miranda. They are consistent with most of Misawa's observations but differ in the fact that in our case neither δ-FeOOH nor amorphous compounds are observed in the internal rust layer. It is worth noting that at least in the beginning of the rust formation, there is no amorphous iron oxihydroxide in the rust layer adjacent to the steel surface. Instead we do find an ultrafine α-FeOOH.

---

† Radiochem. Radioanal. Lett. 36(1) (1978) 49.

* CITEFA, Corrosion Group, Zufriategui y Varela, 1063 V.Martelli, Bs.As.

1) H.Okada, Y.Hosoi, K.Yukawa, H.Naito, Transactions ASM 62 (1969) 278.

2) L. de Miranda, Rapports Techn. du CEBELCOR, RT 222 125 (1974) 1.

3) T. Misawa, K.Asami, K.Hashimoto, S.Shimodaira, Corros. Sci. 14 (1974) 279.

4) I.Dezsi, A.Vértes, L.Kiss, J.Radioanal. Chem. 2 (1969) 183.

5) A.M.Van der Kraan, Thesis, University of Delft (1972).

III.2 Mössbauer study of the behaviour of synthetic corrosion products of nuclear power plants†

M.A.Blesa*, A.J.G.Marotto*, S.I.Passaggio*, F.Labenski and C.Saragovi-Badler

Synthetic corrosion products have been used in simulation studies of the behaviour of the natural ones[1]. Iron oxides are the main components of the circulating particles carried by the fluid in the primary circuit of nuclear power stations. The oxidation state of iron is (II, III) or III, (Fe_3O_4, Fe_2O_3) depending upon the reducing or oxidizing conditions of the medium. In the matrix of these oxides other metal ions may be present as a result of the hydrothermal synthesis produced by the fluid at the high temperature prevailing in the system (~ 250°C). These metals, such as Cr, Ni, Co, Mn, are also released from the structural materials and give rise to ferrite-type structures. We have employed Mössbauer spectroscopy in order to evaluate the method proposed by Fletcher et al.[2] for synthesizing corrosion like products by a wet method.

Synthetic cruds of various compositions were prepared; some of them by

alkaline hydrolysis of iron sulphate under different oxidation conditions; another group using iron chloride instead and also changing the oxidation conditions and a third group preparing mixed oxide samples from a solution containing $FeCl_2 4H_2O$, $NiCl_2.6H_2O$, $MnCl_2.4H_2O$ and $CoCl_2.6H_2$) in oxidizing and air-free conditions. The Mössbauer spectra were taken in transmission geometry and varying the temparature between room and liquid nitrogen temperatures.

The Mössbauer spectra clearly indicate that even small amounts of oxygen do give rise to varying degrees of oxidation, pointed out be the changes in the intensity ratios as well as in the relative proportions of the different phases present (Fe_3O_4, Fe_2O_3) [3]. The replacement of sulphate by chloride in the initial preparation seems to be related to the same end products but the magnetite tends to be a stoichiometric one and the α-Fe_2O_3 proportions decreases. This is probably related to the well-known fact that the nature of the anion is relevant to the mechanism of crystal growth in hydrolyzed Fe (III) solutions. In our case, also, the extent of oxidation seems to be greater when Fe SO_4 is employed instead of Fe Cl_2.

Rather extensive oxidation can take place without disruption of the basic structure (magnetite) in which γ-Fe_2O_3, structurally related to magnetite, is the most important iron containing substance present. It is also confirmed that a short exposure to air at 300°C was enough to produce quantitatively the oxidative lattice transformation from magnetite to hematite.

Although water was not present in this case, the relevance of this result to operating conditions of nuclear power plants is immediate, and is in agreement with proposed methods for physicochemical decontamination involving fast transformation from magnetite and viceversa.

It is therefore concluded that changes in the oxygen content of the coolant in nuclear power stations will reflect itself in changes in the stoichiometry of the magnetite-type solids and, if higher levels of oxygen, or localized attacks take place, the structure of the particles will suffer more drastic changes to hematite in a short time.

+ Rad. Phys. & Chem. 11 (1978) 321.

* Department of Reactor Chemistry.

[1] P.Cohen. Water Coolant Technology of Power Reactors, Gordon Breach, NY, (1969).

[2] W.D.Fletcher, A.Krieg, P.Cohen, WCAP (1961), 1689; W.D.Fletcher WCAP (1964) 3730.

3) R.J.Amstrong, A.H.Morrish, G.A.Sawatzky. Phys. Lett. 23 (1966) 414
O.C.Kistner, A.W.Sunyar. Phys.Rev. Lett. 4 (1960) 412
J.M.Daniels, A.Rosencwaig, J.Phys.Chem. Solids 30 (1969) 1561.

4) B.Montford, Cycling Decontamination Techniques at Douglas Point Generating Station, Atomic Energy Canada Limited AECL-4223, (1973).

III.3 Evidence for the occurrence of a universal type of iron storage in prokaryotic cells: bacteria and mycoplasma†

E.R.Bauminger*, S.G.Cohen*, F.Labenski de Kanter, A.Levy*, S.Ofer and S.Rotten**

Iron in the form of micellar cores of $(FeOOH)_8(FeO.OPO_3H_2)$ is stored in the soluble protein, ferritin, and in its soluble analogue, haemosiderin found in animals and plant tissues[1]. Characteristic ^{57}Fe spectra have been observed in both ferritin and haemosiderin and show that the iron cores are superparamagnetic[2]. Mössbauer studies in E.Coli have established that these bacteria take up iron avidly from the growth media and that it is stored in the form of high spin Fe^{3+}, up to concentrations as large as 1 mg Fe/1 gm cells[3]. Further Mössbauer measurements carried out at low temperatures show that most of the iron in E.Coli cells of high iron content becomes magnetically ordered at 3°K, showing the iron must be present in the form of concentrated aggregates[4]. A soluble iron-storage protein (to be called IS-protein) has been isolated from E.Coli and some of its properties determined[5]. The IS-protein shows morphological similarities to ferritin, as revealed by electron microscopy, but nevertheless has at least two characteristics which distinguish it from ferritin: a) the presence of a distinct chromophore in the IS-protein of E.Coli, whereas no chromophore absorbing in the visible range is found in ferritin; b) the ^{57}Fe Mössbauer spectra and their temperature dependence are very different, indicating that the iron cores of the two proteins have different properties. Mössbauer measurements has now been extended to other species of biological cells grown in media containing enriched ^{57}Fe. Mössbauer spectra, very similar to those observed in whole cells of E.Coli, have now been observed in a) Proteus mirabilis a gram negative bacterium[6], b) Mycoplasma capricolum. In all these cases, magnetically split spectra have been observed at low temperatures, indicating magnetic ordering. In all cases the transition temperature has a range of values, pointing to amorphous structure of small non-uniform particles size. The similarity in behaviour is illustrated in Fig. III.3.1, which shows the relative

strenght of the magnetically unsplit component to the split component as a functionof temperature in E.Coli, M.Capricolum and IS-protein. M.Capricolum is very different from E.Coli and is a fermentative prokaryote belonging to the primitive group of microorganisms known as mycoplasmas, characterized by considerable structural simplicity, consisting of only three organelles: a cells membrane, rib somes and a circular chromosome. The various results point to the exist nce of a universal type of iron storage material and protein in bacterial and mycoplasmal life which differs, in some respects, from the iron storage protein, ferritin, found in higher forms of life.

---

† Accepted for publication on Journal de Physique.

* Racah Insitute of Physics, The Hebrew University, Jerusalem, Israel.

** Biomembrane Research Laboratory, The Hebrew University-Hadassah Medical School, Jerusalem, Israel.

1) S.Granick, P.F.Hahn, J.Biol.Chem. 155 (1944) 661.
J.L.Farrant, Biochem. Biophys. Acta 13 (1954) 569.

2) F.A.Fischabauch et al. J.Ultrastruct.Res. 37 (1971) 495.

3) E.R.Bauminger et al. J.Physique 37, C-6 (1976) 227.

4) E.R.Bauminger et al. J.Physique 40, C-2 (1978) 523.

5) E.R.Bauminger et al. submitted for publication.

6) D.P.E.Dickson, S.Rotten, submitted for publication.

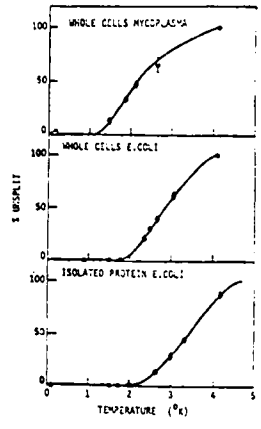

Fig.III.3.1: The ratio (%) of magnetically unsplit part of the spectra as a function of temperature for mycoplasma, E.Coli and the isolated protein

III.4 Clustering of ions in cation exchange membranes: a Mössbauer study †

C.Heitner-Wirguin*, E.R.Bauminger**, F.Labenski de Kanter, A.Levy** and S.Ofer**

Cluster formation in some of cation exchange membranes is already indicated in previous studies[1,2,3], however more details about size of clusters and relative distribution of the ions in them is needed in order to get a better knowledge of the transport properties of these membranes.

In this study, in which Mössbauer spectroscopy was used, the hydrogen ions of the membranes were replaced by tervalent iron ions. The following ion exchanges were studied: a) Nafion (110, 125 and 152)-perfluorosulphonic acid, of ion exchange capacity of 0.6-1.0meq/g; b) Redcat-polyethyleme sulphonic acid acid of 0.94 meq/g ion exchange capacity; c) S.P.S. -sulphonated polysulphone with chlorosulphonic acid. All this membranes in hydrogen form were equilibrated with aqueous or methano solutions of ferric chloride. Nafion 110 equilibrated in methanol solution was measured between 0.05°K and 85°K(4). At 85°K all spectra are composed of two doublets, A and B. In some of the spectra at 85°K a weak sextuple corresponding to a magnetically split spectrum (subspectrum C) could also be discerned. At lower temperature subspectrum C appears in all samples and its relative intensity grows as the temperature is lowered on account of doublet A, whose relative intensity decreases. Subspectrum C is composed of 6 broadened and assymetryc lines. The value of the mean hyperfine field was found to be 560±20 kOe. in all samples, the quadrupole interaction was found to be negligible in these subspectra. The relative intensity and parameters of doublet B do not change with temperature and are characteristic of iron dimers. The behaviour of subspectra A and C correspond to amorphous iron containing clusters with non uniform sizes. Using Neél's formula[5], $f=fo \exp(-CV/kT)$. Thus, for example, using for the constants fo and C the values obtained by Kunding et al.[6] for Fe_2O_3, we find that the doublet A at 4.1°K correspond to clusters smaller than 30Å in diameter, which contain also monomeric iron species. Using the constants derived by Coey et al.[7], the values obtained for the diameters of the clusters are about 10% smaller. Table 1 shows the relative intensities of the three subspectra at 4.1°K. Spectra A correspond to iron species with diameters smaller than 30Å, spectra C to clusters with diameters larger than 30Å, and spectra B to iron dimers[7]. The quadrupole splittings obtained for iron species (spectrumA) are typical of an octahedral iron site (coordinated by 6 oxygens). These parameters are however essentially

lower for Nafion samples (- 0.45 mm/s) than for Redcat and SPS samples (-0.60 mm/s) which is in agreement with infrared measurements[8]. Gierke[2] has recently developed a phenomenological model for the clustering in Nafion membranes. The average size of clusters were estimated from small angle X-ray scattering and water uptake measurements. The sizes of clusters evaluated from Mössbauer measurements are in very good agreement with those evaluated by Gierke[2] (Table III.4.1). The Mössbauer measurements, however supply additional information concerning all the species present and the percentages of them. The model forwarded by Gierke is consistent with the present peasurements if it is assumed that the smaller units (multiplets or monomers) are bridging or channeling between the clusters and thus explain the ion transport through the membrane.

---

† Accepted for publication in "Polymer".

* Dep. of Inorganic and Analytical Chemistry, The Hebrew University, Jerusalem.

** Racah Ins. of Physic, The Hebrew University, Jerusalem, Israel.

1) C.S.Yeo and A.Eisemberg, J.Appl. Polym.Sci. 21 (1977) 875.

2) T.D.Gierke, The Electro-Chemical Society Meeting, October (1977),Atlanta, Georgia.

3) A.J.Hopfinger, et al., The Electro-Chemical Society Meeting, October (1977) Atlanta, Georgia.

4) E.R.Bauminger, F.L. de Kanter, A.Levy, S.Ofer, C.H.Wirguin, J. de Physique, (in press).

5) L.Neél, Ann. Geophysique 5 (1949) 99.

6) J.M.Coey, Earth and Planetary Science Letters, 21 (1973) 45.

7) R.Lechan, et al., J. Chem. Phys., 59 (1973) 3138.

Table III.4.1

Ion Distribution in Membranes at 4.1°K

Sample	Capacity meq/g	(small units)	%B (dimers)	%C (clusters)	% $C/_{A+C}$*	d_o(Å) mean diam. size
Nafion 110(H_2O)	0.91	10	66	24	71	40(41.4)**
Nafion 125(H_2O)	0.83	26	16	59	70	40(37.1)
Nafion 152(H_2O)	0.66	27	45	28	51	30(30)
Nafion 110 (methanol)	0.91	67	14	19	22	20
Redcat (air dried)	0.94	54	12	34	38	28
Redcat (vacuum dried)	0.94	71.5	1.5	27	28	25
S.P.S.	1.2	28	36	35	55	34

* Percentage of clusters ($d > 30$ Å)

**Values in parenthesis are those given by Gierke (2)

III.5 Iron storage in mycoplasma capricolum.†

E.R.Bauminger*, S.J.Cohen*, F.Labenski de Kanter, A.Levy*, S.Ofer M.Kesseel**, and S.Rottem**.

Mössbauer spectroscopic studies of Eschericia coli[1] and Proteus mirabilis[2] cells grown in ^{57}Fe-enriched media have shown that these organisms incorporated substantial quantities of iron from the growth media. The iron was found to be stored in form of aggregates of high spin Fe^{3+}, magnetically ordered at low temperatures[1]. It seems likely that under conditions of iron sufficiency procaryotic cells in general develop the ability to synthesize iron storage material.

The role of the iron storage material in bacteria is still unknown. The Mössbauer spectra of whole Mycoplasma capricolum grown in ^{57}Fe enriched media below 4.1°K are shown in Fig.III.5.1. All the spectra between 4°K and 250°K have the form of a Fe^{3+} quadrupole doublet, whereas at 0.07°K a six line magnetically split spectrum of Fe^{3+} is the main component. All spectra show the presence of a Fe^{2+} doublet which we ascribe to changes produced in the main iron component by thermal recycling. In the magnetically split spectrum at 0.07°K the outer lines are considerably broader than the inner lines indicating that the hyperfine fields at the iron nuclei are spread over a range of values (between 350 and 440KOe). In the transition region between 1.5 and 3.5°K the spectra are composed mainly of 2 subspectra: a) Fe^{3+} quadrupole split doublet (with an isomer shift of 0.51±0.01 mm/s relative to iron metal and a quadrupole splitting of 0.63±0.01 mm/s) whose relative intensity grows with increasing temperature, until above 3.5°K it is the only component that remains and b) a Fe^{3+} magnetically split spectrum, which becomes more smeared out as the temperature is raised and which also shows that the magnetic hyperfine field decreases with temperature until it vanishes at 3.5°K. The temperature dependence of the ratio between the intensity of the 3+ quadrupole split spectrum and the magnetically split spectrum as a function of temperature [3] and the observed spread in the hyperfine fields show that the magnetic transition temperature is not uniquely defined, which indicates an amorphous structure,or the presence of nonuniform particle sizes, or a combination of such factors. In order to account for the presence of a magnetically ordered phase of iron, we must assume the Fe-Fe interatomic distances to be small within a structure containing many iron atoms. These conclusions were further supported by electron microscopy studies. Unstained sections were viewed in a Philip's EM 400 electron microscope at 80kV. The appearance of unstained M.capricolum cells grown with the iron shows a marked concentration of electron dense particles bordering the cell membrane. The particles appear to be preferentially associated with the outer face of the membrane. The particles seem to have a diameter of ~70Å. When M.capricolum cells were osmotically lysed and the soluble fraction was separated from the cell membrane by centrifugation [4], 99% of the iron was found to be associated with the cell membrane fraction. The iron concentration in the membrane preparations was about 5.5 µg ^{57}Fe per mg membrane protein. The main features of the Mössbauer spectra observed in M.capricolum are very similar to those observed in E.Coli and P. mirabilis, yet differ from those obtained in ferritin or hemosiderin. The magnetic ordering temperature of the iron in the procaryotes is about 3°K. whereas the

"blocking" temperature of ferritin or hemosiderin associated with superparamagnetism, is about 40°K[5]. Moreover, the magnetic hyperfine field acting on iron nuclei at magnetic saturation (at 0.08°) in the procaryotes is (430±3)kOe, much smaller than the corresponding field in ferritin or hemosiderin (497±3) kOe(1,5).

Accepted for publication in Bacteriology

* The Racah Institute of Physics, The Hebrew University, Jerusalem. Israel.

** Biomembrane Research Lab., The Hebrew University-Hadassah Medical School, Jerusalem, Israel.

1) E.R.Bauminger et al. J. Physique 40-C2: 523-525

2) D.Dickson and S.Rottem. Biochem J. in press

3) E.R.Bauminger et al. Physique in press.

4) S.Razin, J. Gen. Microbiol. 33 (1963) 471-475.

5) J.F.Boas Australian J.Phys. 19 (1966) 573.

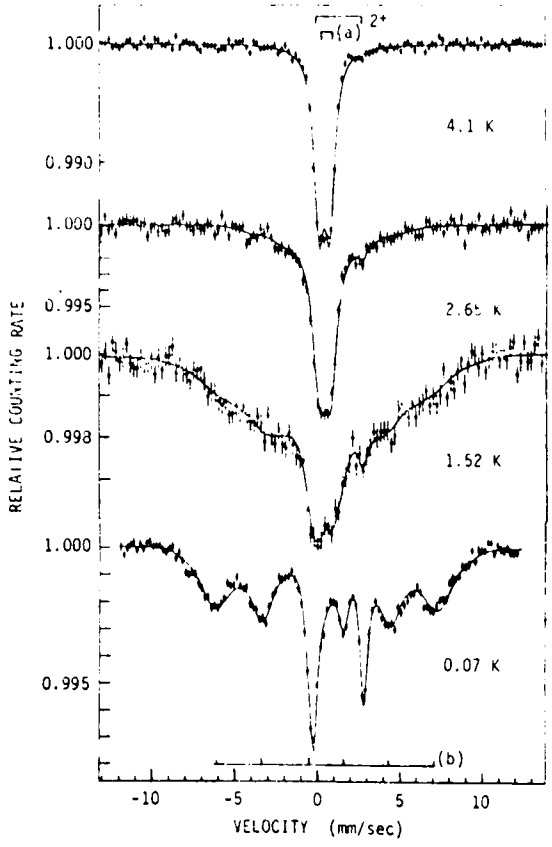

Fig. III.5.1:

Mössbauer spectra of whole M. capricolum cells. The solid lines are least squares computer fits to the spectra, assuming each spectrum to be a sum of Fe^{3+} doublet (subspectra(a)), a magnetically split spectrum (subspectra(b)), and a Fe^{2+} doublet. The position of the Fe^{3+} and Fe^{2+} lines are shown on top of the figure. The position of the lines for a magnetic field H_o are shown in the bottom of the figure.

III.6 Study of a case of corrosion of aluminosilicate refractories using the Mössbauer spectroscopy†

C.Puglisi*, F.Labenski, C.Saragovi-Badler

The Mössbauer effect provides information concerning the local surroundings of the iron ion in any material[1]. This kind of information can be useful in the study of corrosion mechanisms is steelmaking refractories When a molten slag attacks a refractory brick, it penetrates into the brick's porus, dissolving a part of their components and precipitating new solids. The velocity of dissolution is controlled by the mass transport in the liquid phase[2]. Then, as it is well known[3] the molten slag viscosity plays an important rol in the corrosion of aluminosilicate refractories and the iron oxides modify the fluidity of the slag. The accepted model[4] explaining the silicate glasses structure is to suposse a network of tetrahedrons, which are formed by a Si surrounded by 4 oxygen atoms bounded by the vertex and randomly distributed. The addition of mono-divalents ions (Na_2O,CaO,FeO) may alter the continuity of the network and in consequence to produce changes in the properties, in particular the viscosity. The Si^{4+} are "network-former" in tetrahedral positions in a fcc lattice of oxygen anions, while Ca^{2+} or Fe^{2+} are network-modifiers occupying octahedral sites. Al^{3+} or Fe^{3+} can occupy both positions. For example a higher percentage of Fe^{3+} in the octahedral sites of a slag should result in a decreased viscosity and a higher diffusion rate. The purpose of the present work is to investigate the interaction between a real molten slag and an aluminosilicate brick normally used for lining steel-ladle. Two samples were studied using Mössbauer spectroscopy. One of them belonging to a real molten slag and the other one belonging to the reaction product of the slag and an aluminosilicate brick normally used for lining steel-ladle. X-ray diagram of sample I (the slag) showed the presence of $Ca_2Fe_2O_5$ and a low percentage of B-Ca_2SiO_4. The Mössbauer spectrum of the same sample also showed the presence of the crystalline $Ca_2Fe_2O_5$, antiferromagnetic ferrite with one octahedral site and one tetrahedral site for the Fe^{3+}. This is in agreement with the idea[5,6] that in vitreous mixture with a high content of ferric oxide a precipitate of iron oxides or ferrites is formed. This spectrum also indicated the presence of Fe^{2+} in the octahedral sites of a glass[7]. Sample II Mössbauer spectrum shows the presence of Fe^{2+} and Fe^{3+} ions in the octahedral sites of a vitreous phase as well as a relaxation component[8].

A crystalline iron compound is not found which confirms that the iron is

totally incorporated in the vitreous phase when its content is low. The relative concentration of ions Fe^{2+} and Fe^{3+} are calculated. In silicate glasses Fe^{3+} can be found not only in tetrahedral sites but also in octahedral sites[5,7,8]. In our case these ions are in octahedral sites, although it is not possible to decide the coordination number of the Fe^{3+} ions which are responsible of the relaxation spectrum.

---

† Bolet.Soc.Esp.Seram. y vidrio, 18, (1978) 155.

* Centro de Investigaciones para las Industrias Minerales, INTI

1) H.Frauenfelder, "The Mössbauer Effect", W.A.Benjamin Inc. Pub., N.Y. (1963).

2) Y.Oishi, et al., J. Am. Cerm. Soc. 48(2) (1965) 88.

3) S.E.Feldman, et al., Met. Trans. 5 (1974) 249.

4) W.H.Zachariasen, J.Amer.Chem.Soc., 54 (1932) 120; Glastechn. Ber, N2 (1933) 120; J.Chem.Phys. 3 (1937) 162.

5) L.Pargamin, et al. Met. Trans. 3 (1972) 2093.

6) D.W.Collins and L.N.Mulay, J. Am. Ceram. Soc. 54(2) (1971) 69.

7) R.A.Levy, et al. Phys. Chem. Glasses, 17(4) (1976) 94.

8) J.M.D.Coey, J. Physique C6 N° 12,35 (1974) 89.

III.7 Corrosion of refractories in a steel-making electric arch furnace

C.Puglisi* and C.Saragovi-Badler

The aim of this work is to describe the results of a study of two samples of bricks taken at the end of a campaign : one belongs to the roof of an electric arc furnace (sample A) and the other to the slag line (sample B). The furnace is an ultrahigh power one with a 65 Ton capacity. During the campaign under investigation the furnace produced natural hardness steel with a manganese and carbon content of about 1 and 1.45% and of 0.30 and 0.41% respectively. The operation temperature was 1620 °C. Sample A consist of a high alumina brick, sample B is a fired magnesia one and the slag was oxidizing. Their composition is shown below

Average Composition of

slag		brick A		brick B	
Fe 0	3-4%	Al_2O_3	70%	Mg 0	93.5%
Mn 0	4-11%	Si_1O_2	25%	SiO_2	4.5%
Ca 0	33-50%	Fe_2O_3	1.5%	Ca 0	1.5%
Mg 0	2-8%	Alcalis	1.5%	Al_2O_3	0.2%
Si O_2	16-25%			Fe_2O_3	0.3%

The experimental techniques used are X-ray diffraction, Mössbauer spectroscopy and optical microscopy.

Sample A:

The experimental techniques allow the observation of the successives events taking place as the fumes produced during the furnace operation, attack chemically the bricks of the roof. The principal facts are a) in the hot-face a complex process of crystalization takes place when cooling down, with the appearance of calcic ferrite; b) the bricks matrix is completely destroyed and corundum crystals appear semiattacked in the zone next to the hot-face; c) next to it the corundum is attacked with less intensity and appears mixed with magnetite, hematite crystals and high-sized mullite crystals; d) after this zone amortite crystals are found besides the corundum ones, indicating that the silica and lime penetrate deeper than the iron oxides; e) finally a zone analogous to the brick appears. The Mössbauer spectrum identifies the iron compounds present[1], show the imperfect crystalization of them and the high degree of substitution of ions other than Fe in all the cases and together with the phase-diagrams indicate that the attack took place mainly in the matrix.

Sample B:

In this case the sequence of microphotographies of the brick attacked by the slag is the following: in the hot face magnesium ferrite crystals are found, periclase grains attacked, monticellite and silicate crystals and glasses. In going far apart from the hot face these grains are less attacked and the ferrite crystals are disappearing. One can then imagine the process as due to the penetration of the slag containing lime, silica and iron oxides and producing a fluid phase at the service temperature. This phase destroys the binding between the periclase crystals. The monticellite and the silicates, whose fusion is less than 1600 °C, lowered the resistence of the brick structure. When cooling down, a part of the compounds crystallized while the

other formed the glasses. These results agree with those obtained using an empirical diagram (White diagram[2]) which was done by correlating data from different mixtures of MgO, SiO_2 and iron oxides and varying the CaO content.

---

* INTI. Institute of Industrial Technology, Migueletes.

1) N.N.Greenwood, T.C.Gibb: " Mössbauer Spectroscopy" Chapman Hall Ltd., London (1971).

2) J.White in "High Temperature Oxides", Part I, A.M.Alper Editor Academic Press (1970).

III.8 Mössbauer Spectra of iron containing Nafion membranes†

E.R.Bauminger*, F.Labenski de Kanter, A.Levy*, S.Ofer* and C.Heitner-Wirguin**

Ion containing polymers have been intensively studied in recent years in solution as well as in solid state. The common property of this class of compounds is the aggregation of the ions together with the polar solvent (water) into clusters of various sizes in the polymeric matrix[1].

Among the ion containing polymers are also the ion exchange membranes. One of the common used membranes is Nafion (perfluorsulfonic acid). Mössbauer experiments on Nafion membranes have been performed in order to distinguish between the different kinds of iron complexes, to study their structure and magnetic properties and to estimate the size of clusters. For these measurements the hydrogen ions of the membranes were replaced by tervalent irons atoms. For the present study we used three Nafion samples. One sample of equivalent weight 1000 (sample 1) was equilibrated in a methanol solution and two samples of equivalent of 1100 (sample 2) and 1500 (sample 3) are equilibrated in aqueous solutions. Mossbauer spectra of sample 1 were measured between 1.5 °K and 80 °K, and samples 2 and 3, between 1.5 °K and 200 °K. Some of the spectra obtained with sample 1 are shown in fig. III.8.1. At 85 °K the spectrum is composed of doublets, one with a quadrupole splitting of 0.44 mm/s(1) and an isomer shift of 0.51 mm/s(1),(isomer shifts are relative to metallic iron) with relative intensity of ~80%, the other with a quadrupole splitting of 1.68 mm/s(2) and an isomer shift of 0.52 mm/s(2) with relative intensity of 20%. At 4.1 °K and lower temperature the relative

intensity of the first doublet (subspectrum A) decreases and a magnetically split spectrum (subspectrum B) appears instead. The relative intensity of the second doublet, subspectrum C, is 20% at all temperatures. Subspectrum C is attributed to iron-dimers with antiferromagnetic coupling and total spin zero[2]. The temperature dependence of subspectra A and B is characteristic of superparamagnetic particles[3]. Subspectra A and B correspond to iron containing clusters with non uniform sizes. The distribution of sizes of the aggregates can be deduced from data in Fig. III.8.2, using Neél's formula[4] $f=f_0 \exp(-CV/DT)$. Fig. III.8.3 shows the distribution of the diameters of the aggregates. Assuming that the value of f_0 and C are the same as in Fe_2O_3 [3] a value of 20 Å is derived for d in Fig. III.8.3. The spectra of samples 2 and 3 do not change between 4.1°K and 1.5°K and even at 85°K they are composed of three subspectra (A,B,C) with the same parameters as those of sample 1, except that the hyperfine field is about 10% higher (585±5 kOe). The fact that even at 85°K part of the spectra is split shows that these samples contain iron aggregates with d ~ 80 Å. In the Nafion samples examined two k nds of iron species are present: (1) clusters, (2) dimers. In the sample equilibrated with methanol the mean diameter of the clusters in 20 Å. In the water equilibrated samples, there are large clusters, (~ 80 Å) and small clusters (~ 15 Å).

---

† Accepted for publication on Journal de Physique.

* Racah Institute of Physics, The Hebrew University of Jerusalem, Israel,

** Department of Inorganic and Analytical Chemistry, The Hebrew University of Jerusalem, Israel.

1) T.D.Gierke, The Electrochemical Society Meeting, October 1977, Atlanta, Georgia,

2) R.Lechan, C.Nicolini, C.R.Abeledo, R.B.Frankel, J.Chem.Phys. 59 (1973) 3138.

3) W.Kunding et al., Phys. Rev. 142 (1966) 32.

4) L.Neel, Ann. Geophysique 5 (1949) 99.

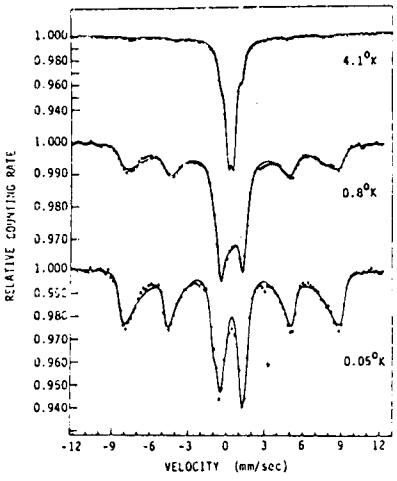

Fig. III.8.1: Mössbauer spectra of ^{57}Fe in Nafion equilibrated with methanol. The solid lines are least squares computer fits to the spectra, assuming 2 quadrupole doublets and a magnetically split spectrum with a distribution of hyperfine fields.

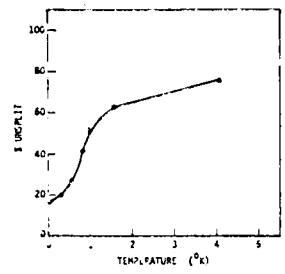

Fig. III.8.2: Ratio (%) between the intensity of subspectrum A and the sum of the intensities of spectra A and B, as a function of temperature.

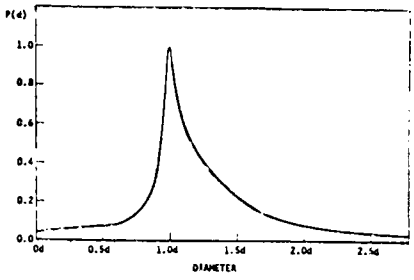

Fig. III.8.3 :

Distribution of cluster diameters in sample 1 .

IV. THEORETICAL SOLID STATE PHYSICS

IV.1 On the calculation of the potential in point-charge lattices by the planewise summation method†.

V.Massidda.

The potential of a lattice of point charges q immersed in a uniform neutralizing background ($\rho = -q/v$, v=volume of the unit cell) is given by the series

$$V(\vec{r}) = \frac{q}{4\pi\varepsilon_0} \sum_{\lambda} \left[\frac{1}{|\vec{r} - \vec{r}_\lambda|} - \frac{1}{v} \int_{v_\lambda} \frac{d\vec{r}'}{|\vec{r} - \vec{r}'|} \right] , \qquad (1)$$

where $\vec{r}_\lambda$ is the distance from the field- to the source-point (λ stands for three integers $\lambda_1,\lambda_2,\lambda_3$ characterizing the cell); the integration is carried out in the $\lambda_1,\lambda_2,\lambda_3$ cell.

As the above series converges very slowly, several methods have been proposed for a rapid calculation. The most well-known of them is the Ewald method[1]. Another, very practical, formula for $V(\vec{r})$ has been found by Sholl[2] using Nijboer and the Wette's planewise summation method[3].

As series (1) gives the potential of a crystal whose unit cell possesses a non-vanishing quadrupole moment, it depends on the shape of the region over which the summation is carried out[4]. The result of Sholl holds for a specimen shaped as a slab cut parallel to two crystal axes, $\vec{a}_1$ and $\vec{a}_2$, for points not lying on an $\vec{a}_1$, $\vec{a}_2$ crystal plane.

We have found a way of relating to each other the values of the potential at a fixed point of the unit cell, in two slabs cut parallel to two different pairs of axes (for instance, $\vec{a},\vec{b}$ and $\vec{b},\vec{c}$). We did that by introducing a suitable dipole layer on the surface of each cell, in such a way that the quadrupole moment of the latter vanishes. The potential inside a crystal with such a cell is shape-independent. All the dipole layers cancel out each other, except those on the external surface of the specimen; for a slab their potential is easily evaluated. Denoting by $V(\vec{r};abc)$ the potential in a slab parallel to the $\vec{a},\vec{b}$ plane (we are assuming that $\vec{a}$, $\vec{b}$ and $\vec{c}$ are mutually perpendicular) we have

$$V(\vec{r};abc) - \frac{qc^2}{24\varepsilon_0 v} = V(\vec{r};bca) - \frac{qa^2}{24\varepsilon_0 v} \quad . \qquad (2)$$

This formula can be applied to supplement Sholl's result for points on or near an a,b plane (in the former case Sholl's formula does not apply, in the latter it has a poor convergence).

We have also found an interpretation for the Ewald result, which gives the potential relative to its average value (instead of to infinity, as (1)) in a crystal of unspecified shape. In fact, we have checked by a numerical calculation that Ewald's result is equal to either side of eq.(2), i.e. it gives the potential relative to infinity inside a crystal with a dipole layer on its surface such that the potential is shape-independent. This result greatly clarifies the situation related to the apparent paradox about the shape-independence of the Ewald formula, which in the past has given rise to many discussions about its meaning and its validity (see for instance ref.5).

---

† Physica 85 B (1977) 311.

1) P.P.Ewald, Ann. d. Phys. 64 (1921) 253.

2) C.A.Sholl, Proc. Phys. Soc. 92 (1967) 434.

3) B.R.A.Nijboer and F.W.de Wette, Physica 24 (1958) 422.

4) C.A.Sholl, Proc. Phys. Soc. 87 (1966) 897.

5) E.S.Campbell, J.Phys. Chem. Solids 24 (1963) 197.

IV.2 Electrostatic energy in ionic crystals by the planewise summation method†.

V.Massidda .

We have derived an expression based upon the "planewise summation method" (see preceding paper) for the potential inside a crystal made of point charges. The crystal has the shape of a slab parallel to a pair of crystal axes, $\vec{a}_1$ and $\vec{a}_2$. The unit cell contains an arbitrary number of charges q_α, $\alpha = 1,2,\ldots,A$, satisfying the neutrality condition:

$$\sum_{\alpha=1}^{A} q_\alpha = 0 \quad .$$

The result is split into two terms, the physical meaning of which is the following . Let us consider for each crystal plane of charges q_α parallel

to $\vec{a}_1$ and $\vec{a}_2$ the uniform average distribution $\Gamma_\alpha = q_\alpha/\omega$ ($\omega = |\vec{a}_1 \times \vec{a}_2|$). Then one of the terms gives the potential of the charges q_α plus their neutralizing distributions $-\Gamma_\alpha$; the other gives the potential of the average distributions Γ_α.

We obtained, as is customary with the planewise summation method, two different expressions, one for field points not belonging to a crystal $\vec{a}_1,\vec{a}_2$ plane, the other for field points at a lattice site. If the field point does belong to a $\vec{a}_1,\vec{a}_2$ crystal plane without coinciding with a lattice site we have expressed the potential in terms of the first of the above expressions, using the result of our preceding paper[1].

Using our result we obtained a general expression for the electrostatic energy of an ionic crystal. We applied it to differently cut slabs of NaCl CsCl and Ba TiO_3, confirming the shape-dependence of the electrostatic energy for ideal crystals with a cell possessing a non-vanishing dipole moment and giving a quantitative explanation of it for the cases dealt with by us.

---

† Physica 95 B (1978) 317.

1) V.Massidda, Physica 85 B (1977) 311.

IV.3 The planewise summation method for triclinic lattices.†

V.Massidda and J.A.Hernando.

The planewise summation method is a very convenient procedure for a rapid evaluation of lattice sums like

$$S_{\ell_1,\ell_2,\ldots,\ell_n} = \frac{\partial}{\partial x_{\ell_1}} \frac{\partial}{\partial x_{\ell_2}} \cdots \frac{\partial}{\partial x_{\ell_n}} \sum_{\lambda_1\lambda_2\lambda_3} \frac{1}{|\vec{r} - \vec{r}_\lambda|} \quad .$$

It was devised by Nijboer and de Wette[1] for n=2, $\vec{r}$ at a lattice point and monoclinic lattices, extended by de Wette and Schacher[2] for n=2, arbitrary $\vec{r}$ and triclinic lattices, by Sholl[3] to $n \geq 1$, $\vec{r}$ not lying on an xy crystal plane and monoclinic lattices and by Sholl[4] and Massidda[5] to n=0, arbitrary $\vec{r}$ and orthorhombic lattices.

In all cases the result given by the planewise summation method refers to a crystal shaped as a slab which is cut parallel to a pair of crystallo-

graphic axes (denoted $\vec{a}_1$ and $\vec{a}_2$). The cartesian axes are chosen so that the xy plane is parallel to the slab.

In this paper we generalize the method to all possible situations, i.e. arbitrary n, arbitrary $\vec{r}$ and lattices with arbitrary symmetry. The procedure followed by us is essentially the same as in refs. 2 and 3 for $\vec{r}$ at a lattice site or $\vec{r}$ not lying on an xy crystal plane and in ref.6 for $\vec{r}$ on an xy crystal plane.

Our formulae furnish a very convenient way of checking the results. In fact, the quantity represented by the above sum can be evaluated in slabs cut in different ways with respect to the crystal axes $\vec{a}$, $\vec{b}$ and $\vec{c}$ ($\vec{a}_1=\vec{a}$, $\vec{a}_2=\vec{b}$ or $\vec{a}_1=\vec{b}$, $\vec{a}_2=\vec{c}$ or $\vec{a}_1=\vec{c}$, $\vec{a}_2=\vec{a}$). The results for the three situations are related to each other by a generalization of the procedure proposed in ref. 6, so that one has three non-equivalent formulae leading to the same quantity.

---

† Physica B, to be published

1) B.R.A.Nijboer and F.W.de Wette, Physica 24 (1958) 422.

2) F.W.de Wette and G.E.Schacher, Phys. Rev. 137 (1965) A78.

3) C.A.Sholl, Proc. Phys. Soc. 87 (1966) 897.

4) C.A.Sholl, Proc. Phys. Soc. 92 (1967) 434.

5) V.Massidda, Physica 95B (1978) 317.

6) V.Massida, Physica 85B (1977) 311.

IV.4 Plattsum: A Fortran Program that evaluates electrostatic lattice sums by the Planewise Summation Method.

J.A.Hernando and V.Massidda.

In this paper we program the equations given in refs.1,2 for calculating the electrostatic potential of a point-charge lattice and its spatial derivatives up to the fourth order. In all cases, in addition to the value of the sum, which may depend on the shape of the crystal, a shape-independent result is obtained. The latter corresponds physically to the same crystal, with a dipole layer on its surface[1]. The use of the Planewise Summation Method implies that these quantities correspond to crystals shaped as slabs cut parallel to two crystallographic axes. There are three slabs cut in this form and the shape-independent quantities calculated in these slabs are related

to each other by means of a rotation matrix. The fact of being able to obtain a given result in three different ways has two important advantages: 1) the computation time can be substantially decreased by adequately choosing the way of cutting the slab; 2) a very sensitive check of the accuracy of the result can be made.

The program can perform the calculations mentioned above an arbitrary number of times. There is no restriction on the lattice symmetry. For field points inside a small parallelepiped centered at a lattice site, the convergence is very slow. The program can do the calculations in this region at the cost of a loss of numerical accuracy and an increase in computation time.

---

[1]) V.Massidda and J.A.Hernando; Physica B to be published (see preceding report).
[2]) F.W.de Wette and G.E.Schacher, Phys. Rev. 137 (1965) A78.

IV.5 Internal fields and ferroelectric ordering in potassium ferrocyanide trihydrate †.

V.Massidda.

Among ferroelectric crystals containing water molecules in their structure, the potassium ferrocyanide trihydrate ($K_4Fe(CN)_6.3H_2O$) is one of the most extensively investigated. The mechanism of its phase transition has been, and still is, the object of considerable controversy. Presently most authors agree that the ferroelectric transition is due to the ordering of the water molecules, but for the orientation of the latter the two models that have been proposed up to now are radically different from each other[1,2].

In this paper we perform a calculation in order to find the true orientation of the water molecules in the ordered phase. The calculation is based upon a physical hypothesis about which is the dominant interaction giving rise to the transition. Relying on the experimental evidence, we assume that the water molecules can reorient themselves more or less freely under the effect of their interactions with the ions of the structure and with each other. Furthermore, as all the distances from the oxygens of the water molecules to the atoms with which H bonds might be formed are long, we assume that the hydrogen bonds in potassium ferrocyanide trihydrate are of a completely electrostatic character. For the water molecules we adopt the

same model that Baur[3] employed with considerable success for explaining the positions of the hydrogens in several hydrated crystals. According to this model each water molecule is replaced by a rigid structure of three point charges, -e on the oxygen and +1/2e on each hydrogen.

We write down the electrostatic energy of the water molecules as a function of their orientation. In doing so we take into account the crystal symmetry, i.e. the fact that the unit cell contains three crystallographically non-equivalent molecules (denoted as I, II and III). In such a way the electrostatic energy is a function of nine variables (the Euler angles of the non-equivalent molecules).

By a computational procedure we find that the energy is at a minimum for two configurations, which differ from each other in the orientation of the water molecules of type I. This means that the latter move in a double-well potential. The two equilibrium positions of the molecules of type I are related to each other by a 180° rotation around the y axis, i.e. they differ in the direction of the projection of their dipole moment onto the xz plane. This suggests that the para- to ferro-electric phase transition basically consists in the ordering of the water molecules of type I into the two equilibrium positions of the double-well potential they see as a result of their electrostatic interactions. Both the direction and the magnitude of the spontaneous polarization agree with experiment.

Our model agrees remarkably well with the NMR data of Kiriyama et al.[1] and with the neutron diffraction data[4]. However, the agreement is reached if the data are given, instead of the interpretation suggested in ref.1 and accepted by other authors[4], a different one; the latter was also suggested by Kiriyama et al.[1], but was judged by these authors less likely than the former. Our model agrees qualitatively with that of Habuda et al.[2], in that the transition is primarily associated with the reorientation of the water molecules of type I.

---

† J.Physics C 11 (1978) 2865.

1) R.Kiriyama, H.Kiriyama, T.Wada, N.Niizeki and H.Hirabayashi, J.Phys. Soc. Japan 19 (1964) 540.

2) S.P.Habuda, A.G.Lundin and E.P.Zeer, Ferroelectrics 1 (1970) 71.

3) W.H.Baur, Acta Crystallogr. 19 (1965) 909.

4) J.C.Taylor, M.H.Mueller and R.L.Hitterman, Acta Crystallogr. A26 (1970) 559 .

IV.6 Order-disorder transition in ionic crystals containing reorientable dipoles[†].

J.A.Hernando and V.Massidda.

The first mechanism to be proposed in order to explain a ferro- to para-electric phase transition was the disordering of the dipole moments of the water molecules. However, the experimental evidence accumulated in most ferroelectrics did not support this hypothesis, so that this mechanism was largely forsaken. Nevertheless, it is believed that for some ferroelectrics ($NaNO_2$ [1], $K_4Fe(CN)_6 . 3\,H_2O$ [2]) the transition is due to the cooperative ordering of permanent dipole moments.

In this paper the dielectric properties of a crystal made of several interpenetrating lattices of ions and reorientable permanent point dipoles are investigated from a statistical point of view. The ions and dipoles are both assumed to be polarizable. A set of functions n_i is introduced to describe the orientational disordering of the permanent dipoles. The electrostatic internal energy is calculated in the mean field approximation, and from it the free energy is obtained in terms of the n_i's. A transcendental system of equations for the latter is derived, from which the equilibrium configuration as a function of T can be found by numerical computation. The model predicts the possible occurrence of an ordered phase (which may be ferro-, antiferro- or ferri-electric) and a disordered, paraelectric phase. The electric susceptibility, specific heat and other quantities of interest are evaluated as functions of T. The formalism is applied to several simple tetragonal structures. In each case a ferro- or antiferro- to para-electric transition is found and the Curie temperature is evaluated. The kind of ordering and the direction of polarization are found to depend on the c/a relation.

[†] Physica 94A (1978) 413.

[1]) H.D.Megaw, Crystal Structures: A Working Approach (1973), p.485 .

[2]) V.Massidda, J. of Phys. C 11 (1978) 2865.

IV.7 Order-disorder transitions in ionic crystals containing reorientable molecules. I. The case T = 0°K.

J.A.Hernando and V.Massidda.

The formalism developed in the preceding paper[1] does not take into account the influence of the shape of the molecules. In other words, we consider there only two of the three orientational degrees of freedom of a rigid molecule. Clearly, the electrostatic interactions make it necessary to consider all of them from the outset.

The first step in this study is to consider the T=0°K case. In such a case the electrostatic energy coincides with the free energy. The electrostatic energy of a molecule in a crystal can be written in terms of its multipole moments. In ref.1 the expression was truncated at the dipole order; in this paper we include the quadrupole moment, so that the three orientational degrees of freedom are included in the electrostatic energy.

An expression for the electrostatic energy of a general crystal containing point charges, dipoles and quadrupoles was written down in terms of the Euler angles of the molecules. Then this expression was applied to tetragonal structures (like those considered in ref.1) containing a sublattice of triangular molecules; the latter were approximated by point distributions with a net charge, a dipole and a quadrupole moment. The equilibrium configuration was obtained by minimizing the above expression.

The main result we obtained is that in some structures the interaction between the quadrupole moment and the ionic charges of the crystal is of fundamental importance in determining the equilibrium configuration. This implies, in many cases, a qualitative modification of the results given in the dipolar approximation. This is of importance in some ferroelectric crystals.

---

[1]) J.A.Hernando and V.Massidda, Physica 94A (1978) 413.

IV.8 Order-disorder transitions in ionic crystals containing reorientable molecules. II. The case T ≠ 0°K.

J.A.Hernando and. V.Massidda

The natural continuation of the work referred to in the two preceding reports would consist in introducing distribution functions $n_i(\phi_i,\theta_i,\psi_i)$

depending on the Euler angles of the molecules, and minimizing the free energy at a general temperature T. This program leads to a system of integral equations which is exceedingly difficult to solve.

We consider two ways of reducing the difficulty of the problems while keeping the quadrupole interaction.

Firstly, we investigate a two-dimensional model consisting of a planar molecule with charge, dipole and quadrupole moment in a two-dimensional crystal.

Secondly, we retain the three-dimensional character of the problem but we relax, to some extent, the rigidity conditions for the molecules. Each molecule is thought of as a spatial distribution of point charges which is replaced by a set of point dipoles. The average values of the angles between these dipoles are introduced as constraints. In this way we obtain a variational problem similar to that in ref. 1, which can now be solved.

The preliminary results support the conclusions reached in the preceding report, particularly in what concerns the role of the charge-quadrupole interaction.

---

1) J.A.Hernando and V.Massidda, Physica 94A (1978) 413.

IV.9 The phase diagram of $NiS_{2-x}Se_x$: intermediate valence effects†

J.Mazzaferro*, H.Ceva and B.Alascio*

$NiS_{2-x}Se_x$ ($0 < x < 2$) exhibit several magnetic and electric phase transitions, as a function of composition, (x), and temperature, T (Ref. 1); it is possible to identify four main phases: paramagnetic insulator; antiferromagnetic insulator (both for small x); antiferromagnetic metal and paramagnetic metal. Most remarkably, for high Se concentration ($x > 1$) the Ni atoms seem to lose their magnetization.

A behaviour similar to the one described in relation with the apparent demagnetization, has been observed previously in rare earth alloys. Theoretically, an intermediate valence (IV) interpretation of these properties is now generally accepted (Ref. 2).

We have applied similar ideas to $NiS_{2-x}Se_x$. This represents one of

the first attemptsto use IV in transition metal alloys. We consider a generalization of the Falicov-Kimball model that includes magnetic interactions between the localized levels' spins, and an hybridization term that leads to the intermediate valence intrepretation of the demagnetization of the compounds. The main effect of the hybridization term is assumed to be the introduction of a finite lifetime $(\Gamma)^{-1}$ for the 3d levels. It has been shown that the numerical consequences are similar to the ones obtained by the use of the Sales and Wohlleben 'ansatz'[3] , namely the replacement of the real temperature T by $T^{eff} = T + \Gamma$ ($\hbar = k_B = 1$). The intrasite term of Falicov-Kimball, and the magnetic interactions were treated in the mean field approximation.

From the resulting free energy we study the behaviour of the number of localized electrons and the magnetization, n and m respectively, as a function of x and T. Adjusting several experimental parameters, it is possible to get a reasonable agreement with published experimental phase diagrams.

---

† Accepted for publication in Phys. Review B.

* Centro Atómico Bariloche, CAB-CNEA.

1) See, for instance, F.Gautier, G.Krill, M.Lapierre, P.Panissod, C.Robert, G.Czjzek, J.Fink, H.Schmidt; Phys.Lett. 53A (1975) 31.

2) R.D.Parks (Ed): Valence instabilities and related narrow band phenomena (Plenum Press, 1977).

3) B.C.Sales and D.Wohlleben , Phys. Rev. Lett. 35 (1975) 1240.

IV.10 The Falicov-Kimball model: an intermediate solution

J.Mazzaferro* and H.Ceva

The Falicov-Kimball model of a metal-insulator transition assumes the existence of a conduction band of uncorrelated electrons and localized states where, due to intratomic correlation effects, it can be at most one hole. There is a gap, Δ, between the localized states and the bottom of the band. Electrons are promoted thermally from the localized sites to the conduction band. The bandwith denoted by W.

The model's Hamiltonian can be written as follows:

$$H = T_0 \sum_{i,\sigma} C^+_{i\sigma} C_{i\sigma} + E \sum_{i,\sigma} b^+_{i\sigma} b_{i\sigma} - G \sum_{i,\sigma,\sigma'} C^+_{i\sigma} C_{i\sigma} b^+_{i\sigma'} b_{i\sigma'} + \sum'_{i,m,\sigma} T_{mi} C^+_{m\sigma} C_{i\sigma}$$

where the c's and b's refer to electrons and holes; the sums are over the sites and spin, and in the last term only nearest neighbor interactions are considered. The intransite G-interaction is assumed to be responsible for the transition.

Depending on the relative values of (G/Δ) and (W/Δ) it is possible to obtain, in the mean field approximation, different behaviours as a function of temperature: a pure insulator, a pure metal, or metal-insulator transitions (either continuous or first order).

Rather recent works (ref. 1,3) have attempted to solve the model using CPA. Unfortunately, there is no agreement between the results of these papers. We have solved the model within the approximation proposed by Hubbard in his first paper on electron correlations (Ref.4): its simplicity makes it very attractive if one is trying to avoid eventual computational problems which seem to be present in the CPA calculations. After obtaining the Green function, the number of conduction electrons, n, is calculated from the grand partition function. The result is shown in the Fig.IV.10.1, for the case of a simple cubic lattice, as a function of reduced inverse temperature, Δ/kT, for $G=21,4\Delta$.

We only found an insulating phase; therefore our result agree, qualitatively, with the work of Ghosh.

A more extended version of this work can be found in Ref.5.

---

* Centro Atómico Bariloche, CNEA.

[1]) M.Plischke Phys. Rev. Letters 28 (1972) 361.

[2]) C.E.T.Concalves da Silva and L.M.Falicov J. Phys. C5 (1972) 906

[3]) D.K.Ghosh Solid State Commun. 18 (1976) 1377.

[4]) J.Hubbard Proc. Roy. Soc. A276 (1963) 238.

[5]) J.Mazzaferro and H.Ceva, Solid State Commun. 29 (1979).137

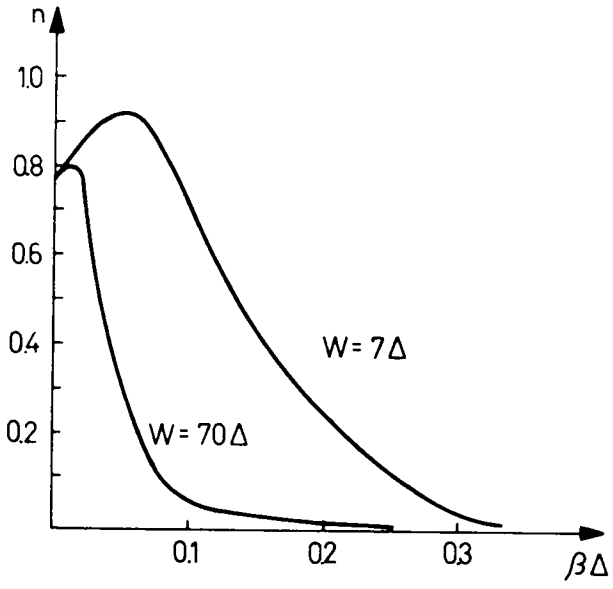

Fig. IV.10.1

IV.11 Theory of disordered systems.

M.Weissmann and N.V.Cohan

In this period we have continued with the study of electronic properties of disordered materials. We have further extended our interests to the study of the structure of microclusters, by the molecular dynamics method. The specific problems considered were:

a) Systems with structural disorder which present a metal-non metal transition[1].

We studied some disordered systems which present a metal-non metal transition such as the impurity bands in doped semiconductors and the alkali metals in supercritical conditions and in noble gas matrices. All these problems can be studied within a single formalism: a tight binding method with a single 1s orbital per atom. In the present work, we consider the effect of the disorder in both, diagonal and non-diagonal matrix elements of the Hamiltonian, in a non orthogonal basis. In the calculations, the intra-atomic electronic repulsion was considered within a self-consistent procedure. The disordered system was represented by random distributions of identical atoms, and the calculations were perfomed in two dimensions for systems of about 150 atoms. The density of states, the localization and the redistribution of charges due to the disorder were calculated as functions of the degree of disorder (or density, as these two variables were taken to be inversely proportional). A metal-non metal transition was obtained for

a value of the density in agreement with experiments.

b) Density of states at the surfaces of graphite.

Local densities of states were calculated in the basal plane (0001) and in two perpendicular planes, $(11\bar{2}0)$ and $(10\bar{1}0)$, of graphite. A basis of four atomic orbitals per carbon atom and the continued fraction formalism were used in the calculations. Trigonal sp^2 hibridization was used in general, but in the case of the $(10\bar{1}0)$ suface, a change in the hibridization of the more external atoms was studied. The densities of states in the three surfaces were very different from each other. In particular, the $(10\bar{1}0)$ surface presents a very pronounced maximum of the local density of states at the Fermi level. This suggests that this surface would be very adequate for adsorption.

This work was presented by R.Farengo as his Seminar in march 1979, in partial fulfillment for the requirements of the Licenciatura en Física at the University of Buenos Aires.

c) Molecular dynamics of microclusters[2]

Two dimensional and adsorbed microclusters of 6,7,8, and 19 rare gas atoms were studied by the molecular dynamics method. All clusters present two distinct regions as a function of temperature: a low temperature regime typical of a solid and a high temperature "liquid" one, in which the clusters remain condensed but the atoms move in a variety of ways, according to the number and shape of the cluster. The systems with close shells of neighbours of the central atom (7 and 19 atoms) present also a "transition" region and further properties at high temperatures typical of a liquid phase. The effect of a weak interaction with a surface becomes important at high temperatures where the clusters evolve to three dimensions as some of the atoms move away from the surface.

---

[1]) N.V.Cohan and M.Weissmann, J.Phys. C Solid St. 12 (1979) 1835.

[2]) M.Weissman and N.V.Cohan, J. Chem. Phys. accepted for publication.

V. DEVELOPMENTS AND SERVICES

V.1 Developments.

V.1.1 High speed digital microdensitometer.

P.König and H.Ceva.

During 1978 the Solid State Physics Division installed a computer assisted equipment for image processing, consisting of a high speed digital microdensitometer Optronics P-1000 model, on line with a Computer Automation, LSI 2-20 processing unit.

The main purpose of this equipment is the digitalization of single X-ray diffraction films for crystal structure analysis. It will also be used for the digitalization of electron micrographs obtained in a Philips EM-300 electron microscope. These will be electron micrographs of the Solid State Physics and the Biological-Radiation-Damage groups.

We are now beginning to work in the software for digitalizing X-ray single crystal diffraction films on the basis of M. Elder's operating system[1].

The minicomputer is planned to be interfaced to a Fourier interferometer of the Raman and Infrared research group.

---

[1]) P.Machin and M.Elder; Internal Report of the Atlas Computer Laboratory (1974).

V.1.2 Developments of the electronic workshop.

A.Rugilo and P. de la Hera.

A stepwise programmable, regulated current source, adjustable from 1 to 2 Amps and from 0 to 300 seconds has been designed and constructed.

It was requested by the Mass Spectrometer group for the filament preparation stage in the transformation of a solution of $NO_3.UO_2$ into UO_3. It has been complemented by an audible alarm device which tells when to stop the process, which is carried out in an automatic way.

V.1.3 Mechanical workshop activities.

N.Gutierrez and I.Petragalli.

A low temperature goniometric Raman X-ray cell was designed and constructed. The purpose of the cell is to grow single crystals at low temperatures, orient them in situ in a Wessemberg camera and obtain polarized Raman spectra.

A stainless steel, high pressure chamber, was constructed by request of the Reactor Chemistry Group. It is to be used in the determination of electrolite conductivities in conditions of pressure and temperature which simulate those prevailing in the primary circuit of pressurized water reactors and is complemented by a hydraulic press, capable of exerting up to 1000 kg/cm^2.

V.2 Services

V.2.1 Services rendered to industry, public and private institutes.

Mössbauer and X-ray analysis of iron oxi-hydroxide samples and of iron patinas exposed to different atmospheric conditions. (Requested by CITEFA).

Identification by Mössbauer spectroscopy of some constituents in attacked and corroded samples. (Requested by LEMIT).

Identification by X-ray diffraction of some manganese-oxide samples. (Requested by Administración Nacional de Aduanas).

Mössbauer study of ^{119}Sn samples and some splat cooled Sn-Pb alloys. (Requested by the Physics Department, Facultad de Ingeniería, UNBA).

X-ray and electron diffraction, and electron microscopy of phosphate minerals of Córdoba province. (Requested by the Minearalogy Group, Facultad de Ciencias, UNC).

X-ray diffraction studies of five samples of metallic salts of sulphonamides. (Requested by Facultad de Bioquímica, Química y Farmacia, UNT).

Electron microscopy of some 80 clay samples from Neuquén and Chubut provinces.

X-ray diffraction study of the dehidration of highly hydrated plancheites. (Requested by the Mineralogy Group, Facultad de Ciencias, UNC).

Identification by Mössbauer spectroscopy of different synthetic organic compounds. (Requested by UNLP).

Differential thermal analysis of different inorganic and organic samples. (Requested by UNLP, UNBA, Instituto de Geoheliofísica and private laboratories).

X-ray diffraction study of quartz monocrystals. (Requested by INTI).

Electron microscopy study of several poliestirene samples. (Requested by a private laboratory).

Infrared spectroscopy analysis of some 100 organic samples. (Requested by private laboratories).

X-ray diffraction studies of zinc oxide samples. (Requested by a private industry).

V.2.2 Services rendered to other CNEA laboratories.

Electron microscopy study of the shape and size of particles obtained during simmulation studies of a nuclear reactor cooling system behaviour. (Requested by Reactor Chemistry Department).

Mössbauer spectroscopy studies of corrosion products obtained from the Atucha reactor cooling system. (Requested by Reactor Chemistry Department).

Differential themal analysis (under different conditions) of several uranium oxide and ammonium di-uranate samples. (Requested by Metallurgic Department).

X-ray diffraction study of some 20 samples of Potasium Fluor-zirconate and several Zr and Hf oxides samples. (Requested by Inorganic Chemistry Division).

X-ray diffraction identification of two forms of zirconium oxide in several samples. (Requested by Analytical Chemistry Division).

Infrared spectrometry determination of 14 samples of Ca-Mg glicerophosphates. (Requested by Radioisotopes Department).

Infrared spectroscopy identification of various samples. (Requested by Chemical Process Department).

X-ray diffraction study of various samples for the Reactor Chemistry, Analytical Chemistry, Heavy Water and Chemical Processes Departments.

Solar Energy

SOLAR ENERGY

Experimental and Theoretical Study of Concentrator Systems

Solar Energy Applications Group*

The final aim of the program is to heat fluids to 300 - 500 C in order to generate steam able to drive a turbogenerator. Intermediate aims are to provide industrial process heat, drive water-pumping systems and refrigeration units for the food industry, etc.

The optical performance of a fixed-faceted-mirror solar concentrator (FFMSC) was simulated with a preliminary program; this was later generalized to a bidimensional analysis valid for any angle of incidence of the solar radiation, which was applied to the study of 5 different types of concentrators having cylindrical symmetry. The results allow to select the optimal parameters for each concentrator and to compare their optimized performance against each other.

Two FFMSC "laboratory prototypes" have been built. Each has a radius of 1 m and a length of 2.4 m. The 110 second-surface flat glass mirrors of each module are 2 cm wide and may be adjusted individually in their tilt in order to optimize concentration. The concentrator's structure itself may be tilted up to 60 degrees with its symmetry axis either in the N - S or in the E - W direction. The receiver is formed by 4 steel tubes 1 cm in diameter, properly insulated and front - covered by a heat - resistant glass. Therminol 66 is used as heating fluid, at atmospheric pressure and up to 320 C. A tracking system was designed and implemented and satisfactorily laboratory tested. The behavior of mirrors of different thicknesses and fixed with several adhesives was followed under atmospheric conditions for several months up to now. Preliminary measurements of the energy flux in the focal plane have been performed. Exhaustive test measurements are due to start. A theoretical study of different selective surfaces led in our case to disregard them as a coating for the receiver tubes; instead, a paint of high absorptance was preferred.

The theoretical treatment of a modified FFMSC having curved mirrors and of a concentrator formed by movable, curved mirrors mounted on a curved frame have been developed. Both show concentration powers significantly higher than that of a FFMSC; difficulties in construction have to be weighted against this advantage.

---

* Work is performed by agreement between the Department of Physics and the Department of Prospective and Special Studies, following programs proposed by the latter.

Appendix

Staff
Publications

PERSONNEL OF THE PHYSICS DEPARTMENT

A. Research Staff

Abriola, D. (1)
Achterberg, E.
Alonso Arias, C. (2)
Badler, C.
Baggio, R.
Benyacar, M. (3)
Berisso, M. (4)
Bes, D.*
Bonadeo, H.* (5)
Burgos, E.*
Ceballos, A. (6)
Ceva, H.*
Dragún, O.
Düering, E. (7)
Dussel, G.*
Etchegoyen, A. (8)
Fernández Niello, J. (9)
Ferrero, A.
Filevich, A. (10)
Frigerio, A.
Gamba, Z.
García Bermúdez, G.*
Halac, B.
Hernando, J.
Huck, H.
König, P.
Kreiner, A.
Labenski, F. (11)
Lanza, H.
Manghi, E.
Maqueda, E.* (12)
Mariscotti, M. (13)

Massidda, V.
Moragues, J.* (14)
Otero, D.
Pacheco, A. (15)
Perazzo, B.
Perazzo, R.* (16)
Pérez, M.
Pérez Ferreira, E. (17)
Pomar, C.
Proto, A.
Reich, S.
Rossi, J.
Saraceno, M.
Scheuer, W.
Sofía, H.
Ventura, E.
Wainer, L.

B. Research Staff Associated to the Physics Department

Behar, M.
Cambiaggio, M.C.*
Cohan, N.
Davidson, J.*
Davidson, M.*
Levi, L.*
Szybisz, L.*
Weissman, M.*

C. Visiting Scholars

Acquadro, J.	(Univ. de Sao Paulo, Brasil)
Amelinckx, S.	(Studiecentrum Voor Kernenergie, Belgium)
Bodenstedt, E.	(Univ. of Bonn, West Germany)
Borello-Lewin, T.	(Univ. de Sao Paulo, Brasil)
Brouers, F.	(Univ. Liege, Belgium)

Browne Moreno, E.	(Lawrence Berkeley Lab., USA)
Döhnert, L.	(Univ. Central de Venezuela)
Donángelo, R.	(Univ. Fed. de Río de Janeiro, Brasil)
Evans, J.	(Univ. of Sussex, U.K.)
Goldring, G.	(Univ. of Rehovot, Israel)
Hahne, F.	(Atomic Energy Board of South Africa)
Krmpotic, F.	(Univ. de Sao Paulo, Brasil)
Lepine, A.	(Univ. de Sao Paulo, Brasil)
López García, A.	(Univ. Nac. de La Plata, Argentina)
Massmann, H.	(Univ. Nac. de Chile)
Massolo, P.	(Univ. Nac. de La Plata, Argentina)
McVoy, K.	(Univ. of Wisconsin-Madison, USA)
Megaw, H.	(Cambridge University, U.K.)
Menchaca Rocha, A.	(Univ. Nac. Autónoma de Méjico)
Mendoza Selis, L.	(Univ. Nac. de La Plata, Argentina)
Moshinsky, M.	(Univ. Nac. Autónoma de Méjico)
Pasquevich, A.	(Univ. Nac. de La Plata, Argentina)
Pereira, D.	(Univ. de Sao Paulo, Brasil)
Piacentini, R.	(Univ. Nac. de Rosario, Argentina)
Plastino, A.	(Univ. Nac. de La Plata, Argentina)
Thieberger, P.	(Brookhaven National Lab., USA)
Toledo Piza, A.	(Univ. de Sao Paulo, Brasil)

D. Research Students

Acuña, C.	(18)
Carcione, J.	(19)
Di Gregorio, D.	(20)
Dukelsky, J.	
Faerman, C.	
Gattone, A.	
Gil, S.	(21)
Levin, N.	
Sa, C.	
Spina, M.	(22)

E. Programming Asistent

Díaz Romero, A.

F. Engineering Staff

Camín, D.	(23)
Fazzini, N.	(24)
González, H.	(25)
Martí, G.	
Mazocchi, A.	(26)
Milberg, J.	
Mónico, J.	
Nicolai, J.	(27)
Requejo, R.	(28)
Tau, S.	(29)

G. Technical Staff

Bolaños, C.	
Bustos, J.	
Boretto, J.	
Carmuega, M.	
Cava, G.	
Collado, A.	(30)
Coralo, J.	
Cordeyro, S.	
D'Agostino, R.	
de la Hera, P.	
Garanzini, J.	
Garay Ramos, E.	
Giménez, C.	
Gutierrez, N.	
Ietri, B.	
Kesque, J.	
Laffranchi, J.	
Lires, S.	

Menéndez, E.
Miguez, C.
Morales, A.
Orecchia, J. (31)
Orecchia, J.D.
Petragalli, I.
Prieto, J.
Professi, M.
Rendina, J.
Riso, J.
Rodríguez, E. (32)
Rodríguez, J.
Rugilo, A.
Satinosky, M.
Schiavino, R.
Swiszcz, S.
Tersigni, A.
Vidallé, J.

H. Secretaries

Cáceres, A.
Ghiotti, B.
Perepitzka, A.
Ursú, C.

I. General Maintenance Staff

Barzola, G.
De Brasi, O.
Gómez, D.
Piccini, G.
Schevenels, L.
Soler, H.

(*) Fellow of the Consejo Nacional de Investigaciones Científicas y Técnicas (CONICET).

(1) Starting May 1979 on leave at State University of New York at Stony Brook, USA.

(2) Terminated September 1979.

(3) Head Solid State Physics Division.

(4) Starting October 1978 on leave at University of Oxford, England.

(5) From September to November 1979 on leave at Istituto di Chimica Fisica, University of Florencia, Italy.

(6) Until December 1979, Head Expèrimental Nuclear Physics Division.

(7) Starting October 1978 on leave at Weizmann Institute, Rehovot, Israel.

(8) Starting October 1978 on leave at University of Oxford, England.

(9) Starting October 1978 on leave at Sektion Physik der Universität, München, West Germany.

(10) Starting December 1979, Head Experimental Nuclear Physics Division.

(11) From June 1978 to October 1979 on leave at Racah Institute of Physics, The Hebrew University of Jerusalem, Israel.

(12) From October 1977 to November 1978 on leave at University of Sussex, England. Starting 1979, Head Theoretical Nuclear Physics Division.

(13) Chairman, Department of Physics.

(14) Head S. .ar Energy Group.

(15) Starting September 1979 on leave at Lawrence Berkeley Laboratory, University of California, USA.

(16) Until December 1978, Head Theoretical Nuclear Physics Division.

(17) Managing Director 20UD TANDAR Project.

(18) Terminated March 1979.

(19) Starting September 1979 on leave at Niels Bohr Institutet, Copenhagen, Denmark.

(20) Starting September 1979 on leave at Oak Ridge National Laboratory, Tennessee, USA.

(21) Starting September 1979 on leave at Nuclear Physics Laboratory, University of Washington, USA.

(22) Starting October 1979 on leave at University of Heidelberg, West Germany.

(23) During January-February 1979 on leave at IAEA, San José de Costa Rica. From June to August 1979 on leave at IAEA, Dublin, Rep. of Ireland.

(24) Until November 1978, Head Technical Assistance and Engineering Division. During 1979 on leave at Oak Ridge National Laboratory, Tennessee, USA.

(25) From August to December 1979 on leave at Oak Ridge National Laboratory, Tennessee, USA.

(26) Terminated July 1979.

(27) From November 1978 to July 1979 on leave at Oak Ridge National Laboratory, Tennessee, USA.

(28) Starting November 1978, Head Technical Assistance and Engineering Division.

(29) Starting December 1979 on leave at Electrostatics International, Inc., Wisconsin, USA.

(30) Terminated September 1979.

(31) Terminated February 1979.

(32) Terminated October 1979.

PUBLICATIONS OF THE PHYSICS DEPARTMENT

A. Papers published or accepted during report period

Nuclear Physics

- Rotational Structures in Doubly Odd Transitional Tl Nuclei.
  A.J.Kreiner, M.Fenzl and W.Kutschera.
  Nucl.Phys. A308 (1978) 147.

- Collective Treatment of the Pairing Hamiltonian (V). Analysis of Transfer Data for 88 < A < 96.
  R.P.J.Perazzo, S.L.Reich and D.R.Bes.
  Nucl.Phys. A311 (1978) 219.

- The Nuclear Field Theory of the Inelastic Scattering of Structureless Particles by Nuclei.
  G.G.Dussel, E.E.Maqueda and R.P.J.Perazzo.
  Phys.Rev. C17 (1978) 2011.

- The Renormalization of Collective States and the Improper Initial and Final States in Nuclear Field Theory.
  D.R.Bes, G.G.Dussel, R.P.J.Perazzo and H.M.Sofía.
  Nucl.Phys. A307 (1978) 402.

- The Nuclear Field Theory.
  D.R.Bes.
  Notas de Física, Instituto de Física, UNAM, Mexico (1978) N° 1.

- On the Convergence of the Nuclear Field Theory Perturbation Expansion for Strongly Anharmonic Systems.
  P.F.Bortignon, R.A.Broglia and D.R.Bes.
  Phys.Lett. 76B (1978) 153.

- Conclusiones Generales. Reunión de Estudio Bariloche I. Acelerador de 20 MV de la CNEA.
  D.R.Bes.
  O.Dragún, R.P.J.Perazzo and J.J.Rossi, ed.. Publicación CNEA-NT 21/78, Buenos Aires (1978) 107.

- Tratamientos Simples de Sistemas Complejos.
  D.R.Bes.
  Anales de la Academia Nacional de Ciencias Exactas, Físicas y Naturales; Tomo 30 (1978) 285.

- Collective Coordinates in Fermi Systems.
  V.Alessandrini, D.R.Bes and V.Machet.
  Nucl.Phys. B142 (1978) 489.

- A Quantum Mechanical Treatment of Rotating Fermion Systems.
  V.Alessandrini, D.R.Bes and V.Machet.
  Phys.Lett. B80 (1978) 9.

- Tratamiento Cuántico de un Sistema de Fermiones en Rotación.
  D.R.Bes.
  Anales de la Academia Nacional de Ciencias Exactas, Físicas y Naturales; Tomo 31 (1978) 13.

- The Alpha Transfer Reactions and the Pairing Vibrational Model.
  R.A.Broglia, L.Ferreira, P.D.Kunz, H.M.Sofía and A.Vitturi.
  Phys.Lett. 79B (1978) 351.

- Multi-detector Arrangements for On-line Measurements of γ-ray and Neutron Multiplicities.
  A.Kerek, J.Kihlgren, T.H.Lindblad, C.Pomar, J.Sztarkier, W.Walus, O.Skeppstedt, J.Bialkowski, J.Kownacki, Z.Sujkowski and A.Zglinski.
  Nucl.Inst. and Meth. 150 (1978) 483.

- Quasi-spin Pairing and the Structure of the Lipkin Model.
  M.C.Cambiaggio and A.Plastino.
  Z.Physik A288 (1978) 153.

- Gamow-Teller β-transition from the 2^- Ground State of ^{88}Rb to the 3^- Excited State of ^{88}Sr.
  L.Szybisz and J.Silbergleit.
  Z.Phys. A284 (1978) 399.

- Induced Scalar Interaction in the Analysis of Superallowed Fermi β-transitions.
  L.Szybisz.
  Z.Phys. A285 (1978) 223.

- The Decay of the T = 1 Isospin Triplet in A = 12 Systems: II. The Induced Interactions in the Anisotropy of Beta-rays.
  L.Szybisz.
  Z.Phys. A287 (1978) 183.

- The First $9/2^+$ State in ^{75}Br and Evidence for Maximum Deformation at N ≈ 42.
  M.Behar, A.Filevich, G.García Bermúdez and M.A.J.Mariscotti.
  Phys.Rev. C17 (1978) 516.

- Digital Multidiscriminator for Use in Gamma-gamma Coincidences Experiments.
  M.Behar, A.Filevich, G.García Bermúdez, M.A.J.Mariscotti, J.Mónico, J.Sinderman, S.Tau and P.Thieberger.
  Nucl.Inst. and Meth. 152 (1978) 531.

- High Spin States in ^{89}Y.
  M.Davidson, J.Davidson, M.Behar, G.García Bermúdez and M.A.J.Mariscotti.
  Nucl.Phys. A306 (1978) 113.

- In Beam Study of ^{70}As.
  A.Filevich, M.Behar, G.García Bermúdez, M.A.J.Mariscotti, E. der Mateosian and P.Thieberger.
  Nucl.Phys. A309 (1978) 285.

- Particle-rotor Model for Doubly Odd Transitional Nuclei of the Tl-region.
  A.J.Kreiner.
  Z. fur Physik A288 (1978) 373.

- The Renormalization of Single Particle and Collective States in Nuclear Field Theory.
  R.P.J.Perazzo and S.L.Reich.
  Lectures delivered at the 1978 Latin American School of Physics; University of Puerto Rico, Mayagüez, Puerto Rico.

- Band Structure in ^{78}Rb.
  M.A.J.Mariscotti, G.García Bermúdez, J.C.Acquadro, A.Lepine, M.N.Rao, W.Seale, E. der Mateosian and P.Thieberger.
  Phys.Rev. C19 (1979) 1301.

- The Decay of the T = 1 Isospin Triplet in A = 12 Systems: III. Higher Order Effects in the Evaluation of the Asymmetry Parameters $\alpha_{\pm}$ for the Electron Emission from Aligned ^{12}B and ^{12}N.
  L.Szybisz.
  Z.Phys. A289 (1979) 315.

- Current State of the Investigation of Superallowed Fermi β Decays.
  L.Szybisz.
  Z.Phys. A292 (1979) 49.

- In-beam γ-ray Spectroscopy in ^{194}Tl.
  A.J.Kreiner, M.Fenzl, U.Heim and W.Kutschera.
  Phys.Rev. C (Dec. 1979).

- Coriolis Interaction.
  A.J.Kreiner.
  Phys.Rev.Lett. 42 (1979) 829.

- Long-lived Positive Parity Isomer in ^{76}Br.
  A.J.Kreiner, G.García Bermúdez, M.A.J.Mariscotti and P.Thieberger.
  Phys.Lett 83B (1979) 31.

- Coriolis Distorted Bands of Common $g_{9/2}$ Parentage in Doubly Odd and Odd N = 41 Nuclei.
  A.J.Kreiner and M.A.J.Mariscotti.
  Phys.Rev.Lett. 43 (1979) 1150.

- A Microscopic Model for the pd → tπ^+ Reaction.
  A.M.Green and E.E.Maqueda.
  Nucl.Phys. A316 (1979) 215-243.

- Number Conserving Derivation of the BCS Equations.
  G.G.Dussel and D.R.Bes.
  Nucl.Phys. A323 (1979) 392.

- Nuclear Field Theory Treatment of the Interacting Boson Model. Interacting Bosons in Nuclear Physics.
  D.E.Bes and R.A.Broglia.
  F.Iachello, ed.. Plenum Press, New York (1979) 143.

- Gamma-gamma Coincidences and Electron Conversion Measurement in ^{141}La.
  A.N.Proto, D.Otero and E.Achterberg.
  J.Phys. G: Nucl.Phys., Vol 5 (1979) 121.

- Study of ^{151}Eu Levels Via the (p,2nγ) Reaction.
  G. Lo Bianco, N.Molho, A.Meroni, S.Hugius, N.Blasi and A.Ferrero.
  J.Physics G: Nucl.Phys. 5 (1979).

- α Emission in Proton Induced Reactions.
  A.Ferrero, E.Gadioli, E.Gadioli Erba, I.Iori, N.Molho and L.Zetta.
  Z.Physik A (1979).

- Quasi-spin Projection in an Exactly Soluble Model.
  M.C.Cambiaggio and A.Plastino.
  Z.Physik A291 (1979) 277.

- A Reformulation of the Mode-coupling Method.
  R.J.Liotta and C.Pomar.
  Letter to Nuovo Cimento (in press).

- In Beam Study of ^{192}Tl.
  A.J.Kreiner, A.Filevich, G.García Bermúdez, M.A.J.Mariscotti, C.Baktash, E. der Mateosian and P.Thieberger.
  Phys.Rev. C (in press).

- Evidence for a Predicted Change of Phase in the Level Staggering of Bands in Doubly Odd Nuclei.
  A.J.Kreiner and M.A.J.Mariscotti.
  Journal of Physics G. Letters (in press).

- The Self-consistent Pseudopotentials in the Thermodynamic Limit. I. The Correlation Field.
  E.S.Hernández, A.Plastino and L.Szybisz.
  Phys.Rev. C (to be published).

- Level Structure of ^{82}Rb, Studied Through the ^{81}Br (α,3n) Reaction.
  M.Behar, A.Filevich, G.García Bermúdez, M.A.J.Mariscotti and L.Szybisz.
  Nucl.Phys. A (to be published).

- Analysis of (^{6}Li,d) and (d,^{6}Li) Reaction in the Nickel and Tin Regions.
  R.A.Broglia, L.Ferreira, P.D.Kunz, A.Vitturi, H.M.Sofía and F.Bortignon.
  Annals of Physics (to be published).

- The Nucleus as a Condensate of Monopole and Quadrupole Pairing Phonons.
  R.A.Broglia, H.M.Sofía, A.Vitturi and K.Matsuyanagi.
  Physics Letters (to be published).

- Non-axisymmetric Focusing Lenses for the Beam of a Mass-separator.
  E.R.Dülering, D.Otero and A.N.Proto.
  Nucl. Inst. and Meth. (to be published).

- Two-nucleon Transfer Reactions Analysis Using a Coupled-channel Formalism for the Isospin-dependent Optical Potentials.
  O.Dragún and E.E.Maqueda.
  Nucl.Phys. (to be published).

Solid State

- Electrostatic Energy in Ionic Crystals by the Planewise Summation Method.
V.Massidda.
Physica 95 B, 317 (1978)

- Internal Fields and Ferroelectric Ordering in Potassium Ferrocyanide Trihydrate.
V.Massidda.
J.Phys. C 11, 2865 (1978).

- Order-disorder Transitions in Ionic Crystals Containing Reorientable Dipoles.
J.A.Hernando and V.Massidda.
Physica 94 A, 413 (1978).

- A new Ferroelectric: Guanidium Uranyl Sulphate Trihydrate.
H.L. de Dussel, L.S. de Wainer and M.A.R. de Benyacar.
Ferroelectrics 17, 487 (1978).

- Symmetry and Phase Transitions in $(AsO_4)\ H_2(UO_2)_2.8H_2O$.
M.A.R. de Benyacar and H.L. de Dussel.
Ferroelectrics 17, 469 (1978).

- The Crystal and Molecular Structure of O-Methyl Armepavine Iodomethylate.
R.F.Baggio and B.O.Perazzo.
Anales Asoc.Quim. Argentina 66, 345 (1978).

- On the Application of Phase Relationships to Complex Structures: XVI. A Random Approach to Structure Determination.
R.F.Baggio, M.M.Woolfson, J.P.Declerq and G.Germain.
Acta Cryst. A34, 883 (1978).

- The Lattice Vibrations of 1, 2, 3, 4, Tetrabromobenzene.
E.Burgos and H.Bonadeo.
Chem.Phys.Letter 57, 125 (1978).

- Lattice Dynamics, Thermodynamic Functions, and Phase Transitions of p-Dichloro and 1, 2, 3, 4 Tetrachlorobenzene.
H.Bonadeo, E.D'Alessio, E.Halac and E.Burgos.
J.Chem.Phys. 68, 4714 (1978).

- Intermolecular Dynamics of Deuterated Benzene.
B.M.Powell, G.Dolling and H.Bonadeo.
J.Chem.Phys. 69, 2428 (1978).

- Study of a Low Alloy Steel Rust Using Mössbauer Spectroscopy.
I.Maier, C.Saragovi-Badler and F.Labenski.
Radio Chem.Radioanal. Lett. 36(1), 49 (1978).

- Electron Microscope Study of Surface Markings Left by Unsteady Cleavage Crack Propagation in NaCl Single Crystals.
L.S.de Wainer and G.A.Bassett.
Phil.Mag. A38, 6, 707 (1978).

- Structure of Sodium Chloride Cleavage Surfaces Etched in Vacuum at Moderate Temperature.
  L.Levi.
  Phil.Mag. A38, 25 (1978).

- Study of the Behaviour of Synthetic Corrosion Products of Nuclear Power Plants.
  F.Labenski de Kanter, C.S. de Badler, M.A.Blessa, A.Marotto and S. Passaggio.
  Rad.Phys. & Chem. 11, 321 (1978).

- Estudio de un Caso de Corrosión de Refracción Silicoaluminosos Mediante Espectroscopía Mössbauer.
  C.Puglisi, F.Labenski de Kanter and C.S. de Badler.
  Bolet.Soc.Esp.Ceram y Vidrio, 18, 155 (1978).

- Crystal Structure of Ice Accretions.
  L.Levi, L.Lubart and E.M. de Achával.
  Il Nuovo Cimento, 1C, 86/92, (1978).

- Crystal Size in Ice Grown by Droplet Accretion.
  L.Levi and F.Prodi.
  J.Atmospheric Sci. 25, 2183/89 (1978).

- The Falicov-Kimball Model: An Intermediate Solution.
  H.Ceva and J.Mazzaferro.
  Solid State Communications, 29, 137 (1979).

- Numerical Study of Systems with Diagonal and Off-Diagonal Disorder in a Nonorthogonal Basis.
  N.V.Cohan and M.Weissmann.
  Journal of Physics C: Solid State Phys. 12, 1835 (1979).

- Mössbauer Spectra of Iron Containing Nafion Membranes.
  E.R.Bauminger, A.Levy, F.Labenski de Kanter, S.Ofer and C.Heitner-Wirguin.
  International Conference of Mössbauer Spectroscopy, September (1979) and (accepted on Journal de Physique).

- Evidence for the Occurrence of a Universal Type of Iron Storage in Prokaryotic Cells: Bacteria and Mycoplasma.
  E.R.Bauminger, S.Cohen, F.Labenski de Kanter, A.Levy, S.Ofer and S. Rottem.
  International Conference of Mössbauer Spectroscopy, September (1979), and (accepted on Journal de Physique).

- Iron Storage in Mycoplasma Capricolum.
  E.R.Bauminger, S.Cohen, F.Labenski de Kanter, A.Levy, S.Ofer, M.Kessel and S.Rottem.
  (Accepted in "Bacteriology").

- Clustering of Ions in Cation Exchange Membranes: a Mössbauer Study.
  C.Heitner-Wirguin, E.R.Bauminger, A.Levy, F.Labenski de Kanter and S.Ofer.
  (Accepted in "Polymer").

- Vibrational Spectra, Packing Calculations and Crystal Structure of 1.2 Diiodobenzene.
  C.Faerman and H.Bonadeo.
  Chem.Phys.Letters (in press).

- Intermolecular Potentials for Some Crystals of Heterocyclic Compounds Containing Nitrogen.
  Z.Gamba and H.Bonadeo.
  Chem.Phys.Letters (in press).

- Decoration Patterns on Cleavage Surfaces of Ferroelectric Crystals.
  L.S.Wainer, H.L. de Dussel and M.A.R. de Benyacar.
  Thin Solid Films (in press).

Solar Energy Group

- Aparato para la Medición de Coeficientes de Reflexión.
  R.P.Platzeck, J.C.Durán, J.A.Moragues, R.O.Nicolás and W.Scheuer.
  Actas de la 4ª Reunión de Trabajo de la ASADES*, La Plata, 381 (1978).

- Utilización de Elementos Cilíndricos en Concentradores Fijos a Espejo facetado.
  R.P.Platzeck.
  Actas de la 4ª Reunión de Trabajo de la ASADES*, La Plata, 155 (1978).

- Concentrador Fijo a Espejo Facetado de la CNEA. Progresos en el Período 1/7/1978 - 30/6/1979.
  J.C.Durán, J.A.Moragues, R.O.Nicolás, R.P.Platzeck, W.Scheuer, J.Di Santo and A.Rapallini.
  Actas de la 5ª Reunión de Trabajo de la ASADES*, Córdoba (1979).(To be published).

- Sistema de Localización y Seguimiento del Foco de un Concentrador Solar.
  J.J.Nicolás.
  Actas de la 5ª Reunión de Trabajo de la ASADES*, Córdoba (1979).(To be published).

- Generalización del Análisis Optico Bidimensional de Concentradores con Simetría Cilíndrica.
  J.C.Durán and R.O.Nicolás.
  Actas de la 5ª Reunión de Trabajo de la ASADES*, Córdoba (1979). (To be published).

- Concentrador Solar Cilíndrico a Espejos Cóncavos Giratorios.
  R.P.Platzeck.
  Actas de la 5ª Reunión de Trabajo de la ASADES*, Córdoba (1979). (To be published).

---

* ASADES: Asociación Argentina de Energía Solar.

B. Papers Presented at Meetings

VII Reunión de la Asociación de Tecnología Nuclear, San Rafael, 1978

- Identificación de los Fragmentos Producidos en la Fisión del Uranio.
  A.N.Proto, J.M.Riso y D.Otero

- La Aniquilación de Positrones en el Estudio de Materiales.
  D.Otero, A.N.Proto y S.Zambrino

Reunión Nacional de Física, Buenos Aires, 1978

- Cuadrupolo Electrostático.
  E.Düering, D.Otero y A.N.Proto.

- Atrapamiento de Vacancias en Plata Templada.
  C.Alonso Arias, J.Fernández Niello, M.Behar, A.Filevich y G.García Bermúdez.

- Isómero de Alto Spin en ^{76}Br.
  A.J.Kreiner, G.García Bermúdez, M.A.J.Mariscotti y P.Thieberger.

- ¿Es necesario atenuar la Interacción de Coriolis?
  A.J.Kreiner.

- Esquema de niveles del ^{78}Br.
  D.Abriola, M.Berisso, J.Fernández Niello, G.García Bermúdez, M.Behar y L.Szybisz.

- Consideraciones sobre la Interacción Multipolar entre Partículas Idénticas.
  D.R.Bes, R.P.J.Perazzo y S.L.Reich.

- Papel de los Campos Locales en la Transición Ferroeléctrica del Ferrocianuro de Potasio Hidratado.
  V.Massida.

- Espectros Vibracionales y Desorden Orientacional en Iodoformo y Bromoformo.
  E.B.Halac, E.Burgos y H.Bonadeo.

- Estructura de Superficies de Clivaje de Cloruro de Sodio Atacadas Térmicamente.
  L.Levi.

- Estudio Teórico de Propiedades Electrónicas de Sistemas con Desorden Estructural.
  N.Cohan y M.Weissmann.

- Solución de Hubbard (I) en el Modelo de Falicov-Kimball para las Transiciones Metal-Aislador.
  H.Ceva y J.Mazzaferro.

- Análisis del funcionamiento de un Concentrador de Radiación Solar a Espejo Facetado
  R.Nicolás, J.Durán. R.Platzeck, J.A.Moragues y W.Scheuer.

Symposium on Pure and Applied Physics, Stockholm, Sweden, August 21-23, 1978

- A Reformulation of the Mode Coupling Method.
  R.J.Liotta, C.Pomar and B.Silvestre-Brac.

- Spin Dissipation in Fusion Reactions with α-particles and ^{12}C ions.
  Sctockholm, Warsaw, Göteburg, Lund, Oslo and Jyväskla, collaborations.

Australian International Conference on Nuclear Interactions, Australian Academy of Science, Canberra, Australia, August 28 - September 2, 1978

- Coulomb Excitation of Even Nd Nuclei.
  C.Fahlander, L.Hasselgren, C.Pomar, A.Bäelin, G.Possnert and J.E.Thun.

International Conference on the Physics of Medium Light Nuclei, Florence, Italia, 1978

- Isospin of Pairing Modes: a charge independent treatment of pairing correlation.
  F.Andreozzi, A.Covello, E.E.Maqueda and R.P.J.Perazzo.

3rd International Conference, Manitoba, Canadá, June 1978

- Measurement and Analysis of Continuous Spectra in Proton Induced Reactions.
  A.Ferrero, E.Gadioli, E.Gadioli Erba, I.Iori, N.Molho and L.Zetta.

International Workshop on Reaction Models for Continuous Spectra of Light Particles, Bad Honnef, 1978

- Study of α Emission in Proton Induced Reactions on Medium-Heavy Nuclei.
  E.Gadioli, E.Gadioli Erba and A.Ferrero.

Seminario de Aprovechamiento de la Energía Solar y Eólica, Centro Espacial San Miguel, Provincia de Buenos Aires, 1978

- Programa y Actividad del Grupo de Energía Solar de la Comisión Nacional de Energía Atómica.
  W.Scheuer, J.A.Moragues

4a Reunión de Trabajo de la Asociación Argentina de Energía Solar, (ASADES), La Plata, 1978

- Concentrador Fijo a Espejo Facetado de la CNEA. Progresos en el período 1/10/77 - 30/6/78.
  R.Nicolás, J.Durán, J.A.Moragues, R.Platzeck y W.Scheuer.

Reunión Nacional de Física, Villa Giardino, Córdoba, 1979

- Coeficientes de conversión en ^{140}Cs: métodos NPG, XPG y coincidencias.
  D.Otero, A.N.Proto, E.Düering y M.L.Pérez.

- Núcleos Impar-Impar cercanos a N = 82: ^{140}Cs y ^{138}Cs.
  D.Otero, A.N.Proto, E.Düering y M.L.Perez.

- Decaimiento Radioactivo de los Núcleos Cercanos al ^{132}Sn.
  H.Huck, M.L.Pérez y J.J.Rossi.

- Una Fuente de Iones y Blanco de Uranio Integrado para el Proyecto IALE.
  H.Huck, M.L.Pérez y J.J.Rossi.

- Estados cuasimoleculares del Sistema $^{10}B + {}^{6}Li$.
  D.Magnac-Valette, C.Gerardin, G.Costa, F.Seltz y J.J.Rossi.

- Renormalización de Estados de Partícula Independiente en la Zona del ^{40}Ca.
  R.P.J.Perazzo y S.L.Reich.

- Tratamiento Perturbativo de un Sistema de Fermiones en Rotación.
  D.R.Bes, G.G.Dussel y R.P.J.Perazzo.

- Estudio de la Estructura $\tilde{\pi}h_{9/2} \otimes \tilde{\nu}i_{13/2}$ en el Núcleo ^{200}Tl.
  A.J.Kreiner, M.A.J.Mariscotti, C.Baktash, E. der Mateosian y P. Thieberger.

- Estados de Alto Momento Angular del ^{74}Br.
  G.García Bermúdez, A.Filevich, A.J.Kreiner, M.A.J.Mariscotti, C. Baktash, E. der Mateosian y P.Thieberger.

- Bandas Distorsionadas de Parentesco Común $g_{9/2}$ en Isótopos Doblemente Impares e Impares con N = 41.
  A.J.Kreiner y M.A.J.Mariscotti.

- Espectros Raman, Estructura Cristalina y Transiciones de Fase del Bromoformo.
  E.B.Halac, E.Burgos y H.Bonadeo.

- Potenciales Intermoleculares en Cristales de Compuestos Heterocíclicos Conteniendo Nitrógeno.
  Z.Gamba y H.Bonadeo.

- Estructura de Dominios en el Ferroelástico $BiVO_4$
  R.Baggio, M.A.R. de Benyacar y L.S. de Wainer.

Second European Conference on Crystal Growth Lancaster University, September 10 - 15, 1979

- Optical and X-ray Characterization of Some Gel Grown Crystals.
  F.Lefaucheux, M.C.Robert, E.Manghi and H.Arend.

Third Latin American Workshop on Self Consistent Theories of Nuclear Matter, Buenos Aires, July 2 - 13, 1979

- Zero Order Crystallization in the Bethe Fermi Homework Problem.
  C.M.Cambiaggio.

- The Correlation Field and the Self-Consistent Pseudopotentials in the Thermodynamic Limit.
  L.Szybisz.

- Renormalization Procedure and Core Polarization.
  S.L.Reich and R.P.J.Perazzo.

7° Reunión del Instituto Argentino de Siderurgia, Mar del Plata, 1979

- Corrosión de Refractarios en un Horno de Arco Eléctrico de Acería.
  C.Puglisi y C.Saragovi-Badler.

VI Simposio Latinoamericano de Física del Estado Sólido, Bogotá, 1979

- Una Solución Intermedia al Proceso de Falicov-Kimball.
  H.Ceva y J.Mazzaferro.

C. Internal Reports

- Equilibrio y Estabilidad MHD en el Confinamiento Magnético para la Fusión Termonuclear.
  D.Otero y A.N.Proto.
  CNEA 454 (1979).

- Concentrador Cilíndrico Fijo a Espejo Facetado para Aprovechamiento de la Energía Solar.
  R.O.Nicolás, J.C.Durán, J.A.Moragues y W.Scheuer.
  CNEA-NT 35/78 (1978).

- Guía de Modelos para el uso de Tarjetas Perforadas en Lenguaje IBM de Control de Trabajo en Sistema Operativo.
  A.M.Díaz Romero.
  CNEA - NT 33/78 (1978).

D. Ph.D. Theses

- Erhard Achterberg.
"Análisis de Espectros Gamma, Calibración de Precisión en Energía y Construcción de Esquemas de Niveles Nucleares Mediante Minicomputadora. Estudio del Decaimiento del ^{139}Xe" (1979).
Universidad Nacional de Cuyo, Bariloche.

- María Cristina Pomposiello.
"Estudio del Cloroformo Cristalino a partir de Datos de Espectroscopía Infraroja y Raman" (1978).
Facultad de Ciencias Exactas y Naturales; Universidad Nac. de Buenos Aires.

E. Licenciatura Theses

- Rubén Osvaldo Nicolás.
"Análisis y Simulación del Comportamiento de un Concentrador Fijo a Espejo Facetado para el Aprovechamiento de la Energía Solar. Diseño y Montaje de Prototipos" (1978).
Facultad de Ciencias Exactas y Naturales; Universidad Nac. de Buenos Aires.

- Ricardo A. Pakula.
"Obtención de los Rendimientos Acumulativos Relativos de Fisión de $^{137,138,139,140,141}Xe$ para la Fisión de ^{235}U con Neutrones Térmicos y Medición del Tiempo de Tránsito de Dichos Productos a Través de un Separador de Isótopos en Línea" (1978).
Facultad de Ciencias Exactas y Naturales; Universidad Nac. de Buenos Aires.

- Jorge Dukelsky.
"Fuente de Iones con Blanco de Oxido de Uranio Incorporado para el Estudio de Productos de Fisión no Gaseosos" (1979).
Universidad Nacional de Cuyo, Bariloche.

- Norberto J. Levin.
"Estudio de la Energía Electrostática de Moléculas de Agua en Cristales Hidratados en Función de su Orientación" (1979).
Facultad de Ciencias Exactas y Naturales; Universidad Nac. de Buenos Aires.

- Carlos Faerman.
"Propiedades Vibracionales y Estructura Cristalina del 1-2 Diclorobenceno" (1978).
Facultad de Ciencias Exactas y Naturales; Universidad Nac. de Buenos Aires.

- Ricardo Farengo.
"Densidad de Estados en las Superficies del Grafito y Adsorción de un Atomo de H" (1979).
Facultad de Ciencias Exactas y Naturales; Universidad Nac. de Buenos Aires.

DEPARTMENT SEMINARS

Armando Ferrero Physics Department CNEA	"Pre-Compound Nuclear Reactions"
Ricardo Baggio Physics Department CNEA	"New Development in Direct Methods for the Determination of Crystal Structures"
Antonio Federico Moreno Planning, Ministry of Defense	"Argentine Position About the River Plate Basin"
Andres Kreiner Physics Department CNEA	"Semidecoupled States in Doubly Odd Nuclei"
Amílcar Jorge Funes Heavy Water Project CNEA	"The Heavy Water Program of the Argentine Atomic Energy Commission"
Víctor Massidda Physics Department CNEA	"Calculation of the Electrostatic Energy of Crystals: some aspects related with the convergence of the lattice sums"
Carlos Suárez Bariloche Foundation San Carlos de Bariloche	"Energy and Development"
Daniel R. Bes Physics Department CNEA	"Functional Methods in Nuclear Field Theory"
Renato Radicella Peru Atomic Center Project CNEA	"Argentine-Peruvian Nuclear Treaty: The Nuclear Research Center of Perú"
Horacio Ceva Physics Department CNEA	"Models of the Metal-Insulator transition"
Edgardo Browne Moreno Lawrence Berkeley Laboratory University of California	"1.Table of Isotopes Project. 2. National and International network for the evaluation of Nuclear data"

Julio Rossi Physics Department CNEA	"Magnetic Spectrometer for the Buenos Aires Tandem"
Gvirol Goldring Director Accelerator "Koffler" Weizmann Institute , Israel	"One Year of Research at the Koffler Accelerator in Rehovot"
Manfred Ahlers Bariloche Atomic Center CNEA	"Alloys with Memory: Martensitic Phase Transformations in Alloys Based on Cu-Zn"
Francisco de la Cruz Bariloche Atomic Center CNEA	"Activities of the Low Temperature Division of the Bariloche Atomic Center"
Néstor Davids Evaluation Department CNEA	"Uranium Resources"
Jaime Moragues Physics Department CNEA	"Activities of the Solar Energy Group (CNEA)"
Luis Sersic Astronomic Observatory Córdoba	"Galaxy Formation and Cosmology"
Roberto Perazzo Physics Department CNEA	"Pairing Rotational Bands"
Jorge Agudin Astronomic Observatory La Plata and CONICET	"Semiclassical Calculation of the Compton Effect"
Hernán Bonadeo Physics Department CNEA	"Inelastic Coherent Neutron Scattering:lattice dynamics of Benzene"
Daniel Camín Physics Department CNEA	"State of the Art of the Electronic Technology"
Bernard Seraphin Optical Sciences Center University of Arizona, Tucson	"Recent Progress in High-Temperature Selective Surfaces for Solar Energy Conversion"

Mario Mariscotti Physics Department CNEA	"Recent Results in the Study of Doubly Odd Nuclei"
Alberto Pignotti Techint	"Charmed Particles"
Rómulo Cabrini Research Manager CNEA	"Activities in the Pure Research Area and Alternatives for its Future Development"
Juan Carlos de Pablo	"Argentine economy: A Review and Perspective"
Carlos Leguizamón Group of Biomathematics CNEA	"Biomathematics: The Intrinsic and Extrinsic Energy Concepts, and the Comorosan Effect"
Emma Pérez Ferreira Physics Department CNEA	"The Electrostatic Accelerator Project: A Progress Report"
Blas Alascio Bariloche Atomic Center CNEA	"Intermediate Valence: Kondo Behaviour in a Simple System"
Carlos Fainstein Bariloche Atomic Center CNEA	"Some Applications of Magnetic Resonance in Solids"
Angel Plastino Physics Department La Plata National University	"Abnormal Bosons"
Osvaldo Civitarese Physics Department La Plata National University	"γ-Multiplicity and Side Feeding Patterns in (heavy ions, xn) Fusion Reactions"
Moni Behar Institute of Physics Federal University of Rio Grande do Sul	"Systematics of Electric Field Gradients in Noble Metals: Jornada Effect"
Manuel Tovar Bariloche Atomic Center CNEA	"Magnetic Ordering in Super Conductors"

Rudi Stammler Development Department CNEA	"Calculation of Thermal Reactors"
Roberto Daniel Lozano Physics Department National Institute for Industrial Research (INTI)	"Colour from a Physical Point of View"
Silvia Reich Physics Department CNEA	"Independent Particle States Renormalization"
Martín Crespi Prospective and Special Studies CNEA	"A Technical Assistance Mission to Ecuador"
J.W.Clark McDonnell Center for Space Sciences and Department of Physics Washington University	"Update of the Crisis in Nuclear-matter Theory
Rubén Barrera Institute of Physics Autonomous National University México	"Magnetism as a Relativistic Quantum Effect"
Raul Colomb Argentine Institute of Radioastronomy	"The Interstellar Space"
Jorge Sábato	"Nuclear Proliferation"
Roberto Cirimello Development Department CNEA	"Technology of Nuclear Fuels"
Luis Roque Argüello L.P.R. Project CNEA	"The Project LPR of the Argentine Atomic Energy Comission"
Nora Cohan Physics Department CNEA	"Molecular Dynamics of micro-clusters"

Emilio Matatagui Development Department CNEA	"Some Technological Aspects of Radiation Detectors"
Elvio Dodero Research Center for Water Desalination National Institute for Industrial Research (INTI)	"Water Desalination"
Dora Anton Department of Radiobiology CNEA	"Recombinant DNA Technique (genetic engineering): its benefits and risks"
Martín Crespi Prospective and Special Studies CNEA	"Energy Resources"
Lewis Pyenson Institute of History and Sociopolitics of Sciences University of Montreal	"Young Man Einstein:The Scientific Education of a Genius" "Bringing Physics to the new world: The rise of exact sciences in Argentine"
Edgardo Browne Moreno Lawrence Berkeley Laboratory University of California	"Structure of the Oak Ridge Nuclear Data Bank"
Felisa Labenski de Kanter Physics Department CNEA	"Mössbauer Spectroscopy Contribution to Biological Studies: Storage Proteins in Bacteria and Pathological Tissues, Specially Blood"

IMPRESO EN CNEA - JULIO 1980

CNEA - NT 32/77.

COMISION NACIONAL DE ENERGIA ATOMICA
DEPENDIENTE DE LA PRESIDENCIA DE LA NACION

CALCULOS DE EFECTOS TERMICOS LOCALES QUE PRODUCEN PARTICULAS DE PuO_2 EN BARRAS COMBUSTIBLES NUCLEARES DE UO_2

Por

G.SANCHEZ SARMIENTO *)
FERNANDO G.BASOMBRIO *)
y ADOLFO MARAJOFSKY **)

*) Centro Atómico Bariloche, C.N.E.A.
Instituto Balseiro, Universidad Nacional de Cuyo.
8400, San Carlos de Bariloche, Río Negro.

**) Gerencia de Desarrollo, C.N.E.A.
Centro Atómico Constituyentes, Buenos Aires
ARGENTINA

San Carlos de Bariloche
Noviembre de 1977

RESUMEN

Se ha realizado un estudio de las sobreelevaciones locales de temperatura que producen, dentro de barras combustibles tipo MZFR con Pu, y tipo Central Nuclear de Atucha con Pu, la presencia de pequeñas partículas (islas) de óxido de plutonio en el interior de las pastillas de óxido de uranio. Mediante el Código AXICUARM, desarrollado en el Centro Atómico Bariloche (que emplea el método de elementos finitos para cualquier geometría con simetría de revolución), se resolvió al efecto la ecuación no lineal de conducción de calor (con conductividades dependientes de la temperatura) para varias posiciones y diferentes tamaños de las partículas dentro de la barra.

A. INTRODUCCION

En la próxima década, el reciclado de plutonio en reactores térmicos moderados con agua pesada se presenta como económicamente promisorio. Dados los lineamientos del Plan Nuclear Argentino, este tipo de ciclo resulta una vía natural de desarrollo.

En este contexto se encuadran los planes de la Gerencia de Desarrollo en cuanto:

a) La adquisición de la tecnología de fabricación de elementos combustibles con plutonio.
b) Los estudios de comportamiento y performance de los mismos para lograr un diseño económico y confiable.

Una tarea que reúne ambos aspectos es la fabricación de un prototipo, en particular el llamado "MZFR-Pu", a ser irradiado en el reactor MZFR de Karlsruhe (Alemania).

Si bien el laboratorio ya ha irradiado prototipos en este reactor, las diferencias principales entre el MZFR-Pu y aquéllos serían:

i) el de alcanzar un mayor quemado (15.000Mwd/Tn)
ii) el de estar enriquecido con plutonio (1.27% total).

Estos puntos hacen necesaria una revisión crítica de las especificaciones de este prototipo:

i) Cálculos realizados en la División Prototipos de dicha Gerencia muestran que para el quemado previsto, las deformaciones acumuladas en la vaina no superan los límites de confianza.

ii) El plutonio se encuentra como PuO_2 en la pastilla de UO_2 y forma solución sólida con este último en un amplio rango de concentraciones y en las temperaturas de trabajo del elemento combustible. Las propiedades físicas relevantes, en cuanto al comportamiento del mismo, son semejantes en el óxido mixto a las del UO_2 (conductividad térmica, punto de fusión, propiedades mecánicas, etc), especialmente en las bajas concentraciones en que será utilizado.

La solución homogénea puede obtenerse por vía húmeda - por ejemplo a partir de la coprecipitación de los nitratos correspon

dientes - pero esta vía resulta menos económica que la del mezclado mecánico de los óxidos, pues deben agregarse etapas de procesamiento en cajas de guantes. El segundo procedimiento, debido a que los bajos coeficientes de difusión catiónica no permiten la homogeneización de la mezcla en las temperaturas y tiempos normalmente utilizados, presenta a su vez problemas:

a) De fabricación: lograr un mezclado y la sinterización que aseguren la densidad requerida y continuidad en las interfases PuO_2 - UO_2.
b) De comportamiento: las islas de la fase PuO_2 en la matriz de UO_2 pueden provocar (debido fundamentalmente a su diferencia en la sección eficaz de fisión):
   b.1) Efectos de autoblindaje;
   b.2) Efectos adversos en el Coeficiente Doppler en transitorios;
   b.3) Puntos de sobrecalentamiento de la matriz.

Resulta entonces de importancia para la especificación del tamaño permisible de las islas, un estudio detallado de los efectos que provocan las mismas. En particular, el punto b.3) es el más importante y su análisis cuantitativo es el objeto del presente trabajo:

Para un cierto nivel de potencia disipada en la barra combustible por la fisión nuclear en ambos materiales, se ha calculado la distribución espacial de la temperatura y del flujo calórico en las islas de PuO_2 y en su radio de influencia térmica, en función de su tamaño, para diversas ubicaciones de ella dentro de la barra.

Por ser el problema también de interés para las barras combustibles de la Central Nuclear de Atucha (C.N.A) con plutonio se ha hecho extensivo el estudio a esta última.

Los valores obtenidos de la temperatura deberán confrontarse a posteriori con las tolerancias permitidas por los criterios de diseño en las zonas críticas:

a) en el centro de la pastilla para evitar la fusión;
b) en la vaina para evitar alteración de las propiedades mecánicas y aceleración de la susceptibilidad a la corrosión.

Con el menor de los diámetros correspondientes a los puntos a) y b) se calcula la probabilidad de que dos islas se encuentren contíguas, y si este valor se encuentra por debajo de los límites de confianza permitidos, se lo elige como valor de especificación del tamaño de isla.

En esencia se trata de un problema tridimensional de distribución de temperatura, pero si la partícula se encuentra sobre el eje de la barra (zona A de la figura 1), la geometría tiene simetría de revolución y sus puntos pueden especificarse con sólo dos coordenadas. Además otras de las situaciones más importantes de considerar son aquéllas en que la partícula está adyacente o muy próxima a la vaina. Como los tamaños que interesan de la partícula (entre 50 y 400 micrones) son muy pequeños respecto de las dimensiones de la barra, es válido resolver el problema para estas últimas situaciones tomando una pequeña porción de la barra cercana a la vaina (zona B de la figura 1) y aproximando la geometría real por una aproximada de simetría axial, con el eje de revolución perpendicular a la vaina.

Se ve entonces que un análisis tridimensional completo para posiciones arbitrarias de la partícula no agregaría una información adicional esencial a la obtenida mediante los análisis bidimensionales planteados. Se realizaron entonces cálculos del carácter mencionado con un código preelaborado en el Centro Atómico Bariloche, llamado AXICUARM /2/, que por el método de elementos finitos resuelve la ecuación de calor estacionaria no lineal en coordenadas cilíndricas para geometrías con simetría axial:

$$\frac{\partial}{\partial r}\left[K(\vec{r},T)\frac{\partial T}{\partial r}\right] + \frac{\partial}{\partial z}\left[K(\vec{r},T)\frac{\partial T}{\partial z}\right] + \frac{K(\vec{r},T)}{r}.T + \rho(\vec{r}) = 0 \qquad (1)$$

donde $\vec{r}=(r,z)$ es la coordenada vectorial de cada punto; $T(\vec{r})$ la temperatura (incógnita a determinar); $K(\vec{r},T)$ la conductividad térmica dependiente del material y de la temperatura; y $\rho(\vec{r})$ la generación de calor por unidad de volúmen.

En la Sección B. se describen los cálculos realizados; en C. los datos empleados en cada uno de ellos; en D. los resultados; y en E. algunas observaciones y conclusiones. En el Apendice I se calculan las respectivas generaciones de calor en cada material.

B.- CALCULOS REALIZADOS

Con cuatro diámetros distintos de partículas de PuO_2 (50, 100, 200 y 400 micrones) y generaciones de calor en el UO_2 y en el PuO_2 (cuya relación entre ellas para un quemado hipotético están calculadas en el Apéndice I), que corresponderían a un dado nivel de potencia por unidad de longitud de la barra si no estuviese la partícula, se resolvió la ecuación (1) para las cuatro siguientes ubicaciones de ésta dentro de la barra:

a) La partícula es esférica y está ubicada sobre el eje de simetría de la barra combustible. Se considera una cierta porción L de la longitud de ésta (zona A de la figura 1), con la partícula en su punto medio, aplicando condiciones de contorno de flujo calórico nulo en ambas superficies extremas a y b, y de temperatura fija T_e (del refrigerante) sobre su superficie lateral c. Por simetría se toma solamente el recinto de cálculo rayado en la figura.

b) La partícula es esférica y yace sobre la superficie exterior de la pastilla, sin afectar el espacio gaseoso entre ésta y la vaina. Se considera la zona B. de la figura 1, aproximando su forma a la de un cilindro con su eje de simetría perpendicular a la vaina, con condiciones de contorno de temperatura fija sobre los lados a' y c', y de flujo calórico nulo sobre su superficie lateral b'. La temperatura sobre a' se determinó previa-

mente calculando en el recinto de la zona A, sin la presencia de la partícula, la temperatura en $r=R_a$.A su vez, la temperatura sobre c' será obviamente la temperatura T_e del refrigerante.

c) La situación es análoga a la b), con la diferencia en que la partícula no es esférica y presenta una superficie máxima en contacto con la vaina, sin afectar la resistencia térmica del espacio gaseoso.

d) La partícula es esférica y está centrada a 4.7 mm del eje de la barra en el caso MZFR - Pu, ó a 4.8 mm del eje para la barra C.N.A. con Pu. Se considera la zona B con las mismas condiciones de contorno de b).

Los cálculos descriptos en a) fueron realizados con la red de elementos finitos triangulares de la figura 2, y los descriptos en b), c) y d) con la de la figura 3. Ambas redes, que corresponden a las partes rayadas de las zonas A y B respectivamente de la figura 1, fueron generadas automáticamente mediante sendos programas. En las figuras se indican las condiciones de contorno impuestas. Para incorporar con distintos diámetros las partículas de PuO_2 se hizo necesario deformar localmente dichas redes. En la figura 4 se muestran las distintas conformaciones de la red de la zona B para las situaciones b) y d), y en la figura 5 las que corresponden a la situación c). Las dimensiones de los poliedros axisimétricos que éstos configuran se eligieron de manera tal que sus volúmenes fuesen iguales a los de las respectivas esferas que ellos representan para las situaciones a), b) y d). En cambio, para la situación c), los elementos simulan exactamente a la geometría de la partícula que se quiere representar.

C.- DATOS DE CALCULO

Se dan a continuación todos los datos físicos y geométricos con los que se realizaron los cálculos para ambos tipos de barras combustibles:

Magnitud	Unidad	Barra MZFR - Pu	Barra C.N.A.- Pu
C. 1. - Datos Físicos:			
Conductividad del Zry-4 dependiente de la temperatura /6/.	w/cm.° C	$K_{zry-4} = 0.1145 + 1.425 \times 10^{-4} T$ (T en °C)	
Conductividad del UO_2 dependiente de la temperatura /6/.	w/cm.° C	$K_{UO_2} = \frac{1}{B+C\,(T+273)} + D\,(T+273)^3$ B=3.3674; C=0.0262; D= 0.478×10^{-12} (T en °C).	
Conductancia del espacio pastilla - vaina (λ) /6/.	$w/cm^2.°C$	1.475	1.375
Conductividad correspondiente del esp.past. -vaina para el esp. ficticio supuesto (K_{int}).	w/cm.°C	1.475×10^{-3}	1.237×10^{-2}
Conductividad del PuO_2 (K_{puO2}).	w/cm.°C	$K_{PuO_2} = K_{UO_2}$	
Potencia disipada en las pastillas por unidad long. barra.	w/cm	616.	687.
Generación de calor en el UO_2 por unidad de volumen. (Q_2).	w/cm^3	728.	775.
Generación de calor en el PuO_2 por un. de vol. (Q_1). ver Ap.	w/cm^3	9.90×10^4	10.55×10^4
Temperatura ext. T_e del refr.	°C	305.	324.
C. 2.-Datos Geométricos.			
Radio exterior R_e de la vaina.	mm	5.74	5.95
Radio interior R_i de la vaina.	mm	5.20	5.40
Radio de la pastilla UO_2.	mm	5.19	5.31
Espesor ficticio del espacio pastilla -vaina considerado.	mm	0.01	0.09
Altura recinto zona B (R_e-R_a).	mm	2.04	2.15
Radio del recinto zona B (R_c).	mm	1.60	1.60
Diámetros de las partíc. PuO_2.	mm	0.05; 0.10; 0.20; 0.40	

C.3. Redes de elementos finitos

C.3.1. Para los cálculos de la situación a):

Número de elementos finitos: 1024
Número de nodos: 561
Número de incógnitas: 528

C.3.2. Para los cálculos de las situaciones b), c) y d):

Número de elementos finitos: 768
Número de puntos nodales: 425
Número de incógnitas: 391

D. RESULTADOS

En las TABLAS I y II se resúmen los resultados más significativos de las cuatro diferentes situaciones para ambos tipos de barras. Se consignan en ellas las temperaturas en los puntos donde se observan las máximas diferencias ΔT entre éstas y las que tendrían en el mismo punto si no estuviese la partícula, y también el valor de estas diferencias, dentro de cada uno de los tres materiales (PuO_2, UO_2 y vaina). Para las situaciones b), c) y d), obviamente en estos puntos no se producen necesariamente las máximas temperaturas. En la situación a), en cambio, ello sí ocurre.

De la información dada en estas tablas puede obtenerse el error introducido por la hipótesis de simetría de revolución para la zona B, antes mencionada, En efecto, si a las temperaturas máximas en la vaina de la barra C.N.A., por ejemplo,(que se producen sobre su superficie exterior) se les resta los correspondientes valores de ΔT (última columna) se obtiene una temperatura de 398°C, que supera en 10°C a la correcta (388°C) obtenida con la red de la figura 3 para la zona A en ausencia de la partícula. Este error evidentemente no tiene importancia para los fines del presente trabajo.

En la misma TABLA II se observa que, para el diámetro de

Situación de la partícula	Diámetro de la partícula (micrones)	Temp. en el punto de máximo incremento en cada material (°C)			Máximo incremento de temperatura (°C)		
		En el PuO_2	En el UO_2	En la vaina	En el PuO_2	En el UO_2	En la vaina
a)	50	2402.	2396.	365.	11.	4.	0.0
	100	2425.	2401.	365.	34.	9.	0.1
	200	2538.	2439.	365.	147.	47.	0.2
	400	3049.	2699.	366.	658.	307.	0.5
b)	50	550.	550.	374.	2.6	2.6	0.3
	100	584.	584.	378.	12.2	12.2	3.7
	200	699.	637.	388.	130.	68.	13.6
	400	1283.	960.	432.	660.	337.	58.
c)	50	518.	517.	374.	1.7	0.7	0.0
	100	541.	527.	376.	25.4	11.2	1.6
	200	631.	573.	386.	114.	57.	11.7
	400	1009.	808.	431.	447.	247.	57.0
d)	50	788.	788.	374.	2.9	2.9	0.0
	100	814.	814.	375.	17.0	17.0	0.3
	200	917.	850.	377.	148.0	82.0	2.6
	400	1510.	1158.	396.	742.0	389.	22.0

TABLA I.- Resultados principales para cada una de las situaciones de una partícula dentro de una barra combustible MZFR - Pu.

Situación de la partícula	Diámetro de la partícula (micrones)	Temperatura en el punto de máximo incremento en cada material (°C)			Máximo incremento de temperatura (°C)		
		En el PuO_2	En el UO_2	En la vaina	En el PuO_2	En el UO_2	En la vaina
a)	50.	2718.	2711.	388.1	9.	5.	0.0
	100.	2740.	2715.	388.1	34.	9.	0.0
	200.	2848.	2750.	388.2	142.	45.	0.1
	400.	3332.	2991.	388.5	626.	286.	0.4
b)	50.	559.	559.	399.	3.	3.	1.
	100.	586.	586.	401.	30.	30.	3.
	200.	777.	692.	410.	185.	136.	12.
	400.	1434.	1001.	458.	753.	445.	60.
c)	50.	579.	579.	399.	4.	4.	1.
	100.	606.	603.	400.	28.	25.	2.
	200.	718.	693.	411.	90.	65.	12.
	400.	1137.	1067.	458.	511.	380.	59.
d)	50.	848.	848.	399.	8.	8.	1.
	100.	860.	860.	399.	30.	30.	1.
	200.	1035.	922.	401.	172.	120.	3.
	400.	1658.	1192.	419.	795.	451.	21.

TABLA II - Resultados principales para cada una de las situaciones de una partícula dentro de una barra combustible tipo C.N.A. con Pu.

200 micrones, los máximos incrementos de temperatura se producen para la posición de la partícula más próxima a la vaina (situación b), mientras que para el diámetro de 400 micrones esto se verifica en la situación c). Esta diferencia es atribuible a una combinación de las características no lineales del problema y del efecto refrigerante de la vaina.

En las figuras 6 y 7 se grafican las distribuciones, en la dirección del radio de la barra que pasa por el centro de la partícula, de la temperatura para los distintos diámetros de la partícula y en ausencia de ésta, en cada una de las situaciones estudiadas. Para mostrar el efecto de la dependencia con la temperatura de la conductividad, se ha incluído en la figura 6 una distribución calculada con conductividades medias independientes de la temperatura [K_{Zry}(350 °C)=0.164w/cm°C; K_{UO_2} (1300 °C) = 0.0235 w/cm°C].

Finalmente, en la figura 8 se muestra una salida por impresora del Programa AXICUARM que muestra la distribución espacial de la temperatura para la situación d) de la partícula en una barra C.N.A., de 400 micrones de diámetro. Los límites de cada franja son isotermas equiespaciadas.

E.- OBSERVACIONES Y CONCLUSIONES

En ausencia de la partícula de PuO_2, las distribuciones de temperatura en la zona B indicada en la Figura 1 y obtenidas baja la hipótesis de simetría de revolución en dicha zona, coinciden satisfactoriamente con las que para posiciones equivalentes se calculan con la red de la zona A, lo que confirma la validez de dicha aproximación adoptada para la primera. Un orden de magnitud de los errores introducidos fue señalado en la sección precedente.

Es notoria la implicancia que tiene sobre los resultados la dependencia con la temperatura de la conductividad del UO_2. Respecto del cálculo lineal (coeficientes independientes de la temperatura), las diferencias mayores son del orden del

10% en ausencia de la partícula (ver Figura 6).

Dado que la temperatura de fusión del UO_2 (y presumiblemente también la del PuO_2) es de aproximadamente 2800°C, los resultados obtenidos para una partícula de 400 micrones en la situación a) en ambos tipos de barras pierden su validez. No obstante, estos han sido también incluídos en las TABLAS I y II en la figura 6, puesto que los incrementos ΔT de temperatura hallados no tienen por qué diferir excesivamente para otros puntos del interior de la pastilla, en que la temperatura máxima correspondiente sea menor que dicho punto de fusión.

El sobrecalentamiento de la vaina es en proporción muy pequeño en todos los casos estudiados. Esto se debe a la acción del refrigerante que mantiene a temperatura constante T_e la superficie exterior de la misma, y a la suposición de que en las situaciones b) y c) la presencia de la partícula no altera la conductividad del espacio gaseoso entre la vaina y la pastilla en el lugar en que aquélla se encuentra. Según se observa en las TABLAS, la máxima temperatura a que dicha superficie llega es de 458°C (caso b; $\emptyset$ = 400 micrones).

Es interesante, por último, cotejar los valores de los incrementos de temperatura obtenidos con los que corresponden a una partícula esférica de PuO_2 en un medio homogéneo e indefinido de UO_2, situación para la cual la ecuación de conducción de calor (1) lineal y estacionaria tiene solución exacta. El valor absoluto de la temperatura obviamente diverge, pero el incremento $\Delta T(r)$ motivado por la presencia de la partícula vale:

En el PuO_2: $$\Delta T(r) = \frac{Q_1 - Q_2}{6K} (3R^2 - r^2)$$

En el UO_2: $$\Delta T(r) = \frac{Q_1 - Q_2}{3K} \frac{R^3}{r}$$

donde Q_1 y Q_2 son las generaciones de calor en el PuO_2 y en el UO_2 respectivamente, K la conductividad común a ambos materiales (aproximación empleada en los cálculos descriptos), y R el radio de la partícula. Los máximos valores de ΔT en cada material serán entonces:

En el PuO_2: $$\Delta T(0) = \frac{Q_1 - Q_2}{2K} R^2$$

En el UO_2: $$\Delta T(R) = \frac{Q_1 - Q_2}{3K} R^2$$

Con los datos de C.1. para el caso de la barra C.N.A.con plutonio, y una conductividad media constante de K=0.0235 w/ cm°C, se obtienen para cada diámetro de la partícula los resultados mostrados en la TABLA III. Se ve que éstos son acordes con los correspondientes resultados de las TABLAS I y II.

Diámetro de la partícula (micrones)	Radio (mm)	$\Delta T(0)$ (°C)	$\Delta T(R)$ (°C)
50	0.025	13	9
100	0.050	55	37
200	0.100	223	149
400	0.200	892	595

TABLA III

AGRADECIMIENTOS

Queremos expresar nuestro agradecimiento a la Sra.Bibiana Cruz, del Centro de Cómputos del C.A.B., por la eficaz colaboración prestada en la construcción automática de las redes de elementos finitos.

APENDICE

CALCULO DE LAS GENERACIONES DE CALOR EN CADA MATERIAL COMBUSTIBLE

Designamos con los subíndices 1 y 2 a las magnitudes correspondientes al óxido de plutonio (PuO_2) y al óxido de uranio (UO_2) respectivamente. En la suposición de que la presencia de la partícula de PuO_2 no afecta al flujo neutrónico térmico $\phi_{term}(\vec{r})$ en el lugar que ocupa dentro de la pastilla de UO_2, la relación entre las generaciones de calor en ambos materiales es:

$$R = \frac{Q_1}{Q_2} = \frac{\sum_f^1 \phi_{term}(\vec{r})}{\sum_f^2 \phi_{term}(\vec{r})} = \frac{(\delta_1/A_1)\ \sigma_f^1}{(\delta_2/A_2)\ \sigma_f^2}$$

donde $\sum_f^1$ y $\sum_f^2$ son las secciones eficaces de fisión para neutrones térmicos; δ_1 y δ_2 las densidades; A_1 y A_2 los pesos moleculares; y σ_f^1 y σ_f^2 las secciones eficaces microscópicas de fisión del PuO_2 y del UO_2 respectivamente.

De [3]:

$\delta_1 = 11.46\ g/cm^3$; $\qquad \delta_2 = 10.96\ g/cm^3$

$A_1 = 274.$ $\qquad A_2 = 270.$

Tomamos para el plutonio la composición isotópica que tiene el generado de un elemento combustible tipo C.N.A. con un quemado de 7.200 MwD/T [4]:

Pu^{239}: 64%

Pu^{240}: 28%

Pu^{241}: 8%

Con los valores de las secciones eficaces de fisión de [5], resulta:

$$\sigma_f^1 = 0.64 \times 742.5 + 0.08 \times 1000.9 = 555 \text{ barns.}$$

$$\sigma_f^2 = 0.0072 \times 582.2 = 4.19 \text{ barns}$$

luego:

$$R = 136.$$

Por ejemplo, para la barra C.N.A., tomamos como generación de calor en el UO_2 a la que corresponde a 687 watios por cm. de longitud de barra combustible si no estuviese la partícula de PuO_2:

$$Q_2 = \frac{687 \text{ w}}{\pi(0.916 \text{ cm})^2 \times 1\text{cm}} = 0.775 \text{ w/mm}^3.$$

Por lo tanto:

$$Q_1 = R.Q_2 = 105.5 \text{ w/mm}^3.$$

REFERENCIAS

[1] CROZIER, R.J.M.; "THISTLE-A Program to Determine the Three-Dimensional, Steady-State Temperature and Heat Flux Distributions in Inhomogeneous Nuclear Fuel Elements". AECL-4253-Chalk River, Ontario (June, 1972)

[2] BASOMBRIO, F.G.; CRUZ, B.; "Resolución por elementos finitos de la ecuación cuasiarmónica bidimensional.(Programas - "CUARM", "AXICUARM", "NOLICUARM")". CAB/1976/2 - Centro Atómico Bariloche, C.N.E.A. (1976).

[3] WEAST, R.C.(Ed.); "Handbook of Chemistry and Physics". CRC-PRESS- 55th Edition (1974-1975).

[4] KUCHLE, M.; PIERONI, N.; "Possibilities of Reactor Physics Experiments with a view to Plutonium Recicling in the Atucha Reactor (Oct.17,1974)-Kernforschungszentrum Karlsruhe.

[5] MUGHABGHAB, S.F.; GARBER, D.I.; "Neutron Cross Sections - Vol.I, Resonance parameters - BNL-325.3th.Edition.Brookhaven National Laboratory (June 1973).

[6] MONTENERO, C.; ROCCA, U.V.; "PIZZA-Código para el análisis termomecánico de barras combustibles tipo C.N.A."-CNEA-NT 18/76 (1976).

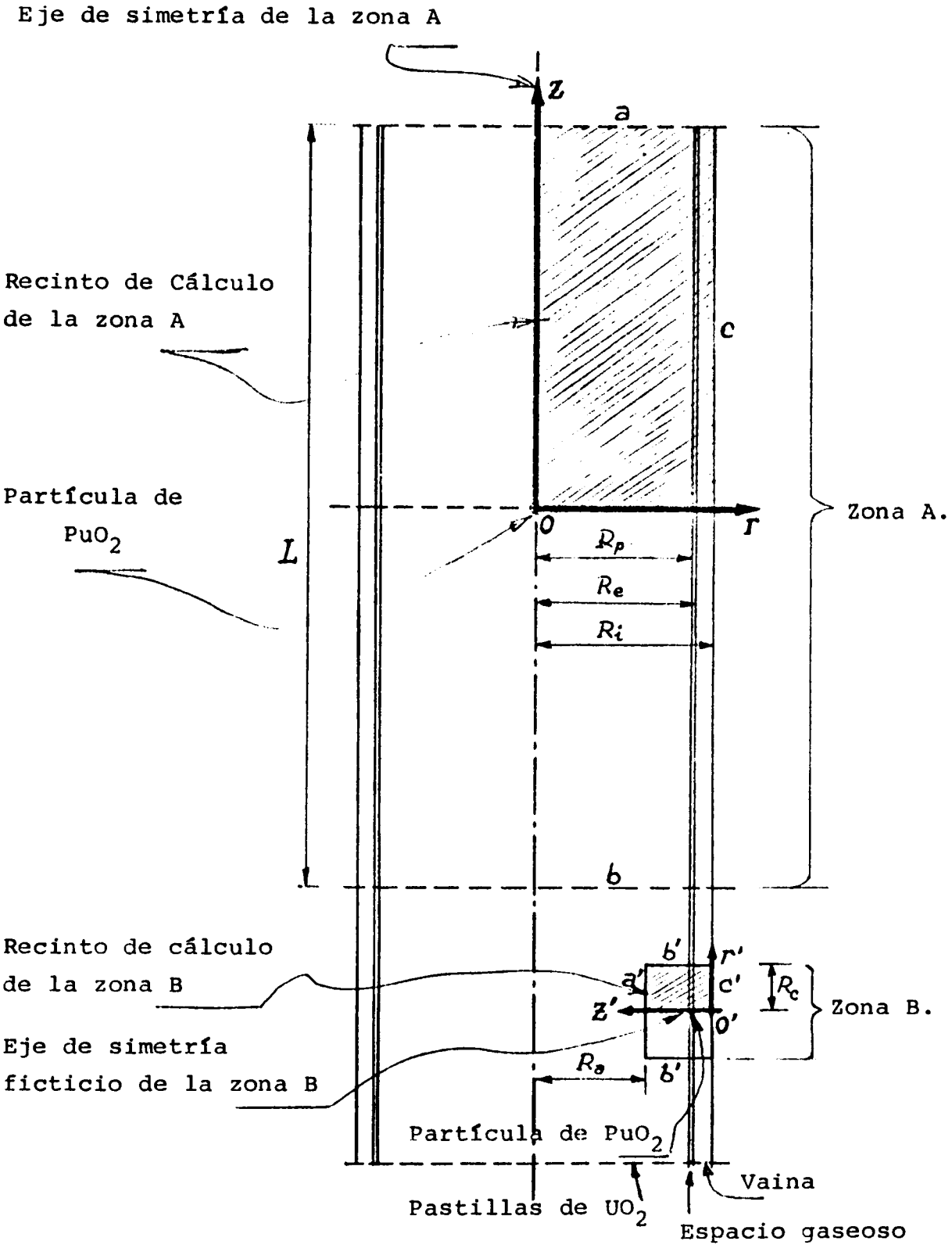

FIGURA 1.- Zonas A y B de la barra combustible y ubicación de sus respectivos recintos de cálculo.

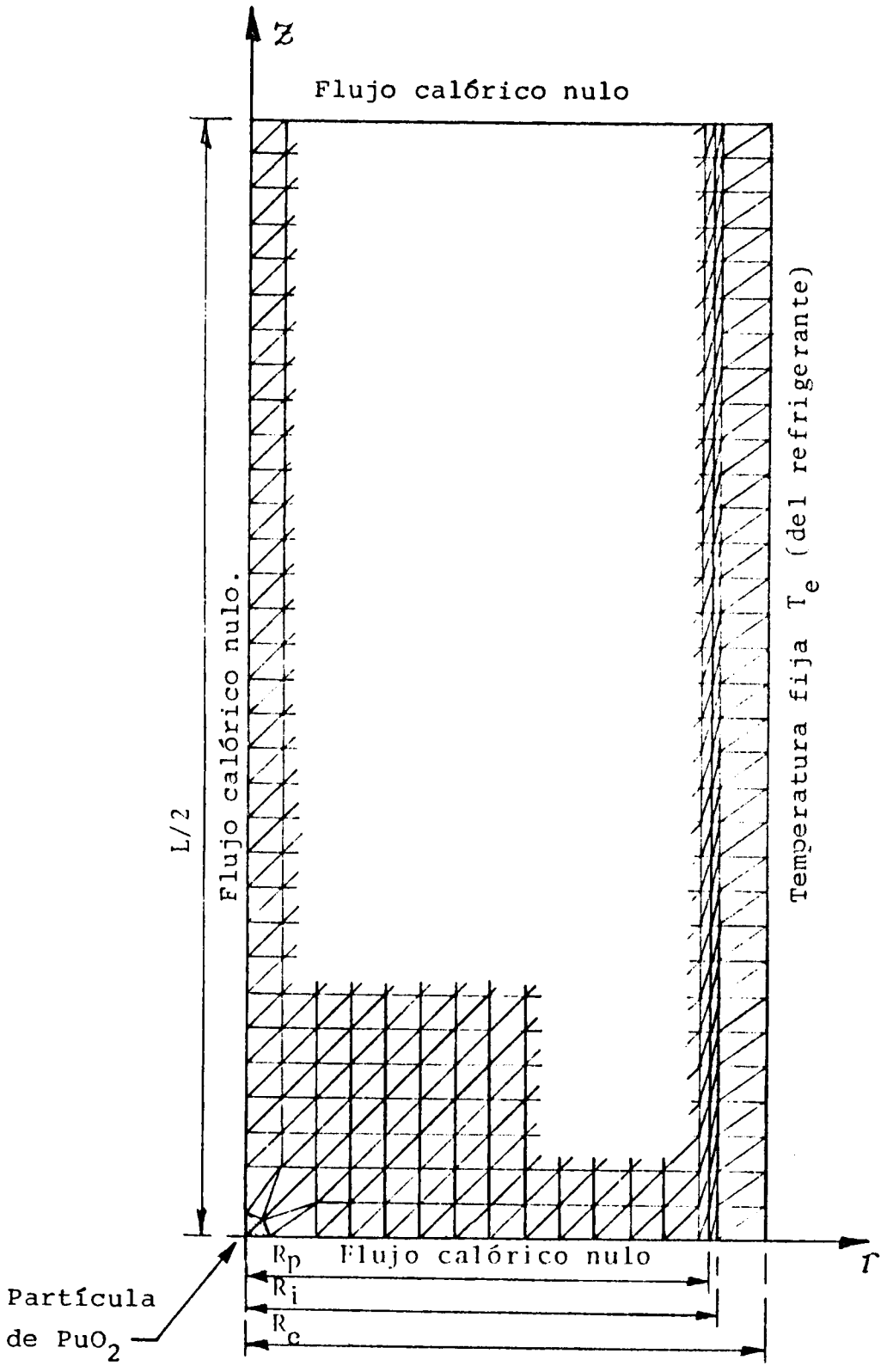

FIGURA 2.- Red de elementos finitos para la zona A.

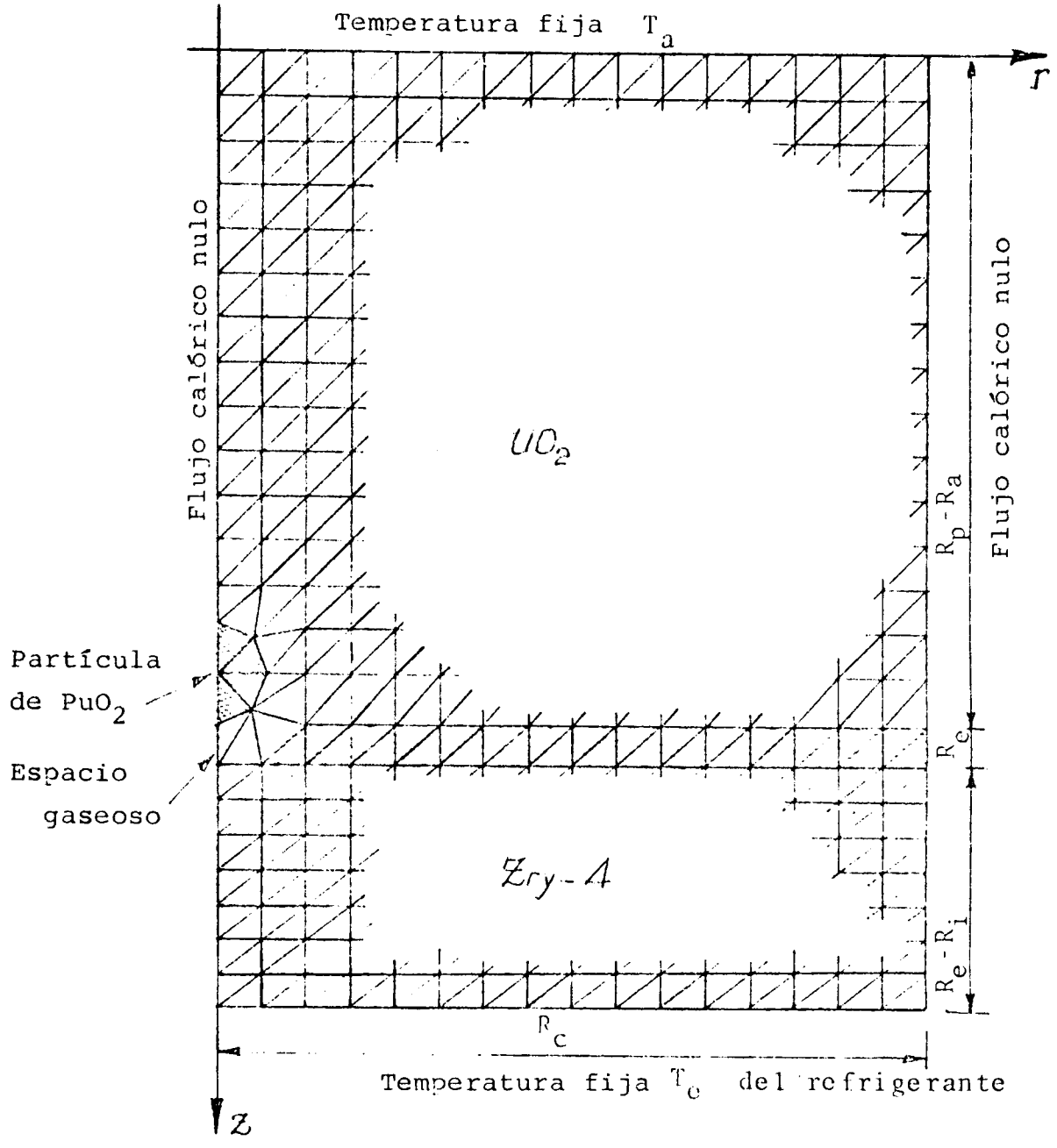

FIGURA 3.- Red de elementos finitos para la zona B, (situación b; ∅ = 200 μ).

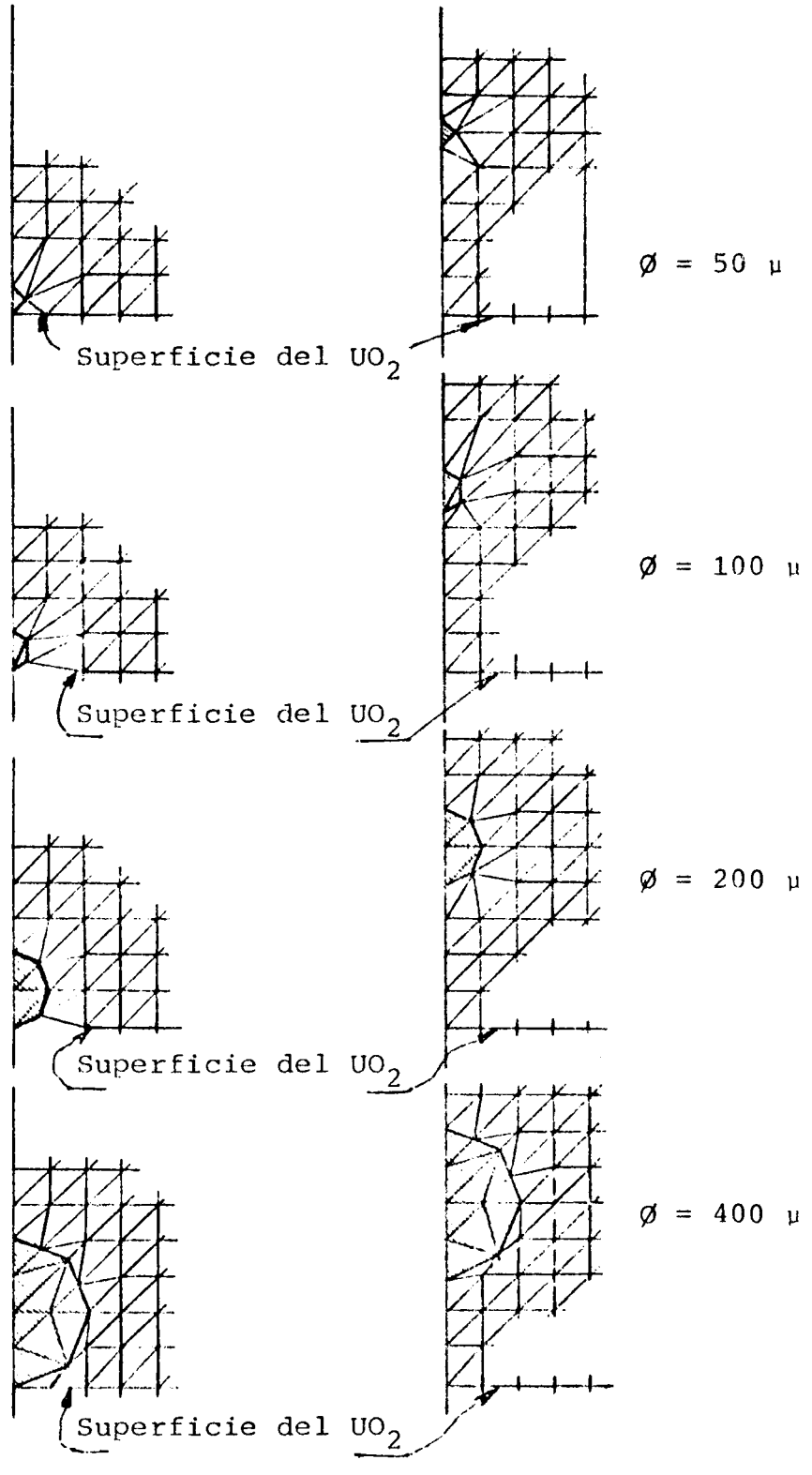

FIGURA 4.- *Conformaciones locales de la red de la figura 3 en el lugar de la partícula de PuO_2, para las situaciones b) y d) y cada uno de los distintos diámetros.*

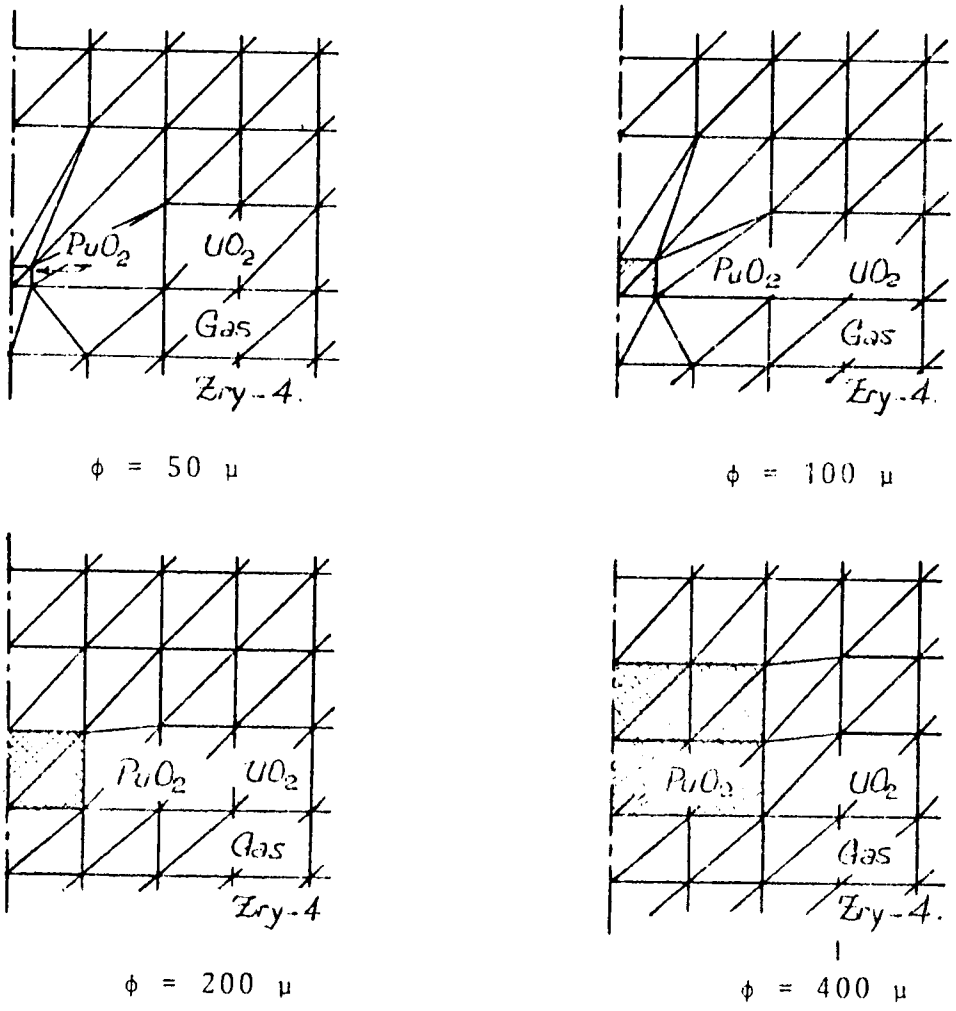

FIGURA 5.- Conformaciones locales de la red de la figura 3 en el lugar de la partícula de PuO_2, para cada dimensión, correspondientes a la situación c).

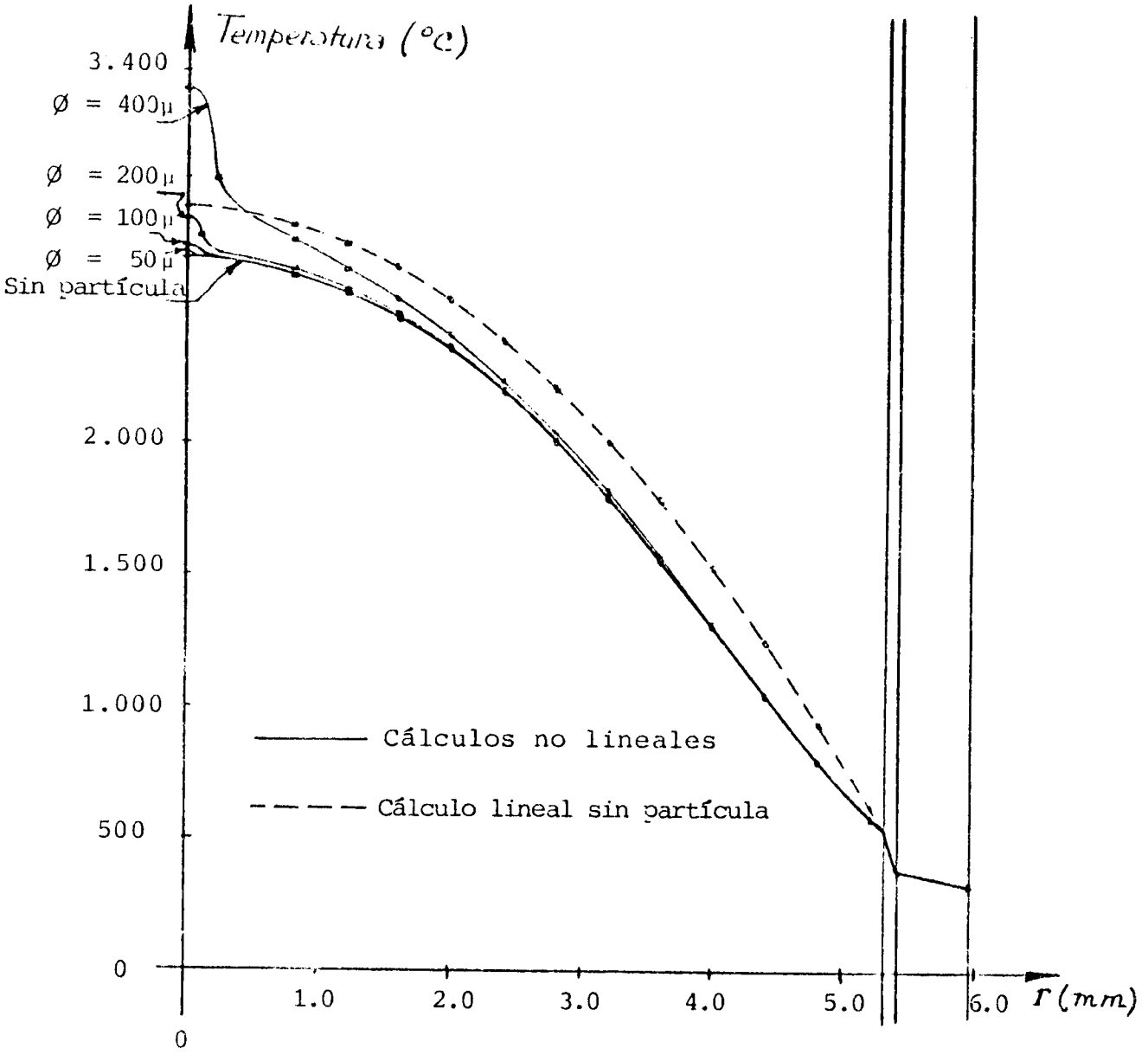

FIGURA 6.- *Distribución radial de la temperatura para la situación a), sobre una recta perpendicular al eje de la barra que pasa por el centro de la partícula. (Caso de la barra C.N.A.)*

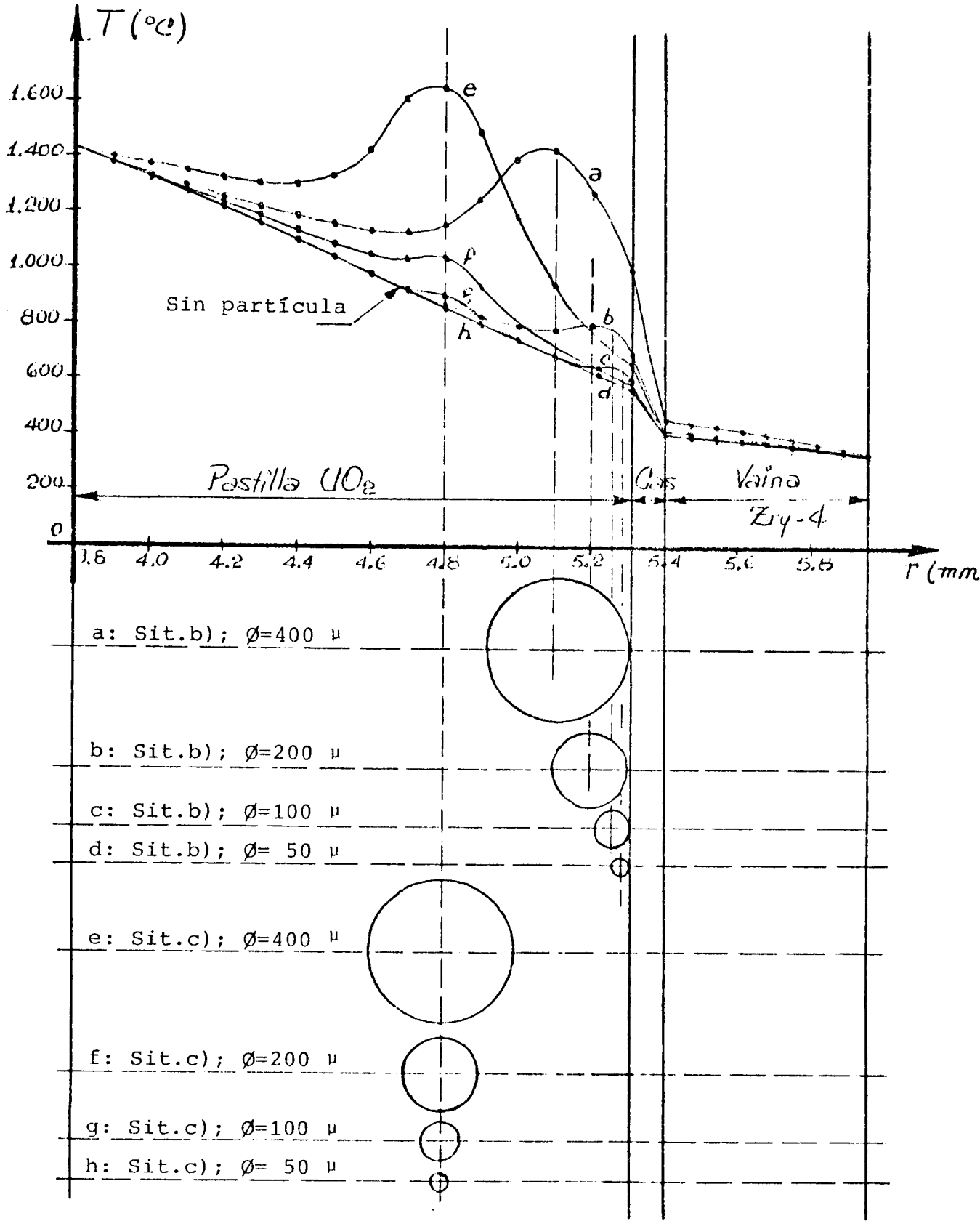

FIGURA 7.- Distribución radial de la temperatura para la situación b) y c), sobre una recta perpendicular a la vaina que pasa por el centro de las partículas. Se indican las posiciones de ésta para cada caso. (Barra combustible C.N.A.)

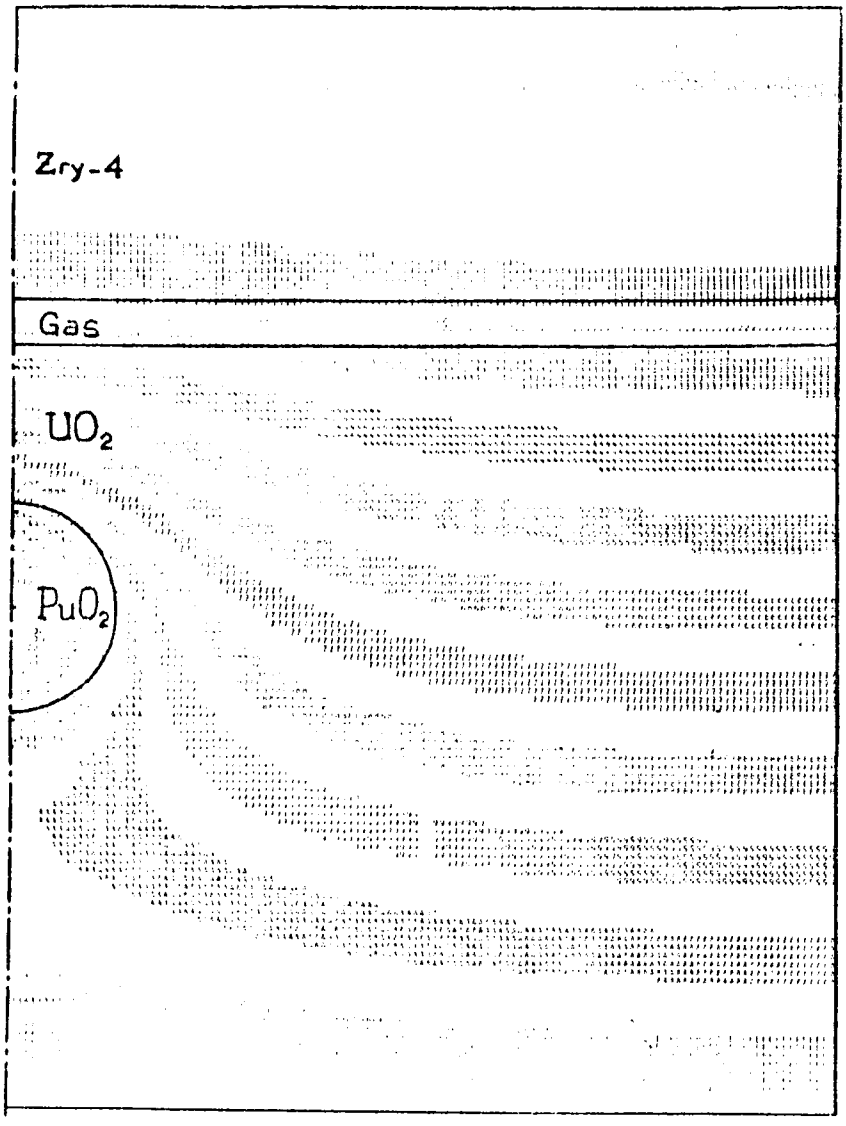

FIGURA 8.- *Distribución espacial de la temperatura para la situación c) y Ø = 400 μ. Los límites de cada franja son isotermas equiespaciadas. (Barra combustible C.N.A.)*